



**UCGE Reports
Number 20293**

Department of Geomatics Engineering

**Real-Time Kinematic Surveying using Tightly-Coupled
GPS and Ultra-Wideband Ranging**

(URL: <http://www.geomatics.ucalgary.ca/research/publications>)

by

Glenn D. MacGougan

August 2009



THE UNIVERSITY OF CALGARY

**Real-Time Kinematic Surveying using Tightly-Coupled GPS and
Ultra-Wideband Ranging**

by

Glenn D. MacGougan

A THESIS

**SUBMITTED TO THE FACULTY OF GRADUATE STUDIES
IN PARTIAL FULFILLMENT OF THE REQUIREMENTS FOR THE
DEGREE OF DOCTOR OF PHILOSOPHY**

DEPARTMENT OF GEOMATICS ENGINEERING

CALGARY, ALBERTA

AUGUST, 2009

© Glenn D. MacGougan 2009

Preface

This is an unaltered version of the authors Doctoral of Philosophy thesis. The thesis was accepted by the Faculty of Graduate Studies in August, 2009. The faculty supervisors for this work were Dr. Kyle O’Keefe and Dr. Richard Klukas. Other members of the examining committee were Dr. Mark Petovello, Dr. Yang Gao, Dr. John Nielsen, and Dr. Yu (Jade) Morton.

Abstract

Ultra-wideband (UWB) ranging radios, an emerging technology that offers precise, short distance, range measurements are investigated as a method to augment carrier-phase GPS positioning. This thesis begins with a discussion of radio-frequency based methods of augmenting high precision GPS and proposes to utilize UWB ranging technology in a tightly-coupled GPS and UWB position estimation filter. This thesis then provides an overview of UWB in the context of ranging applications and assesses the precision and accuracy of UWB ranging from both a theoretical perspective and a practical perspective using real data. Two types of commercially available UWB ranging radios are introduced which are used in testing. Actual ranging accuracy is assessed from line-of-sight testing in benign signal conditions and in outdoor testing with line-of-sight obstructions and strong reflection sources. A tightly-coupled GPS and UWB real-time kinematic (RTK) estimation method is developed and the performance of the system is evaluated in static and kinematic testing. The results of static testing show that the integrated solution provides better accuracy, better ability to resolve integer ambiguities and enhanced fixed ambiguity solution availability compared with GPS alone. The results of kinematic testing demonstrate that UWB errors can be successfully estimated in a real-time filter. In static and kinematic testing in a degraded GPS environment created by artificially inducing a 40° satellite elevation mask, sub-decimetre accuracy was maintained. The tightly-coupled system is also tested to survey several external corner points of an eight story building. The tightly-coupled solution is compared to GPS-only, UWB-only, and loosely-coupled solutions. Sub-metre level solutions are maintained using tight-coupling in conditions where the solutions from the other three approaches are either unavailable or unreliable. The thesis also provides a novel and efficient method for deploying UWB reference stations and performing

the RTK survey. Tightly-coupled GPS+UWB for RTK surveying is a promising new technology that extends RTK surveying to new environments. In addition, in marginal GPS-only surveying environments, position accuracy and RTK solution availability are improved substantially.

Acknowledgements

I owe the completion of this work to many and would like to express my gratitude to those that devoted their ideas, time, and patience to its completion.

- To: My family for their love and support and for keeping me sane and grounded while encouraging me in all of life's endeavors.
- To: My supervisors, Dr. Kyle O'Keefe, for his friendship, patience, and unwavering support of my endeavors, and Dr. Richard Klukas, for his support, guidance and pursuit of excellence.
- To: All of my fellow students who helped me in the sounding of ideas, data collection, editing, and analysis.
- To: The Natural Science Research Council of Canada (NSERC) and the Alberta Ingenuity Fund for their financial support of this research.

Table of Contents

Preface	ii
Abstract	iii
Acknowledgements	v
Table of Contents	vi
Notation	xvi
1 Introduction	1
1.1 Background	2
1.1.1 Satellite augmentation	2
1.1.2 Pseudolites	4
1.1.3 Wideband ground-based ranging systems	5
1.1.4 Ultra-wideband ranging	6
1.1.5 Comparison of augmentation methods	7
1.2 Motivation	9
1.3 Integration methods	9
1.4 Literature review	11
1.4.1 UWB ranging	11
1.4.2 Integration of GPS and UWB	13
1.4.3 Limitation of Previous Work	15
1.5 Research Objectives	16
1.6 Contributions	17
1.7 Outline	18
2 Ultra-wideband ranging	20
2.1 UWB history	21

2.2	UWB defined	21
2.2.1	Emission Limits	23
2.3	UWB categories	26
2.4	Cramer-Rao lower bound for ranging precision	28
2.4.1	Cramer-Rao lower bound discrepancies in the literature	35
2.5	UWB ranging methods	37
2.5.1	A note about time-of-arrival and time-difference-of-arrival UWB positioning systems	39
2.6	Two-way time-of-flight measurement bias	39
2.7	UWB pulse detection and geometric walk error	43
2.8	UWB ranges and multipath	45
2.9	UWB ranging radios	48
2.10	UWB ranging and low pulse repetition frequency UWB	50
2.11	Testing and results	53
2.11.1	Static line-of-sight testing	53
2.11.2	Dynamic line-of-sight testing	56
2.11.3	Multipath and obstruction testing	66
2.12	Time correlation of UWB measurements	71
2.13	Summary	73
3	Tightly-coupled GPS/UWB	74
3.1	Apparatus	74
3.1.1	Measurement synchronization	77
3.2	Selection of the optimal estimator	78
3.3	Summary of the sequential discrete-time extended Kalman filter	80
3.4	Description of the filter	82
3.4.1	Functional models	83

3.4.2	The tightly-coupled discrete sequential extended Kalman filter . . .	86
3.5	Reliability	94
3.5.1	Innovation testing	96
3.6	Differencing the single-difference solution	102
3.7	Ambiguity resolution	104
3.7.1	Integer ambiguity validation	105
3.7.2	Computing the fixed solution	107
3.7.3	Partial fixing	107
3.7.4	When and how to fix ambiguities	109
3.8	Testing overview	109
4	Tightly-coupled GPS/UWB testing	110
4.1	Static testing	110
4.1.1	Results with 13 degree elevation mask	111
4.1.2	Results with a 40 degree elevation mask	118
4.2	Kinematic testing	126
4.2.1	Assessing UWB ranging	128
4.2.2	Tightly-coupled test results	130
4.3	Summary	144
5	Results of testing in a difficult urban environment	145
5.1	Description of the test	145
5.2	Results	147
5.2.1	Test results using the Time Domain Radios	148
5.2.2	Test results using the Multispectral Solutions Radios	161
5.2.3	GPS Pseudorange Errors	172
5.3	Summary	175

6	System and method for tightly-coupled GPS+UWB surveying	177
6.1	UWB radio mounts	178
6.1.1	Tilt sensor	179
6.2	Deployment of the UWB reference stations	179
6.2.1	Deployment over known points	179
6.2.2	Deployment in the field using GPS	181
6.3	The initialization walk	184
6.4	The survey	184
6.5	Details	184
6.6	Summary	185
7	Conclusions and future work	187
7.1	Summary	187
7.2	Conclusions	191
7.3	Future work	192
7.4	Outlook	192

List of Tables

1.1	Comparison of augmentation methods	8
2.1	FCC UWB average power emission limits	25
2.2	GPS Specific FCC Emission Limits	25
3.1	Discrete-time sequential extended Kalman filter equations	81
4.1	Comparison of Horizontal Errors for the Static Test (40° Elevation Mask)	125
4.2	Comparison of Vertical Errors for the Static Test (40° Elevation Mask)	125
4.3	Kinematic test: survey point 1 statistics (GPS+UWB 40° elevation mask vs. GPS-Only 13° elevation mask)	134
4.4	Kinematic test: survey point 2 statistics (GPS+UWB 40° elevation mask vs. GPS-Only 13° elevation mask)	134
4.5	Kinematic test: survey point 3 statistics (GPS+UWB 40° elevation mask vs. GPS-Only 13° elevation mask)	135

List of Figures

1.1	Limited satellite geometry in an urban canyon (from nzbuu (2009))	3
1.2	The near-far problem with pseudolites and GPS	4
1.3	Ground-based augmentation for deep open pit mining	5
1.4	Loose-coupling	10
1.5	Tight-coupling	10
2.1	UWB Fractional Bandwidth	23
2.2	FCC UWB average power emission limits	24
2.3	The Gaussian pulse and its derivatives	27
2.4	Essential bandwidth	30
2.5	Best fit Gaussian pulse given the FCC average power emission limits . . .	33
2.6	Ranging CRLB vs. B_{99} for a Gaussian pulse described by its 99% energy bandwidth	34
2.7	Ranging CRLB vs. SNR for a Gaussian pulse described by its 99% energy bandwidth	35
2.8	Properties of non-bandlimited white noise	37
2.9	Two-way time-of-flight ranging	38
2.10	UWB range measurement turn-around-time bias for various oscillator errors	43
2.11	Threshold energy detection and geometric walk error	45
2.12	Wideband signal with multipath	46
2.13	UWB signal with multipath	47
2.14	Non-line-of-sight measurement	48
2.15	Multispectral Solutions Inc. (left, from MSSI (2007)) and Time Domain Corp. UWB ranging radios (right, from TDC (2008))	49

2.16	The effect of time dithering with 1 GHz, 20 dB bandwidth, Gaussian pulses. 20 pulses of 0.29 ns duration occur within 1000 ns pulse intervals. The sign of the pulse is alternated in the pulse train for both cases to ensure a DC component of zero. The fourier transform, $G(\omega)$, of each pulse is given by Equation 2.5 and the PSD is given by $ G(\omega) ^2$. The use of time dithering clearly reduces peak spectral lines.	52
2.17	Line-of-sight testing	54
2.18	Line-of-sight testing ranging errors results, TDC (left), MSSSI, (right) . . .	56
2.19	Dynamic ranging UWB and GPS using coaxial mounts	58
2.20	Dynamic test trajectory for the TDC radios	59
2.21	Dynamic line-of-sight test: TDC range errors	60
2.22	Dynamic line-of-sight test: MSSSI range errors	61
2.23	Dynamic line-of-sight test: TDC range error distribution for range pair 1 (5 cm bins)	63
2.24	Dynamic line-of-sight test: TDC range error distribution for range pair 2 (5 cm bins)	64
2.25	Dynamic line-of-sight test: MSSSI range error distribution for range pair 1 (5 cm bins)	65
2.26	Dynamic line-of-sight test: MSSSI range error distribution for range pair 2 (5 cm bins)	66
2.27	Plan view (right) of UWB range testing next to a building (left)	68
2.28	TDC Range errors in a multipath environment	69
2.29	MSSSI Range errors in a multipath environment	70
2.30	Time correlation of compensated UWB measurements. This figure shows a static portion of data collected for MSSSI range pair 1 during the dynamic line-of-sight test.	72
3.1	The GPS/UWB survey apparatus	76
3.2	The null hypothesis is that the standardized innovation is normally distributed	98

3.3	Multipath and echo-only GPS signals	101
4.1	Static GPS+UWB RTK test site photo	111
4.2	Static test: number of observations and DOP (13° mask)	112
4.3	Static test: float solution (13° mask)	113
4.4	Static test: float ambiguity estimates (13° mask)	114
4.5	Static test: fixed solution (13° mask)	116
4.6	Static test: fixed solution probability of correct fix (13° mask)	117
4.7	Static test: number of observations and DOP (40° mask)	119
4.8	Static test: float solution (40° mask)	120
4.9	Static test: float ambiguities (40° mask)	121
4.10	Static test: fixed solution (40° mask)	123
4.11	Static test: fixed solution probability of correct fix (40° mask)	124
4.12	The kinematic test	127
4.13	The kinematic test trajectory	128
4.14	Kinematic test: UWB Ranging Errors. The top row of subplots show the raw measured UWB range and the reference GPS RTK derived range vs. time. At this scale, only data gaps and UWB range blunders are apparent. The difference between the UWB range and the GPS RTK derived range vs. time is shown in the second row of subplots. This is the UWB ranging error. The bottom row of subplots shows the UWB ranging error plotted as a function of the GPS RTK derived range. These plots show the error characteristics of the UWB measurements as a function of the best estimate of the true distance being measured. In each plot of the bottom row, a line fit of the data obtained by post-processing is shown. Of note: the bottom left subplot shows two distinct trend lines. It is possible that the turn-around-time bias changed during the test due to warming of the radios' oscillators.	129
4.15	Kinematic test: GPS+UWB observations and DOP. The number of double difference ambiguities drops from 6 to 2 and there are large jumps in the DOP values when the 40° elevation mask is applied.	131

4.16 Kinematic test: survey points 1, 2, and 3 (GPS+UWB 40° elevation mask)	133
4.17 Kinematic test: baseline differences)	136
4.18 Kinematic test: UWB bias estimate. Convergence of the bias estimate only occurs after the user begins to move. The estimate of the bias converges after a sufficient range of motion is observed via the initialization walk.	138
4.19 Kinematic test: UWB scale factor estimate. Convergence of the scale factor estimate only occurs after the user begins to move. The estimate of the scale factor converges after a sufficient range of motion is observed via the initialization walk.	139
4.20 Kinematic test: UWB ranges and blunders. The subplots show the raw measured UWB range measurements (i.e. no corrections applied) and the reference GPS RTK derived range values. UWB range measurement blunders are clearly apparent in the plots. The blunders rejected by the filter are shown in red.	141
4.21 Kinematic test: Raw and corrected UWB range measurement errors. These subplots show the difference between the raw UWB range measurements and the reference GPS RTK derived ranges (i.e. UWB range error estimates). They also show the difference between the corrected UWB range measurements (using the estimated bias and scale factor estimates output by the filter for each epoch) and the reference GPS RTK derived ranges. The bias and scale factor corrections result in reduced UWB measurement error levels but systematic effects are not fully removed.	143
5.1 Photo of test area	146
5.2 TDC test trajectory on left and MSSSI test trajectory on right	147
5.3 GPS-only results of test with TDC radios	151
5.4 UWB-only results of test with TDC radios	151
5.5 GPS+UWB results of test with TDC radios	152
5.6 Loosely coupled solution using the TDC radios	152
5.7 UWB ranges and rejected measurements for the TDC UWB-Only solution	153
5.8 UWB ranges and rejected measurements for the TDC GPS+UWB solution	154

5.9	UWB range error histogram for range pair 1 (10 cm bin size)	156
5.10	UWB range error histogram for range pair 2 (10 cm bin size)	157
5.11	UWB range error histogram for range pair 3 (10 cm bin size)	158
5.12	UWB range error histogram for range pair 1 (2 cm bin size)	159
5.13	UWB range error histogram for range pair 2 (2 cm bin size)	160
5.14	UWB range error histogram for range pair 3 (2 cm bin size)	161
5.15	GPS-only results of test with MSSSI radios	163
5.16	UWB-only results of test with MSSSI radios	163
5.17	GPS+UWB results of test with MSSSI radios	164
5.18	Loosely coupled solution using the MSSSI radios	164
5.19	MSSSI UWB-Only solution UWB ranges and rejected measurements for the MSSSI UWB-Only solution	166
5.20	UWB ranges and rejected measurements for the MSSSI GPS+UWB solution	167
5.21	UWB range error histogram for range pair 1	169
5.22	UWB range error histogram for range pair 2	170
5.23	UWB range error histogram for range pair 3	171
5.24	Code-minus-carrier for PRN 22	174
5.25	Code-minus-carrier for PRN 16	175
6.1	MSSSI UWB radio mount	178
6.2	An UWB reference station over a known point	181
6.3	Surveying an UWB reference station over a new point	183
6.4	The GPS+UWB survey method	186

Notation

Symbols

$\hat{\mathbf{a}}$	vector of float ambiguities
$\tilde{\mathbf{a}}$	vector of fixed ambiguities
$\tilde{\mathbf{a}}_{\mathbf{B}}$	vector of fixed ambiguities using bootstrapping
\hat{b}	An estimated UWB bias error state
\hat{b}_a	An estimated UWB bias error state
\hat{b}_b	An estimated UWB bias error state
\hat{b}_c	An estimated UWB bias error state
$\hat{\mathbf{b}}$	vector of states (excluding ambiguity states to be fixed)
$\tilde{\mathbf{b}}$	vector of states (excluding fixed ambiguities)
	conditioned by the fixed ambiguities
\mathbf{B}	Differencing matrix from single-difference ambiguities to the double-difference ambiguities
B_b	essential bandwidth at baseband (Hz)
B_{b99}	B_b which contains 99% of the signal energy(Hz)
B_{b99}^{fit}	B_b which contains 99% of the signal energy and best fits the available FCC emission limits (Hz)
c	light speed (299792458.0 m/s in vacuum)
$d\rho$	orbital error (m)
dT	GPS receiver clock offset (s)
$dT_{reference}$	GPS reference receiver clock offset (s)
\mathbf{D}	Differencing matrix from the single-difference to the double-difference solution
E	energy
F	ratio value
e_A	error in the requester's oscillator (ppm)
e_B	error in the responder's oscillator (ppm)
f	frequency (Hz)
f_C	center frequency (Hz)
f_H	upper bound frequency (UWB 10 dB bandwidth in Hz)
f_L	lower bound frequency (UWB 10 dB bandwidth in Hz)
\mathbf{h}_i	i^{th} design vector
\mathbf{h}_p	the pseudorange design vector
\mathbf{h}_u	the UWB range design vector
\mathbf{H}_0	null hypothesis

\mathbf{H}_a	alternative hypothesis
I	Ionospheric delay (m)
\mathbf{I}	Identity matrix
k	An UWB scale factor error state
\mathbf{k}_i	Kalman gain vector for measurement i
l_i	a measurement
N	integer ambiguity (cycles)
N_0	noise spectral density
P	pseudorange measurement (m)
\mathbf{P}_k	Variance-covariance matrix of the states at epoch k
\mathbf{P}_{sd}	Single-difference variance-covariance matrix
\mathbf{P}_{dd}	Double-difference variance-covariance matrix
\mathbf{Q}_k	Process noise matrix at epoch k
$\mathbf{Q}_{\hat{a}}$	covariance matrix of the float double-difference ambiguities
$\mathbf{Q}_{\hat{b}}$	covariance matrix of the states (excluding ambiguity states to be fixed)
$\mathbf{Q}_{\hat{b}a}$	A submatrix of \mathbf{P}_{dd}
$\mathbf{Q}_{\hat{z}}$	covariance matrix of the float z-space double-difference ambiguities
$\hat{\mathbf{r}}$	vector of double-difference carrier phase residuals
R	UWB range measurement (m)
SNR	signal to noise ratio (dB)
t_f	time of flight (s)
t_i	standardized test statistic
t_{rt}	round trip time (s)
t_{ta}^d	turn-around-time design value (s)
t_{ta}^{true}	true turn-around-time (s)
$t_{ta}^{responder}$	the responder's turn-around-time ($= t_{ta}^d$) (s)
$t_{rt}^{requester}$	the requester's measurement of round trip time (s)
T	tropospheric delay (m)
v_i	i^{th} measurement innovation
\mathbf{w}_k	white noise sequence at epoch k
x, y, z	Unknown ECEF user coordinates
x_s, y_s, z_s	ECEF GPS satellite coordinates
x_u, y_u, z_u	ECEF UWB reference station virtual antenna position coordinates
$\hat{\mathbf{x}}_k$	vector of unknown parameters at epoch k
$\hat{\mathbf{x}}_{sd}$	vector of unknown single-difference parameters
$\hat{\mathbf{x}}_{dd}$	vector of unknown double-difference parameters
$\hat{\mathbf{z}}$	vector of z-space ambiguities
$\check{\mathbf{z}}$	vector of fixed integer z-space ambiguities
$\check{\mathbf{z}}_B$	vector of fixed integer z-space ambiguities using bootstrapping
\mathbf{Z}	LAMBDA Z-transformation matrix

α	significance level
β	effective bandwidth (Hz)
β	UWB bias
$\hat{\delta}_x$	error state vector
$\hat{\delta}_x, \hat{\delta}_y, \hat{\delta}_z$	ECEF user position error states
δT	signal difference clock offset error state (s)
ΔP	single-difference pseudorange measurement (m)
ΔT	single-difference GPS clock offset (s)
ϵ_f	error in the time of flight estimate (s)
ϵ_i	measurement noise
ϵ	noise
ϵ_P	pseudorange measurement noise and multipath error
ϵ_Φ	carrier phase measurement noise and multipath error
η	ambiguity error state
κ	UWB scale factor
λ	wavelength (m)
ρ	geometric range (m)
$\rho_{reference}$	geometric range between the reference GPS antenna and a GPS satellite (m)
ρ_u	geometric range between two UWB antennas (m)
σ	standard deviation
σ_i^2	measurement variance
$\sigma_{v_i}^2$	variance of an innovation
τ	time delay (s)
Φ	A GPS carrier phase measurement
$\Phi_{k-1,k}$	state transition matrix from epoch $k - 1$ to epoch k
$\Phi(y)$	an alternate form for the cumulative distribution function of the normal distribution
χ_{\min}^2	a smallest sum-of-squares
ω	angular frequency (radians/s)
$\nabla\Delta\lambda N$	double-difference ambiguity (m)
$\nabla\Delta\Phi$	double-difference phase measurement
$\nabla\Delta\rho$	double-difference geometric range

Abbreviations and Acronyms

CRLB	Cramer-Rao Lower Bound
DGPS	Differential GPS
DOP	Dilution of Precision
ECEF	Earth-Centered Earth-Fixed
ECMA	European Computer Manufacturers Association
EGNOS	European Geostationary Navigation Overlay Service
EIRP	Equivalent Isotropically Radiated Power
FCC	Federal Communications Commission
GPS	Global Positioning System
GNSS	Global Navigation Satellite System
HDOP	Horizontal Dilution of Precision
IEEE	Institute of Electrical and Electronics Engineers
ISM	Industrial, Scientific and Medical
LAMBDA	Least-squares Ambiguity Decorrelation Adjustment
LOS	Line-of-Sight
MSAS	Multi-functional Satellite Augmentation System
MSSI	Multispectral Solution Inc.
NLOS	Non-Line-of-Sight
OFDM	Orthogonal Frequency-Division Multiplexing
PCF	Probability of Correct Fix
PDOP	Position Dilution of Precision
ppm	parts-per-million
PRF	Pulse Repetition Frequency
RF	Radio Frequency
RMS	Root Mean Square
RTK	Real-Time Kinematic
SBAS	Satellite Based Augmentation System
SNR	Signal to Noise Ratio
SRC	Stored Template Reference Correlation
STD	Standard Deviation
TDC	Time Domain Corp.
TDOA	Time-Difference-of-Arrival
TOA	Time-of-Arrival
TRC	Transmit-Reference Correlation
UWB	Ultra-Wideband
VDOP	Vertical Dilution of Precision
WAAS	Wide Area Augmentation System

Chapter 1

Introduction

Ultra-wideband (UWB) ranging technology is low cost, low complexity, multipath resistant and high precision albeit short range. This makes UWB an excellent candidate for ground-based augmentation of real time kinematic (RTK) positioning using the Global Positioning System (GPS) for applications where short operational range is suitable. The Global Positioning System is a satellite based L-band radio-frequency (RF) navigation system comprised of more than 24 satellites orbiting approximately 20000 km above the earth. Using differential carrier phase techniques centimetre level RTK positioning is possible using GPS. The goal of this work is to improve and extend the ability to perform RTK surveying in difficult environments using UWB. This chapter describes the problem with GPS RTK systems and introduces current radio frequency (RF) based augmentation methods. There are other methods to augment high precision GPS surveying techniques. For example GPS can be integrated with inertial navigation units. However, this research only considers RF based methods of GPS augmentation. The objectives of the thesis are to examine UWB ranging technology from both a theoretical and practical perspective and to develop a tightly-coupled estimation approach for combining GPS and UWB measurements for high precision surveying.

This chapter begins by providing background information and discusses the motivation for using UWB technology to augment GPS RTK. This is followed by a literature review of UWB ranging studies and attempts to integrate GPS and UWB. The limitations of previous work are described and the objectives of this research are stated. The outline

of this thesis follows a summary of the contributions related to this research.

1.1 Background

Real time kinematic positioning using the Global Positioning System provides centimetre-level accuracy when there is high satellite availability and good quality solution geometry. RTK surveying is now common in industry but is limited in application primarily due to signal masking and multipath in hostile environments. Urban canyons, forests and congested construction sites are prime examples of environments where GPS RTK surveying fails to operate well. At a minimum, GPS RTK requires 4 satellites with good positioning geometry. In fact, many commercial systems often fail to fix carrier phase ambiguities unless five satellites are visible. Hence, in order to maintain centimeter-level accuracies under sub-optimal conditions, a method to augment GPS RTK is required.

As GPS is well known and well described by textbooks such as [Misra and Enge \(2004\)](#), this thesis may not introduce or may be brief about some GPS concepts.

This section first discusses different satellite and ground-based methods previously proposed and used to augment GPS to improve observability. The advantages and drawbacks of each method are discussed and then a new method of ground-based augmentation using ultra-wideband is proposed to improve and extend the ability to perform RTK surveying in difficult environments.

1.1.1 Satellite augmentation

Increasing the number of available satellites is one method to improve RTK availability. This can be achieved by utilizing satellite based augmentation systems (SBAS,

e.g. WAAS, EGNOS, MSAS) and other Global Navigation Satellite Systems (GNSS, e.g. Galileo, GLONASS). For example [Wanniger and Wallstab-Freitag \(2007\)](#) recently investigated the current integration of GPS, GLONASS and SBAS for RTK. The additional signal processing requirements add complexity and cost to the RTK receiver used for surveying. In deep urban canyons, high buildings block satellite signals with low to medium elevation angles and significantly degrade the solution geometry, or dilution of precision (DOP). This in turn drastically reduces the improvement achieved when using additional satellite systems. **Figure 1.1** provides an intuitive example of how geometry is a limiting factor in an urban environment. Additional satellites always benefit a navigation solution but the DOP is essentially limited by signal masking. Thus, additional augmentation is still required.



Figure 1.1: Limited satellite geometry in an urban canyon (from [nzbuu \(2009\)](#))

1.1.2 Pseudolites

GPS RTK can be successfully augmented using pseudolites, which are ground based in-band GPS-like (i.e. pseudo-satellite) transmitters (Cobb, 1997). A GPS receiver requires software modifications to enable the use of pseudolites but generally no additional receiver hardware is required. The near-far problem, illustrated in **Figure 1.2**, applies to pseudolites because as the GPS receiver approaches the pseudolite transmitter the pseudolite signal becomes strong enough to jam the relatively weak signals from the distant GPS satellites. This can be somewhat mitigated using pulsed signals (Cobb, 1997). The use of pseudolites is constrained by the need for licenses to transmit within the protected GPS frequency bands. Pseudolites also require timing synchronization with GPS. Due to these constraints, pseudolites are well suited for RTK applications where fixed infrastructure is available such as deep, open pit mining (Stone and Powell, 1998). This application is shown in **Figure 1.3**. Deformation monitoring (Dai et al., 2002) and precision approach and landing systems for aircraft (Bartone and Kiran, 2001) are also applications well suited to using pseudolites.

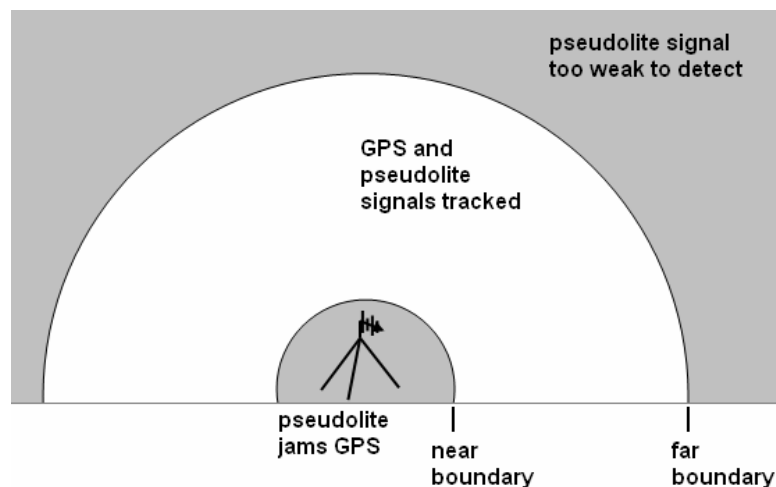


Figure 1.2: The near-far problem with pseudolites and GPS

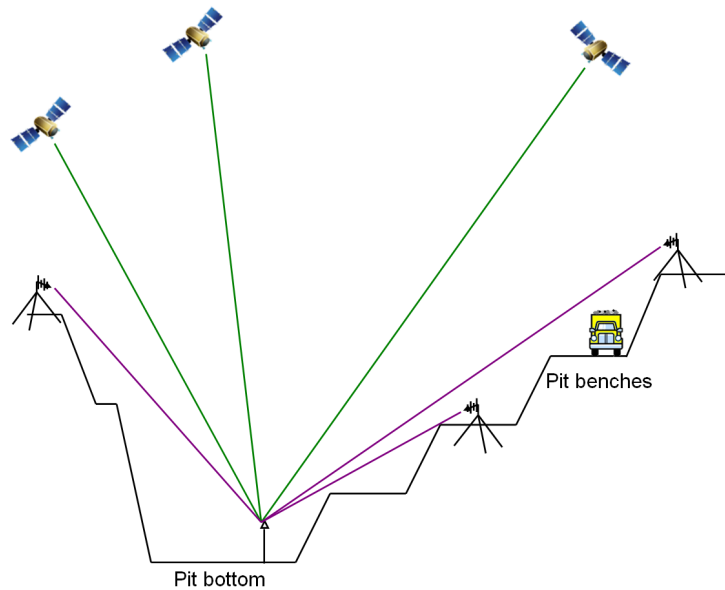


Figure 1.3: Ground-based augmentation for deep open pit mining

1.1.3 Wideband ground-based ranging systems

Augmentation with wideband ground-based ranging systems (80-100 MHz bandwidth) that operate in unlicensed bands such as presented in [Zimmerman et al. \(2005\)](#) and in [Barnes et al. \(2006\)](#) extend RTK capabilities using carrier phase processing techniques similar to those used in GPS. [Zimmerman et al. \(2005\)](#) describes a system operating using X-band signals (9.5 to 10.0 GHz) and the system described in [Barnes et al. \(2006\)](#) operates using ISM signals centered at 2.4 GHz. These are time-of-arrival systems and synchronized timing is, therefore, required. The time-synchronization requirements for these systems are high if centimetre level positioning is desired. This requirement also implies that these systems are difficult to deploy rapidly or on an ad-hoc basis for temporary surveying. These systems are very applicable to surveying in an environment suitable for fixed infrastructure. In fact, these systems derive from research into the

use of pseudolites and offer solutions that resolve the pseudolite near-far problem and that do not require licensing. The primary disadvantages of these systems are high cost and the complexity of integration with GPS.

1.1.4 Ultra-wideband ranging

The precision of ranging measurements by means of timing using modulated radio frequency (RF) signals is a function of the received signal to noise ratio (SNR) and the bandwidth of the signal employed. Moreover, as will be shown, the Cramer-Rao lower bound (CRLB), a lower bound precision estimate, is, for a timing delay estimator (range estimator), inversely proportional to the signal bandwidth but inversely proportional to only the square root of the SNR (Kay, 1993). Hence, increasing signal bandwidth is a significant means of improving measurement precision.

There is intense interest in ultra-wideband (UWB), a term which refers to very large relative or very large absolute bandwidth systems, due to the release of 7.5 GHz of unlicensed spectrum by the United States Federal Communications Commission (FCC) in 2002 for use by UWB systems (FCC, 2002). The term UWB was actually coined by the U.S. Department of Defense in 1989 (OSD-DARPA, 1990); however, UWB signals have long been part of the radio frequency (RF) spectrum. In fact, some of the first RF experiments were performed using spark-gap transmitters which have large relative bandwidth (DiBenedetto et al., 2006). However, it has taken many years and the confluence of numerous technological and political circumstances to enable practical, large scale UWB usage. UWB has many advantages including signal robustness (to interference), high communications capacity (e.g. 400 Mbps), resistance to multipath, and fine time resolution (e.g. cm level).

UWB can be used in synchronous time-of-arrival systems or in a method of asyn-

chronous ranging referred to as two-way time-of-flight ranging. Pulse-based UWB methods are prevalent in available ranging systems and carrier phase based techniques similar to GPS are not necessary. UWB is of particular interest to position and navigation applications because of the huge bandwidth available for time transfer (i.e. high precision ranging). The level of complexity to deploy and integrate UWB with other systems is very low because asynchronous ranging techniques can be used. With low cost, low complexity, high resistance to multipath, and the potential for centimetre level range measurements, UWB technology is very suitable to augment high precision surveying equipment such as GPS RTK.

The primary problem with UWB ranging is limited operational range. Commercially available ranging systems are currently limited to about 200 m for unlicensed operation and up to 600 m for licensed US government customers (e.g. [MSSI \(2007\)](#)). Experimental results in [Fontana \(2002\)](#) have shown operational ranges up to 2 km although the system tested would not likely meet FCC specifications in terms transmitted power. It is expected that the operational range can be increased while still meeting the FCC specifications but it will not likely match that of wideband ranging systems. Another drawback concerning UWB augmentation is that the FCC states that outdoor UWB systems are not to be used as fixed infrastructure. This limits the application of UWB for augmentation purposes to temporary usage unless a license is obtained. Applications like deep open-pit mining will require a license. In this case the operational range of the radios can likely be extended with higher emission limits to match that of wideband systems.

1.1.5 Comparison of augmentation methods

Table 1.1 provides an overview of the advantages and disadvantages of RF based methods used to augment GPS for high precision RTK surveying. The best approach

is a combination of satellite augmentation and ground-based augmentation.

Table 1.1: Comparison of augmentation methods

Method	Advantages	Disadvantages
Satellite Augmentation	<ul style="list-style-type: none"> • Improved measurement redundancy • No need for additional receivers 	<ul style="list-style-type: none"> • Limited by signal masking • Moderate increase in receiver complexity and cost
Pseudolite Augmentation	<ul style="list-style-type: none"> • Improved measurement redundancy • No need for additional receivers 	<ul style="list-style-type: none"> • Near-far problem • Moderate increase in receiver complexity and cost • Synchronized timing required • Special emission license required
Wideband Augmentation	<ul style="list-style-type: none"> • Improved measurement redundancy 	<ul style="list-style-type: none"> • Additional receivers required or complex combined receiver needed • Synchronized timing required • Large increase in receiver complexity and cost
UWB Augmentation	<ul style="list-style-type: none"> • Improved measurement redundancy • Low cost • Low complexity (asynchronous ranging) • Easily deployed • Multipath resistant 	<ul style="list-style-type: none"> • Limited operation range (without license) • Additional receivers required • Not suitable for fixed infrastructure unless a license is obtained

1.2 Motivation

With the advent of commercially available pulse-based UWB ranging devices, a study of GPS RTK augmented with multiple UWB ranges is feasible. The primary objective of this research is to assess how augmenting GPS RTK with UWB range measurements affects the ability to perform RTK when GPS signal conditions and GPS satellite availability are degraded. This requires a fundamental understanding of how the UWB range measurements are generated and of the associated error processes that affect UWB range measurement precision. Once the error processes are understood, an estimation method can be developed to use both UWB and GPS measurements with a tightly-coupled approach. The reason for selecting the tightly-coupled approach is discussed in the following.

1.3 Integration methods

There are two general classifications for combining systems and measurements. These are termed the loosely-coupled and tightly-coupled approaches. Position (and sometimes velocity) are desired unknown parameters computed by the estimation method. The GPS position solution and associated covariance matrix are often used as input (i.e. as a measurement) with either measurements from another system or the position solution obtained by another system. This method is called loose-coupling. Tight-coupling uses the measurements from different systems as input to a combined estimation method. The two methods are shown in **Figure 1.4** and **Figure 1.5**. The main advantage of tight-coupling is the added measurement redundancy. This allows a solution to be computed when there is an insufficient number of observations for one or the other system to compute a solution and also improves the ability to detect measurement blunders using reliability testing. For example, consider a 2D positioning

case with two independent systems, each with 2 range measurements. Both systems can compute a unique position solution with no redundancy. If a measurement blunder is present, it may be possible to detect the discrepancy between the two solutions but it is not possible to detect which system is in error. The tightly-coupled approach results in a redundancy of 2 and a measurement blunder can potentially be detected. In the case that one system loses one measurement, the loosely-coupled integration fails since one of the two systems cannot compute a solution. In the tightly coupled case, the remaining observation would continue to be used in a redundant integrated solution.

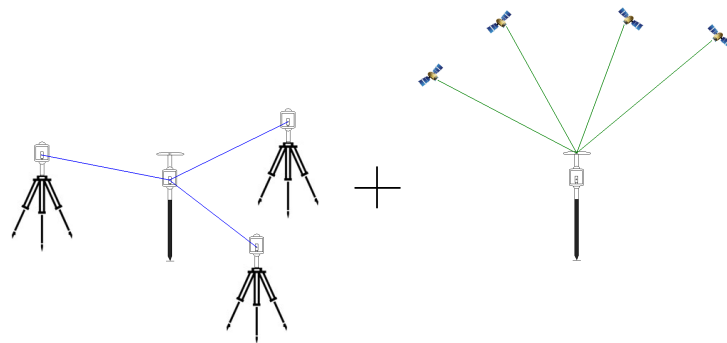


Figure 1.4: Loose-coupling

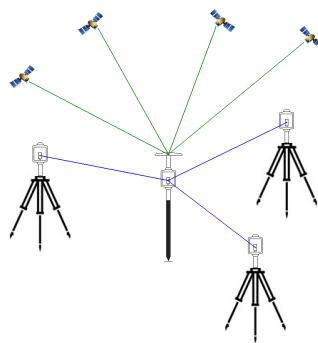


Figure 1.5: Tight-coupling

1.4 Literature review

1.4.1 UWB ranging

[Gezici et al. \(2005\)](#) discusses localization using UWB ranging in general and is a good introductory reference with some description of error sources. The ranging application using UWB is specifically addressed by an IEEE standard ([IEEE802-15.4a, 2007](#)) and by the European ECMA standard ([ECMA-368, 2006](#)).

Theoretical UWB ranging precision is assessed in numerous papers such as [Cardinali et al. \(2005\)](#), [Cardinali et al. \(2006\)](#), [Chung and Ha \(2003\)](#), [Guvenc and Sahinoglu \(2005\)](#), [Sahinoglu and Gezici \(2006\)](#), and [Yu \(2006\)](#). It should be noted that there are problems in the literature concerning the CRLB for time delay estimates. [Kay \(1993\)](#), [Poor \(1988\)](#), and [Urkowitz \(1983\)](#) are consistent with the equation for CRLB provided. [Cardinali et al. \(2006\)](#) and [Gezici et al. \(2005\)](#) provide the CRLB for a time delay estimate which differs from [Kay \(1993\)](#) by a factor of 1/2. It is also troubling that multiple technical papers such as [Sahinoglu and Gezici \(2006\)](#), [Lanzisera et al. \(2006\)](#), [Chung and Ha \(2003\)](#) and also [Yu \(2006\)](#) provide unclear or erroneous descriptions for the CRLB of a timing delay estimate. Misinterpretation of the term 'effective bandwidth' or misinterpretation of the definition of white noise are potential reasons for these problems. The review of these papers led to the submission of a letter to the IEEE ([MacGougan et al., 2009](#)) that attempts to clarify this situation. A full discussion of this is given in Section 2.4.1.

Multipath and oscillator bias induced UWB ranging error effects are reasonably well described in the literature. Oscillator bias induced error effects for two-way-time-of-flight ranging are discussed in ([IEEE802-15.4a, 2007](#)). [Yang and Giannakis \(2004\)](#) provides an introductory comparison of the impact of multipath on wideband and UWB signals. [Gezici et al. \(2005\)](#) discusses multipath and non-line-of-sight signal measurement and

UWB. [Lee and Scholtz \(2002\)](#) examined indoor UWB ranging and found that there are significant propagation delays due to line-of-sight blockage materials. These delays are a result of refraction and measurement of a dominant non-line-of-sight signal. [Denis et al. \(2003\)](#) performed a similar study which focusses on the impact of non-line-of-sight signal propagation. In the context of GPS/UWB integration and using real UWB measurements indoors, [Opshaug and Enge \(2001\)](#) quantified the multipath channel in terms of average delay and delay spread and found several cases where multipath components were stronger than the direct signal. They also mention that UWB technology has potential for avoiding ranging accuracy degradation for all but very short delay multipath. The indoor studies indicate that measurements based on reflected signals when the line-of-sight is occluded will be biased measurements. This extends to the outdoor environment, the focus of this research, and detection of exclusion of UWB measurement blunders is needed.

[Shimizu and Sanada \(2003\)](#) discuss the impact of clock jitter on ranging performance when correlation and a delay lock loop is used to synchronize to incoming pulses at the receiver. The clock jitter sets the performance floor and improvement can be achieved by increasing the averaging period of the loop filter.

The various techniques of pulse detection used with UWB pulses are well described in [Guvenc et al. \(2006\)](#). Pulse detection is performed by variants of one of three techniques. The first is threshold energy detection. It is the oldest and simplest pulse detection method. The second is stored template reference correlation (SRC) pulse detection. It uses (potentially coherent) correlation with an ideal received waveform to perform pulse detection. This is known as a matched filter receiver and has been used in narrowband systems and some wideband systems (such as GPS) for decades. The third method is transmit-reference correlation (TRC) pulse detection. TRC uses pilot pulses which are gathered by the receiver and used to correlate with the data pulses.

The main sources of inaccuracy in pulse based ranging systems using threshold energy detection are noise-generated timing jitter and geometric walk timing error. Jitter in timing determines the precision of the range measurement. This is primarily a function of the received SNR. Pulse amplitude and shape variations create timing error in the fine time-pickoff circuit and this error is called geometric walk error ([Amann et al., 2001](#)).

The fine time-pickoff circuit utilizes some form of time discriminator. The task of the discriminator is to observe fine time information from the electric pulse derived from the received RF signal. In pulse based laser ranging, commonly used discriminator designs include leading edge timing (constant amplitude), zero crossing timing (derivation, first moment timing (integration), and constant fraction timing ([Amann et al., 2001](#)). This is discussed in detail in Section 2.7.

Threshold detection receivers, also known as leading edge detection receivers, set a threshold signal value and any incoming pulse that crosses the threshold is detected and demodulated. This receiver design requires calibration to set the threshold such that the number of false alarms (false pulses) corresponding to noise spikes that happen to cross the threshold are within a desired operation range. In radar, this type of receiver is often called a constant false alarm rate receiver. A tunnel diode is often used as the pulse detector in these receivers ([Reed, 2005](#)).

1.4.2 Integration of GPS and UWB

[Opshaug and Enge \(2002\)](#) performed stand-alone GPS and DGPS simulations with covariance analysis to show that combined GPS and UWB has great potential for improving navigation performance by means of improving the solution geometry, solution availability, and by increasing the solution redundancy. [Tan and Law \(2007\)](#) performed

a similar study.

In a patent, [Fontana \(2000\)](#) discusses an UWB precision geolocation system which uses UWB pulses for time-difference-of-arrival (TDOA) measurements for high precision (centimeter level) applications. “With the ability to achieve range resolutions at centimeter levels (time-of-flight measurements to better than a few tens of picoseconds), UWB can also be used to provide a precise geolocation capability similar to that achieved with real-time kinematic (RTK) GPS solutions” (from [Fontana \(2000\)](#)). He goes on to suggest that an UWB solution can replace or augment conventional GPS RTK systems. The system described is untethered (i.e. no wires connecting any of the UWB reference transceivers). “In accordance with an embodiment of the present invention, a precision geolocation system, comprises a set of untethered, wireless ultra wideband transceivers positioned at precisely surveyed positions, and an untethered ultra wideband receiver/processor located at the point in space (e.g. a movable object, target or platform) whose absolute spatial coordinates are to be measured or detected wherein the processor resolves the position of the point in space based on the coordinates of the fixed points and time-of-flight measurements of the ultra wideband pulse” (from [Fontana \(2000\)](#)). In one implementation, the system utilizes a self-synchronizing scheme that makes time-of-flight measurements based on an initiation pulse from a mobile or stationary UWB transceiver. In another implementation, an external timing source (such as GPS) is used for determining the pulse arrival times at the mobile or stationary reference points. The method described uses TDOA UWB measurements at the receiver to obtain precise positions. Surveying is performed beforehand to determine the position of reference UWB transceivers. Experimental results of the aforementioned method are described in [Fontana \(2002\)](#) and in [Fontana et al. \(2003\)](#); however, in both examples, systems using UWB measurements only are described.

Estimation methods using GPS and UWB with experimental results using commer-

cially available UWB systems are discussed in [Gonzalez et al. \(2007\)](#), [Fernandez-Madrigal et al. \(2007\)](#), [Moore et al. \(2007\)](#), and [Tanigawa et al. \(2008\)](#). All of these papers except [Moore et al. \(2007\)](#) use a loosely-coupled approach by combining GPS positions and associated covariance information with UWB range measurements. [Moore et al. \(2007\)](#) does not present a coupled GPS and UWB solution but instead shows the performance of UWB only and GPS solutions (RTK in some cases). [Chiu \(2008\)](#) provides the first tight integration of GPS and UWB primarily using GPS pseudorange and UWB range measurements for low precision applications. Limited analysis is provided using tight-coupling with GPS carrier phase measurements for a combined float solution but a fixed ambiguity RTK solution is not provided and UWB bias and scale factors are treated by calibration in post-processing. The research presented in [Chiu \(2008\)](#) is in fact preliminary work performed in collaboration with this research.

1.4.3 Limitation of Previous Work

The ranging precision possible using UWB as defined in [FCC \(2002\)](#) is not well addressed in the literature. As discussed, there are problems and discrepancies in the descriptions of the CRLB used for assessing potential ranging precision. It is very important that the potential precision of UWB ranging measurements is well understood and hence it is an objective of this work to provide robust CLRb analysis for UWB ranging.

Ranging errors associated with two-way time-of-flight delay estimates have been assessed theoretically in the literature. No studies assessing the performance of available commercial UWB ranging radios are known. Hence, it is an objective of this work to assess the two types of commercial UWB systems available at the University of Calgary.

Fontana (2000) discusses the potential for augmenting GPS RTK with UWB TDOA measurements. Gonzalez et al. (2007), Fernandez-Madrigal et al. (2007), and Tanigawa et al. (2008) (for example) have examined the loosely-coupled approach. Compared to the loosely-coupled approach, that combines independent GPS and UWB position solutions, tight-coupling is particularly useful in sub-optimal environments since a position can still be obtained when fewer than 4 GPS or 3 UWB measurements are available. Tight-coupling can also significantly improve the ability to detect and mitigate measurement blunders as redundancy is improved.

Chiu (2008) has done some preliminary research (in collaboration with this research) integrating GPS with two-way time-of-flight UWB range measurements. However, tightly-coupled integration of GPS and UWB measurements, especially for high precision RTK (i.e. centimeter level) applications, is novel research. This is the primary focus of this work.

1.5 Research Objectives

The research described in this thesis has the following objectives.

1. To characterize UWB ranging technology from a Geomatics perspective.
2. To assess the potential precision of UWB ranging based on time delay estimation using Cramer-Rao lower bound analysis.
3. To assess and characterize UWB range measurement errors and error sources using commercially available UWB ranging devices.
4. To develop a tightly-coupled RTK estimation filter using GPS and UWB measurements.

5. To assess the reliability of UWB range measurements and develop methods to detect, isolate and adapt to potentially biased UWB range measurements.
6. To refine the estimation filter using state augmentation as needed to compensate for UWB error effects.
7. To develop a method and apparatus that facilitates practical use of GPS and UWB in the field.
8. To perform field testing of the UWB augmented GPS RTK solution and assess the impact of including UWB range measurements.

1.6 Contributions

Work presented in this thesis has been published or submitted for publication as follows:

- Chiu, D.S., G.D. MacGougan and K. O’Keefe (2008). UWB assisted GPS RTK in hostile environments. Proceedings of ION NTM 2008, 28-30 January, 2008, San Diego CA, U.S. Institute of Navigation, Fairfax VA
- G.D. MacGougan, O’Keefe K., and D. Chiu (2008). Multiple UWB range assisted GPS RTK in hostile environments. Proceedings of ION GNSS 2008, 15-19 Sept, 2008, Savannah, Georgia, U.S. Institute of Navigation, Fairfax VA, *best paper award*.
- K. O’Keefe, G.D. MacGougan, and D.S. Chiu (2008). System and methods for real time kinematic surveying using GNSS and ultra wideband ranging. United States provisional patent application. Filed in September 2008.

- G.D. MacGougan, and K. O’Keefe (2009). Real time UWB error estimation in a tightly-coupled GPS/UWB positioning system,” Proceedings ION ITM 2009, 26-28 Jan 2009, Anaheim California.
- G.D. MacGougan, K. O’Keefe, and R. Klukas (2009). Tightly-coupled GPS/UWB positioning. Proceedings of IEEE Conference on UWB, 9-11 Sept, 2009, Vancouver, Canada. *accepted*.
- G.D. MacGougan, K. O’Keefe, and R. Klukas (2009). On the Cramer-Rao lower bound for UWB ranging. IEEE Transactions on Vehicular Technology. *submitted*.
- G.D. MacGougan, K. O’Keefe and R. Klukas (2009). Ultra-wideband ranging precision and accuracy. Journal of Measurement Science. *accepted*.
- G.D. MacGougan, K. O’Keefe and R. Klukas (2009). Tightly-coupled GPS/UWB integration. The Journal of Navigation. *submitted*.
- G.D. MacGougan, K. O’Keefe, R. and Klukas (2009). Accuracy and reliability of tightly-coupled GPS/ultra-wideband positioning for surveying in urban environments. GPSSolutions, *submitted*.
- G.D. MacGougan and K. O’Keefe (2009). Method and Apparatus for High Precision GNSS/UWB Surveying. ION GNSS, Savannah, GA, Sept. 24 *abstract accepted*.

1.7 Outline

The remainder of this thesis is organized into six chapters. Chapter 2 discusses UWB in general, the potential precision of UWB ranging, UWB ranging methods, and potential sources of UWB ranging errors. It also includes a description of the UWB radio

types used for this research and the results of UWB range measurement testing in benign line-of-sight conditions. Chapter 3 describes the GPS/UWB surveying apparatus that was developed, the estimation method used to tightly integrate GPS and UWB measurements, the ambiguity resolution and validation strategy used to obtain a fixed ambiguity solution, and the reliability method used to detect measurement blunders. Chapter 4 provides the results of static and kinematic testing in a degraded GPS signal environment created artificially by excluding GPS satellites from the solution using elevation masking. Chapter 5 assesses the feasibility of the tightly-coupled approach of combining GPS and UWB measurements for RTK surveying in a realistic urban canyon environment. Chapter 6 describes a novel method of deploying the GPS/UWB equipment in order to efficiently perform an RTK survey. Concluding remarks are provided in Chapter 7.

Chapter 2

Ultra-wideband ranging

UWB is of particular interest for position and navigation applications because of the huge bandwidth available for time transfer. The precision of ranging measurements by means of timing using modulated radio frequency (RF) signals is a function of the received signal-to-noise ratio (SNR) and the bandwidth of the signal employed. Moreover, as will be shown, the Cramer-Rao lower bound (CRLB) for a timing delay estimator (range estimator) is a lower bound precision estimate that is inversely proportional to the signal bandwidth but inversely proportional to only the square root of the SNR (Kay, 1993). Hence, increasing signal bandwidth is a significant means of improving measurement precision.

Measurement precision is defined as the consistency of a group of observations about the mean value. However, the mean value may be biased. Accuracy is defined as the closeness of the measurements to the true value. CRLB analysis assesses the theoretical best performance of UWB for ranging in terms of precision but real testing is needed to assess the accuracy of practical UWB ranging.

In this chapter, two types of commercially available UWB ranging radios are examined and potential sources of measurement error are described. Actual ranging accuracy is assessed from line-of-sight testing in benign signal conditions by comparison to high accuracy electronic distance measurements and to ranges derived from GPS real-time kinematic positioning. In addition, range measurements obtained in outdoor testing with line-of-sight obstructions and strong reflection sources are compared to ranges derived from classically surveyed positions.

2.1 UWB history

Research and development relevant to today's UWB began in the 1960's by Ross and Robbins at the Sperry Rand Corporation, by Harmuth at the Catholic University of America, by Paul van Etten at the US Air Force Rome Air Development Center, and also by Russians researchers ([Barrett, 2001](#)). Most notably, in 1973, the US patent office awarded Ross a landmark patent, US 3278632, on UWB communications ([Ross, 1973](#)). This patent included all the major components necessary for an impulse radio system. Developments led to the use of UWB for radar, ground penetrating radar, and communications systems. Many systems were developed covertly for the military. In 1994, T. E. McEwan invented micropower impulse radar which provided, for the first time, extremely low power (i.e. microwatt) UWB radar ([McEwan, 1995](#)). The First Report and Order released by the U.S. Federal Communications Commission (FCC) in 2002 ([FCC, 2002](#)) brought UWB into the spotlight with the release of 7.5 GHz of unlicensed spectrum. The FCC also issued a Second Report and Order in 2005 ([FCC, 2005](#)) which amended the Part 15 non-UWB regulations to permit the use of peak emissions levels, similar to the levels applied to UWB devices. These documents provide the most pertinent definition of an UWB signal. For an in depth history of UWB consult [Barrett \(2001\)](#).

2.2 UWB defined

In the United States, Part 15 is an often-quoted section of the FCC rules and regulations. More specifically, it is part of Title 47 of the Code of Federal Regulations and mainly deals with unlicensed transmissions. It regulates everything from spurious emissions to unlicensed low-power broadcasting. The FCC 15.517 (indoor) and FCC 15.519 (hand held, i.e. outdoor with no fixed infrastructure) specifications pertain to

UWB and Subpart F, p.103 of [FCC \(2002\)](#), provides the following definition for UWB.

Section 15.503 Definitions. (a) UWB Bandwidth. For the purpose of this subpart, the UWB bandwidth is the frequency band bounded by the points that are 10 dB below the highest radiated emission, as based on the complete transmission system including the antenna. The upper boundary is designated f_H and the lower boundary is designated f_L . The frequency at which the highest radiated emission occurs is designated f_M . (b) Center frequency. The center frequency, f_C , equals $(f_H + f_L)/2$. (c) Fractional bandwidth. The fractional bandwidth equals $2(f_H - f_L)/(f_H + f_L)$. (d) Ultra-wideband (UWB) transmitter. An intentional radiator that, at any point in time, has a fractional bandwidth equal to or greater than 0.20 or has a UWB bandwidth equal to or greater than 500 MHz, regardless of the fractional bandwidth.

Figure 2.1 illustrates this definition graphically. The concept of the 10 dB bandwidth is shown with the frequency of highest power which may or may not be the same as the center frequency. Transmitters with center frequencies at or above 2.5 GHz are considered UWB emitters if they have a 10 dB bandwidth greater than 500 MHz. UWB systems with center frequencies less than 2.5 GHz will have a fractional bandwidth equal to or greater than 0.20.

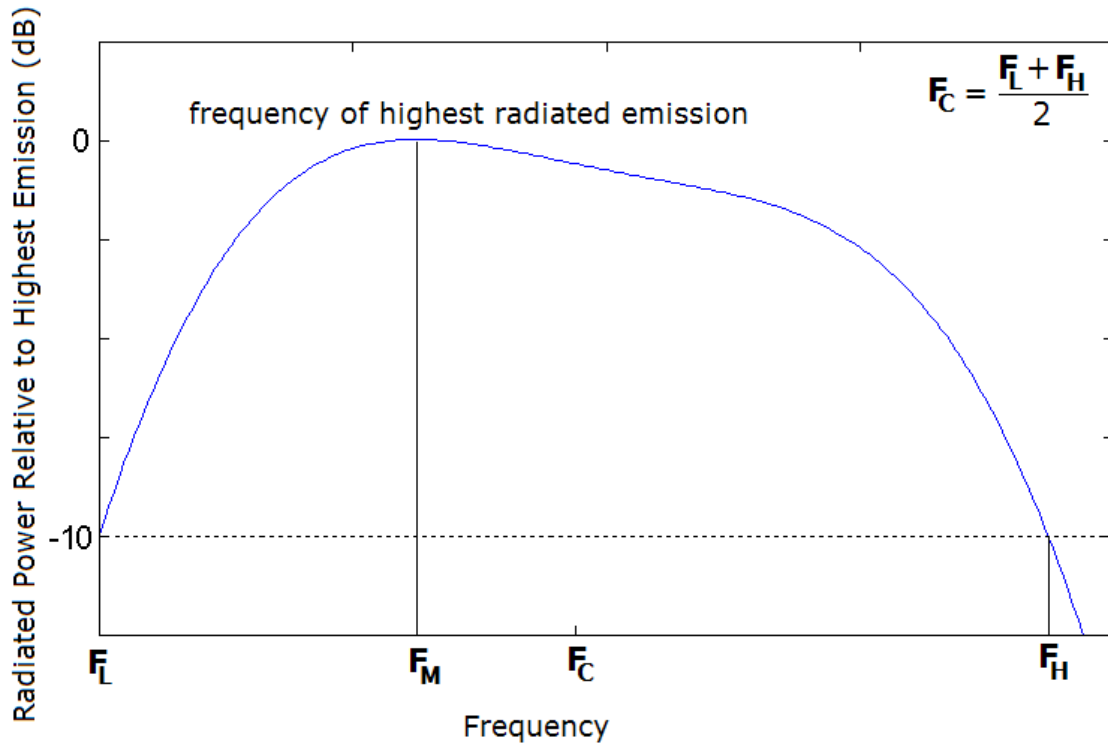


Figure 2.1: UWB Fractional Bandwidth

2.2.1 Emission Limits

The FCC provides average power density and peak power emission limits for compliant operation (FCC, 2002). For outdoor usage, the hand-held category of emission limits is applicable. The average power emission limits are shown in **Figure 2.2** and provided in **Table 2.1**. The peak emission limit is 0 dBm equivalent isotropically radiated power (EIRP) for the emissions contained within a 50 MHz bandwidth centered on the frequency at which the highest radiated emission occurs. For pulse based UWB signals with low pulse repetition frequencies (PRF), the peak limit is likely the defining standard. This is discussed further in **Section 2.10**.

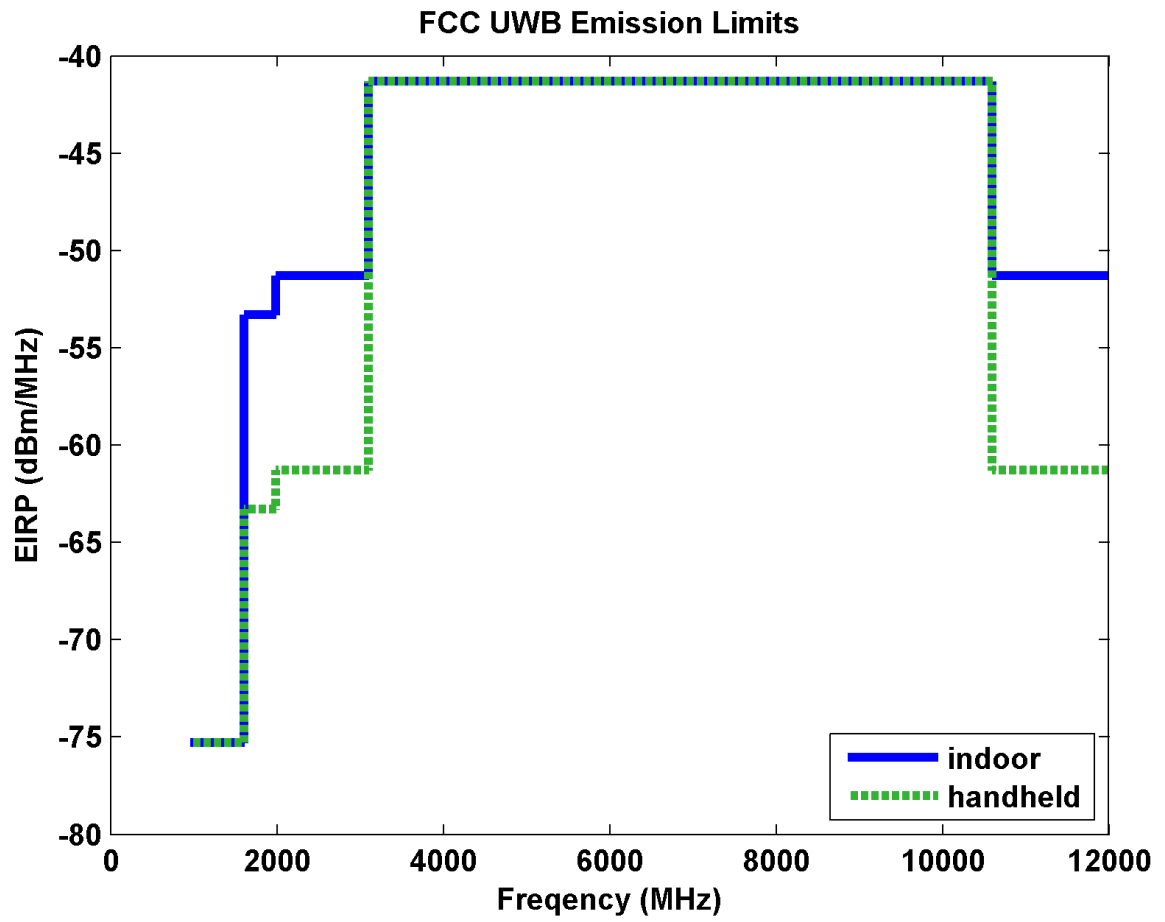


Figure 2.2: FCC UWB average power emission limits

Table 2.1: FCC UWB average power emission limits

Frequency Range (MHz)	Indoor EIRP (dBm/MHz)	Hand-held EIRP (dBm/MHz)
Below 960	refer FCC Part 15.209	refer FCC Part 15.209
960-1610	-75.3	-75.3
1610-1990	-53.3	-63.3
1990-3100	-51.3	-61.3
3100-10600	-41.3	-41.3
Above 10600	-51.3	-61.3

In addition to the average and peak emission limits, particular attention was also paid to avoid interference below 2 GHz where the RF spectrum is most heavily occupied and especially for the GPS bands to avoid serious detrimental impact on public safety. **Table 2.2** shows the emission limits that protect GPS signal bands including GPS L1, L2, and L5 when measured with a resolution bandwidth of no less than 1 KHz.

Table 2.2: GPS Specific FCC Emission Limits

Frequency Range (MHz)	Indoor EIRP (dBm/MHz)	Hand-held EIRP (dBm/MHz)
1164-1240 (GPS L2, L5)	-85.3	-85.3
1559-1610 (GPS L1)	-85.3	-85.3

2.3 UWB categories

UWB is broadly categorized into short pulse based (impulse) UWB (e.g. nanosecond long Gaussian pulses) and multi-carrier UWB (e.g. Orthogonal frequency-division multiplexing (OFDM)). Impulse methods sometimes make use of a carrier to better use the spectrum available given the FCC constraints. Historically, UWB signals are synonymous with impulse radio but large bandwidth multicarrier methods, such as OFDM, can also be considered UWB based on the FCC definition. A few studies, such as [Parikh and Michalson \(2008\)](#) and [Xu et al. \(2007\)](#), have examined multi-carrier methods for UWB ranging. Ranging based on impulse UWB is more prevalent in the literature and commercial systems that use this technique are already available. As of yet, no commercial systems that use the multi-carrier method for ranging are known.

Simple analytic pulse waveforms can be obtained from the Gaussian pulse and its derivatives. The Gaussian pulse is described by

$$p(t) = e^{-(t-\mu)^2/(2\sigma^2)} \quad (2.1)$$

where σ is related to the pulse width (to be discussed in the ensuing section), and μ is the midpoint of the pulse in time. The Gaussian pulse and its first three derivatives are shown in **Figure 2.3**. The first derivative of the Gaussian pulse is referred to as a Gaussian monocycle.

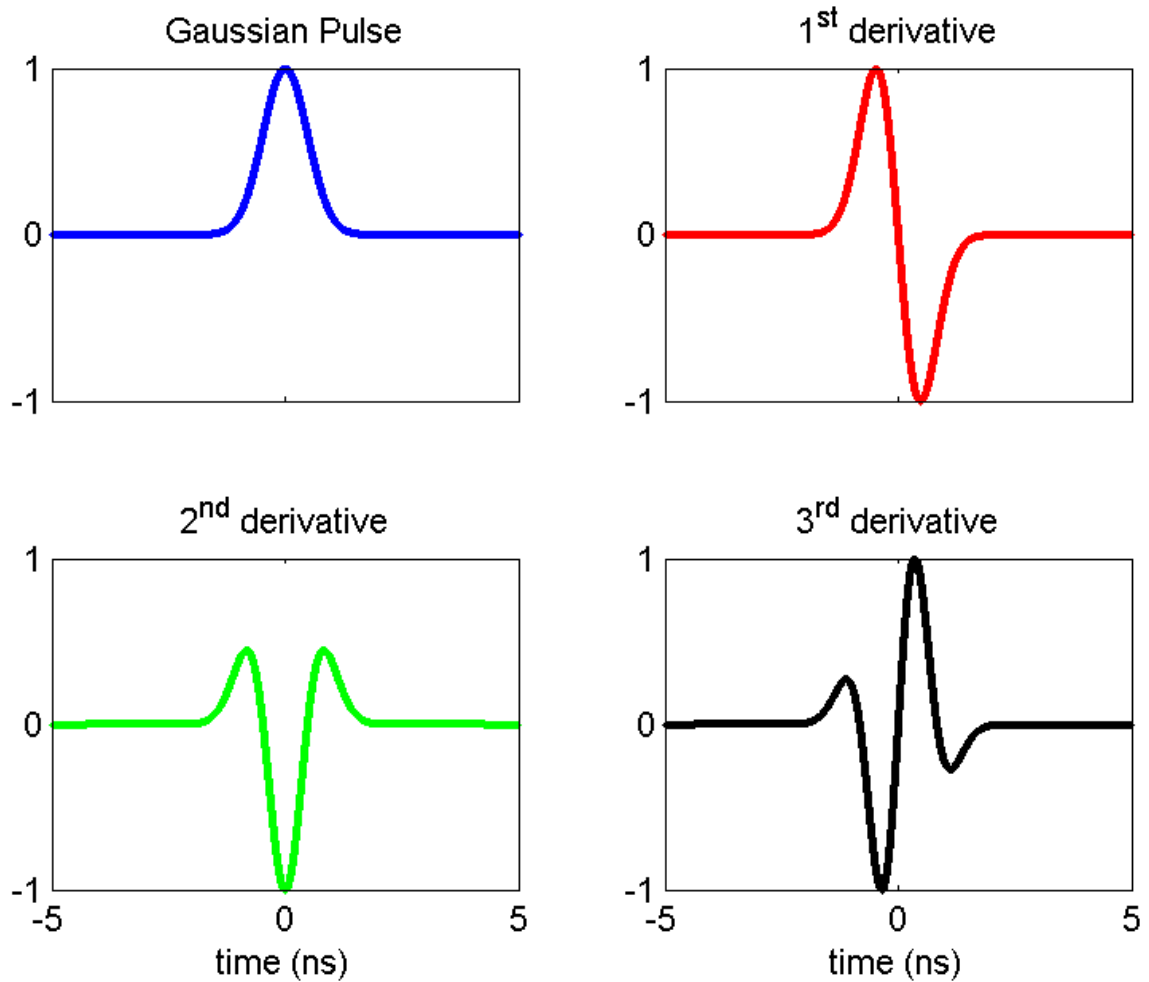


Figure 2.3: The Gaussian pulse and its derivatives

These pulses, while convenient for analytic purposes, are not directly suited for practical application because of the need to fit the available spectrum as mandated by the FCC. For example, to make the most use of the FCC allocation in the 3.1 GHz to 10.6 GHz band, a Gaussian pulse can modulate a 6.85 GHz carrier signal. Modulating a carrier, pulse shaping, and bandpass filtering of the basic Gaussian derived waveforms are effective means of generating FCC compliant pulses.

2.4 Cramer-Rao lower bound for ranging precision

The Cramer-Rao lower bound (CRLB) is a statistical measure described well by [Kay \(1993\)](#) that states that the variance of any unbiased estimator will be no lower than the inverse of the Fisher information. The CRLB provides a benchmark for the performance analysis of any unbiased estimator. For ranging methods, it provides a means to assess the theoretical best performance of an estimator. The CRLB for a time delay estimate, with any pulse waveform, is given by [Kay \(1993\)](#), [Poor \(1988\)](#), and [Urkowitz \(1983\)](#) as

$$\text{var}(\hat{\tau}) \geq \frac{1}{\frac{E}{N_0/2}\beta^2} = \frac{1}{\text{SNR} \cdot \beta^2} \quad (2.2)$$

where β is called effective bandwidth or mean square bandwidth, E is the energy of the pulse, N_0 is noise spectral density, and $E/(N_0/2)$ is SNR ([VanTrees, 1968](#)). Effective bandwidth is given by

$$\beta^2 = \frac{\int_{-\infty}^{\infty} (2\pi f)^2 |S(f)|^2 df}{\int_{-\infty}^{\infty} |S(f)|^2 df} \quad (2.3)$$

where f is frequency (Hz), and $S(f)$ is the Fourier transform of the transmitted signal, $s(t)$. Note that effective bandwidth is not related to the half-power bandwidth or noise bandwidth. Clearly, larger effective bandwidth implies better ranging precision. SNR, which is strongly influenced by operating conditions and transmit energy, has less effect but still contributes to ranging precision.

The effective bandwidth, β^2 , is provided in [Kay \(1993\)](#) for the Gaussian pulse as

$$\beta^2 = \frac{1}{2\sigma^2} \quad (2.4)$$

where σ can be related to the pulse width in the time domain or bandwidth in the frequency domain. A useful bandwidth to relate to σ is the 99% energy bandwidth.

To demonstrate the performance potential for UWB ranging, the CRLB associated with a 99% energy bandwidth for a Gaussian pulse can be determined. This corresponds to

bandwidth cutoff at -20 dB. The following proof shows the relationship between σ and the 20 dB bandwidth.

The Fourier transform of the Gaussian pulse is described analytically on page 85 of [Lathi \(1998\)](#) as

$$G(\omega) = \sigma\sqrt{2\pi}e^{-\sigma^2\omega^2/2}e^{-j\omega\mu} \quad (2.5)$$

where ω is angular frequency. Furthermore, the energy spectral density (ESD) for this pulse is defined analytically as

$$\Psi(\omega) = |G(\omega)|^2 = 2\pi\sigma^2e^{-\sigma^2\omega^2} \quad (2.6)$$

The complete energy for a single Gaussian pulse determined analytically using Parseval's theorem is

$$\begin{aligned} E &= \frac{1}{2\pi} \int_{-\infty}^{\infty} \Psi(\omega) d\omega \\ E &= \frac{1}{2\pi} \int_{-\infty}^{\infty} 2\pi\sigma^2e^{-\sigma^2\omega^2} d\omega \\ E &= \int_{-\infty}^{\infty} \sigma^2e^{-\sigma^2\omega^2} d\omega \end{aligned} \quad (2.7)$$

The following integral lemma is useful.

$$I(a) = \int_{-\infty}^{\infty} e^{-ax^2} dx = \sqrt{\frac{\pi}{a}}, a > 0 \quad (2.8)$$

The total signal energy is determined to be

$$E = \int_{-\infty}^{\infty} \sigma^2e^{-\sigma^2\omega^2} d\omega = \sigma^2\sqrt{\frac{\pi}{\sigma^2}} = \sigma\sqrt{\pi} \quad (2.9)$$

Essential bandwidth, B_b , describes the bandwidth that contains a certain percentage of the total signal energy. The concept of essential bandwidth is illustrated in **Figure 2.4**.

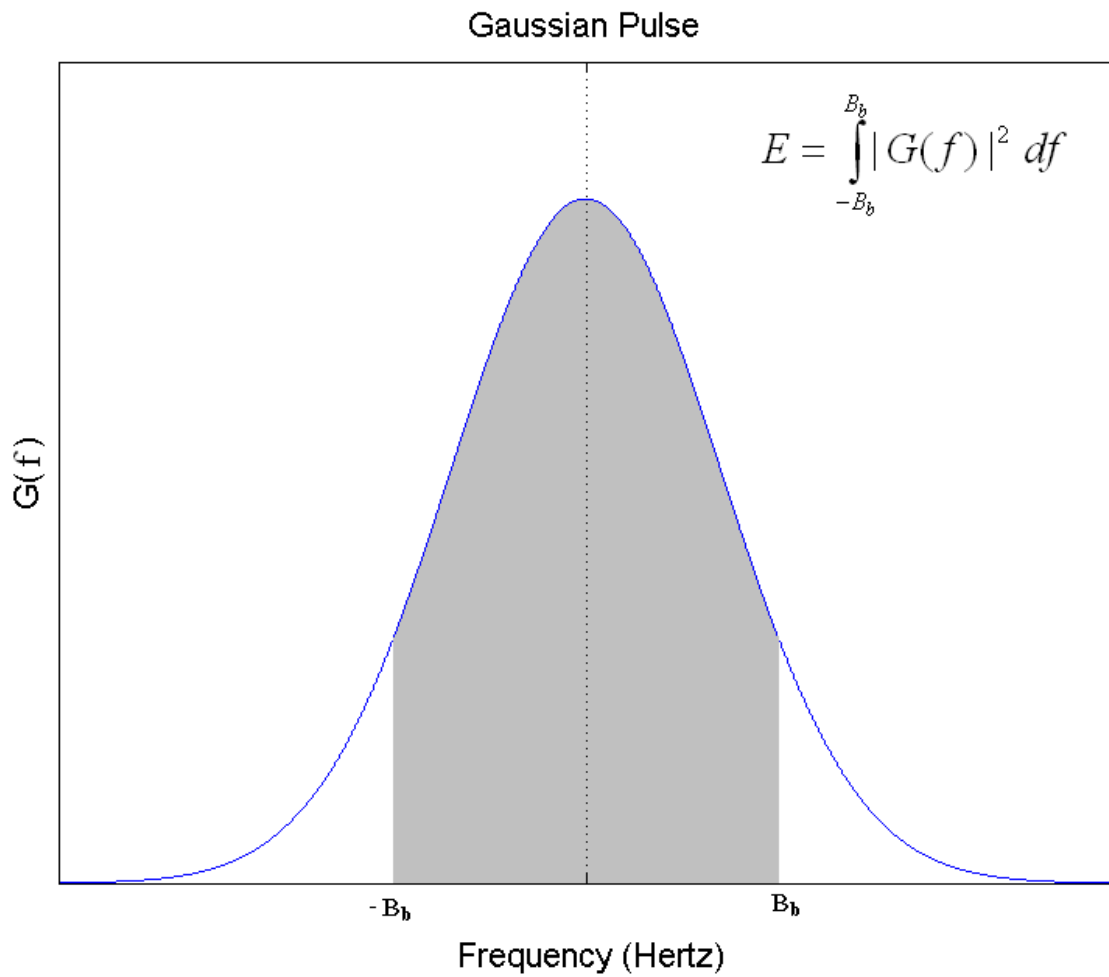


Figure 2.4: Essential bandwidth

The relationship between energy and essential bandwidth at baseband, B_b , is described on page 117 of [Lathi \(1998\)](#) as

$$E_B = \frac{1}{2\pi} \int_{-2\pi B_b}^{2\pi B_b} 2\pi\sigma^2 e^{-\sigma^2\omega^2} d\omega = \int_{-2\pi B_b}^{2\pi B_b} \sigma^2 e^{-\sigma^2\omega^2} d\omega \quad (2.10)$$

The following integral lemma is useful to evaluate the above expression.

$$\begin{aligned} \int_{-z}^z e^{-cx^2} dx &= \sqrt{\frac{\pi}{4c}} \operatorname{erf}(\sqrt{cx}) \Big|_{-z}^z, \operatorname{erf}(-y) = -\operatorname{erf}(y) \\ \int_{-z}^z e^{-cx^2} dx &= 2\sqrt{\frac{\pi}{4c}} \operatorname{erf}(\sqrt{cx}) = \operatorname{erf}(\sqrt{cz}) \sqrt{\pi/c} \end{aligned} \quad (2.11)$$

where erf , is the Gauss error function. For $c = \sigma^2$ and $z = 2\pi B_b$, this is

$$E_B = \sigma^2 \operatorname{erf}(2\pi B_b \sigma) \sqrt{\frac{\pi}{\sigma^2}} = \operatorname{erf}(2\pi B_b \sigma) \sigma \sqrt{\pi} \quad (2.12)$$

The essential bandwidth which contains 99% of the signal energy is related to σ by

$$\begin{aligned} 0.99E &= E_B = 0.99\sigma\sqrt{\pi} = \operatorname{erf}(2\pi B_{b99}\sigma)\sigma\sqrt{\pi} \\ B_{b99} &= \operatorname{erf}^{-1}(0.99)/(2\pi\sigma), \\ \sigma &= \operatorname{erf}^{-1}(0.99)/(2\pi B_{b99}) \end{aligned} \quad (2.13)$$

Combining **Equation 2.4** with the expression for σ using B_{b99} in the previous equation results in

$$\beta^2 = \frac{1}{2\sigma^2} = \frac{1}{2} \left(\frac{2\pi B_{b99}}{\operatorname{erf}^{-1}(0.99)} \right)^2 = \frac{2\pi^2 B_{b99}^2}{(\operatorname{erf}^{-1}(0.99))^2} \quad (2.14)$$

This results in the CRLB for a time delay estimate for a Gaussian pulse described by its 99% energy bandwidth or 20 dB bandwidth. This is given by

$$\operatorname{var}(\hat{\tau}) \geq \frac{(\operatorname{erf}^{-1}(0.99))^2}{\operatorname{SNR} \cdot 2\pi^2 B_{b99}^2} \approx \frac{1}{5.95 \cdot \operatorname{SNR} \cdot B_{b99}^2} \quad (2.15)$$

Keep in mind that this CRLB is not for a band limited signal. The signal is just described by its 99% energy bandwidth. However, since 99% of the signal energy is contained by this bandwidth it is a fair assumption that the CRLB for a bandlimited signal would be close to **Equation 2.15**, provided that the signal is not bandlimited to less than the essential bandwidth.

The Gaussian pulse described by the 99% energy baseband bandwidth (20 dB bandwidth), possible given the FCC average power emission constraints, can be determined

analytically. The proof starts with **Equation 2.6** and proceeds as follows.

$$\begin{aligned}
\Psi(\omega) &= 2\pi\sigma^2 e^{-\sigma^2\omega^2} \\
\Psi(0) &= 2\pi\sigma^2 \\
10 \log_{10}(\Psi(2\pi \cdot 3.75 \text{ GHz})) &= 10 \log_{10}(\Psi(0)) - 20 \\
10 \log_{10}(\Psi(2\pi \cdot 3.75 \text{ GHz})) &= 10 \log_{10}(2\pi\sigma^2) - 20 \\
10 \log_{10}(2\pi\sigma^2) - 20 &= 10 \log_{10}(2\pi\sigma^2) - 10 \log_{10}(100) = 10 \log_{10}(2\pi\sigma^2/100) \\
10 \log_{10}(\Psi(2\pi \cdot 3.75 \text{ GHz})) &= 10 \log_{10}(2\pi\sigma^2/100) \\
2\pi\sigma^2 e^{-\sigma^2(2\pi \cdot 3.75 \text{ GHz})^2} &= 2\pi\sigma^2/100 \\
e^{-\sigma^2(2\pi \cdot 3.75 \text{ GHz})^2} &= 1/100 \\
\ln(e^{-\sigma^2(2\pi \cdot 3.75 \text{ GHz})^2}) &= -\sigma^2(2\pi \cdot 3.75 \text{ GHz})^2 = \ln(1/100) \\
\sigma^2 &= \frac{-\ln(1/100)}{(2\pi \cdot 3.75 \text{ GHz})^2}
\end{aligned} \tag{2.16}$$

Using **Equation 2.13**, the 99% baseband bandwidth which describes the best fit Gaussian pulse is determined.

$$\begin{aligned}
\sigma &= \text{erf}^{-1}(0.99)/(2\pi B_{b99}^{\text{fit}}) \\
\sigma &= \text{erf}^{-1}(0.99)/(2\pi B_{b99}^{\text{fit}}) = \sqrt{-\ln(1/100) \frac{1}{(2\pi \cdot 3.75 \text{ GHz})^2}} \\
B_{b99}^{\text{fit}} &= \frac{\text{erf}^{-1}(0.99)}{2\pi \sqrt{-\ln(1/100) \frac{1}{(2\pi \cdot 3.75 \text{ GHz})^2}}} \\
B_{b99}^{\text{fit}} &= 3.182808485.9... \text{ GHz} \\
B_{b99}^{\text{fit}} &\approx 3.182808 \text{ GHz}
\end{aligned} \tag{2.17}$$

Thus, a carrier modulated Gaussian pulse which best fits the available bandwidth given the FCC emission limits has a 99% energy bandwidth of 3.182808 GHz with a 6.85 GHz carrier. This signal is illustrated in **Figure 2.5**.

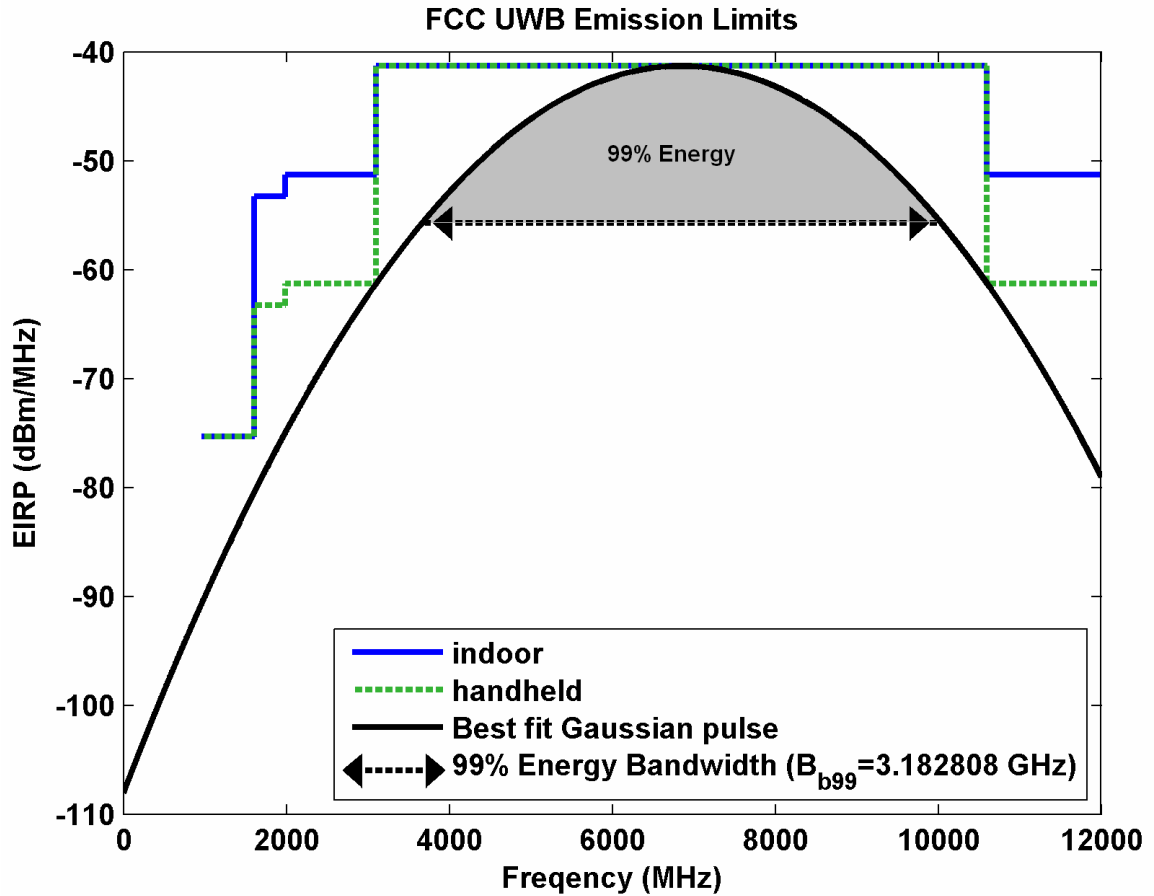


Figure 2.5: Best fit Gaussian pulse given the FCC average power emission limits

Figure 2.6 illustrates the ranging CRLB for Gaussian pulse signals with various SNR values and as a function of the 99% energy bandwidth up to the best fit maximum bandwidth given the FCC average emission limits. Figure 2.7 describes the CRLB for various 99% energy bandwidths as a function of the SNR. These figures show that UWB ranging has real potential for sub-decimetre precision. These results are for synchronous one-way time of arrival ranging.

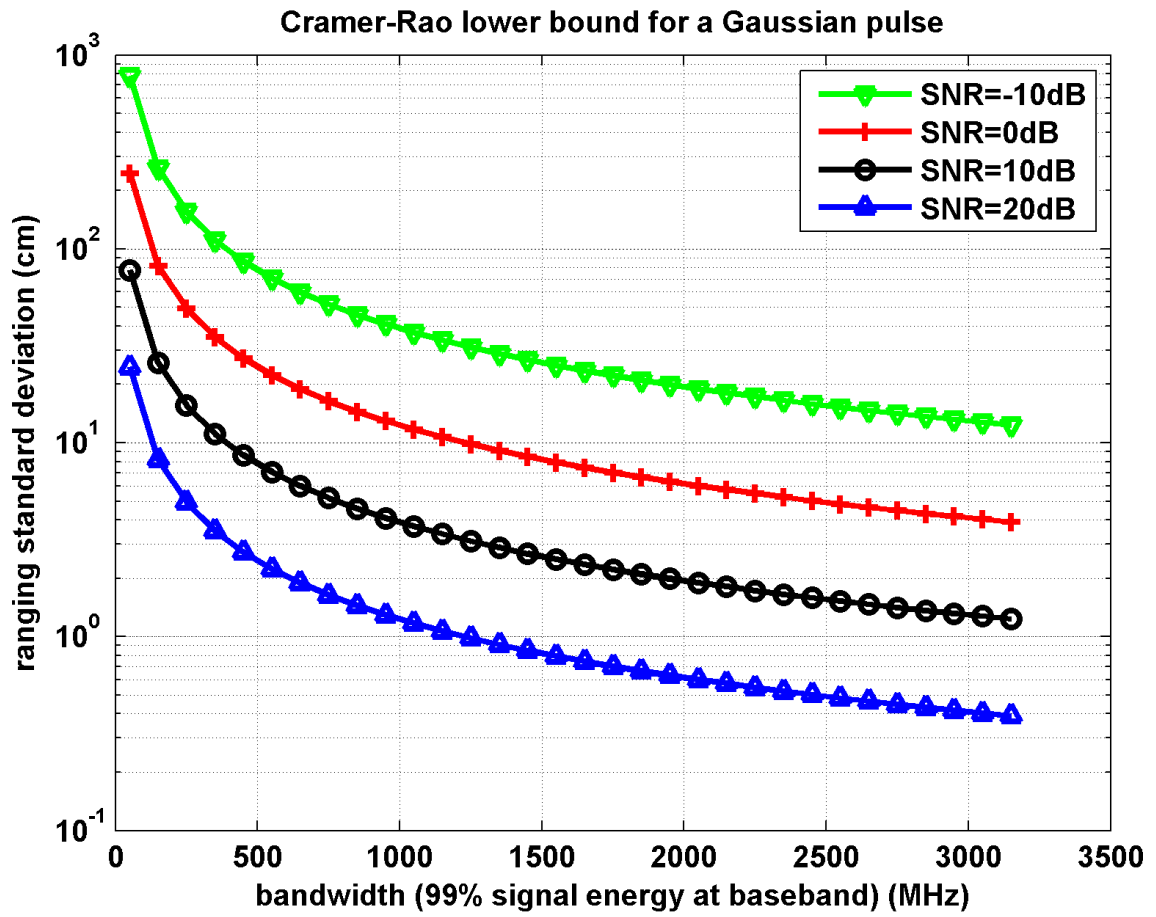


Figure 2.6: Ranging CRLB vs. B_{99} for a Gaussian pulse described by its 99% energy bandwidth

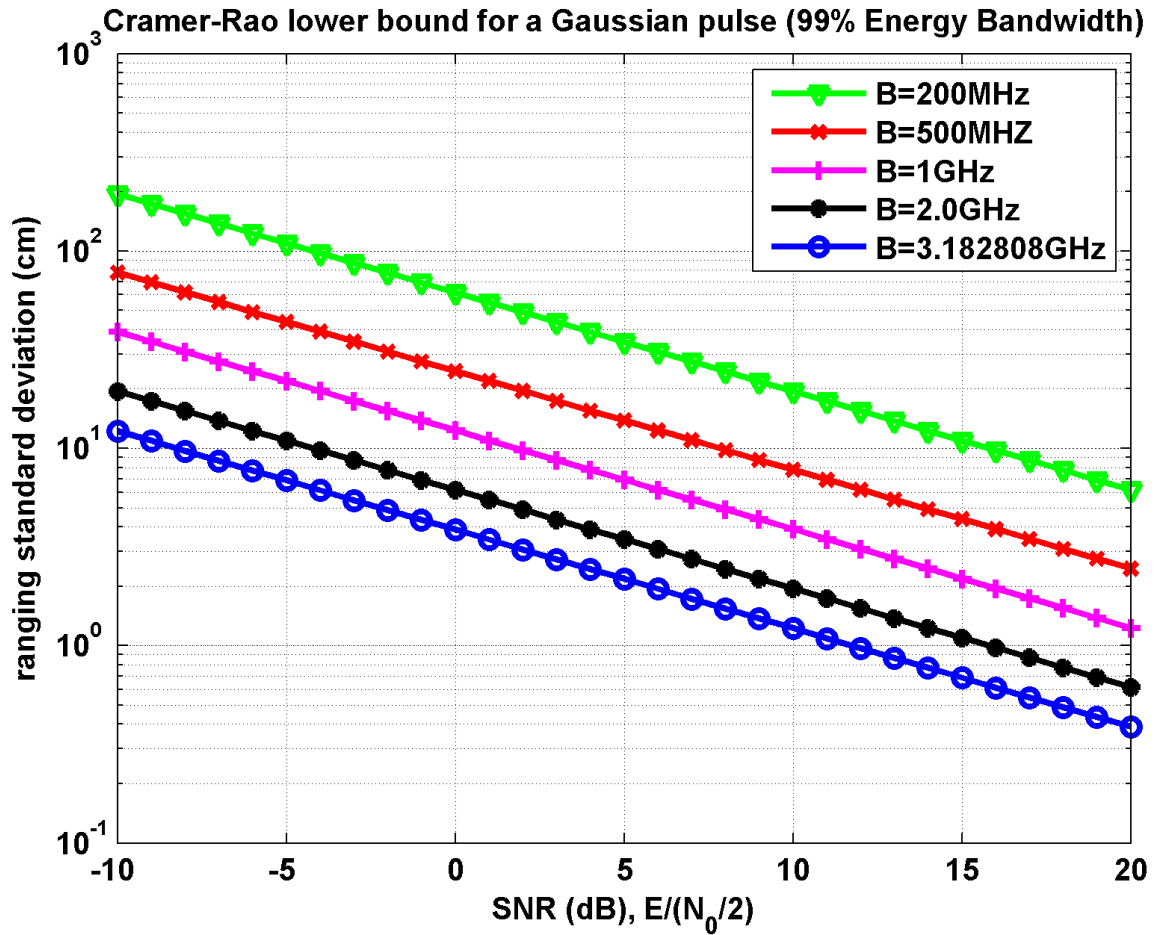


Figure 2.7: Ranging CRLB vs. SNR for a Gaussian pulse described by its 99% energy bandwidth

2.4.1 Cramer-Rao lower bound discrepancies in the literature

There are peer reviewed papers which state the CRLB in accordance with [Kay \(1993\)](#), [Poor \(1988\)](#), and [Urkowitz \(1983\)](#) (**Equation 2.2**). This is the case in [Saberinia and Tewfik \(2008\)](#). However, there is discrepancy in the literature concerning the CRLB for a time delay estimator using UWB.

The CRLB given in two peer reviewed journal papers, is optimistic by a factor of two compared to **Equation 2.2**. In [Cardinali et al. \(2006\)](#), the CRLB for a time delay estimator is given as

$$\text{var}(\hat{\tau}) \geq \frac{1}{2E/(N_0/2)\beta^2} \quad (2.18)$$

which differs by $\frac{1}{2}$. This paper does not provide a full derivation but cites [Urkowitz \(1983\)](#) even if it disagrees. In [Gezici et al. \(2005\)](#), which cites [Poor \(1988\)](#) the CRLB is given as

$$\sqrt{\text{var}(\hat{d})} \geq \frac{1}{2\sqrt{2\pi}\sqrt{\text{SNR}}\beta_f} \quad (2.19)$$

where \hat{d} is the time delay estimate and $\beta_f = \beta/(2\pi)$. This can be reformulated to

$$\text{var}(\hat{d}) \geq \frac{1}{2\text{SNR}\beta^2} \quad (2.20)$$

which also differs from [Kay \(1993\)](#), [Poor \(1988\)](#), and [Urkowitz \(1983\)](#) by $\frac{1}{2}$. Thus [Gezici et al. \(2005\)](#) disagrees with [Poor \(1988\)](#) despite the citation. Another paper, [Barton and Rao \(2001\)](#), cites [Gezici et al. \(2005\)](#) in its discussion of the CRLB hence propagating the $\frac{1}{2}$ factor.

In multiple conference papers (e.g. [Chung and Ha \(2003\)](#), [Lanzisera et al. \(2006\)](#), and [Yu \(2006\)](#)) the bandwidth term of the CRLB equation is simply described as 'bandwidth' which is incomplete and misleading. Both [Chung and Ha \(2003\)](#), [Lanzisera et al. \(2006\)](#) cite [Urkowitz \(1983\)](#) but differ from it by a factor of $\frac{1}{2}$. Another conference paper, [Sahinoglu and Gezici \(2006\)](#), which cites [Poor \(1988\)](#), also differs by a factor of $\frac{1}{2}$. The $\frac{1}{2}$ factor also appears in [Galler et al. \(2006\)](#) which cites [Gezici et al. \(2005\)](#) and in [Dardari et al. \(2006\)](#), which cites [VanTrees \(1968\)](#), and states SNR as E/N_0 rather than $E/(N_0/2)$.

This common problem of differing by a factor of $\frac{1}{2}$ is most likely due to the misinterpretation of E/N_0 as SNR rather than $E/(N_0/2)$. A non-bandlimited white noise process, $w(t)$ is a stationary random process with constant power spectral density

(PSD), $S_x(f) = N_0/2$. The autocorrelation function (ACF) of $w(t)$ is an impulse function $R_x(\tau) = \delta(\tau)N_0/2$. This is illustrated in **Figure 2.8**. The variance of the noise is given by $R_x(0)$ which is $N_0/2$. Clearly SNR is given by $E/(N_0/2)$.

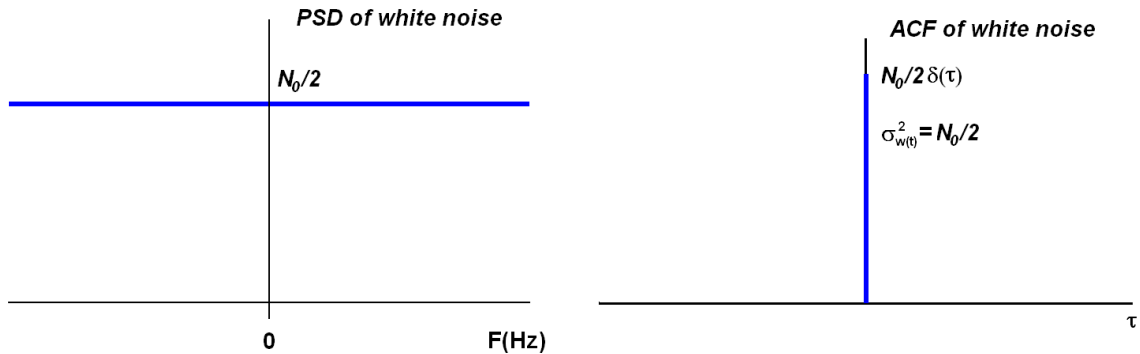


Figure 2.8: Properties of non-bandlimited white noise

The simple form of the CRLB given in **Equation 2.2** is very useful for the description of the potential performance of UWB ranging devices. Simple forms like this are often used in many papers as a foundation for further analysis. Estimates based on the equation provided in [Cardinali et al. \(2006\)](#) and [Gezici et al. \(2005\)](#) are optimistic by a factor of 2. Use of the incorrect CRLB may result in pessimistic conclusions regarding the performance of an estimator, or nonsensical comparisons between estimators that have been benchmarked to different bound values.

2.5 UWB ranging methods

Ranging observations cannot be produced directly from time-of-arrival (TOA) measurements unless both the transmitter and receiver are synchronized in time. Asynchronous ranging, ranging in the absence of clock synchronization, is a method of obtaining a range measurement wherein the requester device uses knowledge of its own clock and a

known turn-around-time in the responder to measure a two-way range as shown in **Figure 2.9**. This method, two-way time-of-flight ranging, is used by the two commercial manufacturers of UWB ranging equipment evaluated in this research.

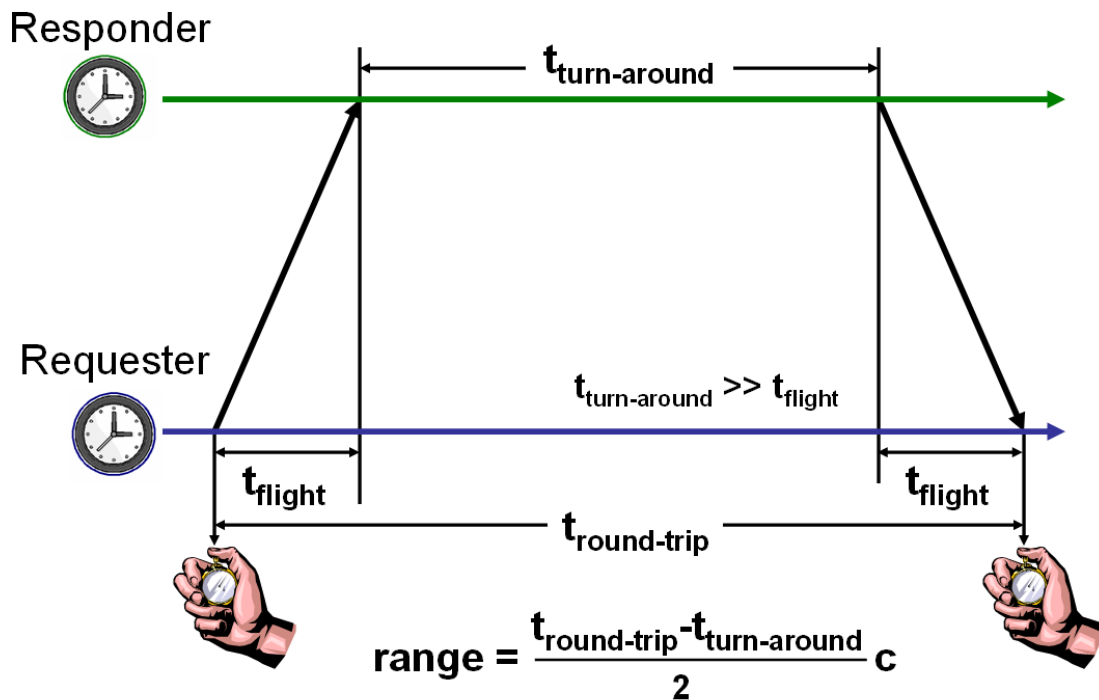


Figure 2.9: Two-way time-of-flight ranging

It is important to note that the speed of light used for UWB ranging is light speed 'in air' and is a function of the temperature, pressure, and water vapour pressure (Rüeger, 1990). The velocity correction can vary from approximately 270 ppm to nearly 400 ppm (with respect to light speed in a vacuum) at level sea pressure (1013.25 mb) and a temperature of 20°C when the partial pressure of water vapour varies from 0 to 30 mb.

2.5.1 A note about time-of-arrival and time-difference-of-arrival UWB positioning systems

Time-of-arrival (i.e. pseudorange) or time-difference-of-arrival techniques can be used to produce positions if all transmitters are synchronized (i.e. multiple synchronous transmitters and a single receiver on the unit to be located) or all receivers are synchronized (i.e. multiple synchronous receivers and a single transmitter on the unit to be located). UWB is used in commercial real-time location systems using these techniques such as the Sapphire DART product offered by Multispectral Solutions Inc. (well described by [Fontana \(2000\)](#)), the PLUS RTS system provided by Time Domain Corp., and the Series 7000 system offered by Ubisense Inc.

During the scope of this research, these products were not available with the option to produce raw time-of-arrival measurements and thus were not evaluated. The TOA or TDOA systems available are designed for indoor use and meet the indoor FCC specification (FCC 15.517). Two-way time-of-flight systems are better suited for outdoor use given the FCC restriction that outdoor systems must not be fixed infrastructure. The TOA or TDOA systems likely require fixed infrastructure for synchronization of the system.

2.6 Two-way time-of-flight measurement bias

A two-way time-of-flight measurement is made as follows. The requester, shown in **Figure 2.9**, sends a ranging request, consisting of an encoded series of pulses, to the responder. The responder is able to synchronize to the incoming pulse train and generate a ranging response, consisting of a series of encoded return pulses. One of the return pulses corresponds to a ranging pulse which has a fixed turn-around-time with

respect to one of the pulses in the requester signal. The requester detects the return pulse from the response pulse train and determines the time-of-flight by the equation:

$$\hat{t}_f = \frac{\hat{t}_{rt} - t_{ta}^d}{2} \quad (2.21)$$

where \hat{t}_f is the estimated time-of-flight, \hat{t}_{rt} is the total time estimated by the requester for the two-way round trip measurement and t_{ta}^d is the design value for the turn-around-time.

Time measurements are based on frequency standards and these standards often have a bias or frequency offset (Sullivan et al., 1990). This bias is typically expressed in parts-per-million. The direct result of frequency biases in the requester and responder is a small scale factor error in the range measurement (due only to the requester's oscillator) and a relatively much larger bias in the range measurement. This is discussed in the IEEE 802.15.4a standard (IEEE802-15.4a, 2007) and a more thorough derivation of the error equation is now provided.

Let e_A represent the error due to the requester's oscillator and e_B represent the error due to the responder's oscillator. The requester measures the round-trip time with a biased frequency standard resulting in an error in the round-trip time given by

$$t_{rt}^{requester} = (1 + e_A)(2t_f + t_{ta}^{true}) \quad (2.22)$$

where t_{ta}^{true} is the true turn-around-time. The true turn-around-time is not equal to the design value because of error due to the responder's oscillator. The responder perceives that the design value for the turn-around-time has elapsed and this results in a true turn-around-time which depends on the responder's oscillator.

$$\begin{aligned} t_{ta}^d &= t_{ta}^{responder} = (1 + e_B)(t_{ta}^{true}), \\ t_{ta}^{true} &= \frac{t_{ta}^d}{1+e_B}, \\ e_B &\ll 1 \therefore \frac{1}{1+e_B} \approx (1 - e_B), \\ t_{ta}^{true} &\approx (1 - e_B)t_{ta}^d \end{aligned} \quad (2.23)$$

Thus, given **Equations 2.21, 2.22** and **2.23**, the error in the time-of-flight estimate is given by

$$\begin{aligned}
\hat{\epsilon}_f &= \hat{t}_f - t_f \\
\hat{\epsilon}_f &= \frac{1}{2}(\hat{t}_{rt}^{requester} - t_{ta}^d) - t_f \\
\hat{\epsilon}_f &= \frac{1}{2}((1 + e_A)(2t_f + t_{ta}^{true}) - t_{ta}^d) - t_f \\
\hat{\epsilon}_f &= \frac{1}{2}((1 + e_A)(2t_f + (1 - e_B)t_{ta}^d) - t_{ta}^d) - t_f \\
\hat{\epsilon}_f &= \frac{1}{2}(2t_f + 2e_A t_f + (1 + e_A)(1 - e_B)t_{ta}^d - t_{ta}^d - 2t_f) \\
\hat{\epsilon}_f &= \frac{1}{2}(2e_A t_f + t_{ta}^d + e_A t_{ta}^d - e_B t_{ta}^d - e_A e_B t_{ta}^d - t_{ta}^d) \\
\hat{\epsilon}_f &= \frac{1}{2}(2e_A t_f + e_A t_{ta}^d - e_B t_{ta}^d - e_A e_B t_{ta}^d) \\
\hat{\epsilon}_f &= e_A t_f + \frac{1}{2}(e_A - e_B)t_{ta}^d - \frac{1}{2}(e_A e_B)t_{ta}^d
\end{aligned} \tag{2.24}$$

This can be simplified to

$$\hat{\epsilon}_f \approx e_A t_f + \frac{1}{2}(e_A - e_B)t_{ta}^d \because e_A e_B \approx 0 \tag{2.25}$$

The first part of the error equation describes a scale factor error. The second part of the error equation describes a bias term. The turn-around-time is much greater than the time-of-flight since it includes all the time necessary for the UWB radio protocol to facilitate the ranging measurement.

As an example, imagine a $0.333 \mu s$ true time-of-flight in a vacuum (approximately $99.83 m$) using a system with a design turn-around-time of $205 \mu s$ with worst case oscillator error for the requester of $20 ppm$ and for the responder of $-20 ppm$. The responder receives the ranging pulse and waits for its perceived value of the turn-around-time to elapse. Note that the $205 \mu s$ turn-around-time is used by the Multi-spectral Solutions Inc ranging radio. The true time elapsed during the turn-around-time is approximately $205.0041 \mu s$, $(205(1 - 20/1000000))$. The requester perceives the total round-trip time as $(1 + 20/1000000)(2 * 0.333 \mu s + 205.0041 \mu s)$ resulting in a perceived round-trip time of $205.6742 \mu s$. The requester estimates the time-of-flight

as $0.33505 \mu s, 0.5(205.6742 - 205)$. This is a range measurement of approximately $101.062 m$. The measurement is in error by approximately $1.231 m$. The scale factor component of this error is approximately $2 mm$. The turn-around-time bias accounts for $1.229 m$.

Clearly, the turn-around-time bias can result in a significant measurement error. The behaviour of this error will parallel the behaviour of the oscillator. Most crystal frequency standards exhibit very stable frequency generation over short intervals such as a few hundred milliseconds. For the UWB measurements considered, over distances of 0 to 200 m, this bias is very stable during a short measurement interval. Over longer intervals, frequency drift can occur due to, for example, aging, temperature variation, and mechanical stress (Sullivan et al., 1990). This may result in a slowly changing ranging bias during testing.

Oscillators ranging from 2 ppm to 80 ppm are discussed in the IEEE 802.15.4a standard (IEEE802-15.4a, 2007). The turn-around-time bias as a function of the turn-around-time is given in **Figure 2.10** for various oscillator errors.

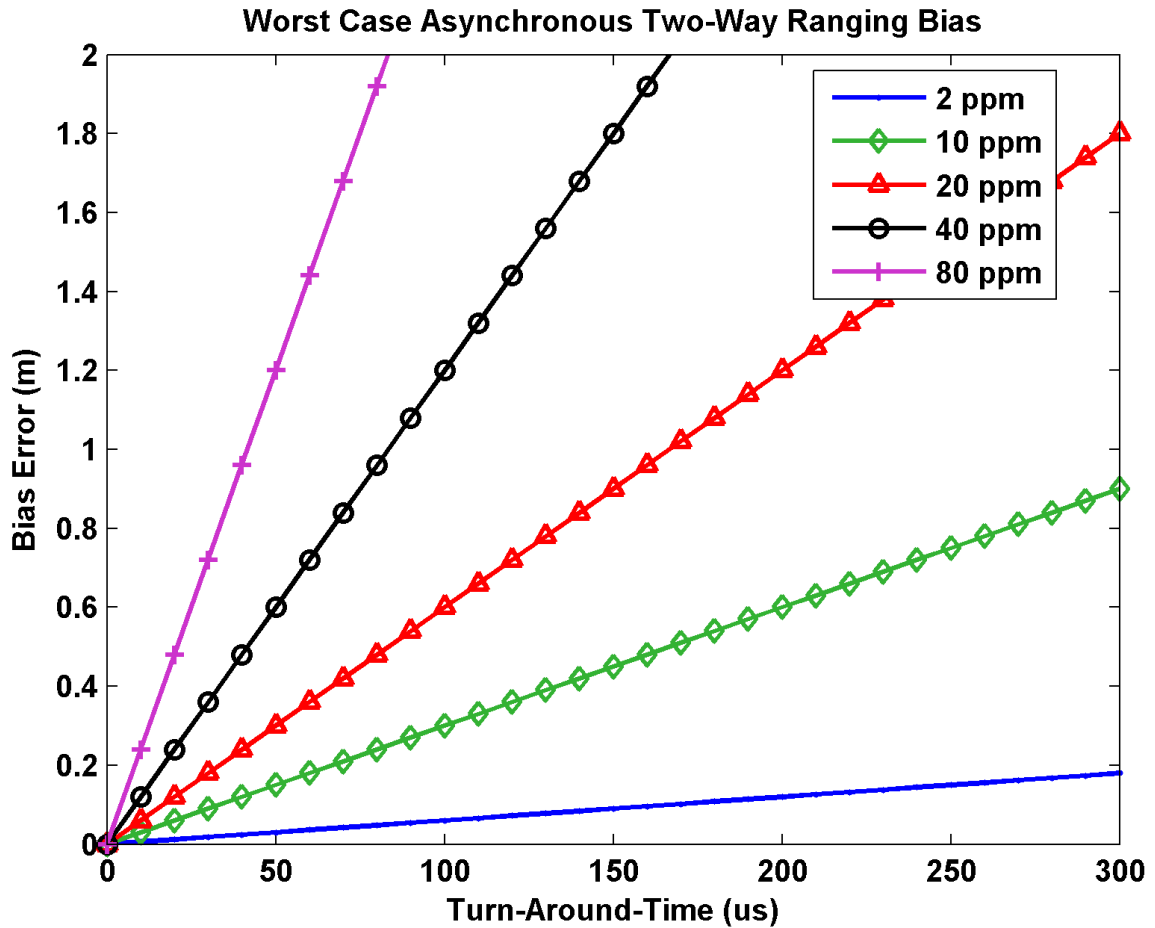


Figure 2.10: UWB range measurement turn-around-time bias for various oscillator errors

2.7 UWB pulse detection and geometric walk error

The main sources of inaccuracy in pulse-based ranging systems are noise-generated timing jitter and geometric walk timing error ([Amann et al., 2001](#)). Jitter in timing determines the precision of the range measurement. This is primarily a function of the received SNR. Pulse amplitude and shape variations create timing error in the fine time-pickoff circuit and this error is called geometric walk error.

The fine time-pickoff circuit utilizes some form of time discriminator. The task of the discriminator is to observe fine time information from the pulse signal received. In pulse-based laser ranging, commonly used discriminator designs include leading edge timing (constant amplitude), zero crossing timing (derivation), first moment timing (integration), and constant fraction timing ([Amann et al., 2001](#)).

Threshold detection receivers, also known as leading edge detection receivers, set a threshold signal value and any incoming pulse that crosses the threshold is detected and demodulated. This receiver design requires calibration to set the threshold such that the number of false alarms (false pulses), that are noise spikes which happen to cross the threshold, are within a desirable operational range. In radar, this type of receiver is often called a constant false alarm rate receiver. A tunnel diode is often used as a pulse detector in these receivers ([Reed, 2005](#)). One of the UWB receiver types evaluated in this thesis uses this type of architecture with a tunnel diode pulse detector and a threshold value based on an estimate of internal receiver noise. The threshold is generally set once, shortly after turning on the receiver ([Fontana, 1999](#)).

Threshold detection receivers suffer from a geometric walk error that is a function of the signal amplitude with respect to the threshold value selected. This is discussed in ([Amann et al., 2001](#)). **Figure 2.11** provides an intuitive graphic illustration of the effect of geometric 'walk', given a set threshold, as signal strength decreases. Signal strength decreases proportionally to the inverse square of the distance between the two UWB radios and thus a scale factor is apparent.

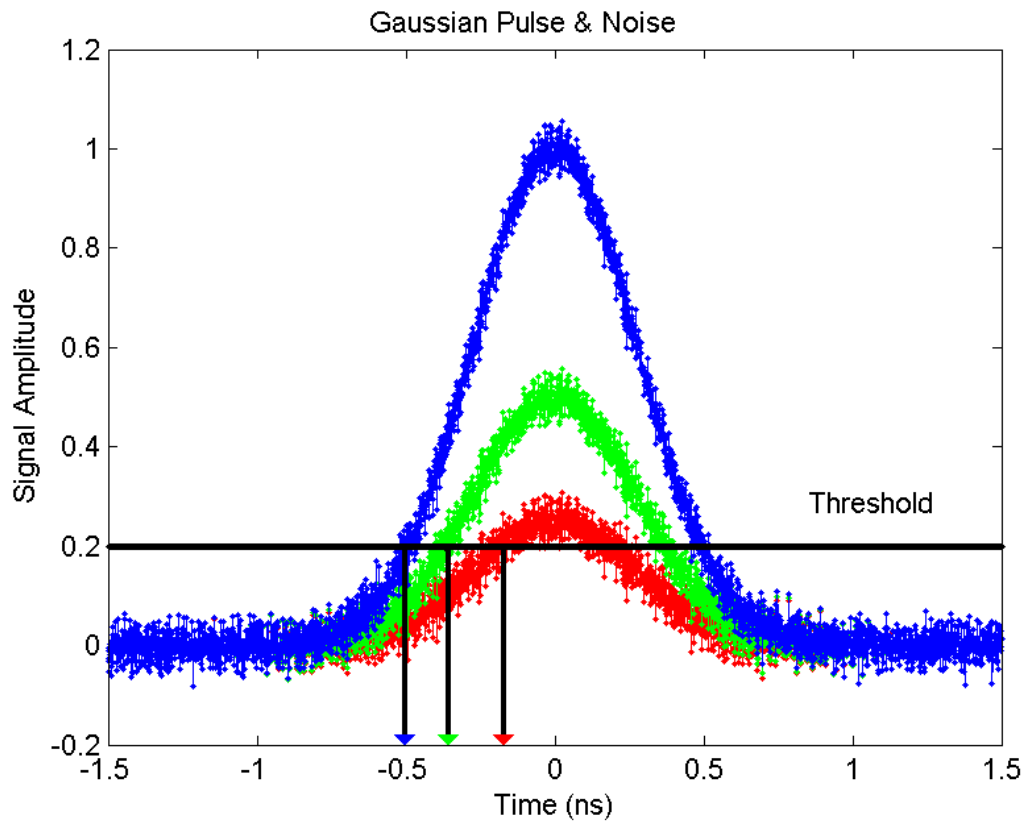


Figure 2.11: Threshold energy detection and geometric walk error

2.8 UWB ranges and multipath

Signals that can be classified as UWB facilitate differentiation between the line-of-sight response and most multipath. To demonstrate this, a GPS-like wideband signal with multipath is shown in **Figure 2.12**. An UWB signal with multipath signals of the same delay is shown in **Figure 2.13**. In the case of this wideband signal, the peak of the received signal occurs approximately 6 ns earlier than that of the line-of-sight signal resulting in a ranging error of approximately 2 m. For an UWB signal subject to

the same multipath, there is no discernable difference between the peak of the received signal and that of the line-of-sight signal.

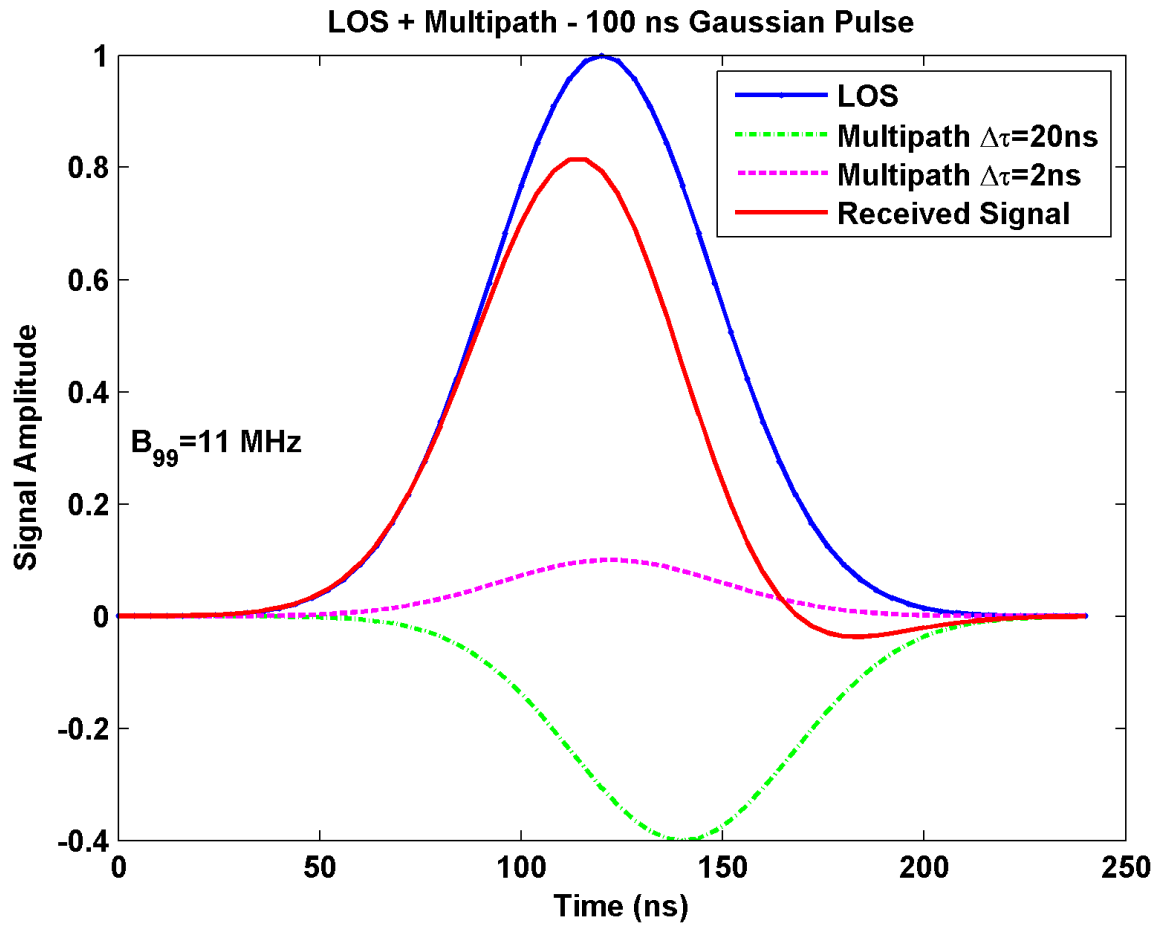


Figure 2.12: Wideband signal with multipath

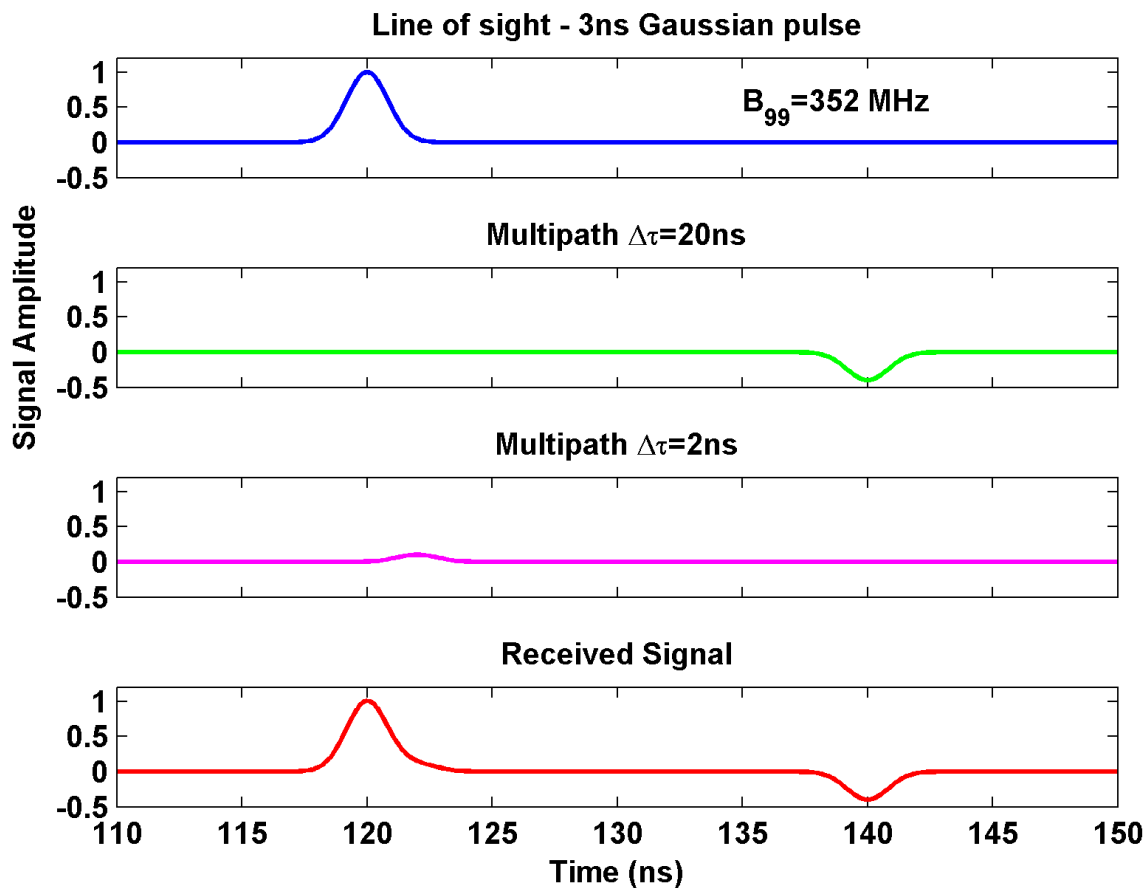


Figure 2.13: UWB signal with multipath

In general, any multipath that occurs with a delay less than the width of the line-of-sight pulse will result in distortion of the received pulse shape and the multipath cannot be distinguished. Maximum delay estimate error induced by multipath is one half of the pulse width (99% energy pulse width).

While UWB is very good at distinguishing between the line-of-sight response and multipath when the line-of-sight signal is detectable, there is a significant danger of measuring the first strongest multipath otherwise. This is demonstrated in **Figure 2.14**. This figure shows a weak line-of-sight signal, a multipath signal with 7 ns delay,

and a multipath signal with 20 ns delay. If the line-of-sight signal is too weak to be detected, the first multipath detected above the threshold will be measured and a metre level measurement blunder is likely.

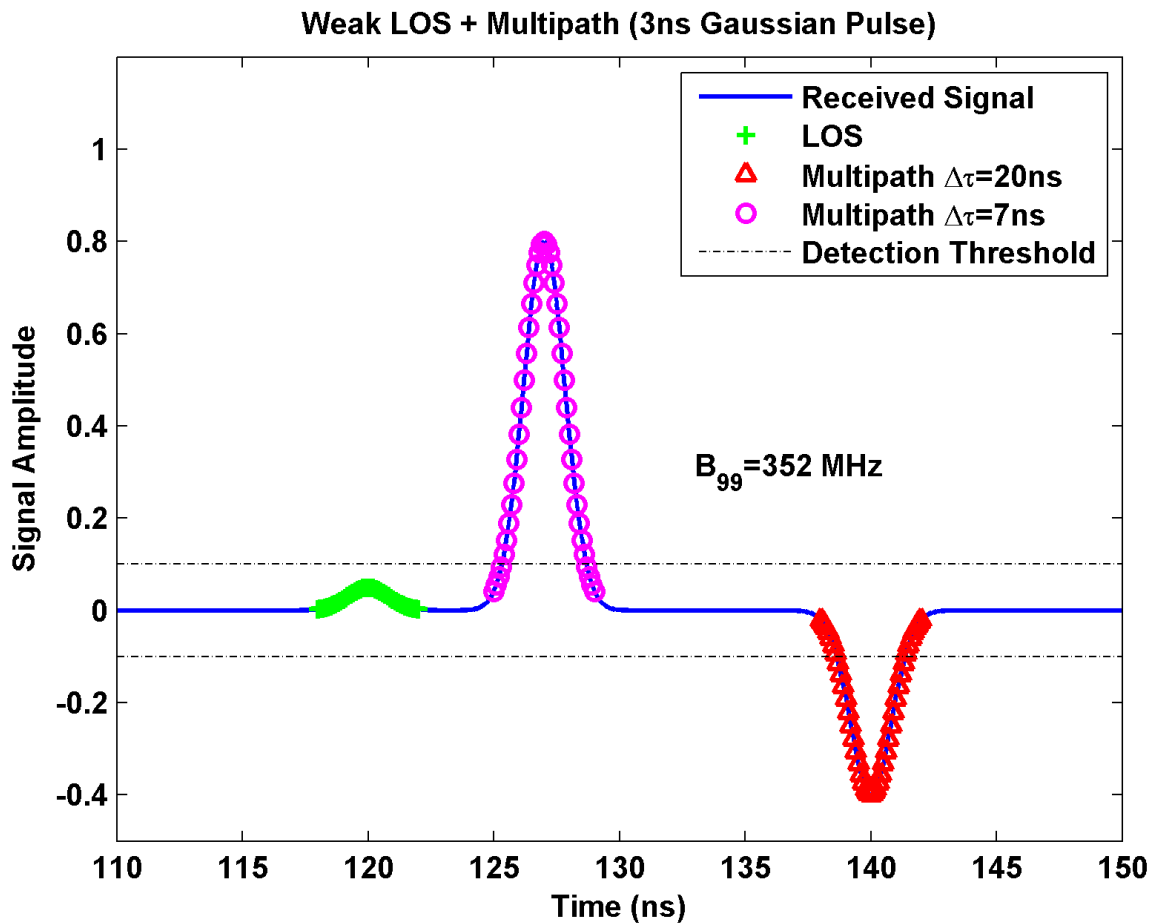


Figure 2.14: Non-line-of-sight measurement

2.9 UWB ranging radios

The University of Calgary obtained four ranging radios from each of Multispectral Solutions Inc (MSSI) and Time Domain Corp. (TDC) suitable for testing and analysis.

Both radio types utilize impulse UWB signals and two-way time-of-flight ranging.

The TDC Pulse-On 210 radios utilize a Gaussian monocycle pulse of approximately 0.23 ns duration with high pass filtering below 3 GHz to meet the FCC 15.517/15.159 specifications. This results in a signal with a center frequency of approximately 4.7 GHz and a 10 dB bandwidth of 3.2 GHz. Many aspects of the radio design are described in [Kelly et al. \(2002\)](#) and [Petroff et al. \(2003\)](#). The ranging measurement has a precision of 1-3 cm (one standard deviation) but raw measurement accuracy suffers due to turn-around-time bias and scale factor error.

The MSSSI ranging radios modulate a 6.35 GHz C-Band carrier with a Gaussian-like pulse of approximately 3 ns duration resulting in a signal with a 10 dB bandwidth of approximately 500 MHz. The radio design is described well by the US patent 5901172 ([Fontana, 1999](#)). The ranging measurement has a precision of better than 15 cm (one standard deviation); however, the radios quantize their range measurement output to half of one nanosecond (approximately 15 cm). Raw measurement accuracy also suffers due to turn-around-time bias and scale factor error. The radios are shown in **Figure 2.15**.



Figure 2.15: Multispectral Solutions Inc. (left, from [MSSI \(2007\)](#)) and Time Domain Corp. UWB ranging radios (right, from [TDC \(2008\)](#))

2.10 UWB ranging and low pulse repetition frequency UWB

For UWB ranging applications, the pulse repetition rate can be very low compared to UWB communications systems. With lower pulse repetition frequency, pulses can have more energy and hence provide sufficient operational ranging performance. However, if time dithering of the pulse within a pulse interval is not used, low PRF signals generate strong spectral lines and risk exceeding the peak FCC emission limits (FCC, 2005). The peak emission limit and low PRF systems are described further by FCC (2005) in the following excerpt:

As previously stated by the Commission, low PRF UWB systems can have a higher potential for causing interference than high PRF UWB systems. Operation with a low PRF results in closer frequency spacing of the spectral emission lines. This, in turn, increases the probability that emissions will appear within the bandwidth of a victim receiver. Further, as the PRF decreases, the peak to average ratio increases. For UWB systems employing a low PRF, the peak emission limit becomes the defining standard and the average emission level decreases below the limit specified in the regulations. Accordingly, UWB devices employing a low PRF are constrained in their output levels by the limit on peak emission levels, not by the limit on average emission levels. Conversely, high PRF systems would be limited by the average limit established under the rules and not by the peak limit. Further, if the pulse repetition frequency of the UWB signal is much greater than the bandwidth of a receiver, the emission may appear to be random noise or a continuous wave (CW) signal, the effect of which is proportional to the average power in the UWB signal within the receivers bandwidth. However, if the PRF is much less than the receivers bandwidth, the UWB

signal may appear to the receiver as impulsive noise and the effect is proportional to the peak power of the UWB signal unless some type of signal processing is incorporated in the victim receiver.

Time dithering of the location of an individual pulse within a pulse interval can be used to mitigate the peak spectral lines that are problematic for low PRF systems. For example, if pulses occur once every 1000 ns, the pulse position within the 1000 ns can be dithered using a pseudorandom sequence. This is discussed in [Kissick \(2001\)](#). If the pulse position is not dithered, the power spectrum will show discrete spectral lines at harmonics of the pulse repetition rate. Dithering makes the spectrum look much more noise like. The importance of using the dithering technique is demonstrated in Figure 2.16 which shows the power spectrum for a pulse train with 20 Gaussian pulses with and without time dithering of the pulse train. Modulating the pulse trains using on/off keying, pulse position modulation, and binary phase shift keying (antipodal modulation), and gating may also result in reduction of these spectral peaks. Gating refers to the turning on and off the UWB pulse trains such that gated bursts of data are transmitted.

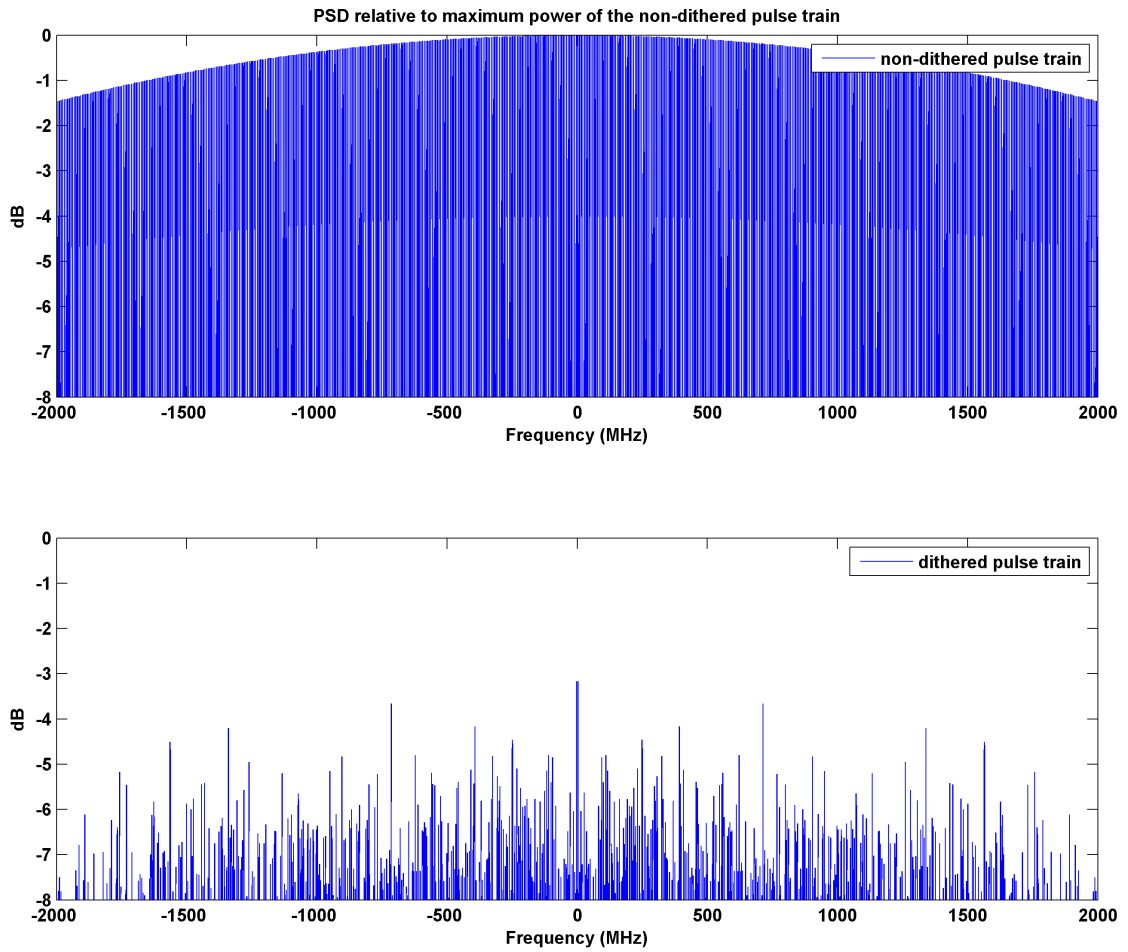


Figure 2.16: The effect of time dithering with 1 GHz, 20 dB bandwidth, Gaussian pulses. 20 pulses of 0.29 ns duration occur within 1000 ns pulse intervals. The sign of the pulse is alternated in the pulse train for both cases to ensure a DC component of zero. The fourier transform, $G(\omega)$, of each pulse is given by Equation 2.5 and the PSD is given by $|G(\omega)|^2$. The use of time dithering clearly reduces peak spectral lines.

2.11 Testing and results

Before integration with GPS, the radios were evaluated using line-of-sight testing to assess their ranging performance and ranging error behaviour. This was done using static line-of-sight testing and comparison with electronic distance measurement and with kinematic line-of-sight testing and comparison with GPS RTK-derived ranges.

2.11.1 Static line-of-sight testing

Line-of-sight testing was performed with the ranging radios at Shouldice Park, Calgary, Alberta, Canada. The testing location was a soccer field with a very level surface. There were few, if any, sources of signal reflection other than the operators, the equipment and the ground. **Figure 2.17** provides a photo of the test site and equipment. Horizontal distances were measured using a total station (i.e. using electronic distance measurement) and points were established up to 100 m apart. Multiple pairs of radios of the set of 4 radios per radio type were used. In addition, multiple independent tests at different times were performed with some of the radio pairs to assess run-to-run behaviour.

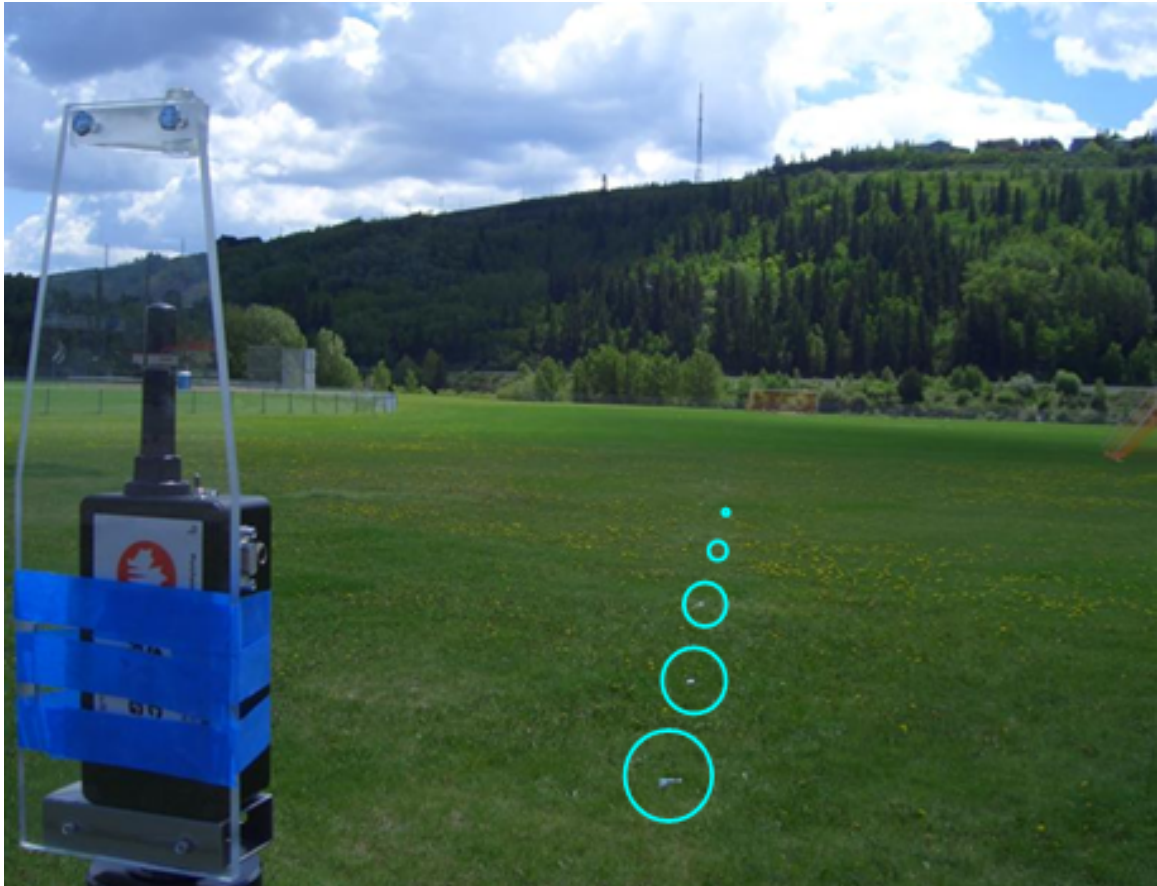


Figure 2.17: Line-of-sight testing

Measurement points were occupied for a few minutes and the number of samples collected typically ranged from 250 to 1000 range measurement samples. The number of outliers detected was typically less than 1%. Measurement outliers were removed from the data by recursively removing any measurements that were three standard deviations away from the mean value for each range measured.

The TDC radios were able to consistently obtain ranges up to 70 m. Most of the MSSSI ranging pairs were able to obtain ranges up to 100 m. The measured ranges were averaged after outlier removal and the average error at each distance was determined.

The mean range error as a function of distance for both radio types is shown in **Figure 2.18**. Line fits for each ranging radio pair are also shown in the figure. The estimated bias based on the line fit for the TDC radios is less than a decimetre and less than half a metre for the MSSSI radios. There is significant scale factor error for both radio types. The slope of the line fit (shown in parts per million (ppm) in the figure) ranges from 2300 ppm to 3900 ppm for the TDC radios and 3900 ppm to 4700 ppm for the MSSSI radios. The cause of the common trend behaviour of the MSSSI radios is unknown. One theory is that the common effect is due to the quantization of the range measurement output. Another postulate is that the behaviour is due to the nature of the geometric walk in the leading edge pulse detection.

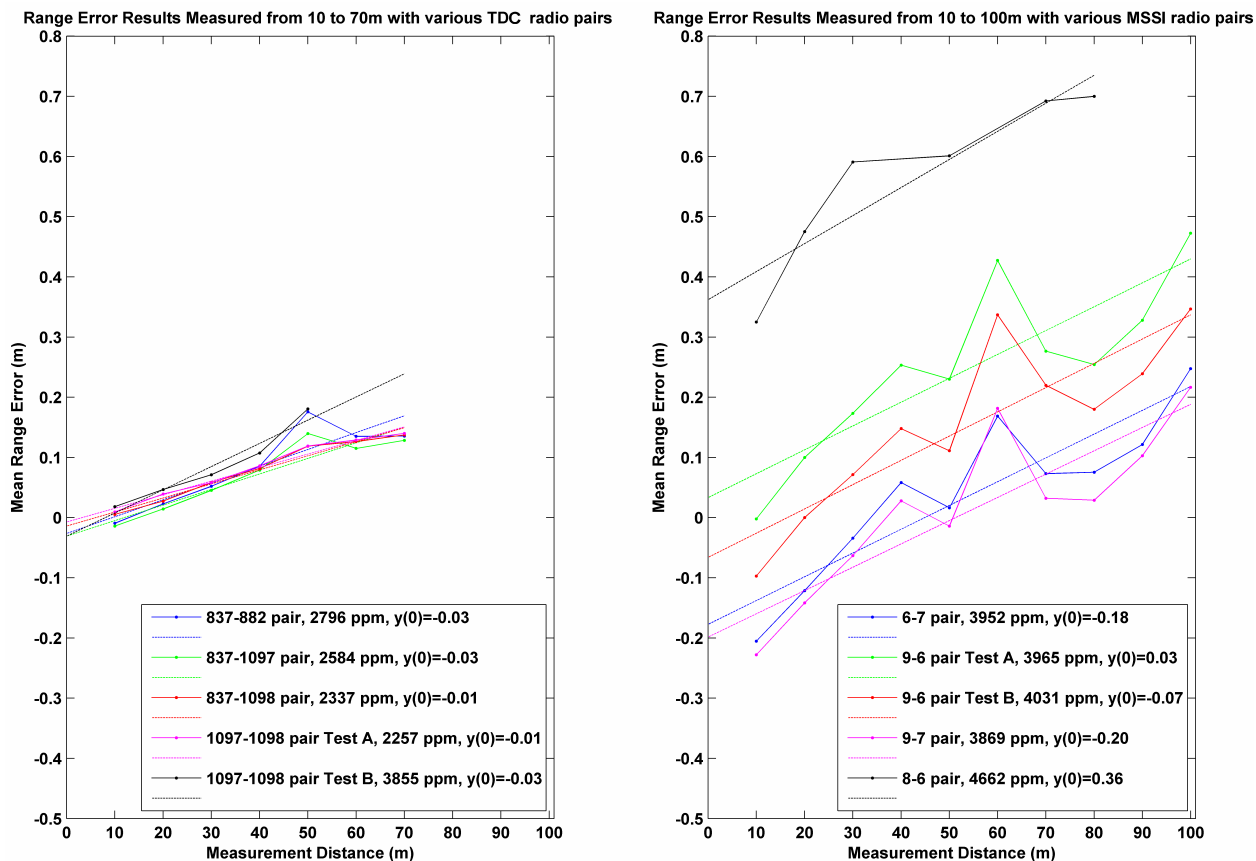


Figure 2.18: Line-of-sight testing ranging errors results, TDC (left), MSSSI, (right)

2.11.2 Dynamic line-of-sight testing

The ranging performance for both the MSSSI and the TDC radios was assessed in a dynamic line-of-sight test by comparison with ranges derived from GPS real-time kinematic (RTK) positioning. RTK positioning with GPS utilizes double-differenced carrier phase observations and requires solving the associated unknown integer valued carrier phase ambiguities. This is well described in GPS texts such as [Misra and Enge](#)

(2004). The horizontal accuracy of RTK is 2 cm to 3 cm given good GPS conditions.

Two of the UWB radios were mounted on tripods over surveyed positions. These were used to obtain ranges to a pole mounted UWB radio. The pole mounted UWB radio was mounted beneath the phase center of the GPS antenna using coaxial mounts. A MSSSI radio mounted on a tripod and a TDC radio mounted on a survey pole are shown in **Figure 2.19**.

The test consisted of walking a 60 m loop multiple times. The ranges between the UWB radios were generally line-of-sight except for occasional obstruction by the operators. The test trajectory is shown in **Figure 2.20**. A test with each radio type was performed with two tripod mounted radios and one pole mounted radio. This results in two ranging measurements per epoch. The results of the test compare the RTK derived range to the UWB range measurement.

The difference between the UWB ranges and RTK derived ranges are shown in **Figure 2.21** and **Figure 2.22** for the TDC radios and the MSSSI radios respectively. The data is can be modeled with a linear fit for both radios. However, some higher order behaviour is present but it is a good first step to remove the 1st order trend from the data. The TDC trend line corresponds well with the static line-of-sight testing results. However, the scale factor errors for the MSSSI radios are more than double the values observed in the static case. The MSSSI radios set their threshold for pulse detection only when the units are turned on and this threshold will be based on internal noise. A change in the threshold value changes the scale factor error. It is possible that the external temperature plays a role in the threshold value selected. The static testing was performed at 5°C to 10°C whereas the dynamic test was performed at -10°C to -5°C.



Figure 2.19: Dynamic ranging UWB and GPS using coaxial mounts

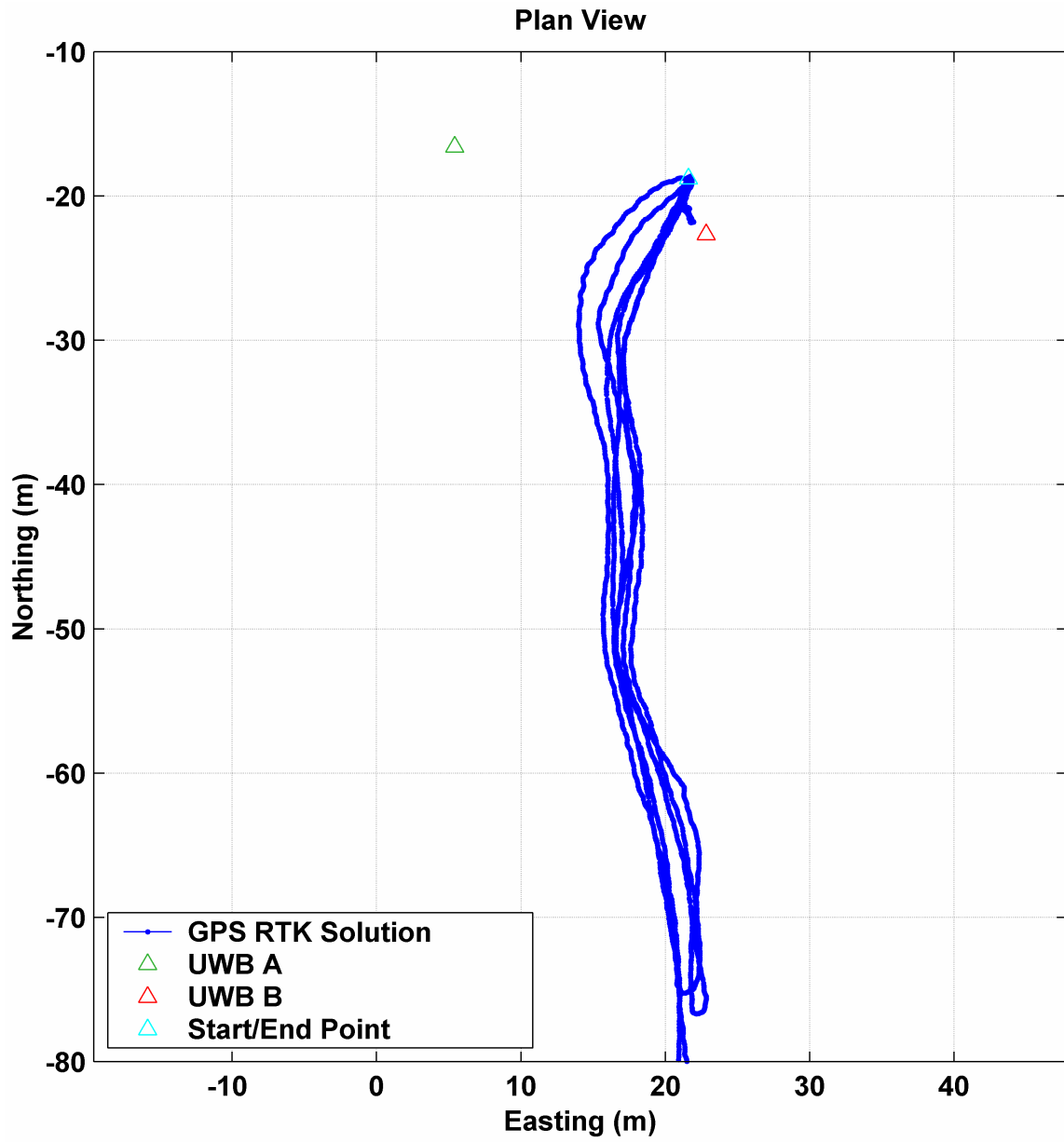


Figure 2.20: Dynamic test trajectory for the TDC radios

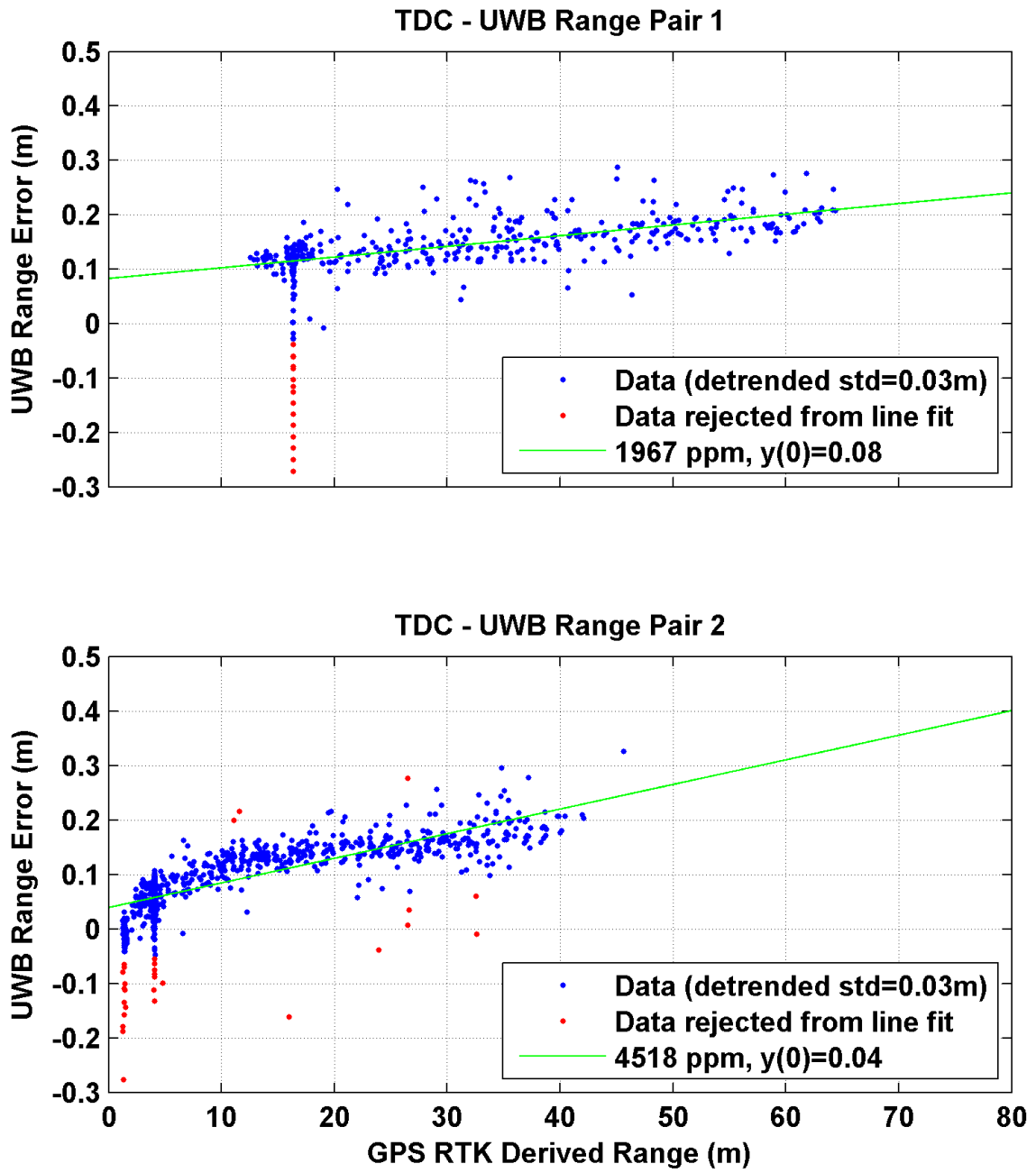


Figure 2.21: Dynamic line-of-sight test: TDC range errors

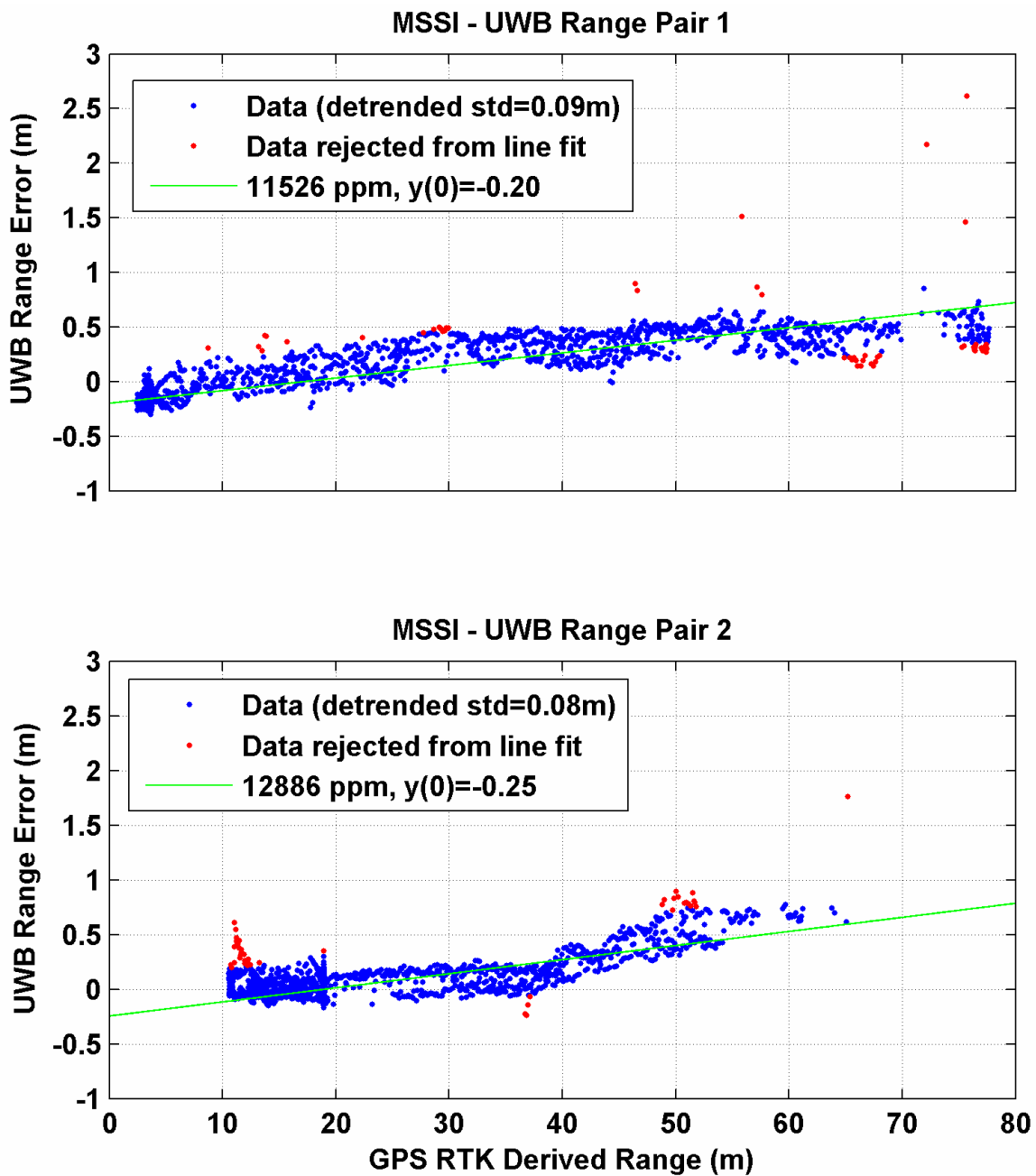


Figure 2.22: Dynamic line-of-sight test: MSSSI range errors

It is useful to examine the distributions of the range errors after detrending the data.

This allows an assessment of the potential to model the UWB range error using a bias and a scale factor for each range pair. The goal is to have normally distributed range errors after correcting the UWB ranges for the first order trend. If the remaining errors are normally distributed, then the bias and scale factor error model can be considered sufficient for the corrected observations to be used in an estimation method expecting unbiased observations. The histograms of the corrected range errors (i.e. detrended range errors, outliers excluded) for the TDC results are shown in **Figure 2.23** and in **Figure 2.24** for range pair 1 and 2 respectively. The histograms of the corrected range errors (i.e. detrended range errors) for the MSSSI results are shown in **Figure 2.25** and in **Figure 2.26** for range pair 1 and 2 respectively. The distributions are approximately normally distributed with zero mean and standard deviations of 3 cm for the TDC range errors and 9 cm for the MSSSI range errors. Based on these figures, modeling the UWB range errors with a bias and scale factor in a real-time filter should benefit the solution. This does not mean that systematic effects are going to be removed completely. For example, the trend for range pair two in **Figure 2.22** would appear to be better modeled using a second order polynomial. It is reasonable to use a linear model for the UWB range errors as a first step in improving the use of UWB ranges in an estimation filter and these results do not show any reason to pursue a more advanced error model.

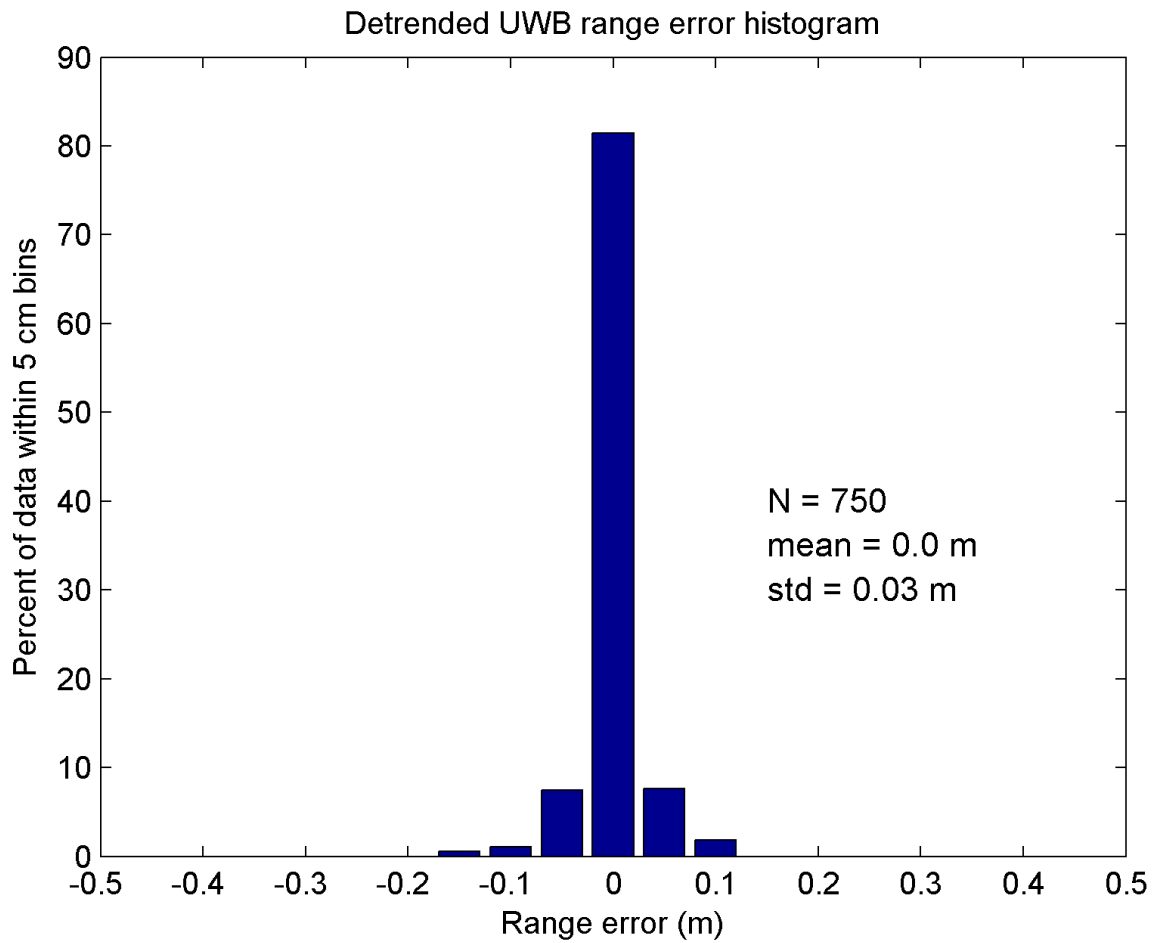


Figure 2.23: Dynamic line-of-sight test: TDC range error distribution for range pair 1 (5 cm bins)

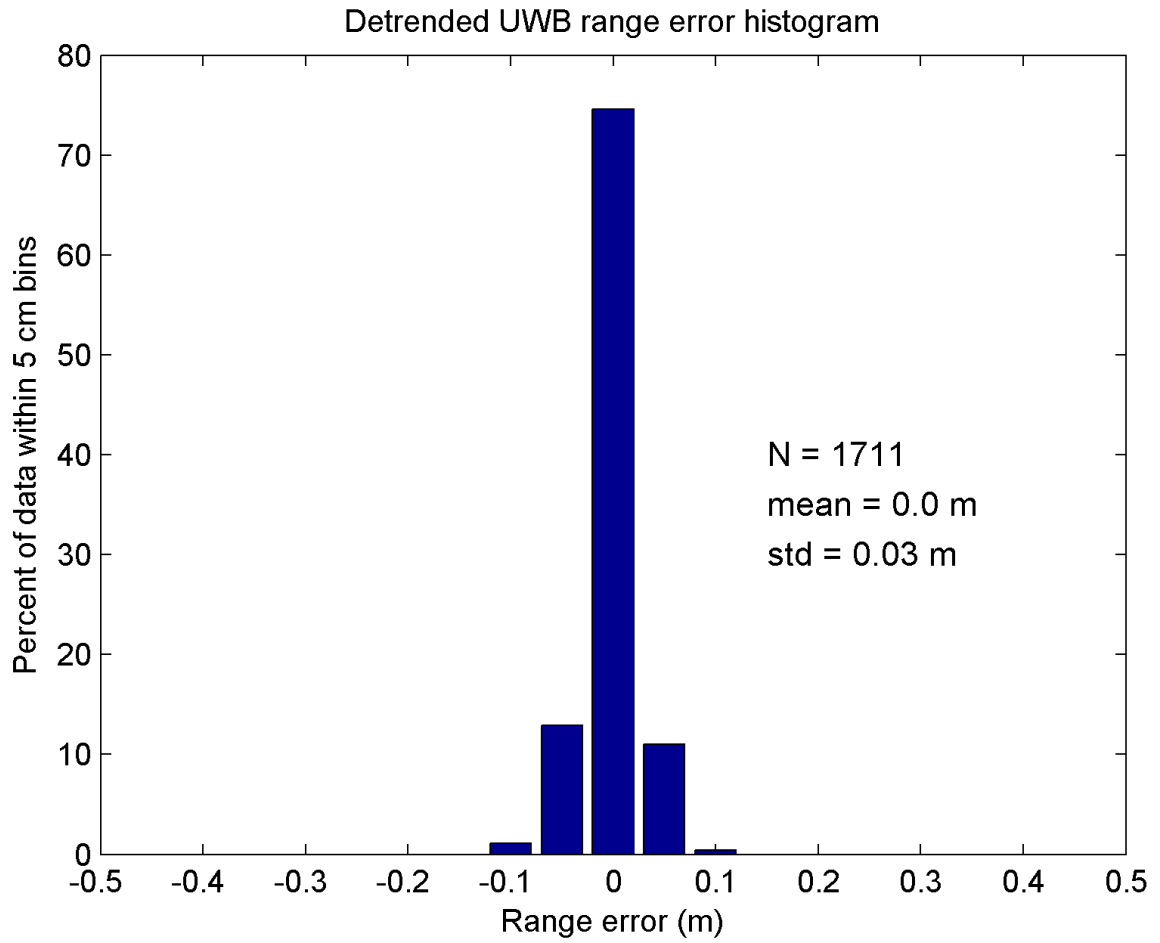


Figure 2.24: Dynamic line-of-sight test: TDC range error distribution for range pair 2 (5 cm bins)

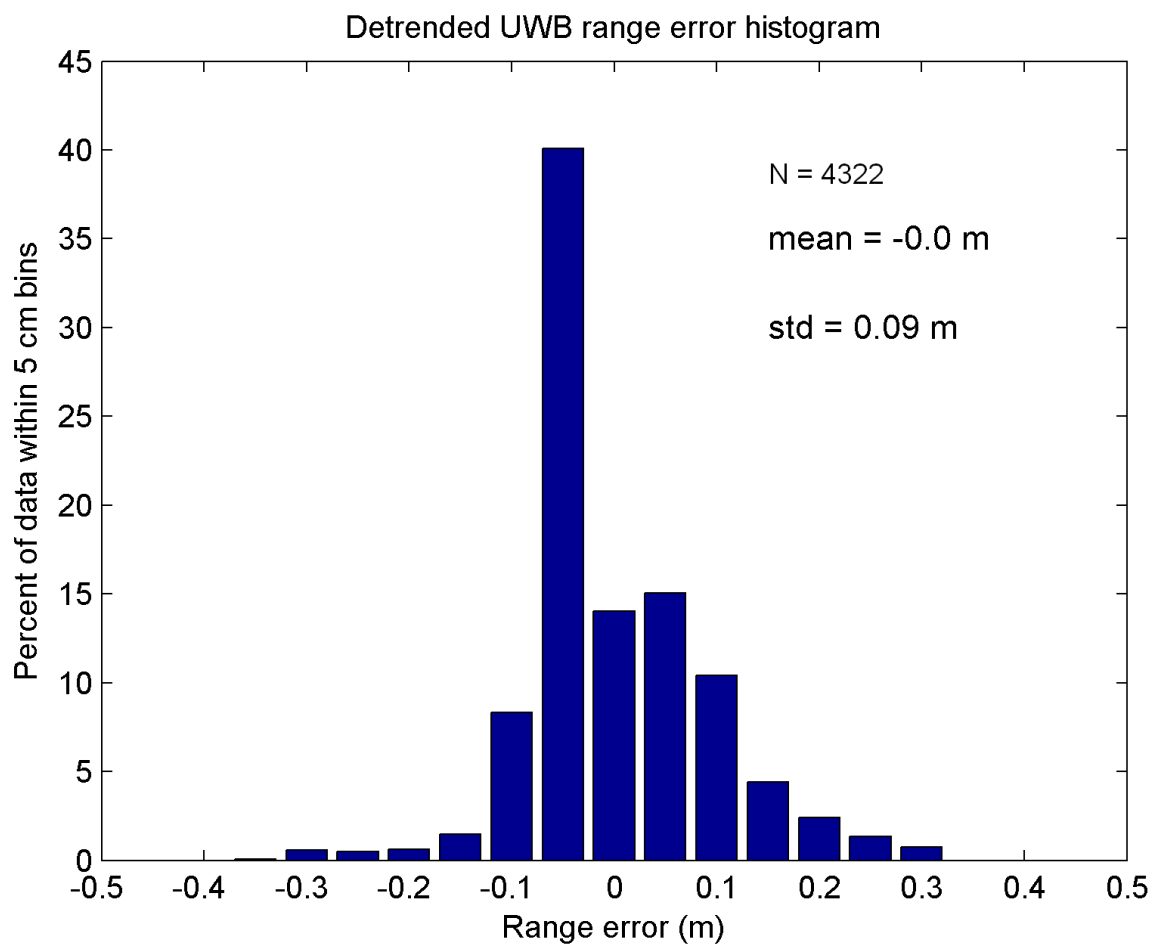


Figure 2.25: Dynamic line-of-sight test: MSSSI range error distribution for range pair 1 (5 cm bins)

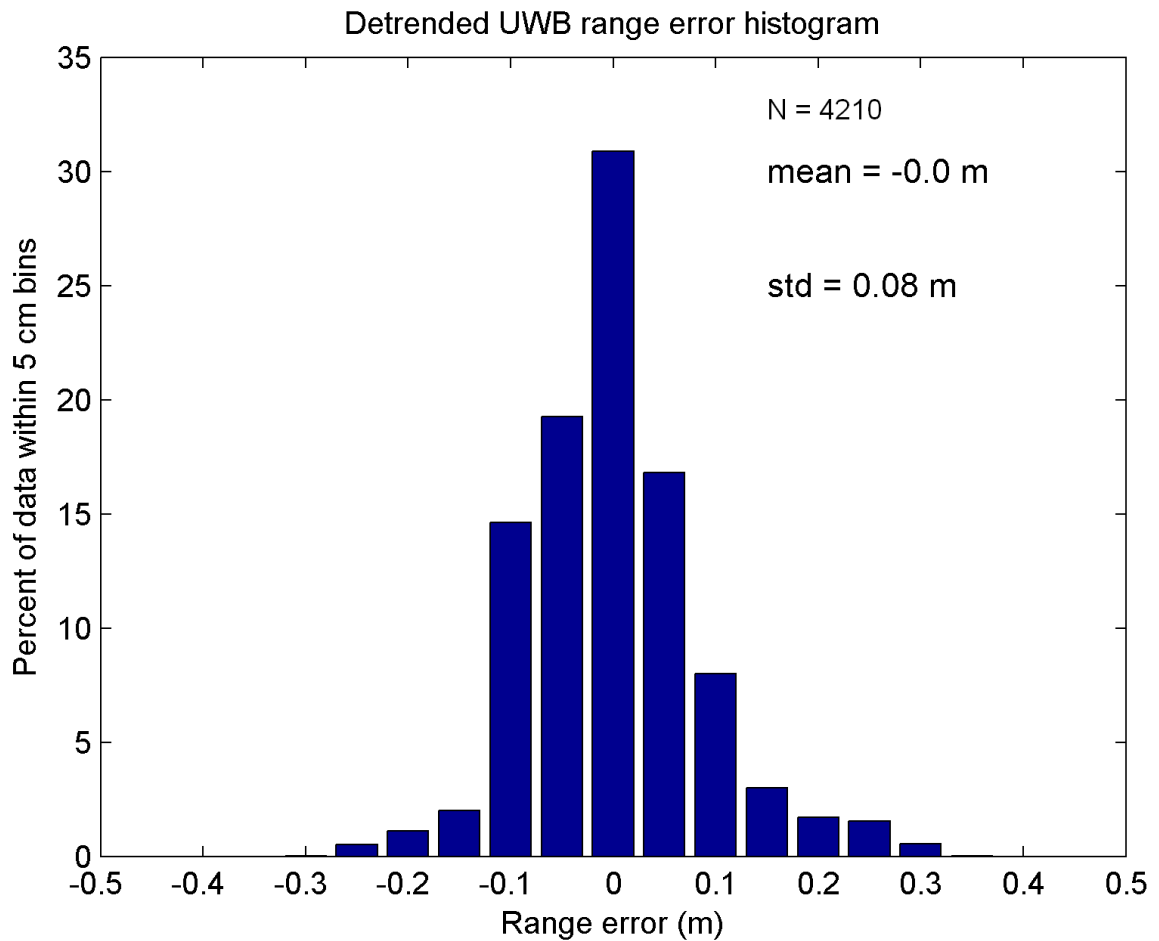


Figure 2.26: Dynamic line-of-sight test: MSSI range error distribution for range pair 2 (5 cm bins)

2.11.3 Multipath and obstruction testing

Both types of UWB radios were used to measure ranges obtained close to a large glass and metal building, shown in **Figure 2.27**, the ICT building at the University of Calgary. The external surface of this building acts as a likely source of strong multipath signals. Three tripod mounted UWB radios were set up over surveyed positions. A pole mounted UWB radio at a pre-surveyed test point observed ranges to each of the

three UWB reference stations. Differencing the UWB ranges with those derived from the surveyed coordinates of the occupied points, results in UWB range errors. A plan view of the test point and the three UWB reference stations is also shown in **Figure 2.27**. The range measurements between the surveyed test point and UWB reference station 3 were obstructed by a large metal sign (shown in the lower center of the photo in **Figure 2.27**).

The TDC range errors are shown in **Figure 2.28** for the ranges measured between the test point and each of the three UWB reference stations. The range pair for reference station 1 consistently measures a range delayed by approximately 12.6 m. The range pair for reference station 2 has ranging errors up to 20 m and appears to measure multiple discrete reflected signals and noise. The range pair for reference station 3, which is obstructed by the metal sign, managed only three range measurements during the 75 second test with errors of 2 m to 7 m.

The MSSSI range errors are shown for the three ranging pairs in **Figure 2.29**. The first two ranging pairs are likely observing line-of-sight signals and the measurements include both a bias and a scale factor error. The line-of-sight signal for the third ranging pair is obstructed by the metal sign and multiple range errors are observed. These errors correspond well with the distance from the test point to the building.

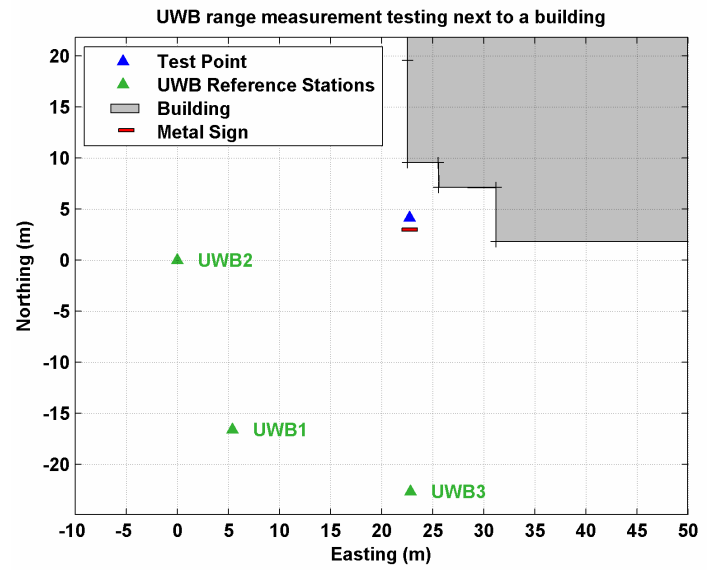
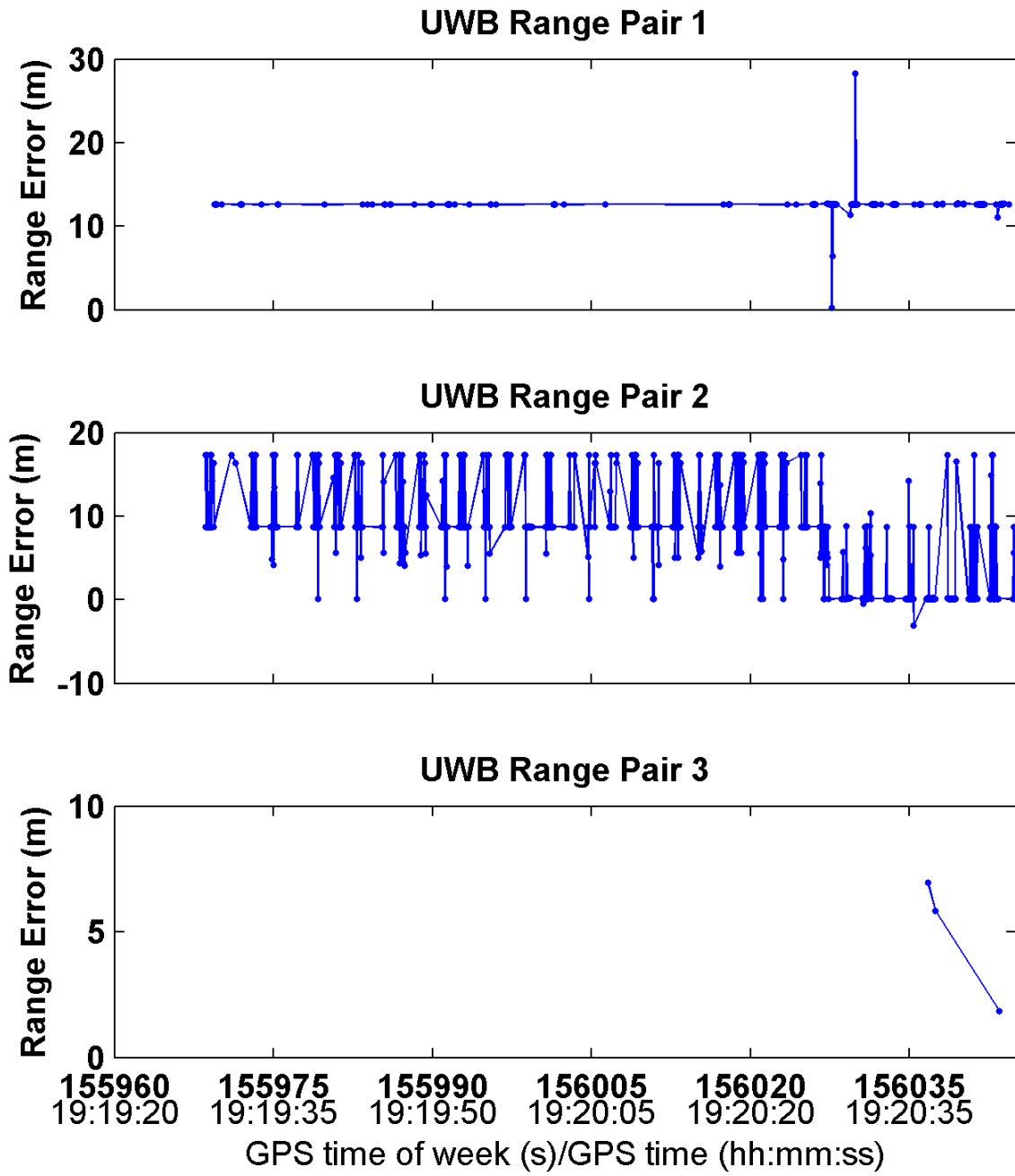


Figure 2.27: Plan view (right) of UWB range testing next to a building (left)



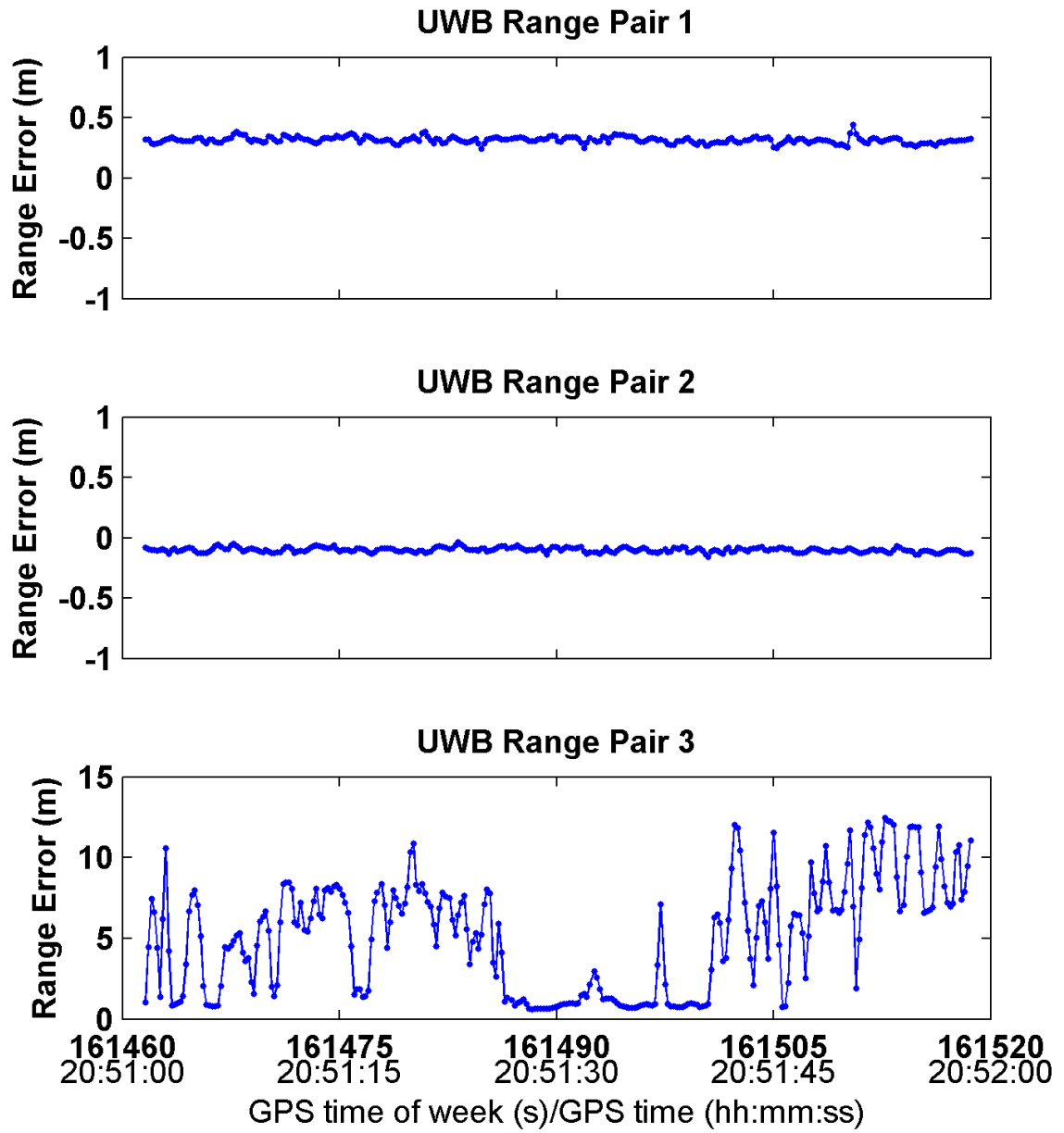


Figure 2.29: MSSSI Range errors in a multipath environment

2.12 Time correlation of UWB measurements

The UWB range errors can be reasonably well modeled using a 1st order line-fit. However, based on the results of the static and dynamic line-of-sight testing performed, there would still be some systematic error left after removing the 1st order trend. This results in UWB measurement ‘noise’ that is correlated in time. This is shown in **Figure 2.30** for a period of static data collected during the dynamic line-of-sight test for MSS1 range pair 1. The compensated range measurements are still biased and hence are correlated in time. During motion, the residual systematic error decorrelates due to scale factor error.

Coloured measurement noise violates a key assumption in standard Kalman filtering. If measurement noise is correlated in time, the estimated precision of the solution will be optimistic. A common, but not optimal, method of dealing with this is to raise the measurement noise variance used in the filter so that the solution is no longer optimistic. In this case, the remaining UWB measurement bias will affect the solution but at least the estimated solution precision is appropriate.

In the case of the compensated UWB measurements, since the residual systematic error is small (typically less than 10 cm RMS), the measurement noise model used by the estimation process will be adjusted (i.e. increased measurement noise) to compensate for the time correlated measurement noise.

This method of dealing with time correlated measurement noise is used with GPS pseudorange measurements as well. The pseudorange measurements are typically affected by low frequency multipath errors in low dynamic applications. This results in time correlated pseudorange measurement noise. The standard Kalman filter must be modified to optimally compensate for coloured measurement noise such as discussed in [Bryson and Johansen \(1965\)](#), [Bryson and Henrikson \(1968\)](#), and more recently in

Petovello et al. (2005). However, increasing the measurement noise level in the measurement model, while not optimal, works well to ensure that the estimated solution precision is not optimistic.

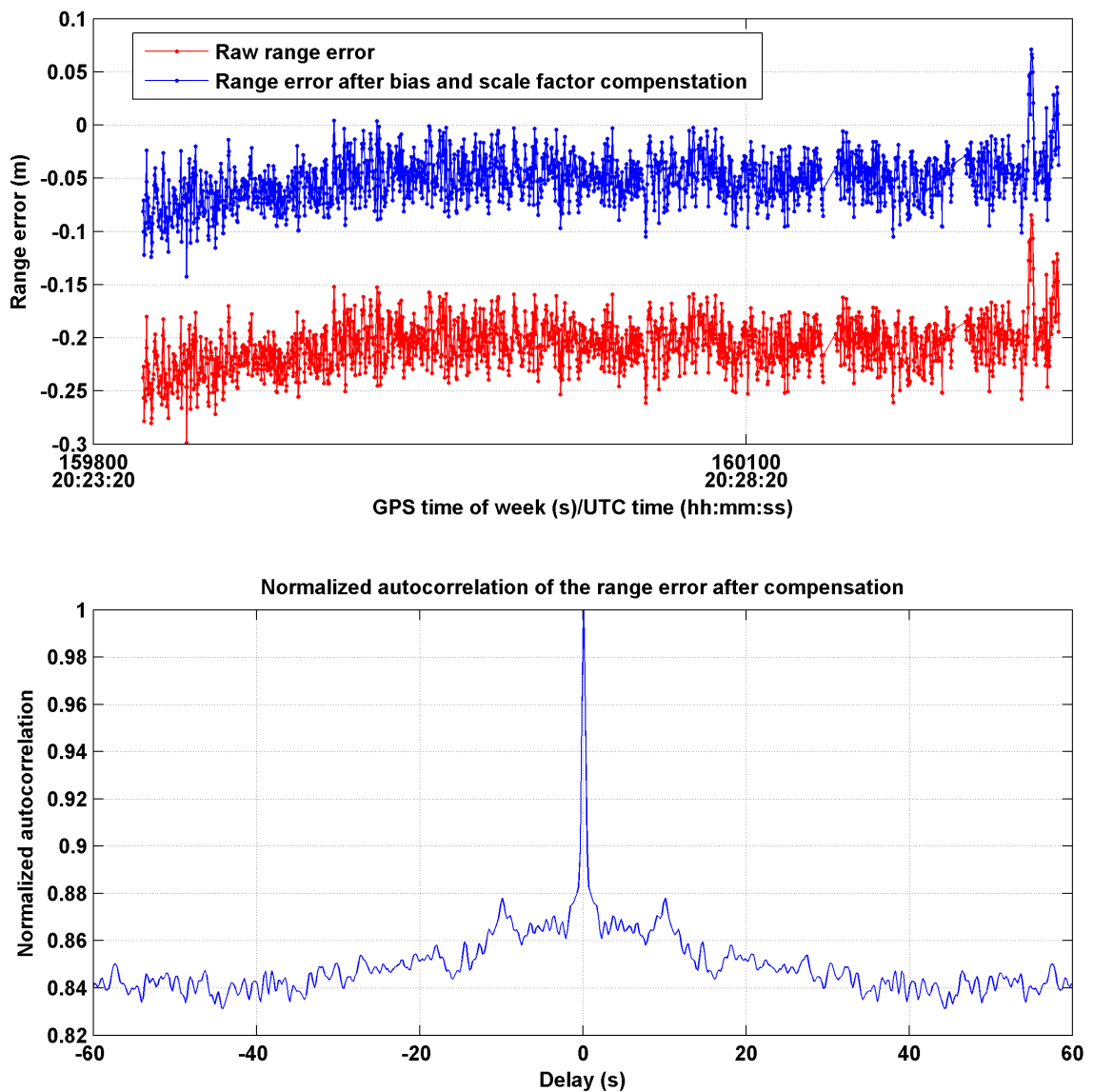


Figure 2.30: Time correlation of compensated UWB measurements. This figure shows a static portion of data collected for MSSSI range pair 1 during the dynamic line-of-sight test.

2.13 Summary

This chapter described UWB ranging technology from both a theoretical and practical perspective. With an understanding UWB ranging technology and the estimated accuracy and error effects associated with two-way time-of-flight ranging, a method to integrate UWB measurements with GPS measurements in tightly-coupled estimation can now be developed. This is the focus of the next chapter.

Chapter 3

Tightly-coupled GPS/UWB

This chapter introduces the apparatus used to combine GPS and UWB systems and describes the estimation and reliability method used to obtain filtered position solutions. The apparatus allows UWB measurements to be related to the phase center of the GPS antenna and it is the position of this phase center that is computed by the estimator. A sequential discrete-time extended Kalman filter is the estimator selected for the tight-integration of GPS and UWB. Single-difference (between receiver) GPS measurements and UWB range measurements are used to update the filter. It includes states for the position, a single-difference GPS receiver clock state, bias and scale factor states for each UWB range pair, and states for the single-difference GPS carrier-phase ambiguities. The filter uses innovation testing to try to identify GPS and UWB measurement blunders before they can impact the solution. A single-difference float solution is employed rather than a double-difference float solution. The reasons and advantages for this choice are discussed. This chapter concludes with an explanation of the integer ambiguity resolution method used to provide a RTK solution.

3.1 Apparatus

Before discussion of the filter design, it is necessary to describe the apparatus used to integrate the GPS and UWB equipment. To integrate the UWB transceivers with the GPS antenna, co-axial GPS/UWB antenna mounts were built (one type for each UWB radio type used). The mount designs are such that the phase centers of the GPS

receiver and the UWB antenna are vertically co-linear. An UWB range measurement is made between a reference UWB transceiver and an UWB transceiver on the survey system (e.g. pole mounted). It is desirable to use the UWB range measurement to estimate the phase center of the GPS antenna without having to deal with any lever arm offsets between the UWB antenna and the GPS antenna (on both the reference and survey systems). The following example, describes how this is possible.

Consider a single GPS baseline survey, with one GPS antenna mounted over a known location and the other GPS antenna mounted on a survey pole. By mounting the reference UWB transceiver and the survey system UWB transceiver a fixed distance below the GPS antennas, the UWB range measurement is equivalent to the GPS baseline. **Figure 3.1** makes this obvious.

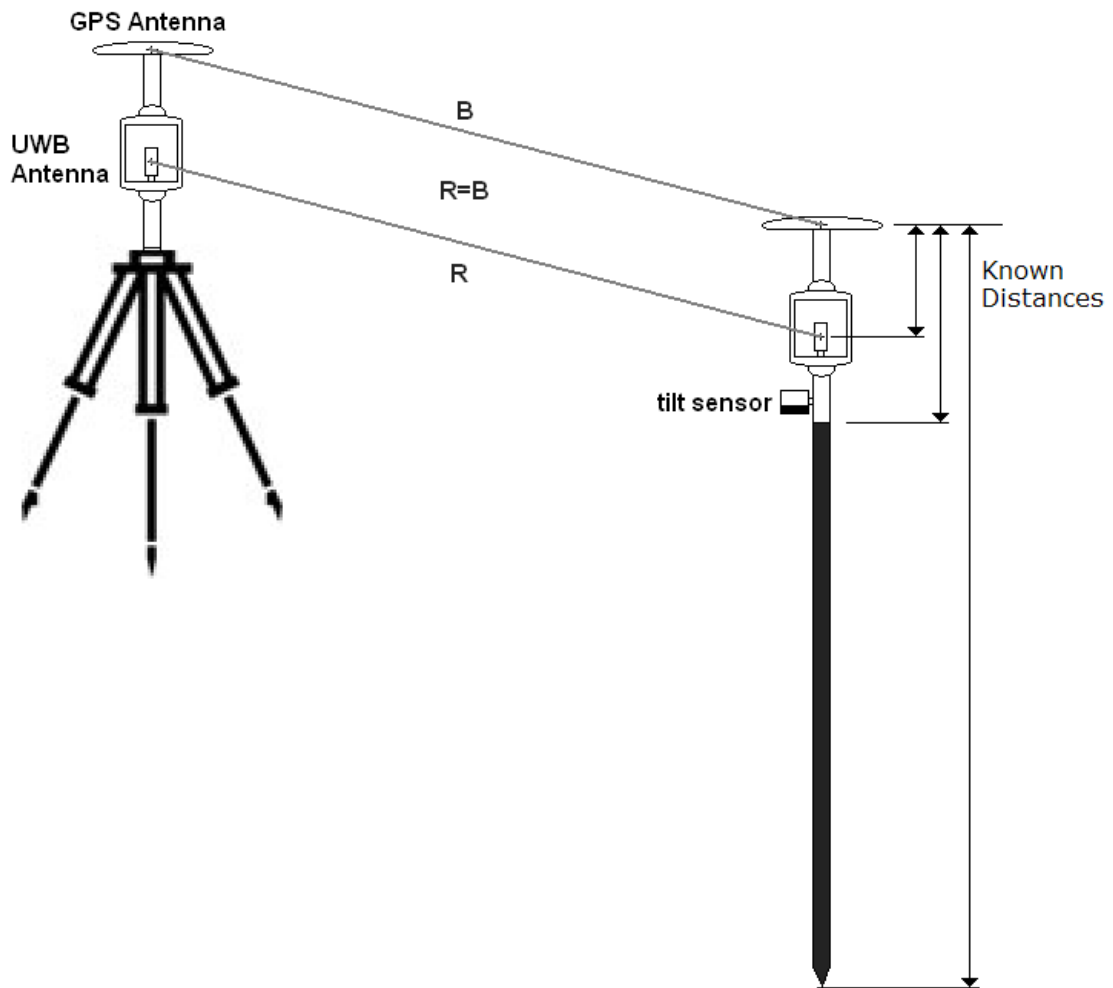


Figure 3.1: The GPS/UWB survey apparatus

As long as the UWB reference station is surveyed with GPS using the co-axial mounts and the GPS/UWB survey system uses the same mount, the UWB range measurements can be translated so that the apparent UWB reference station antenna position is the same as the surveyed GPS antenna phase center on the reference station. The UWB range measurements on the survey system can then be translated to estimate the GPS

antenna phase center on the survey system.

Thus, the position of the phase center of the GPS antenna is estimated by the estimation filter. This method is dependant on the phase center of the UWB antenna and the phase center of the GPS antenna being aligned co-linearly to the local gravity vector. If the system is not level, a lever arm is introduced. A tilt sensor with an accuracy of about 3° (obtained via the RMS tilt value for 20 minutes of static data when measuring a tilt of 0°) is used to monitor this lever arm. The tilt sensor employed is model EZ-TILT-1000-008 made by Advanced Orientation Systems Inc. The estimated standard deviation of the UWB measurement, as used by an estimation filter, can be increased based on the tilt angle to de-weight observations. The approximate lever arm between the GPS antenna and the UWB antenna is 10 to 12 cm for both UWB radio types. At a tilt of 20° , this adds approximately 4 cm of measurement bias. Monitoring the tilt is important when the user is moving. The bias varies with the pole motion while moving and is typically correlated for about 1-5 seconds. The effect induced by the level arm effect is relatively small and thus, while not optimal, it is reasonable to just increase the measurement noise for the UWB range measurements. When the user is stationary over a point, a bubble level attached to the pole is used to manually level the system.

3.1.1 Measurement synchronization

Measurement synchronization between different systems is a concern for kinematic data collection. In kinematic testing, the UWB ranges collected are time tagged using the time of the data collection computer. This computer is synchronized to GPS time using software written to capture the pulse-per-second output of the GPS receiver. The software developed was released at the open source website SourceForge.Net (<http://sourceforge.net/projects/gpsppsync>). The accuracy of the ability to set the

computer time using this method is approximately 20 ms. When in motion for land surveying using the pole mounted system, the maximum velocity is maximum walking speed or about 6 km/hr. This implies a maximum time synchronization error of about 4 cm. This is accounted for in the filter by using a slightly larger measurement variance.

3.2 Selection of the optimal estimator

The task of integrating GPS and UWB measurements to compute a tightly-coupled solution requires the selection of an appropriate estimation method. Gelb (1974) describes the selection of the optimal estimator as the method that processes measurements to determine a minimum error estimate of the unknown parameters of a system by utilizing: knowledge of the system and measurement dynamics, assumed statistics of system noises and measurement noises, and initial condition information. The optimal estimator is determined subjectively based on the selection of the minimum error criterion. In systems with more measurements than unknown parameters (i.e. non-unique solutions), the optimal estimator is most often selected based on the minimum sum of square errors ($\sum_{i=1}^n (\hat{x} - x_i)^2 = \min$). The minimum sum of square errors is more prevalent than the minimum sum of absolute errors ($\sum_{i=1}^n |\hat{x} - x_i| = \min$) because of the difficulties in implementing the latter method. Consistency (the estimate converges to the true value), unbiasedness ($E[\hat{\mathbf{x}}] = \mathbf{x}$), minimum variance ($E[(\hat{\mathbf{x}} - E[\hat{\mathbf{x}}])^T(\hat{\mathbf{x}} - E[\hat{\mathbf{x}}])] = \min$), and computational efficiency (especially for real-time systems such as RTK surveying) are the most important properties of a good estimator. The best estimator should also use all available information to produce the solution. Thus, if there is knowledge of the system dynamics, a recursive minimum variance estimation method is better than a epoch-by-epoch least squares estimation method. In addition, if knowledge of the maxima and minima values for some unknown parameters are available, this information should be used to constrain the estimator

behaviour.

The task of designing the estimator begins with modelling the relationship between the observations and the unknown parameters (functional model) and then requires modelling of the stochastic behaviour of the states and the observations (stochastic model). The stochastic model generally describes measurement noises as random processes with normal distributions. Gross measurement outliers (i.e. blunders) are not described by the stochastic model. Statistical testing is often used to identify and exclude measurement blunders in the estimation process. If the estimation method cannot practically deal with measurement blunders, a robust estimator, one that aims to be insensitive to deviations in the stochastic model, is necessary. In the context of this research, a robust estimator is not warranted as it is assumed most measurement blunders can be dealt with practically using statistical testing.

The discrete-time extended Kalman filter is the often preferred choice of estimator in many navigation applications. A Kalman filter is an efficient (unbiased and minimum variance) recursive filter that estimates the error states of a dynamic system provided the system is linear and the measurement noise is Gaussian ([Brown and Hwang, 1997](#)). As many systems have a nonlinear functional model relating the measurements to the estimated parameters and only require discrete updates, the discrete-time extended Kalman filter is often utilized. A linearized functional model is derived by a first order Taylor series expansion about a linearization point. In other words, the filter estimates error states about the linearized trajectory. It produces optimal estimates provided the assumptions of the underlying stochastic model are correct. An error in the design of the dynamic stochastic model is readily discovered with appropriate field testing during development. However, the measurement stochastic model is frequently incorrect when measurement blunders occur and, as a result, measurement fault detection using statistical testing is a very important part of the estimation process.

The implementation of the discrete-time extended Kalman filter is made more computationally efficient by adding statistically independent measurements sequentially (Petovello et al., 2003) (i.e. updating the filter one measurement at a time). The sequential method is algebraically equivalent to the batch (all processed at once) method as discussed on page 250 of Brown and Hwang (1997) provided the measurements are uncorrelated. The sequential update strategy, according to Brodie (2001), also improves the ability to detect pseudorange measurement faults provided the measurements are added with increasing likelihood of a measurement fault.

3.3 Summary of the sequential discrete-time extended Kalman filter

Table 3.3 provides a summary of the equations for the sequential discrete-time extended Kalman filter. This is a useful reference in the ensuing sections as the filter is described.

Table 3.1: Discrete-time sequential extended Kalman filter equations

Functional Model <i>(linearized form)</i>	$z_i = \mathbf{h}_i \hat{\boldsymbol{\delta}}_x$	$\hat{\boldsymbol{\delta}}_x$: error state vector \mathbf{h}_i : i^{th} design vector
Measurement Model	$v_i = z_i + \epsilon_i = l_i - \hat{l}_i$	v_i : i^{th} measurement innovation $l_i - \hat{l}_i$: measured - estimated value ϵ_i : measurement noise
Dynamics Model <i>from epoch k-1 to k</i>	$\hat{\mathbf{x}}_k = \Phi_{k-1,k} \hat{\mathbf{x}}_{k-1} + \mathbf{w}_{k-1}$	$\hat{\mathbf{x}}_k$: vector of unknown parameters $\Phi_{k-1,k}$: state transition matrix \mathbf{w}_{k-1} : white noise sequence
Stochastic Model <i>normally distributed</i> <i>independent measurements</i> <i>not correlated in time</i> <i>driven by white noise</i> <i>not correlated in time</i> <i>independence assumption</i>	$\epsilon_i \sim N(0, \sigma_i^2)$ $E[\epsilon_i \epsilon_j] = 0$ $E[\epsilon_k \epsilon_{k-1}] = 0$ $\mathbf{w}_k \sim N(\mathbf{0}, \mathbf{Q}_k)$ $E[\mathbf{w}_k \mathbf{w}_{k-1}^T] = \mathbf{0}$ $E[\mathbf{w}_k \epsilon_i] = \mathbf{0} \forall k, i$	allows sequential processing \mathbf{Q}_k : Process noise matrix
Initial Conditions	$E[\mathbf{x}_0] = \hat{\mathbf{x}}_0$ $E[\hat{\mathbf{x}}_0 \hat{\mathbf{x}}_0^T] = \mathbf{P}_0$	
Covariance Prediction	$\mathbf{P}_k^- = \Phi_{k-1} \mathbf{P}_{k-1}^+ \Phi_{k-1}^T + \mathbf{Q}_{k-1}$	$-$ superscript means pre-update $+$ superscript means post-update
Update <i>updates are applied</i>	$\hat{\boldsymbol{\delta}}_{\mathbf{x}_{k_i}}^- = \mathbf{0}$ $\hat{\boldsymbol{\delta}}_{\mathbf{x}_{k_i}}^+ = \mathbf{k}_i v_i$ $\hat{\mathbf{x}}_{k_i}^+ = \hat{\mathbf{x}}_{k_i}^- + \hat{\boldsymbol{\delta}}_{\mathbf{x}_{k_i}}^+$	\mathbf{k}_i : Kalman gain vector
Kalman Gain	$\mathbf{k}_i = \mathbf{P}_{k_i}^- \mathbf{h}_i^T \frac{1}{\sigma_{v_i}^2}$ $\sigma_{v_i}^2 = \mathbf{h}_i \mathbf{P}_{k_i}^- \mathbf{h}_i^T + \sigma_i^2$	scalar inversion $\sigma_{v_i}^2$: variance of the innovation computationally efficient!
Covariance Update	$\mathbf{P}_{k_i}^+ = [\mathbf{I} - \mathbf{k}_i \mathbf{h}_i] \mathbf{P}_{k_i}^-$	performed sequentially

bold lowercase indicates a **vector**, **BOLD** uppercase indicates a **matrix**, scalar otherwise.

i indicates the i^{th} measurement for a given epoch, k .

3.4 Description of the filter

This section focuses on the development of a discrete-time sequential extended Kalman filter using tightly-coupled GPS and UWB measurements. The standard GPS RTK extended Kalman filter is augmented with additional error states to accommodate for UWB ranging errors. The maximum and minimum values for the UWB bias and scale factor parameters used to model the UWB ranging errors are known to a certain extent. This allows the use of inequality constraints, applied as pseudo-measurement updates as described by [Richards \(1995\)](#), to utilize this information to the benefit of the filter.

A two-stage estimation approach is used. First, using sequential updates, the filter utilizes single-difference GPS pseudorange measurements, UWB range measurements, and single-difference GPS carrier-phase measurements. The unknown position, single-difference GPS receiver clock offset, UWB bias and scale factor estimates (for each UWB range pair) and single-difference GPS ambiguities are estimated. The single-difference float solution ambiguity estimates are then differenced between satellites and the LAMBDA method (well described by [DeJonge and Tiberius \(1996\)](#)) is used to obtain double-difference integer ambiguities which are used to produce an RTK position solution. The equivalence of hyperbolic positioning and pseudoranging methods makes this possible ([Shen and Xu, 2008](#)). This equivalence and the advantages of using this approach are discussed further in **Section 3.6**.

The filter accepts 5 Hz UWB range measurements as well as 5 Hz differential GPS L1 pseudorange and carrier-phase measurements. This study utilizes differential GPS L1 measurements with relatively short baselines (less than 1 km). Most GPS RTK systems utilize both L1 and L2 measurements. Utilizing GPS L2 phase measurements aids the ability to estimate fixed integer ambiguities but the focus of this research is examination of the impact of UWB range augmentation and this impact is assessed

well with L1 only (for short baselines).

3.4.1 Functional models

The first step in designing an estimator is determining the functional relationship between the measurements and the unknown parameters. In the following, the non-linear and linearized measurement functional models are derived for the single-difference GPS pseudorange measurement, the UWB range measurement, and the single-difference GPS carrier-phase measurement.

The non-linear undifferenced GPS pseudorange functional model is

$$\begin{aligned} P &= \rho + c(dT) \\ \rho &= \sqrt{(x_s - x)^2 + (y_s - y)^2 + (z_s - z)^2} \end{aligned} \quad (3.1)$$

where P is a pseudorange measurement, ρ is the geometric range from the phase center of the GPS antenna to the satellite, c is the speed of light, dT is the unknown receiver clock offset, x_s , y_s , and z_s are the earth centered earth fixed (ECEF) coordinates of the satellite, and x , y , and z are the unknown ECEF coordinates of the GPS antenna. It follows that the non-linear single-difference (between receivers) GPS pseudorange functional model for the test receiver and the reference receiver at a known location is

$$\begin{aligned} \Delta P &= (\rho + c(dT)) - (\rho_{\text{reference}} + c(dT_{\text{reference}})) \\ \Delta P &= (\rho - \rho_{\text{reference}}) + c(dT - dT_{\text{reference}}) \\ \Delta P &= \Delta\rho + c(\Delta T) \end{aligned} \quad (3.2)$$

where ΔP is a single-difference pseudorange measurement, $\rho_{\text{reference}}$ is a deterministic value, and ΔT is the single-difference receiver clock offset. Using Taylor's series

expansion, the corresponding linearized functional model is

$$\Delta P = \Delta \hat{P} + \frac{\partial \Delta P}{\partial x}(x - \hat{x}) + \frac{\partial \Delta P}{\partial y}(y - \hat{y}) + \frac{\partial \Delta P}{\partial z}(z - \hat{z}) + \frac{\partial \Delta P}{\partial c(\Delta T)}(c\Delta T - c\Delta \hat{T})$$

$$\mathbf{h}_p = \begin{bmatrix} \frac{\partial \Delta P}{\partial x} & \frac{\partial \Delta P}{\partial y} & \frac{\partial \Delta P}{\partial z} & \frac{\partial \Delta P}{\partial c\Delta T} \end{bmatrix} = \begin{bmatrix} \frac{-(x_s - \hat{x})}{\hat{\rho}} & \frac{-(y_s - \hat{y})}{\hat{\rho}} & \frac{-(z_s - \hat{z})}{\hat{\rho}} & 1 \end{bmatrix}$$

$$\hat{\boldsymbol{\delta}}_{x_p} = \begin{bmatrix} x - \hat{x} \\ y - \hat{y} \\ z - \hat{z} \\ c\Delta T - c\Delta \hat{T} \end{bmatrix} = \begin{bmatrix} \hat{\delta}_x \\ \hat{\delta}_y \\ \hat{\delta}_z \\ c\delta \hat{T} \end{bmatrix} \quad (3.3)$$

$$\hat{v} = \Delta P - \Delta \hat{P} = \mathbf{h}_p \hat{\boldsymbol{\delta}}_{x_p}$$

where $\Delta \hat{P}$, $\hat{\rho}$, \hat{x} , \hat{y} and \hat{z} are the estimated values at the point of expansion, \hat{v} is a pseudorange measurement innovation, \mathbf{h}_p is the pseudorange design vector, and $\hat{\boldsymbol{\delta}}_{x_p}$ is the vector of estimated error states for the pseudorange measurement.

The non-linear UWB range functional model is

$$\begin{aligned} R &= \kappa \rho_u + \beta \\ \rho_u &= \sqrt{(x_u - x)^2 + (y_u - y)^2 + (z_u - z)^2} \end{aligned} \quad (3.4)$$

where R is the UWB range measurement, κ is a scale factor, β is a bias, and x_u , y_u , and z_u are the ECEF coordinates of the reference UWB station. The corresponding

linearized model is

$$\begin{aligned} R &= \hat{R} + \frac{\partial R}{\partial x}(x - \hat{x}_0) + \frac{\partial R}{\partial y}(y - \hat{y}) + \frac{\partial R}{\partial z}(z - \hat{z}) + \frac{\partial R}{\partial \beta}(\beta - \hat{\beta}) + \frac{\partial R}{\partial \kappa}(\kappa - \hat{\kappa}) \\ \mathbf{h}_u &= \begin{bmatrix} \frac{\partial R}{\partial x} & \frac{\partial R}{\partial y} & \frac{\partial R}{\partial z} & \frac{\partial R}{\partial \beta} & \frac{\partial R}{\partial \kappa} \end{bmatrix} = \begin{bmatrix} \frac{-\kappa(x_u - \hat{x})}{\hat{\rho}_u} & \frac{-\kappa(y_u - \hat{y})}{\hat{\rho}_u} & \frac{-\kappa(z_u - \hat{z})}{\hat{\rho}_u} & 1 & \hat{\rho}_u \end{bmatrix} \\ \hat{\boldsymbol{\delta}}_{\mathbf{x}_u} &= \begin{bmatrix} x - \hat{x} \\ y - \hat{y} \\ z - \hat{z} \\ \beta - \hat{\beta} \\ \kappa - \hat{\kappa} \end{bmatrix} = \begin{bmatrix} \hat{\delta}_x \\ \hat{\delta}_y \\ \hat{\delta}_z \\ \hat{b} \\ \hat{k} \end{bmatrix} \end{aligned} \quad (3.5)$$

$$\hat{v}_u = R - \hat{R} = \mathbf{h}_u \hat{\boldsymbol{\delta}}_{\mathbf{x}_u}$$

where \hat{R} , $\hat{\beta}$, $\hat{\kappa}$, and $\hat{\rho}_u$ are the estimated values at the point of expansion, \hat{v}_u is an UWB range measurement innovation, \mathbf{h}_u is the UWB range measurement design vector, and $\hat{\boldsymbol{\delta}}_{\mathbf{x}_u}$ is the vector of estimated error states for the UWB range measurement.

The non-linear functional model for a GPS carrier-phase measurement is given by

$$\Phi = \rho + c(dT) + \lambda N \quad (3.6)$$

where Φ is the carrier-phase measurement and λN is an integer ambiguity in units of metres. Note that each carrier-phase measurement has a different integer ambiguity. It follows that the non-linear single-difference (between receivers) GPS carrier-phase functional model for the test receiver and the reference receiver at a known location is

$$\begin{aligned} \Delta\Phi &= (\rho + c(dT) + \lambda N) - (\rho_{reference} + c(dT_{reference} + \lambda N_{reference})) \\ \Delta\Phi &= (\rho - \rho_{reference}) + c(dT - dT_{reference}) + (\lambda(N - N_{reference})) \\ \Delta\Phi &= \Delta\rho + c(\Delta T) + \lambda\Delta N \end{aligned} \quad (3.7)$$

Using Taylor's series expansion, the corresponding linearized model is

$$\Delta\Phi = \Delta\hat{\Phi} + \frac{\partial\Phi}{\partial x}(x - \hat{x}) + \frac{\partial\Phi}{\partial y}(y - \hat{y}) + \frac{\partial\Phi}{\partial z}(z - \hat{z}) + \frac{\partial\Phi}{\partial c(\Delta T)}(cdT - c\Delta\hat{T}) + \frac{\partial\Phi}{\partial \lambda\Delta N}(\lambda\Delta N - \lambda\Delta\hat{N})$$

$$\mathbf{h}_{\Phi} = \left[\begin{array}{ccccc} \frac{\partial\Phi}{\partial x} & \frac{\partial\Phi}{\partial y} & \frac{\partial\Phi}{\partial z} & \frac{\partial\Phi}{\partial cdT} & \frac{\partial\Phi}{\partial \lambda N} \end{array} \right] = \left[\begin{array}{ccc|cc} \frac{-(x_s - \hat{x})}{\hat{\rho}} & \frac{-(y_s - \hat{y})}{\hat{\rho}} & \frac{-(z_s - \hat{z})}{\hat{\rho}} & 1 & 1 \end{array} \right]$$

$$\hat{\boldsymbol{\delta}}_{\mathbf{x}_{\Phi}} = \left[\begin{array}{c} x - \hat{x} \\ y - \hat{y} \\ z - \hat{z} \\ c\Delta T - c\Delta\hat{T} \\ \lambda\Delta N - \lambda\Delta\hat{N} \end{array} \right] = \left[\begin{array}{c} \hat{\delta}_x \\ \hat{\delta}_y \\ \hat{\delta}_z \\ c\hat{\delta}T \\ \lambda\hat{\eta} \end{array} \right] \quad (3.8)$$

$$\hat{v}_{\Phi} = \Phi - \hat{\Phi} = \mathbf{h}_{\Phi}\hat{\boldsymbol{\delta}}_{\mathbf{x}_{\Phi}}$$

where $\hat{\Phi}$ and $\lambda\hat{\eta}$ are the estimated values at the point of expansion, \mathbf{h}_{Φ} is the carrier-phase design vector, $\hat{\boldsymbol{\delta}}_{\mathbf{x}_{\Phi}}$ are error states associated with the carrier-phase measurement, and \hat{v}_{Φ} is a carrier-phase measurement innovation.

3.4.2 The tightly-coupled discrete sequential extended Kalman filter

Given the three linearized measurement models, the combined error state vector for the sequential extended Kalman filter can be composed. There are three position error states and one single-difference GPS receiver clock offset error state. The filter is set up for a maximum of three UWB range measurements (range pairs a, b, and c). For three UWB range measurements there are three corresponding bias error states and three scale factor error states. There are also integer ambiguity error states for each single-difference carrier-phase measurement. The resulting sequential extended Kalman filter

error state vector is:

$$\hat{\boldsymbol{\delta}}_{\mathbf{x}} = \left[\hat{\delta}_x \quad \hat{\delta}_y \quad \hat{\delta}_z \quad c\delta\hat{T} \quad \hat{b}_a \quad \hat{b}_b \quad \hat{b}_c \quad \hat{k}_a \quad \hat{k}_b \quad \hat{k}_c \quad \lambda\hat{\eta}_1 \quad \lambda\hat{\eta}_2 \quad \dots \quad \lambda\hat{\eta}_n \right]^T \quad (3.9)$$

where $\hat{\delta}_x$, $\hat{\delta}_y$, and $\hat{\delta}_z$ are the error states corresponding to the unknown ECEF coordinates x , y , and z , $c\delta\hat{T}$ is the error state corresponding to the single-difference GPS receiver clock offset, \hat{b}_a , \hat{b}_b , and \hat{b}_c are the error states corresponding to the unknown UWB bias parameters for UWB range pairs a, b, and c, \hat{k}_a , \hat{k}_b , and \hat{k}_c are the error states corresponding to the unknown UWB scale factor parameters for UWB range pairs a, b, and c, and $\lambda\hat{\eta}_i$ is the single-difference ambiguity error state for the i^{th} carrier-phase ambiguity.

The unknown parameters corresponding to the error states in **Equation 3.9** in vector form are

$$\hat{\mathbf{x}} = \left[\hat{x} \quad \hat{y} \quad \hat{z} \quad c\Delta\hat{T} \quad \hat{\beta}_a \quad \hat{\beta}_b \quad \hat{\beta}_c \quad \hat{\kappa}_a \quad \hat{\kappa}_b \quad \hat{\kappa}_c \quad \Delta\lambda\hat{N}_1 \quad \Delta\lambda\hat{N}_2 \quad \dots \quad \Delta\lambda\hat{N}_n \right]^T \quad (3.10)$$

where x , y , z are the ECEF position states, $c\Delta\hat{T}$ is the single-difference GPS receiver clock offset state, $\hat{\beta}_a$, $\hat{\beta}_b$, and $\hat{\beta}_c$ are the UWB bias states, $\hat{\kappa}_a$, $\hat{\kappa}_b$, and $\hat{\kappa}_c$ are the UWB scale factor states, and $\Delta\lambda\hat{N}_i$ is the single-difference ambiguity state for the i^{th} carrier-phase ambiguity.

The extended Kalman filter comprises two basic steps, a prediction step and an update step. The prediction step applies, from epoch $k - 1$ to epoch k , to the unknown parameters and associated covariance matrix as

$$\begin{aligned} \hat{\mathbf{x}}_{\mathbf{k}} &= \boldsymbol{\Phi}_{\mathbf{k}-1,\mathbf{k}}\hat{\mathbf{x}}_{\mathbf{k}-1} \\ \mathbf{P}_{\mathbf{k}}^+ &= \boldsymbol{\Phi}_{\mathbf{k}-1,\mathbf{k}}\mathbf{P}_{\mathbf{k}-1}^-\boldsymbol{\Phi}_{\mathbf{k}-1,\mathbf{k}}^T + \mathbf{Q}_{\mathbf{k}-1} \end{aligned} \quad (3.11)$$

where $\boldsymbol{\Phi}_{\mathbf{k}-1,\mathbf{k}}$ is the state transition matrix, $\mathbf{P}_{\mathbf{k}}$ is the variance-covariance matrix of the states (and error states), and $\mathbf{Q}_{\mathbf{k}-1}$ is the process noise matrix.

Selection of dynamic model

The dynamic model determines the choice of the state transition matrix and the process noise matrix.

For low dynamic operations such as pole-mounted RTK land surveying, it is sufficient to model the position states as random walk processes with process noise suitable for mildly dynamic operations. A random walk process is given by

$$\mathbf{x}_k = \mathbf{x}_{k-1} + \mathbf{w}_{k-1}, \mathbf{Q}_k \quad (3.12)$$

Modelling the dynamic behaviour of the single-difference GPS receiver clock offset is a problem. Quartz crystal based frequency standards are used for GPS receiver oscillators. Temperature, vibration (especially shock), acceleration, and power supply voltage all affect crystal oscillators (Cantor et al., 1999). Even if all of these effects are taken into account in the dynamics model for the single-difference clock offset, GPS receiver manufacturers often steer their receiver clock or perform integer millisecond jumps to keep the receiver clock time close to GPS time. This deterministically alters the GPS receiver clock dynamics and this information is often not provided to the user. Thus, the single-difference GPS receiver clock offset is modelled by a random walk process with very large process noise so that it is fully estimated at each update (i.e. it is not filtered). This is not considered a problem because the clock offset term is eliminated later when a differencing operation is applied to the single-difference solution. In fact, fully estimating the clock at each epoch is required to maintain the equivalence between hyperbolic positioning and pseudorangeing. If the clock could be modelled, the single-differencing approach used here could be used to possibly obtain a better position solution than the equivalent double-differencing method (a topic for further research, i.e. outside the scope of this thesis).

Each UWB bias state is modeled as a random walk process with process noise that

allows the bias to change slowly over time. The bias may change over time since the two-way time-of-flight bias is a function of the stability of the UWB radio oscillators which likely vary with temperature. Each UWB scale factor state is modeled as a random walk process with very little process noise as it is not expected to change while the UWB radios are powered up (almost random constant). For both radios types, this is reasonable given previous empirical testing as discussed in Chapter 2. More specifically, for the MSSSI ranging radios, this is reasonable since the threshold used for the leading edge detector is set once when the device is turned on and remains constant during the test (Fontana, 1999).

An enhancement in terms of determining the process noises for the position states is possible using the tilt sensor. When the user is stationary over a point, a bubble level attached to the survey pole is used to manually level the system. The tilt sensor also indicates level operation. The tilt sensor has an output rate of approximately 10 Hz. When the tilt is less than a threshold value (3°) for more than 1 second, the process noises are adjusted for nearly static operation. This threshold is based on the behaviour observed during testing and is empirical in design. It was found that the pole was static and level whenever this condition was observed and not static otherwise.

For pole-mounted land surveying, a user may walk up to 6 km/hour or approximately 1.7 m/s. This corresponds to a horizontal position error of 1.7 m for prediction over a 1 second interval using a random walk model. A process noise of $(1.7 \text{ m/s})^2$ is used by the filter to provide enough uncertainty such that the update using the measurements will be sufficient to estimate the precise position. This is the default value for the horizontal process noise used in the filter. The default vertical process noise is selected at $(0.4 \text{ m/s})^2$ which is sufficient for pole-mounted land surveying. The GPS receiver Doppler measurements are not used in the estimation filter. If they were, the velocity states would drive the position states. To simplify the work performed in this

research, the simple random walk model for the position states was selected. However, an enhancement is possible using a least-squares solution for the GPS velocity of the pole-mounted system. This solution is computed in parallel with the filter solution. The GPS velocity output provides an additional means of setting the process noise value for the position states. For example, if a velocity solution of 1.0 m/s northeast is deemed good and useable, the process noise values are reduced accordingly. Note that the velocity computed is not used to predict the position. It is only used to adjust the process noise.

The single-difference GPS ambiguity states are constant values and are thus modelled as random constants with no process noise.

In summary, the state transition matrix selected is simply the identity matrix and the process noise is a diagonal matrix. Both are given in the following equation.

$$\Phi = \mathbf{I}$$

$$\mathbf{Q} =$$

$$\begin{bmatrix} (q_X \Delta t)^2 & 0 & 0 & 0 & 0 & 0 & 0 & 0 & 0 & 0 & 0 & 0 \dots 0 \\ 0 & (q_Y \Delta t)^2 & 0 & 0 & 0 & 0 & 0 & 0 & 0 & 0 & 0 & 0 \dots 0 \\ 0 & 0 & (q_Z \Delta t)^2 & 0 & 0 & 0 & 0 & 0 & 0 & 0 & 0 & 0 \dots 0 \\ 0 & 0 & 0 & (q_{c\Delta T} \Delta t)^2 & 0 & 0 & 0 & 0 & 0 & 0 & 0 & 0 \dots 0 \\ 0 & 0 & 0 & 0 & (q_{\beta_a} \Delta t)^2 & 0 & 0 & 0 & 0 & 0 & 0 & 0 \dots 0 \\ 0 & 0 & 0 & 0 & 0 & (q_{\beta_b} \Delta t)^2 & 0 & 0 & 0 & 0 & 0 & 0 \dots 0 \\ 0 & 0 & 0 & 0 & 0 & 0 & (q_{\beta_c} \Delta t)^2 & 0 & 0 & 0 & 0 & 0 \dots 0 \\ 0 & 0 & 0 & 0 & 0 & 0 & 0 & (q_{\kappa_a} \Delta t)^2 & 0 & 0 & 0 & 0 \dots 0 \\ 0 & 0 & 0 & 0 & 0 & 0 & 0 & 0 & (q_{\kappa_b} \Delta t)^2 & 0 & 0 & 0 \dots 0 \\ 0 & 0 & 0 & 0 & 0 & 0 & 0 & 0 & 0 & (q_{\kappa_c} \Delta t)^2 & 0 & 0 \dots 0 \\ 0 & 0 & 0 & 0 & 0 & 0 & 0 & 0 & 0 & 0 & 0 & 0 \dots 0 \\ \vdots & \vdots \dots \vdots \\ 0 & 0 & 0 & 0 & 0 & 0 & 0 & 0 & 0 & 0 & 0 & 0 \dots 0 \end{bmatrix} \quad (3.13)$$

Sequential update

Following the prediction step, update steps are performed for each measurement. The update step proceeds as follows for each observation. First, compute the design vector

for each measurement. The design vector is one of the following vectors.

$$\begin{aligned}
\mathbf{h}_{p_1} &= \begin{bmatrix} \frac{-(x_{s_1}-\hat{x})}{\hat{\rho}} & \frac{-(y_{s_1}-\hat{y})}{\hat{\rho}} & \frac{-(z_{s_1}-\hat{z})}{\hat{\rho}} & 1 & 0 & 0 & 0 & 0 & 0 & 0 & 0 \dots & 0 \end{bmatrix} \\
&\vdots \\
\mathbf{h}_{p_n} &= \begin{bmatrix} \frac{-(x_{s_n}-\hat{x})}{\hat{\rho}} & \frac{-(y_{s_n}-\hat{y})}{\hat{\rho}} & \frac{-(z_{s_n}-\hat{z})}{\hat{\rho}} & 1 & 0 & 0 & 0 & 0 & 0 & 0 & 0 \dots & 0 \end{bmatrix} \\
\mathbf{h}_{u_a} &= \begin{bmatrix} \frac{-\kappa_a(x_u-\hat{x})}{\hat{\rho}_{u_a}} & \frac{-\kappa_a(y_u-\hat{y})}{\hat{\rho}_{u_a}} & \frac{-\kappa_a(z_u-\hat{z})}{\hat{\rho}_{u_a}} & 0 & 1 & 0 & 0 & \hat{\rho}_{u_a} & 0 & 0 & 0 \dots & 0 \end{bmatrix} \\
\mathbf{h}_{u_b} &= \begin{bmatrix} \frac{-\kappa_b(x_u-\hat{x})}{\hat{\rho}_{u_b}} & \frac{-\kappa_b(y_u-\hat{y})}{\hat{\rho}_{u_b}} & \frac{-\kappa_b(z_u-\hat{z})}{\hat{\rho}_{u_b}} & 0 & 0 & 1 & 0 & 0 & \hat{\rho}_{u_b} & 0 & 0 \dots & 0 \end{bmatrix} \\
\mathbf{h}_{u_c} &= \begin{bmatrix} \frac{-\kappa_c(x_u-\hat{x})}{\hat{\rho}_{u_c}} & \frac{-\kappa_c(y_u-\hat{y})}{\hat{\rho}_{u_c}} & \frac{-\kappa_c(z_u-\hat{z})}{\hat{\rho}_{u_c}} & 0 & 0 & 0 & 1 & 0 & 0 & \hat{\rho}_{u_c} & 0 \dots & 0 \end{bmatrix} \\
\mathbf{h}_{\Phi_1} &= \begin{bmatrix} \frac{-(x_{s_1}-\hat{x})}{\hat{\rho}_1} & \frac{-(y_{s_1}-\hat{y})}{\hat{\rho}_1} & \frac{-(z_{s_1}-\hat{z})}{\hat{\rho}_1} & 1 & 0 & 0 & 0 & 0 & 0 & 0 & 1 & 0 \dots & 0 \end{bmatrix} \\
&\vdots \\
\mathbf{h}_{\Phi_n} &= \begin{bmatrix} \frac{-(x_{s_n}-\hat{x})}{\hat{\rho}_n} & \frac{-(y_{s_n}-\hat{y})}{\hat{\rho}_n} & \frac{-(z_{s_n}-\hat{z})}{\hat{\rho}_n} & 1 & 0 & 0 & 0 & 0 & 0 & 0 & 0 \dots & 1 \end{bmatrix}
\end{aligned} \tag{3.14}$$

where \mathbf{h}_p is a design vector for a single-difference GPS pseudorange measurement, \mathbf{h}_{u_a} , \mathbf{h}_{u_b} , and \mathbf{h}_{u_c} are design vectors for UWB range pairs a, b, and c, and \mathbf{h}_{Φ_1} and \mathbf{h}_{Φ_n} are the first and n^{th} single-difference GPS carrier-phase measurements. The next step is to form the innovation corresponding to this measurement based on the predicted measurement.

$$v_i = l_i - \hat{l}_i \tag{3.15}$$

where l_i is the measured value and \hat{l}_i is the estimated measurement. Next, the Kalman gain vector is computed.

$$\mathbf{k}_i = \mathbf{P}_{k_i}^- \mathbf{h}_i^T \left(\frac{1}{\mathbf{h}_i \mathbf{P}_{k_i}^- \mathbf{h}_i^T + \sigma_i^2} \right) \tag{3.16}$$

where \mathbf{k}_i is the Kalman gain vector, $\mathbf{P}_{k_i}^-$ is the pre-update covariance matrix of the states at epoch k for measurement i , \mathbf{h}_i is the design vector for the i^{th} measurement, and σ_i^2 is the variance of the measurement. The error state vector is computed next. The error state vector is not propagated. Instead, the unknown parameters are always updated with each update step. This means that the pre-update error state vector is

always zero.

$$\begin{aligned}
\hat{\delta}_{\mathbf{x}_{\mathbf{k}_i}}^- &= \mathbf{0} \\
\hat{\delta}_{\mathbf{x}_{\mathbf{k}_i}}^+ &= \mathbf{k}_i v_i \\
\hat{\mathbf{x}}_{\mathbf{k}_i}^+ &= \hat{\mathbf{x}}_{\mathbf{k}_i}^- + \hat{\delta}_{\mathbf{x}_{\mathbf{k}_i}}^+
\end{aligned} \tag{3.17}$$

The covariance matrix of the states is then updated using the following equation.

$$\mathbf{P}_{\mathbf{k}_i}^+ = [\mathbf{I} - \mathbf{k}_i \mathbf{h}_i] \mathbf{P}_{\mathbf{k}_i}^- \tag{3.18}$$

Inequality constraints

Since the range of the UWB bias is known based on the quality of the oscillators used ([IEEE802-15.4a, 2007](#)) (e.g. for 20 ppm, the worst case bias is 1.23 m), and the range of the UWB scale factor error is well known from line-of-sight testing, inequality constraints are used in the filter. After each measurement update, the UWB bias and scale factor values are checked to determine if the minimum or maximum value is exceeded. If a boundary has been crossed, a pseudo-measurement update is performed to force the solution to the known range of values. This method of applying inequality constraints to an extended Kalman filter adds a minimal amount of information to the filter to achieve the constraint ([Richards, 1995](#)).

The application of inequality constraints to an UWB range bias is examined in the following. If the maximum value is exceeded, a pseudo-measurement at the minimum value is used to update the filter. The measurement innovation, v_β , the measurement variance for this pseudo-measurement, σ_β^2 , and the corresponding design vector, h_{β_a} (range pair a for example), are given by:

$$\begin{aligned}
v_\beta &= \beta_{\min} - \hat{\beta} \\
\sigma_\beta^2 &= P_{k_{\beta_a}}^+ \frac{\beta_{\max} - \beta_{\min}}{\hat{\beta} - \beta_{\max}} \\
h_{\beta_a} &= \begin{bmatrix} 0 & 0 & 0 & 0 & 1 & 0 & 0 & 0 & 0 & 0 & 0 \dots 0 \end{bmatrix}
\end{aligned} \tag{3.19}$$

where $\hat{\beta}$ is the value of the bias after an update step (which now exceeds the maximum bias value), β_{\min} is the minimum value and also the value of the pseudo-measurement, $P_{k\beta_a}^+$ is the element of the state covariance matrix corresponding to the state which has exceeded the maximum, and β_{\max} is the maximum value. If the minimum value is exceeded, a pseudo-measurement at the maximum value is used to update the filter. The innovation, measurement variance for the pseudo-measurement and its design vector in this case are given by:

$$\begin{aligned} v_\beta &= \beta_{\max} - \hat{\beta} \\ \sigma_\beta^2 &= P_{k\beta_a}^+ \frac{\beta_{\max} - \beta_{\min}}{\beta_{\min} - \hat{\beta}} \\ h_{\beta_a} &= \begin{bmatrix} 0 & 0 & 0 & 0 & 1 & 0 & 0 & 0 & 0 & 0 & 0 \dots 0 \end{bmatrix} \end{aligned} \quad (3.20)$$

where $\hat{\beta}$ is the value of the bias after an update step (which now exceeds the minimum bias value) and β_{\max} is the value of the pseudo-measurement.

The application of inequality constraints to an UWB range scale factor is examined in the following. If the maximum value is exceeded, a pseudo-measurement at the minimum value is used to update the filter. The measurement innovation, v_κ , the measurement variance for this pseudo-measurement, σ_κ^2 , and the corresponding design vector, h_{κ_a} (range pair a for example), are given by:

$$\begin{aligned} v_\kappa &= \kappa_{\min} - \hat{\kappa} \\ \sigma_\kappa^2 &= P_{k\kappa_a}^+ \frac{\kappa_{\max} - \kappa_{\min}}{\hat{\kappa} - \kappa_{\max}} \\ h_{\kappa_a} &= \begin{bmatrix} 0 & 0 & 0 & 0 & 0 & 0 & 0 & 1 & 0 & 0 & 0 \dots 0 \end{bmatrix} \end{aligned} \quad (3.21)$$

where $\hat{\kappa}$ is the value of the scale factor after an update step (which now exceeds the maximum value value), κ_{\min} is the minimum value and also the value of the pseudo-measurement, $P_{k\kappa_a}^+$ is the element of the state variance covariance corresponding to the state which has exceeded the maximum, and κ_{\max} is the maximum value. If the minimum value is exceeded, a pseudo-measurement at the maximum value is used to

update the filter. The innovation, measurement variance for the pseudo-measurement and its design vector in this case are given by:

$$\begin{aligned}
 v_{\kappa} &= \kappa_{\max} - \hat{\kappa} \\
 \sigma_{\kappa}^2 &= P_{k_{\kappa a}}^+ \frac{\kappa_{\max} - \kappa_{\min}}{\kappa_{\min} - \hat{\kappa}} \\
 h_{\kappa a} &= \begin{bmatrix} 0 & 0 & 0 & 0 & 0 & 0 & 0 & 1 & 0 & 0 & 0 \dots 0 \end{bmatrix}
 \end{aligned} \tag{3.22}$$

where $\hat{\kappa}$ is the value of the scale factor after an update step (which now exceeds the minimum bias value) and κ_{\max} is the value of the pseudo-measurement.

The application of inequality constraints using this method causes the state to be adjusted to the extrema value; however, all the unknowns are adjusted. In some cases, another state can exceed its inequality constraint and thus some iteration of the application of the constraints can occur in the filter.

The explanation of the filter is now complete given the assumption that there are no measurement blunders. The next section will discuss the detection and exclusion of outliers.

3.5 Reliability

In estimation, the uncertainty in the measurements is described by the stochastic model. The stochastic model describes noise in the measurements as random processes with normal distributions. For a radio-frequency based time delay estimate the variance of the measurement noise is a function of the received signal-to-noise ratio and the bandwidth of the system (Kay, 1993). Interference due to multipath also distorts the measurement and to a certain extent this is dealt with by increasing the measurement variance used in the estimation filter. Gross measurement outliers (i.e. blunders) are not described by the stochastic model. The relationship between the unknown

estimated parameters and the measurements is described by the functional mathematic model used by the estimation filter. This model also has no way to account for outliers. The impact of an outlier in the estimation filter invalidates the assumption that the measurements are unbiased. This is reflected by inaccuracy in the solution. In other words, an undetected fault has a very negative impact on accuracy. Statistical testing is used to try to identify and exclude measurement blunders in the estimation process.

Reliability refers to the ability to detect measurement faults. Statistical reliability quantifies the ability to identify blunders. It is subdivided into internal and external reliability (Baarda, 1968). Internal reliability refers to the ability to detect a blunder by statistical testing. This is also called local testing of the measurements. The minimum blunder that can be detected is referred to as the marginally detectable blunder or the minimum detectable bias (MDB). External reliability quantifies the impact of an undetected blunder on the estimated parameters. In other words, external reliability assesses the impact of the MDB on the solution.

Internal reliability can be implemented in an epoch-by-epoch sense using least squares (Leick, 2004) or by testing of the innovations (predicted residuals) in Kalman filtering (Teunissen and Salzmann, 1989). For most GPS applications testing of the innovations is more robust because the Kalman filter utilizes a dynamic model. It can also be implemented such that uncorrelated measurements can be used in estimation one at a time. This is not possible using epoch-by-epoch least squares because the least squares normal matrix is not invertible when there are fewer observations than parameters.

Petovello et al. (2003) compared sequential and simultaneous Kalman filter update approaches for statistically independent sets of observations. Double-difference pseudorange, double-difference Doppler, and double-difference carrier-phase measurements comprised the three sets evaluated in the study. Note that a set of observations was used in a sequential update (not individual measurements). The order in which the sets

of observations were used in the update step was evaluated. The sequential method was shown to be much more computationally efficient than the simultaneous method. This is well known and a major advantage for real time systems. [Petovello et al. \(2003\)](#) also showed that there is very little difference in the two methods in terms of ability to detect blunders.

[Brodie \(2001\)](#) shows that by adding pseudorange measurements sequentially as updates to a discrete-time extended Kalman filter and by using the knowledge that measurements of high elevation satellites are less likely to be blunders there is an improvement in the ability to detect blunders overall.

3.5.1 Innovation testing

Assuming no errors in the dynamic model for the filter and that no blunders have already affected the solution, the following local testing of the innovations is valid.

The variance of the innovation, $\sigma_{v_i}^2$, in the case of sequential processing (assuming uncorrelated measurement noise) is given by:

$$\sigma_{v_i}^2 = \mathbf{h}_i \mathbf{P}_{\mathbf{k}}^- \mathbf{h}_i^T + \sigma_i^2 \quad (3.23)$$

where σ_i^2 is the measurement variance and $\mathbf{h}_i \mathbf{P}_{\mathbf{k}}^- \mathbf{h}_i^T$ is the predicted variance of the parameters mapped into the observation domain.

A measurement innovation is considered bias free by the null hypothesis.

$$v_i \Big|_{H_0} \sim N(0, \sigma_{v_i}^2) \quad (3.24)$$

Otherwise, the alternative hypothesis states that a bias, δ_v is present.

$$v_i \Big|_{H_a} \sim N(\delta_v, \sigma_{v_i}^2) \quad (3.25)$$

It is more convenient to apply a test to a normalized test statistic.

$$t_i \Big|_{H_0} \sim N(0, 1) \tag{3.26}$$

$$t_i \Big|_{H_a} \sim N(\delta_0, 1)$$

where t_i is given by:

$$t_i = \frac{v_i}{\sqrt{\sigma_{v_i}^2}} \tag{3.27}$$

The null hypothesis is that a standardized innovation is normally distributed with zero mean and variance of 1. This is rejected if $t_i < n_{\alpha/2}$ or $t_i > n_{1-\alpha/2}$, where α is the significance level of the test and $n_{\alpha/2}$ and $n_{1-\alpha/2}$ are points such that

$P(n_{\alpha/2} < t_i < n_{1-\alpha/2}) = 1 - \alpha$. This is illustrated by **Figure 3.2**. For example, the three sigma test, $P(-3\sigma < t_i < 3\sigma) = 99.74\%$, considers an α value of 0.26%.

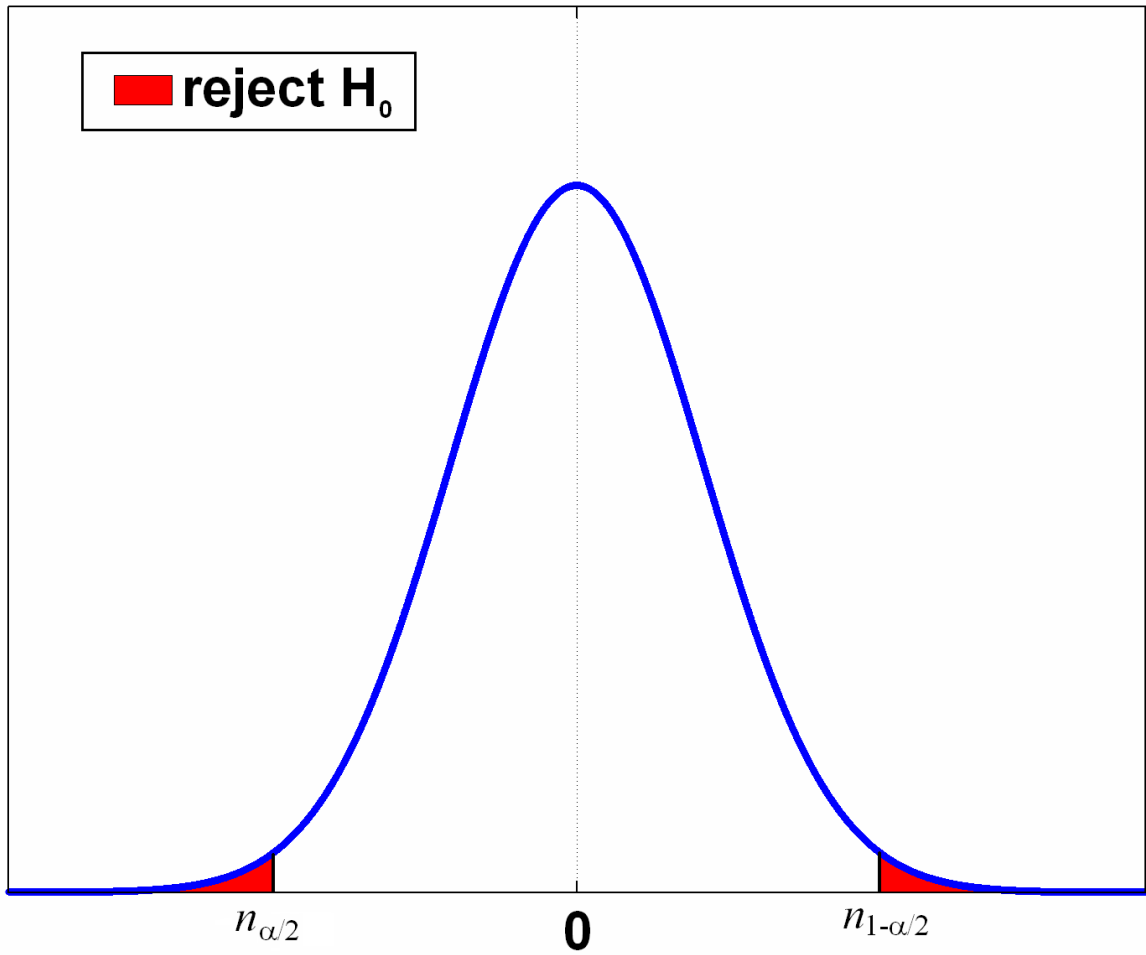


Figure 3.2: The null hypothesis is that the standardized innovation is normally distributed

The innovation test occurs before the states are updated and if the null hypothesis is rejected the measurement is simply not used to update the filter. Thus, there is no need to recompute the solution or correct for the blunder. Note that by sequential testing of the innovations, no assumptions have been made about the number of blunders at each epoch.

The problem with single-difference innovation testing

There is a problem with the ability to detect a blunder for the first measurement update because the single-difference receiver clock offset is not filtered. The pseudorange measurements are the first group of measurements used to update the filter. The high process noise for the single-difference receiver clock offset state results in the variance of the first innovation given by the following equation. ¹

$$\begin{aligned}\sigma_{v_0}^2 &= \mathbf{h}_0 \mathbf{P}_k^- \mathbf{h}_0^T + \sigma_0^2 \\ \mathbf{h}_0[3] &= 1.0 \\ \mathbf{P}_k^- [3][3] &= 1000000.0 \\ \sigma_{v_0}^2 &\approx 1000000.0\end{aligned}\tag{3.28}$$

This results in

$$t_0 \approx \frac{v_0}{1000.0}\tag{3.29}$$

and t_0 will be small and very likely it is not possible to detect a blunder for the first update as it is used solely to observe the single-difference GPS receiver clock offset. It is important that the first few updates do not contain blunders as the ability to detect them is limited until the clock offset is observed.

To address this problem, a parallel least squares position solution utilizing only pseudorange measurements is computed independently of the filtered solution. The least squares estimation uses residual testing (Leick, 2004) to identify blunders. The filter checks if the first pseudorange measurements were identified as blunders by the parallel least squares solution and insures that a blunder free pseudorange is the first measurement used on each update cycle. This first measurement observes the clock offset and for subsequent measurements an appropriate estimated innovation standard deviation is available for innovation testing.

¹The process noise used for the GPS clock bias state for each prediction step is $(1000m)^2$

However, this method fails if fewer than 4 satellites are available for the least squares solution and for future work a more robust method is desirable.

The order of the sequential updates

Traditional methods of reliability testing for the identification of GPS measurement outliers assume equal likelihood of occurrence amongst the set of observations. In fact, there is a functional relationship between the likelihood of an outlier and the user to satellite geometry in some situations. An ordered sequential measurement processing strategy used by the estimation filter improves the ability to detect measurement outliers for these cases. [Brodie \(2001\)](#) demonstrates this for GPS positioning with an extended Kalman filter that utilizes pseudorange measurements.

The principle sources of GPS measurement outliers are tracking errors caused by reflected signals. There are two cases in this regard shown in **Figure 3.3**. Often the receiver tracks a line-of-sight signal combined with reflected signals. This is referred to as multipath error. The error magnitude for the GPS pseudorange measurement is a function of the correlator-based mitigation techniques used by the receiver ([van Dierendonck et al., 1992](#)). Occasionally situations arise in which obstructions block the direct satellite signals while strong specular reflections from other surfaces are tracked. The tracking of echo-only signals leads to large measurement errors greater than the maximum possible multipath error regardless of the type of correlator-based mitigation techniques used by the receiver ([MacGougan, 2008](#)).

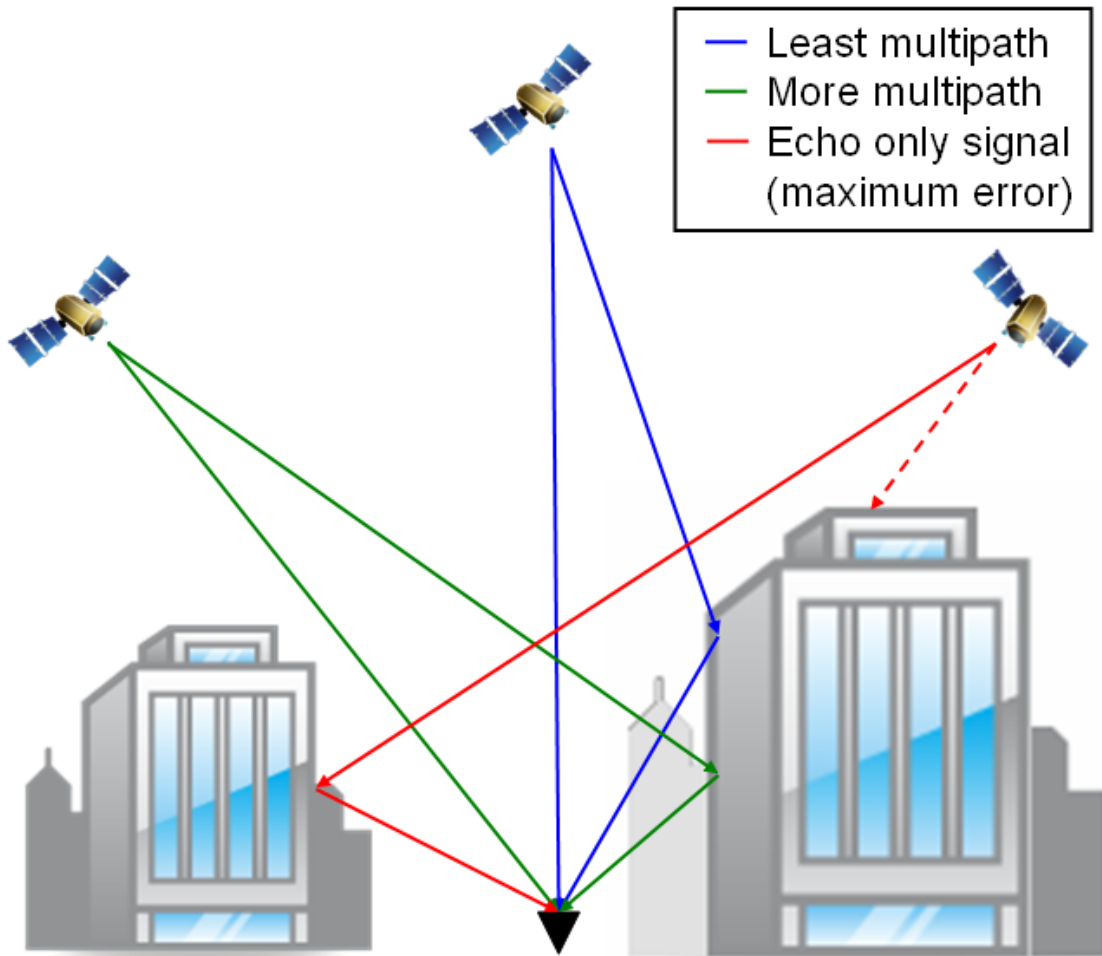


Figure 3.3: Multipath and echo-only GPS signals

The urban canyon environment with large buildings having smooth glass and steel surfaces is very problematic for GPS positioning and navigation because of measurement blunders due to multipath and echo-only signals. It is intuitive from **Figure 3.3** that the incidence of outliers is a function of elevation angle. High elevation satellites are unlikely to suffer from much multipath tracking error and are also unlikely to be tracked as an echo only signal. [MacGougan \(2008\)](#) performed extensive testing with

three types of receivers in the downtown cores of two large cities. Pseudorange measurement errors were analyzed as a function of elevation angle and the occurrence of gross outliers decreased with higher elevation angles. While Brodie (2001) and MacGougan (2008) only provide analysis of pseudorange measurements, the likelihood that there is correlation between blunders and elevation angle for carrier-phase measurements is high.

Given that it is difficult to identify blunders in the first measurements used to update the filter and that the incidence of blunders increases as satellite elevation angle decreases, the updates in this filter implementation are ordered from highest to lowest satellite elevation angle.

The pseudorange measurements are added first, followed by the UWB range measurements, and lastly the carrier-phase measurements are used to update the filter.

3.6 Differencing the single-difference solution

In order to apply the LAMBDA method, double-difference ambiguities are required. Though the LAMBDA method can be applied to any general integer least squares problem, in GPS RTK applications, double differences must be used to insure that the ambiguities are indeed integer. If single difference ambiguities and a receiver clock offset are estimated simultaneously, it is impossible to fully separate the ambiguities and the clock offset. This is the main reason for double differencing of observations, but as shown below the same result can be obtained by differencing the ambiguity states. To obtain double-difference ambiguities, the single-difference float filter solution ($\hat{\mathbf{x}}_{sd}$) is differenced using the following operation to obtain the double-difference solution

$(\hat{\mathbf{x}}_{\text{dd}})$.

$$\hat{\mathbf{x}}_{\text{dd}} = \mathbf{D}\hat{\mathbf{x}}_{\text{sd}}$$

$$\mathbf{D} = \begin{bmatrix} 1 & 0 & 0 & 0 & 0 & 0 & 0 & 0 & 0 & 0 & 0 & 0 \dots \\ 0 & 1 & 0 & 0 & 0 & 0 & 0 & 0 & 0 & 0 & 0 & 0 \dots \\ 0 & 0 & 1 & 0 & 0 & 0 & 0 & 0 & 0 & 0 & 0 & 0 \dots \\ 0 & 0 & 0 & 0 & 1 & 0 & 0 & 0 & 0 & 0 & 0 & 0 \dots \\ 0 & 0 & 0 & 0 & 0 & 1 & 0 & 0 & 0 & 0 & 0 & 0 \dots \\ 0 & 0 & 0 & 0 & 0 & 0 & 1 & 0 & 0 & 0 & 0 & 0 \dots \\ 0 & 0 & 0 & 0 & 0 & 0 & 0 & 1 & 0 & 0 & 0 & 0 \dots \\ 0 & 0 & 0 & 0 & 0 & 0 & 0 & 0 & 1 & 0 & 0 & 0 \dots \\ 0 & 0 & 0 & 0 & 0 & 0 & 0 & 0 & 0 & 1 & 0 & 0 \dots \\ 0 & 0 & 0 & 0 & 0 & 0 & 0 & 0 & 0 & 0 & 0 & \mathbf{B} \end{bmatrix} \quad (3.30)$$

$$\mathbf{B} = \begin{bmatrix} -1 & 1 & 0 & 0 & \dots & 0 \\ -1 & 0 & 1 & 0 & \dots & 0 \\ -1 & 0 & 0 & 1 & \dots & 0 \\ \vdots & \vdots & \vdots & 0 & \dots & 1 \dots & 0 \\ -1 & 0 & 0 & 0 & \dots & 1 \end{bmatrix}$$

This operation removes the single-difference GPS clock state and differences the ambiguity states between a common ambiguity. The covariance matrix of the single-difference solution ($\mathbf{P}_{\text{sd}} = \mathbf{P}_{\mathbf{k}}^+$) is transformed into the covariance matrix for the double-difference solution (\mathbf{P}_{dd}) by:

$$\mathbf{P}_{\text{dd}} = \mathbf{D}\mathbf{P}_{\text{sd}}\mathbf{D}^T \quad (3.31)$$

The advantages of this method of differencing the single-difference solution include:

- the ability to update the extended Kalman filter sequentially (uncorrelated measurements);
- the ability to perform innovation testing using an ordered strategy from highest to lowest elevation; satellites (i.e. with increasing likelihood of a blunder and increasing ability to detect a blunder);
- simple implementation with much less housekeeping in the C/C++ source code;
- and very computationally efficient.

The main disadvantage of this approach is that the uncertainty in the single-difference GPS receiver clock offset affects the ability to detect measurement blunders until the clock offset is observed. This is an area for improvement in the method as discussed in **Section 3.5.1**.

3.7 Ambiguity resolution

Real-time kinematic positioning with GPS utilizes double-differenced carrier-phase observations and solving the associated unknown integer valued carrier-phase ambiguities. This is well described in GPS texts such as [Misra and Enge \(2004\)](#) and is only briefly introduced herein.

After the double-difference float solution is computed, the goal is to find the best set of integer ambiguity values. The optimal choice is the set of integer ambiguities which minimizes the norm of the difference between the float and integer ambiguities scaled by the covariance matrix of the float ambiguities.

$$\chi_{\min}^2 = \min_{\check{\mathbf{a}} \in \mathbb{Z}} ((\hat{\mathbf{a}} - \check{\mathbf{a}})^T \mathbf{Q}_{\hat{\mathbf{a}}}^{-1} (\hat{\mathbf{a}} - \check{\mathbf{a}})) \quad (3.32)$$

where χ_{\min}^2 is the smallest quadratic sum-of-squares, $\hat{\mathbf{a}}$ is the vector of float ambiguities, $\tilde{\mathbf{a}}$ is the vector of integer ambiguities, and $\mathbf{Q}_{\hat{\mathbf{a}}}$ is the covariance matrix of the float double-difference ambiguities (a block submatrix of \mathbf{P}_{dd}). This method is referred to as integer least squares search. A search is required because there is no explicit mathematical method to resolve the optimal integer vector.

The LAMBDA method provides a very efficient method to resolve the integer least squares solution (Teunissen (1993) and DeJonge and Tiberius (1996)). The method involves decorrelation of the original set of ambiguities by means of a permissible transformation (\mathbf{Z}) which preserves the integer nature of the ambiguities and has a determinant of one (i.e. volume of the search space is equivalent). The transformation is given by:

$$\begin{aligned}\hat{\mathbf{z}} &= \mathbf{Z}^T \hat{\mathbf{a}} \\ \mathbf{Q}_{\hat{\mathbf{z}}} &= \mathbf{Z}^T \mathbf{Q}_{\hat{\mathbf{a}}} \mathbf{Z}\end{aligned}\tag{3.33}$$

Following decorrelation, the search is performed in the transformed space (z-space) to find the optimal integer vector. The LAMBDA method does not change the solution but reduces the size of the search space. The minimum norm in z-space is given by:

$$\chi_{\min}^2 = \min_{\tilde{\mathbf{z}} \in \mathbb{Z}} ((\hat{\mathbf{z}} - \tilde{\mathbf{z}})^T \mathbf{Q}_{\hat{\mathbf{z}}}^{-1} (\hat{\mathbf{z}} - \tilde{\mathbf{z}}))\tag{3.34}$$

3.7.1 Integer ambiguity validation

It is very important that integer ambiguities are validated before presenting a solution conditioned on the integer values. An incorrect fixed integer solution can introduce a decimetre to metre level position error. A common method to validate the integer ambiguities uses a fixed threshold value ratio test. This method is often empirical and ad-hoc based on testing experience. Verhagen (2004) discusses some of the different ratio tests and problems associated with these methods. In addition to the ratio test, it is important to compute the probability of correct fix (PCF). The PCF should be

high (very close to 1.0) to deem to ambiguities valid for use in fixing. The PCF cannot be computed easily for integer least squares; however, a useful lower bound is available using the probability of correct fix using bootstrapping (after the LAMBDA decorrelation step) [Teunissen \(1998\)](#). This research employs a practical and slightly conservative approach to ambiguity validation using a fixed ratio test and a PCF test. For more rigorous ambiguity validation consult [Teunissen and Verhagen \(2008\)](#).

The so-called F-ratio test is often used to validate integer ambiguity search procedures ([Counselman and Abbot, 1989](#)). The ratio test indicates relative strength, in terms of the *closeness* of the fixed solution to the float solution, of the best set of integer ambiguities compared to the second best set obtained during the least squares search. The ratio value is given by

$$F = \frac{\Omega + (\hat{\mathbf{a}} - \check{\mathbf{a}}_1)^T \mathbf{Q}_{\hat{\mathbf{a}}}^{-1} (\hat{\mathbf{a}} - \check{\mathbf{a}}_1)}{\Omega + (\hat{\mathbf{a}} - \check{\mathbf{a}}_0)^T \mathbf{Q}_{\hat{\mathbf{a}}}^{-1} (\hat{\mathbf{a}} - \check{\mathbf{a}}_0)} \quad (3.35)$$

$$\Omega = \hat{\mathbf{r}}^T \mathbf{P}_{\text{dd}} \hat{\mathbf{r}}$$

where $\hat{\mathbf{r}}$ is the vector of double-difference carrier-phase residuals ($\hat{r} = \nabla \Delta \Phi - \nabla \Delta \hat{\Phi}$), $\hat{\mathbf{a}}_1$ is the second best set of integer ambiguities and $\hat{\mathbf{a}}_0$ is the best set of integer ambiguities (based on the minimum quadratic norm achieved).

The probability of correct fix for bootstrapping ([Teunissen, 1998](#)) is given by:

$$P(\check{\mathbf{a}}_{\mathbf{B}} = \mathbf{a}) = \prod_{i=1}^n \left(2 \Phi \left(\frac{1}{2\sigma_{\hat{\mathbf{a}}_{i|I}}} \right) - 1 \right) \quad (3.36)$$

$$\Phi(y) = \frac{1}{2} \operatorname{erfc} \left(\frac{-y}{\sqrt{2}} \right)$$

where $\Phi(y)$ is an alternate form for the cumulative distribution function of the normal distribution, $\hat{\mathbf{a}}_B$ is the vector of bootstrapped integer ambiguities, $\sigma_{\hat{\mathbf{a}}_{i|I}}$ is the variance of the i^{th} ambiguity obtained through a conditioning on the previous $I = \{1, \dots, (i-1)\}$ sequentially rounded ambiguities.

3.7.2 Computing the fixed solution

Once the set of integer ambiguities is deemed valid, the fixed solution and its covariance matrix is computed by the following (DeJonge and Tiberius, 1996):

$$\begin{aligned}
 \check{\mathbf{b}} &= \hat{\mathbf{b}} - \mathbf{Q}_{\hat{\mathbf{b}}\hat{\mathbf{a}}} \mathbf{Q}_{\hat{\mathbf{a}}}^{-1} (\hat{\mathbf{a}} - \check{\mathbf{a}}) \\
 \mathbf{Q}_{\check{\mathbf{b}}} &= \mathbf{Q}_{\hat{\mathbf{b}}} - \mathbf{Q}_{\hat{\mathbf{b}}\hat{\mathbf{a}}} \mathbf{Q}_{\hat{\mathbf{a}}}^{-1} \mathbf{Q}_{\hat{\mathbf{a}}\hat{\mathbf{b}}} + \mathbf{Q}_{\hat{\mathbf{b}}\hat{\mathbf{a}}} \mathbf{Q}_{\hat{\mathbf{a}}}^{-1} \mathbf{Q}_{\check{\mathbf{a}}} \mathbf{Q}_{\hat{\mathbf{a}}}^{-1} \mathbf{Q}_{\hat{\mathbf{a}}\hat{\mathbf{b}}} \\
 \mathbf{Q}_{\check{\mathbf{b}}}^* &\approx \mathbf{Q}_{\hat{\mathbf{b}}|\check{\mathbf{a}}} = \mathbf{Q}_{\hat{\mathbf{b}}} - \mathbf{Q}_{\hat{\mathbf{b}}\hat{\mathbf{a}}} \mathbf{Q}_{\hat{\mathbf{a}}}^{-1} \mathbf{Q}_{\hat{\mathbf{a}}\hat{\mathbf{b}}} \\
 \hat{\mathbf{x}}_{\text{dd}} &= \begin{bmatrix} \hat{\mathbf{b}} \\ \hat{\mathbf{a}} \end{bmatrix} \\
 \mathbf{P}_{\text{dd}} &= \begin{bmatrix} \mathbf{Q}_{\hat{\mathbf{b}}} & \mathbf{Q}_{\hat{\mathbf{b}}\hat{\mathbf{a}}} \\ \mathbf{Q}_{\hat{\mathbf{a}}\hat{\mathbf{b}}} & \mathbf{Q}_{\hat{\mathbf{a}}} \end{bmatrix}
 \end{aligned} \tag{3.37}$$

* $\mathbf{Q}_{\hat{\mathbf{b}}\hat{\mathbf{a}}} \mathbf{Q}_{\hat{\mathbf{a}}}^{-1} \mathbf{Q}_{\check{\mathbf{a}}} \mathbf{Q}_{\hat{\mathbf{a}}}^{-1} \mathbf{Q}_{\hat{\mathbf{a}}\hat{\mathbf{b}}}$ is often neglected in practice (Teunissen, 1989b) because it is assumed that the fixed ambiguities are perfectly known quantities

where \mathbf{b} is the vector of non-ambiguity states of the double-difference state vector, \mathbf{a} is the vector of the double-difference ambiguity states, and $\mathbf{Q}_{\hat{\mathbf{b}}}$, $\mathbf{Q}_{\hat{\mathbf{b}}\hat{\mathbf{a}}}$, $\mathbf{Q}_{\hat{\mathbf{a}}\hat{\mathbf{b}}}$, and $\mathbf{Q}_{\hat{\mathbf{a}}}$ are the associated sub-matrices of the double-difference covariance matrix.

3.7.3 Partial fixing

There is no requirement to fix the ambiguities, $\hat{\mathbf{a}}$, in the original ambiguity space (a-space), compared to fixing the ambiguities, $\hat{\mathbf{z}}$, in the transformed ambiguity space (z-space). There is also no requirement to fix *all* ambiguities in either space. The reason for partial fixing is that the PCF and ratio tests may not validate a fully fixed solution but will validate a partially fixed solution. A simple method of partial fixing is based on the bootstrapped probability of a correct fix in z-space.

The decorrelation step in LAMBDA results in an generally ordered (but not perfectly ordered) covariance matrix from the most precise to the least precise. If $\mathbf{Q}_{\hat{\mathbf{z}}}$ is given by

$$\mathbf{Q}_{\hat{\mathbf{z}}} = \begin{bmatrix} \sigma_{z_0}^2 & \sigma_{z_0} \sigma_{z_1} & \dots & \sigma_{z_0} \sigma_{z_n} \\ \sigma_{z_1} \sigma_{z_0} & \sigma_{z_1}^2 & \dots & \sigma_{z_1} \sigma_{z_n} \\ \vdots & \dots & \ddots & \vdots \\ \sigma_{z_{n-1}} \sigma_{z_0} & \dots & \dots & \sigma_{z_{n-1}}^2 \end{bmatrix} \tag{3.38}$$

then $\sigma_{z_{n-1}}^2$ is generally (but not always) less than $\sigma_{z_{n-2}}^2$ and $\sigma_{z_{n-2}}^2$ is generally (but not always) less than $\sigma_{z_{n-3}}^2$ and so on. This means that the z-space ambiguities are ordered in such a fashion that bootstrapping from the n^{th} ambiguity toward the 1^{st} ambiguity will usually result in the most partially fixed ambiguities with the largest PCF.

The procedure is straight forward. The probability of correct fix for bootstrapping (Teunissen, 1998) the z-space ambiguities is given by:

$$P(\check{\mathbf{z}}_{\mathbf{B}} = \mathbf{z}) = \prod_{i=n}^{j, i=i-1} \left(2 \Phi \left(\frac{1}{2\sigma_{\hat{\mathbf{z}}_{i|I}}} \right) - 1 \right) \quad (3.39)$$

where $\hat{\mathbf{z}}_{\mathbf{B}}$ is the vector of bootstrapped integer ambiguities, $\sigma_{\hat{\mathbf{z}}_{i|I}}$ is the variance of the i^{th} ambiguity obtained through a conditioning on the previous $I = \{n, n-1, \dots, j\}$ sequentially rounded ambiguities. The PCF is calculated from the n^{th} to the j^{th} ambiguities and when the threshold PCF is exceeded, the set of partially fixed ambiguities is known. The integer search is performed and if the ratio test passes, the solution is conditioned based on the subset of fixed ambiguities in z-space. If the ratio test fails, the set is reduced by one ambiguity and the process is repeated.

Equation 3.37 can be transformed easily such that it pertains to the z-space ambiguities and $\check{\mathbf{z}}_{\mathbf{s}}$ contains the set of fixed ambiguities and $\check{\mathbf{b}}_{\mathbf{z}}$ includes the ambiguities which are not to be fixed ($\check{\mathbf{z}}_{\text{nf}}$).

$$\begin{aligned} \check{\mathbf{b}}_{\mathbf{z}} &= \hat{\mathbf{b}}_{\mathbf{z}} - \mathbf{Q}_{\hat{\mathbf{b}}_{\mathbf{z}}\hat{\mathbf{z}}_{\mathbf{s}}} \mathbf{Q}_{\hat{\mathbf{z}}_{\mathbf{s}}}^{-1} (\hat{\mathbf{z}}_{\mathbf{s}} - \check{\mathbf{z}}_{\mathbf{s}}) \\ \mathbf{Q}_{\check{\mathbf{b}}_{\mathbf{z}}} &\approx \mathbf{Q}_{\hat{\mathbf{b}}_{\mathbf{z}}|\check{\mathbf{z}}_{\mathbf{s}}} = \mathbf{Q}_{\hat{\mathbf{b}}_{\mathbf{z}}} - \mathbf{Q}_{\hat{\mathbf{b}}_{\mathbf{z}}\hat{\mathbf{z}}_{\mathbf{s}}} \mathbf{Q}_{\hat{\mathbf{z}}_{\mathbf{s}}}^{-1} \mathbf{Q}_{\hat{\mathbf{z}}_{\mathbf{s}}\hat{\mathbf{b}}_{\mathbf{z}}} \\ \hat{\mathbf{x}}_{\text{dd}} &= \begin{bmatrix} \hat{\mathbf{b}} \\ \hat{\mathbf{a}} \end{bmatrix} = \begin{bmatrix} \hat{\mathbf{b}} \\ \mathbf{Z}^T \hat{\mathbf{a}} \end{bmatrix} = \begin{bmatrix} \hat{\mathbf{b}} \\ \hat{\mathbf{z}} \end{bmatrix} \\ \hat{\mathbf{z}} &= \begin{bmatrix} \hat{\mathbf{z}}_{\text{nf}} \\ \hat{\mathbf{z}}_{\mathbf{s}} \end{bmatrix} \\ \hat{\mathbf{b}}_{\mathbf{z}} &= \begin{bmatrix} \hat{\mathbf{b}} \\ \hat{\mathbf{z}}_{\text{nf}} \end{bmatrix} \\ \hat{\mathbf{x}}_{\text{dd}} &= \begin{bmatrix} \hat{\mathbf{b}}_{\mathbf{z}} \\ \hat{\mathbf{z}}_{\mathbf{s}} \end{bmatrix} \\ \mathbf{P}_{\text{dd}} &= \begin{bmatrix} \mathbf{Q}_{\hat{\mathbf{b}}} & \mathbf{Q}_{\hat{\mathbf{b}}\hat{\mathbf{a}}} \\ \mathbf{Q}_{\hat{\mathbf{a}}\hat{\mathbf{b}}} & \mathbf{Q}_{\hat{\mathbf{a}}} \end{bmatrix} = \begin{bmatrix} \mathbf{Q}_{\hat{\mathbf{b}}} & \mathbf{Q}_{\hat{\mathbf{b}}\hat{\mathbf{a}}}\mathbf{Z} \\ \mathbf{Z}^T \mathbf{Q}_{\hat{\mathbf{a}}\hat{\mathbf{b}}} & \mathbf{Z}^T \mathbf{Q}_{\hat{\mathbf{a}}}\mathbf{Z} \end{bmatrix} = \begin{bmatrix} \mathbf{Q}_{\hat{\mathbf{b}}} & \mathbf{Q}_{\hat{\mathbf{b}}\hat{\mathbf{z}}} \\ \mathbf{Q}_{\hat{\mathbf{z}}\hat{\mathbf{b}}} & \mathbf{Q}_{\hat{\mathbf{z}}} \end{bmatrix} = \begin{bmatrix} \mathbf{Q}_{\hat{\mathbf{b}}_{\mathbf{z}}} & \mathbf{Q}_{\hat{\mathbf{b}}_{\mathbf{z}}\hat{\mathbf{z}}_{\mathbf{s}}} \\ \mathbf{Q}_{\hat{\mathbf{z}}_{\mathbf{s}}\hat{\mathbf{b}}_{\mathbf{z}}} & \mathbf{Q}_{\hat{\mathbf{z}}_{\mathbf{s}}} \end{bmatrix} \end{aligned} \quad (3.40)$$

3.7.4 When and how to fix ambiguities

Using the methods described herein, the decision to fully fix ambiguities or partially fix ambiguities depends on the research topic in question. The filter is set up to perform the ambiguity resolution on an epoch-by-epoch basis. It can also propagate previously determined (at an earlier epoch) fixed ambiguities and ignore the results of the epoch-by-epoch output. In the results chapters to follow, the specific methods used will be stated explicitly.

3.8 Testing overview

The following chapters use the apparatus and the estimation method described in this chapter. Chapter 4 provides the results of static and kinematic testing in a degraded GPS signal environment created artificially by excluding GPS satellites from the solution using elevation masking. The bias and scale factor values are first calibrated by post-processing and the improvement in RTK using tight-coupling of GPS and UWB is analyzed. The ability to estimate the bias and scale factor values in the filter is then examined. Chapter 5 then assesses the feasibility of the tight-coupled approach of combining GPS and UWB measurements for RTK surveying in a realistic urban canyon environment.

Chapter 4

Tightly-coupled GPS/UWB testing

This chapter presents results for static and kinematic testing using an artificially high satellite elevation mask to create a challenging GPS environment. This allows the GPS-only RTK solution obtained with a nominal elevation mask of 13° to be used as a benchmark for comparison. The initial testing results are obtained only with the MSSSI UWB radios as there were difficulties obtaining more than one range pair from the TDC UWB radios. This was resolved for the testing presented in the next chapter where a more realistic challenging GPS environment was used.

4.1 Static testing

Trimble R8 GPS and MSSSI UWB range data was collected at a static point at the University of Calgary as shown in **Figure 4.1**. The static point was surrounded by three UWB reference ranging transceivers that were set up at pre-established surveyed positions. The GPS base station was located approximately 140 m away on the roof of the engineering building. This test assesses the performance of RTK using GPS only and combined GPS with UWB ranges for four minutes using a 13° elevation mask angle. The UWB bias and scale factor errors were pre-determined by post-processing and were not estimated by the filter in this case.

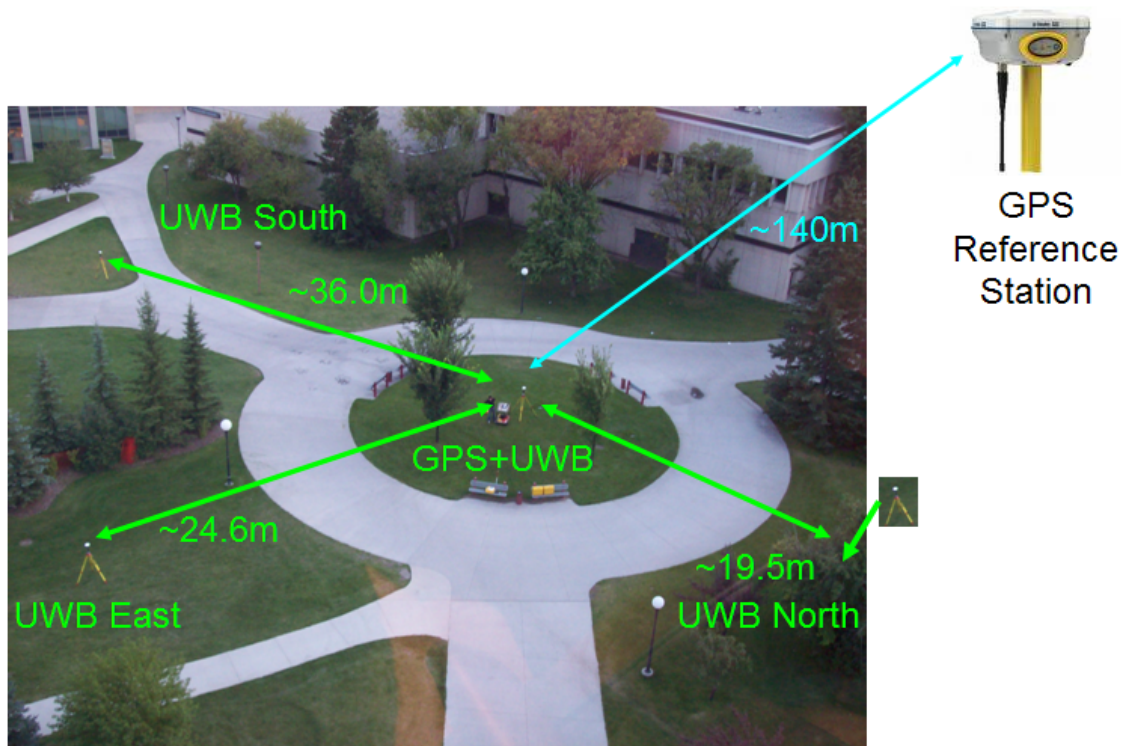


Figure 4.1: Static GPS+UWB RTK test site photo

4.1.1 Results with 13 degree elevation mask

The number of available GPS satellites and UWB range measurements are shown in **Figure 4.2** along with the resulting horizontal dilution of precision (HDOP) and vertical dilution of precision (VDOP) values using GPS-only and GPS+UWB. The UWB reference stations and the test station are on a horizontal plane and thus the HDOP was improved directly by the additional observations. VDOP also improves since less of the GPS observation set is required to estimate the horizontal position and can thus contribute more to the vertical solution.

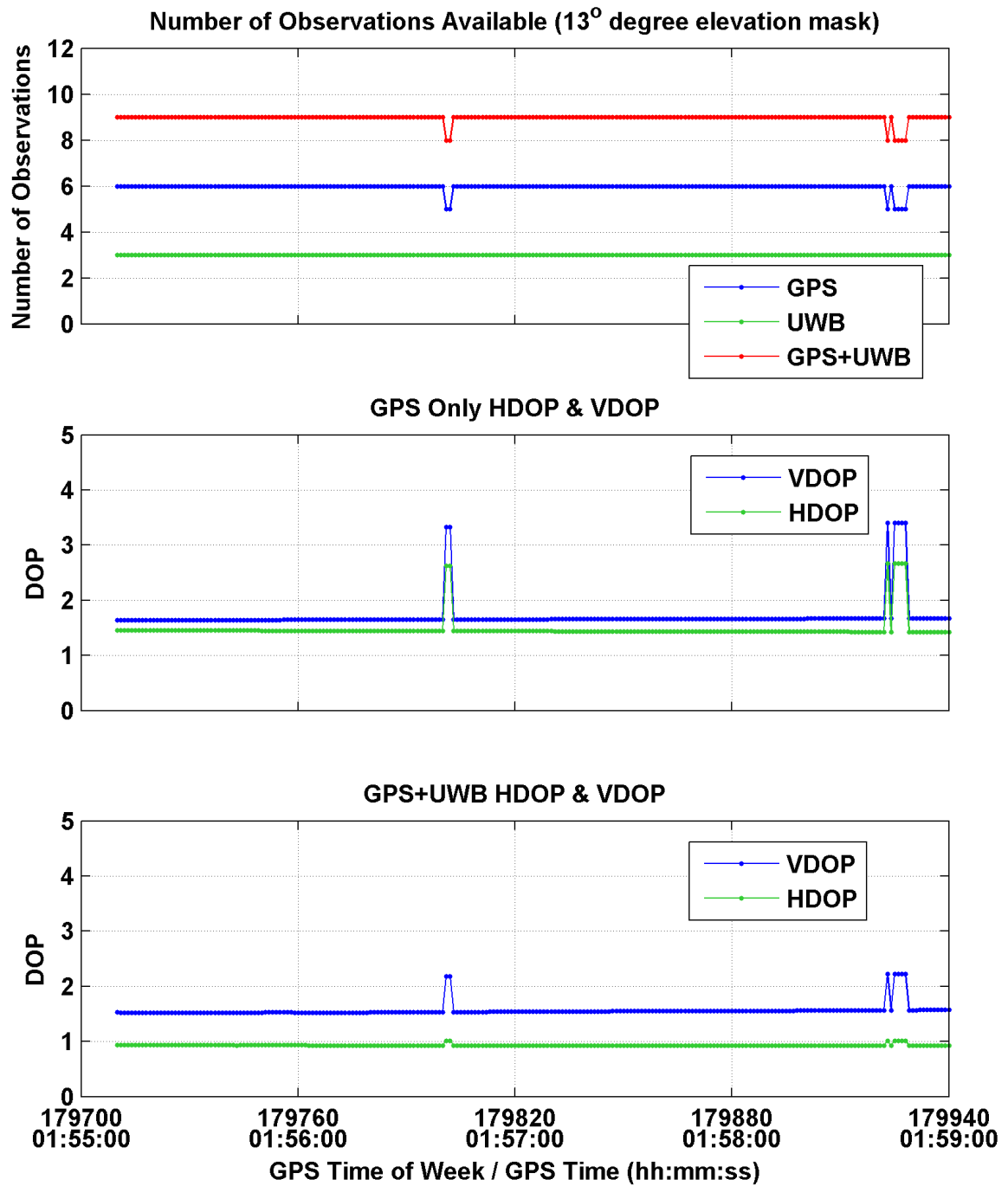


Figure 4.2: Static test: number of observations and DOP (13° mask)

The float solution position errors are shown in **Figure 4.3**. The GPS-only solution has errors close to half a metre. The GPS+UWB solution has sub-decimetre level accuracy in this case because the UWB bias and scale factor errors are well calibrated.

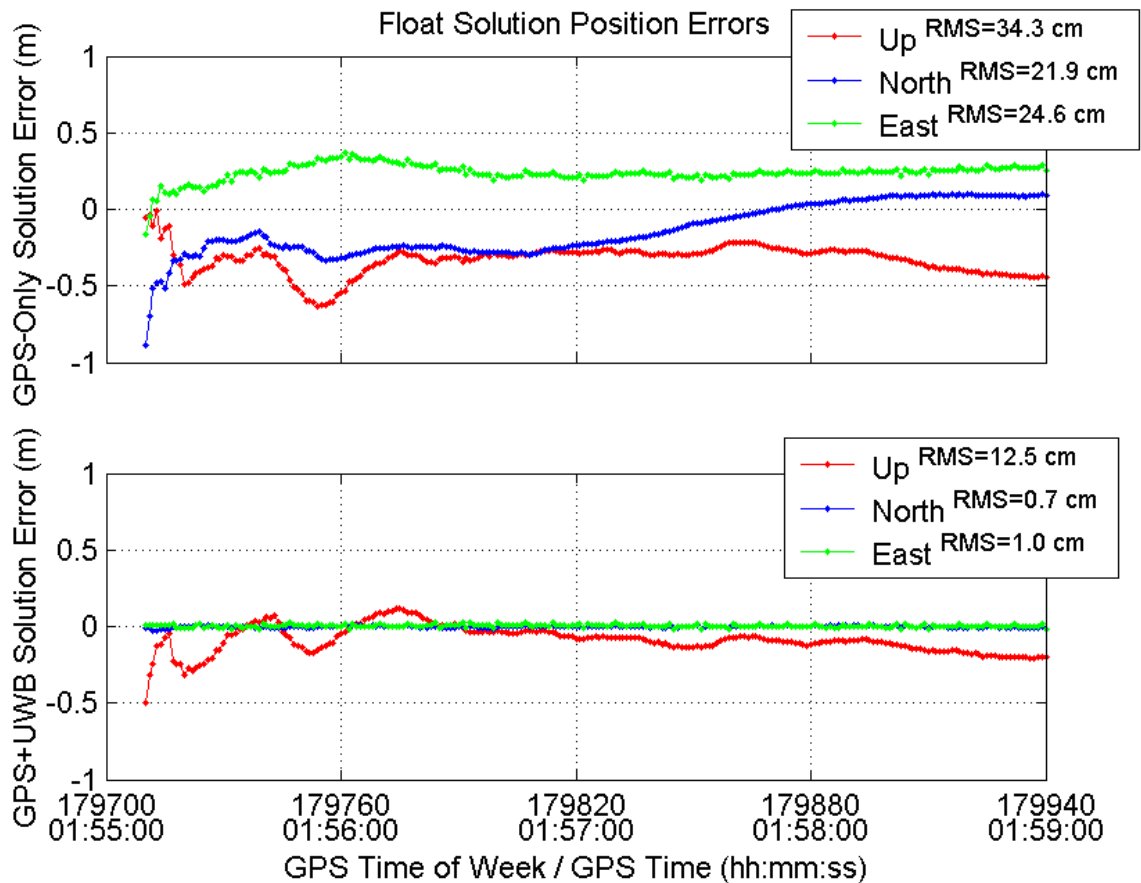


Figure 4.3: Static test: float solution (13° mask)

The difference between the float solution double-differenced carrier phase ambiguity estimates and the known fixed double-differenced ambiguity values are shown in **Figure 4.4**. There is clearly improvement in the ambiguity convergence time with the inclusion of the UWB ranges. This is clearly shown in the figure with difference values closer to zero in general for the GPS+UWB solution compared to the GPS-only solution.

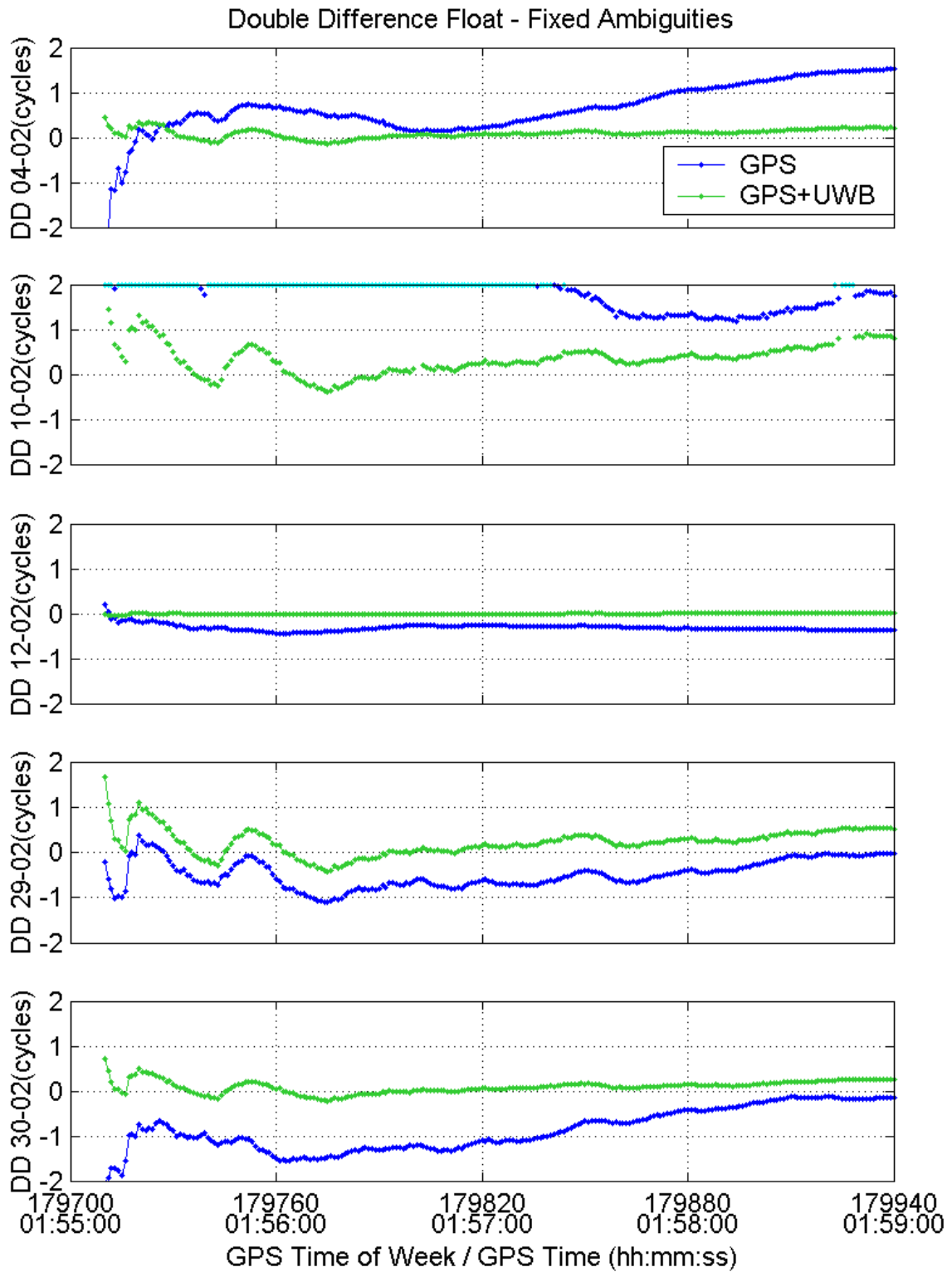


Figure 4.4: Static test: float ambiguity estimates (13° mask)

The LAMBDA method was applied to the float solution at every epoch (i.e. epoch by epoch ambiguity fixing) by first double differencing the estimated single-difference float ambiguities. This approach is identical to double differencing the observations as any residual clock effect on the single-difference ambiguities is canceled in the differencing process. With such a short baseline, and good DOP, both the GPS and GPS+UWB solutions are able to fix ambiguities correctly. The resulting fixed solution position errors are shown in **Figure 4.5**. The accuracy obtained after fixing correctly is identical and driven by the precision of the carrier phase measurement. The GPS+UWB solution fixed ambiguities correctly on the first epoch. The GPS only solution required 12 s to fix correctly.

The F-ratio test (given in **Equation 3.35**) was often used to validate integer ambiguities with a critical value of 2.0 (e.g. [Euler and Landau \(1996\)](#)). The ratio values computed at each epoch for the GPS only and GPS+UWB solutions are shown in **Figure 4.5**. The ratio values achieved for the GPS-only and the GPS+UWB solutions both provide strong confidence in the ambiguity set found compared to the second best set. The GPS+UWB ratio values are much larger than those of the GPS only solution and, therefore, the relative confidence is much higher.

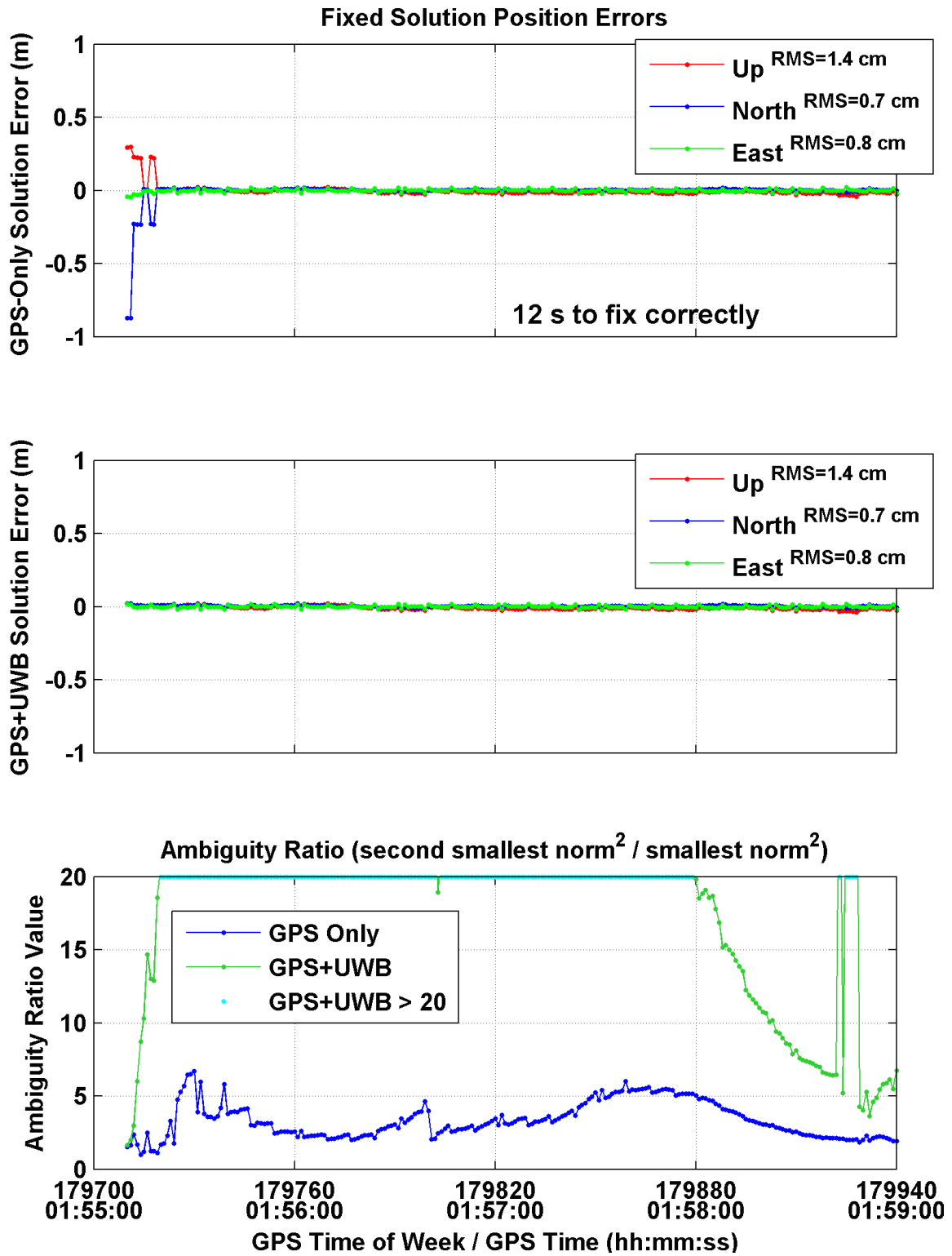


Figure 4.5: Static test: fixed solution (13° mask)

The probability of correct fix was determined on an epoch by epoch basis using **Equation 3.36** and is shown in **Figure 4.6**. The tightly-coupled solution reaches a high probability value very quickly (i.e. within 20 s) whereas it takes more than two minutes for the GPS-only solution to achieve the same confidence. The initial sawtooth behaviour of the GPS-only PCF values is due to changes in the LAMBDA Z transformation (which changes the set of z-space ambiguities used in calculating the bootstrapped PCF value). This behaviour was expected and has been previously described by O'Keefe et al. (2007).

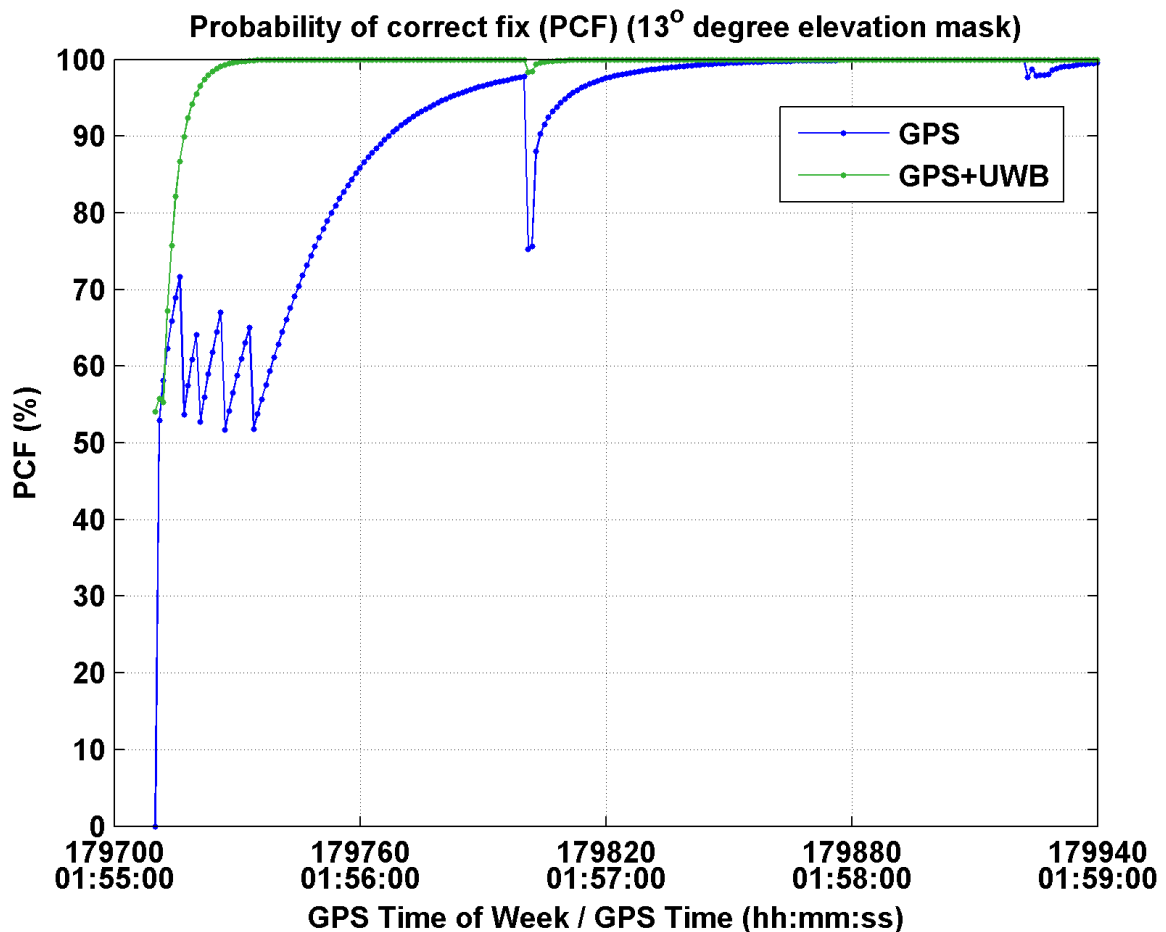


Figure 4.6: Static test: fixed solution probability of correct fix (13° mask)

4.1.2 Results with a 40 degree elevation mask

The static data was reprocessed using a 40° elevation mask to simulate RTK operation in an urban canyon or perhaps a deep open pit mine. The number of satellites available and the number of UWB range measurements available are shown in **Figure 4.7**. Only 4 satellites are available and thus the GPS only solution has no redundancy. The resulting DOP values are also shown in **Figure 4.7**. The GPS only solution has very poor DOP values whereas the GPS+UWB solution still has reasonable HDOP while VDOP is somewhat poor.

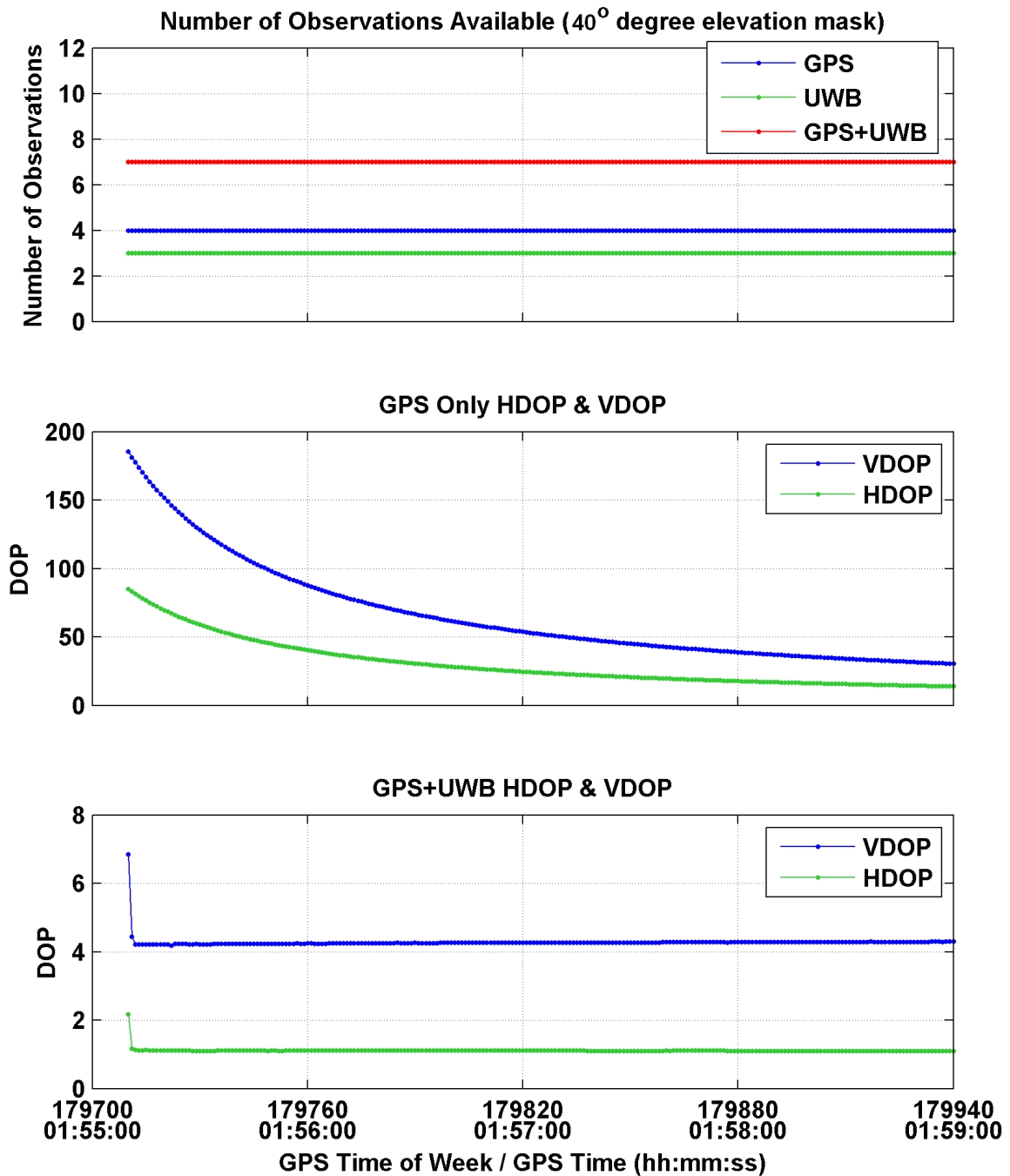


Figure 4.7: Static test: number of observations and DOP (40° mask)

The float solution position errors are shown in **Figure 4.8**. The GPS+UWB horizontal position still has sub-decimetre accuracy. It takes nearly a minute for the GPS only solution to converge to sub-metre level accuracy.

The differences between the float solution double differenced carrier phase ambiguity estimates and the known fixed double differenced ambiguity values are shown in **Figure 4.9**. The double difference ambiguities all converge to within half a cycle of the true values for the GPS+UWB solution. The GPS only ambiguities are off by 1 to 2 cycles after 4 minutes.

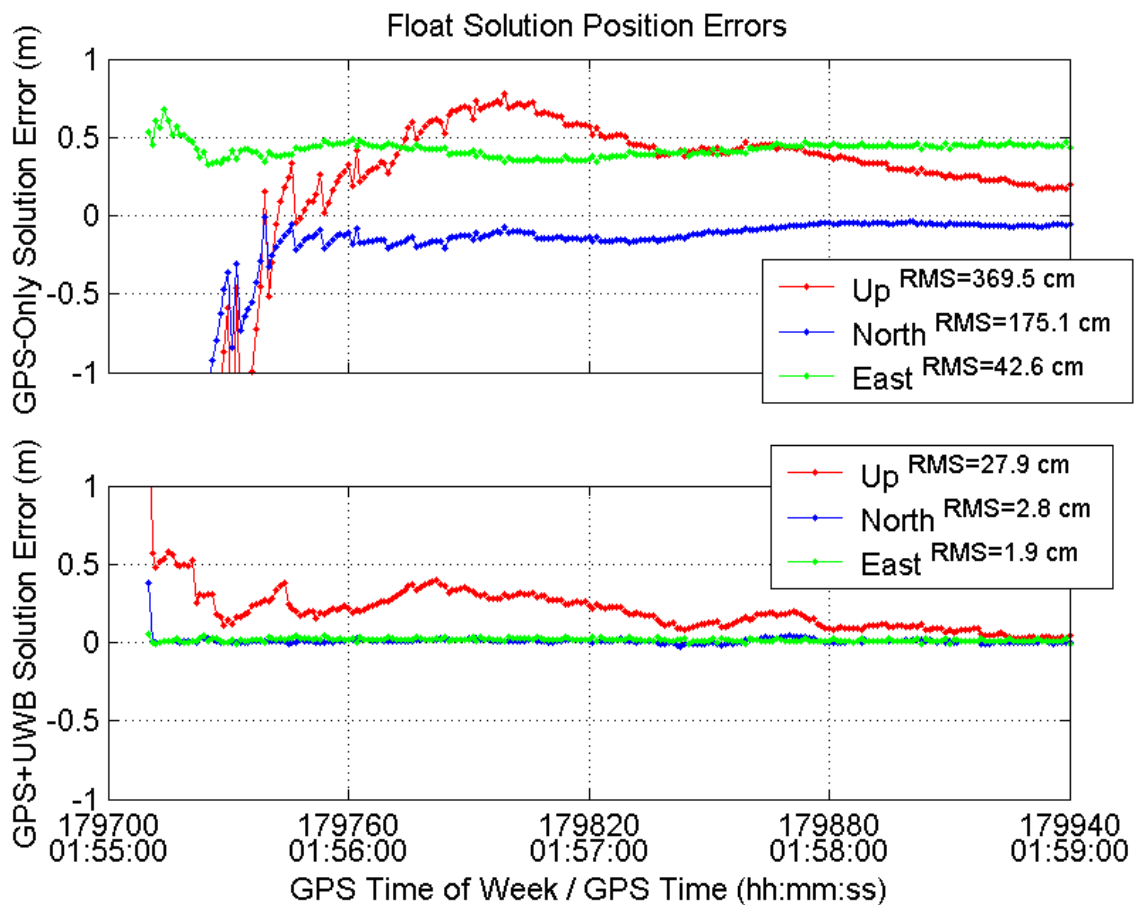


Figure 4.8: Static test: float solution (40° mask)

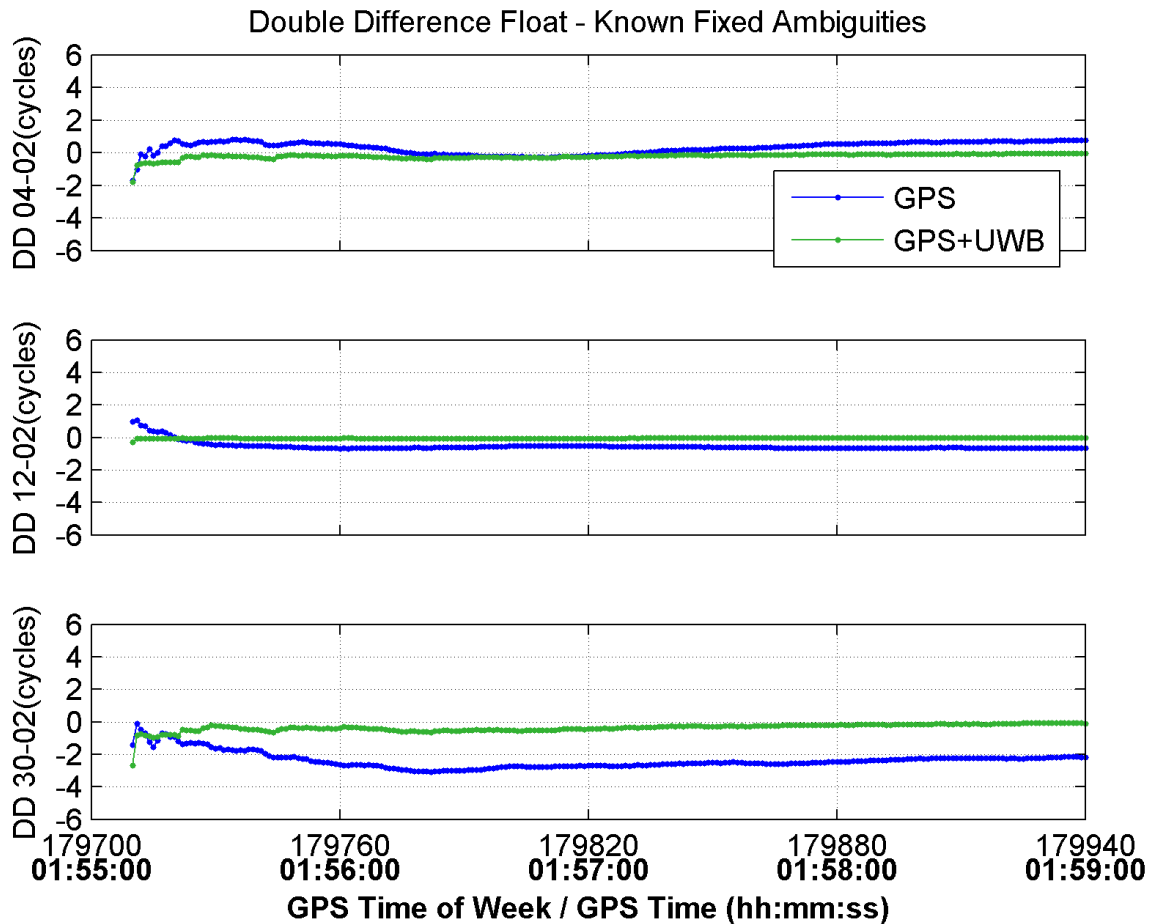


Figure 4.9: Static test: float ambiguities (40° mask)

The LAMBDA method was applied to the float solution at every epoch (i.e. epoch by epoch ambiguity fixing). The resulting fixed solution position errors are shown in **Figure 4.10**. The GPS+UWB solution fixes correctly after 12 s. The GPS only solution rarely fixes correctly during the test. It should be noted that in the GPS only case, the fixed solution is displayed even though it fails the validation test. Throughout, different incorrect ambiguity sets are selected as shown by the biased, but precise, position solutions. The discontinuities in the solution correspond to changes in the integer estimate.

This is reflected by the ratio test values shown in **Figure 4.10**. The GPS+UWB solution ratio values are well above 2.0 after 12 s whereas the GPS only solution fails to reach suitable values to justify integer solution validity.

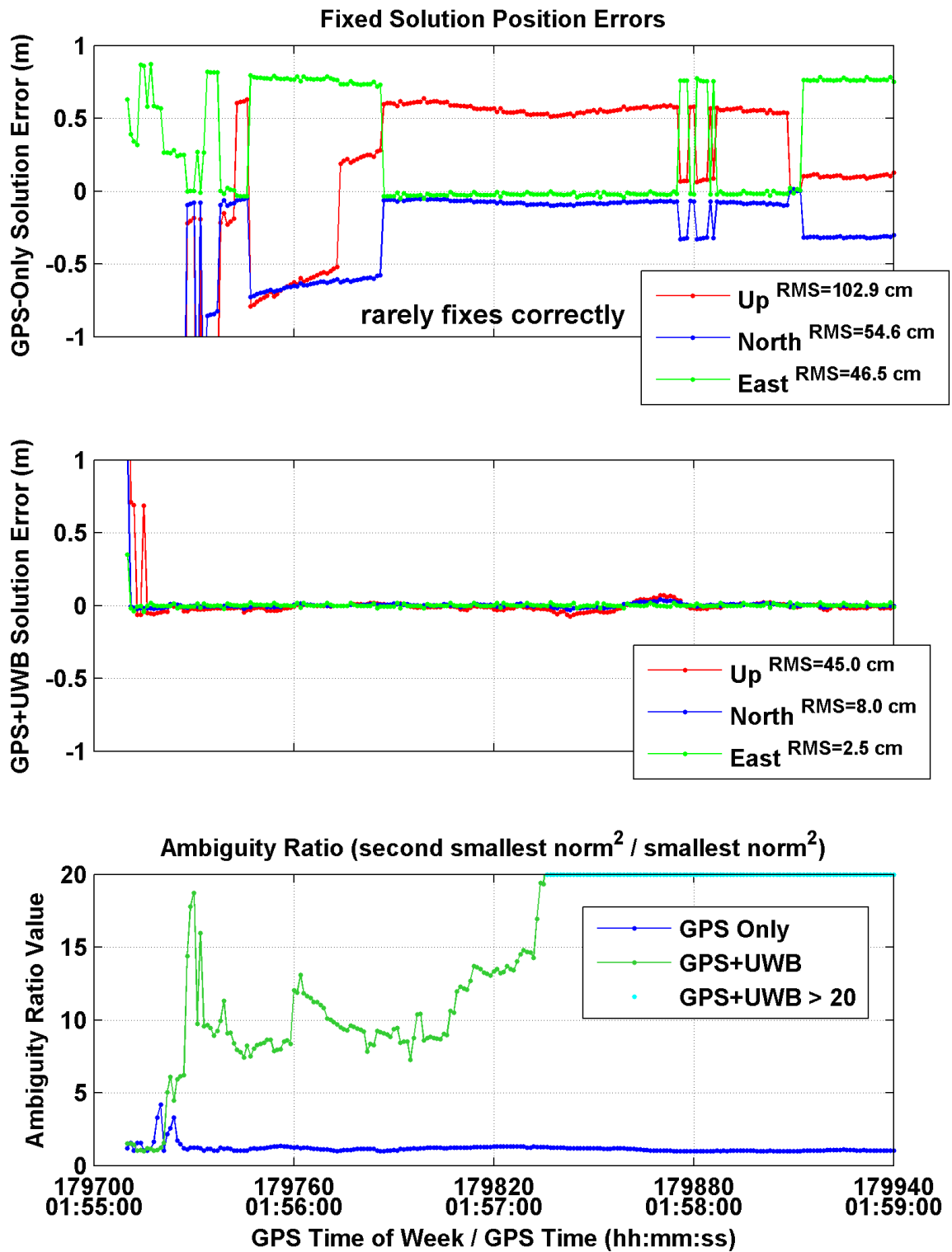


Figure 4.10: Static test: fixed solution (40° mask)

The probability of correct fix was again determined on an epoch by epoch basis using **Equation 3.36** and is shown in **Figure 4.11**. The tightly-coupled solution reaches a high probability value (99%) after three minutes whereas the GPS-only solution does not exceed a PCF of 35% after 4 minutes.

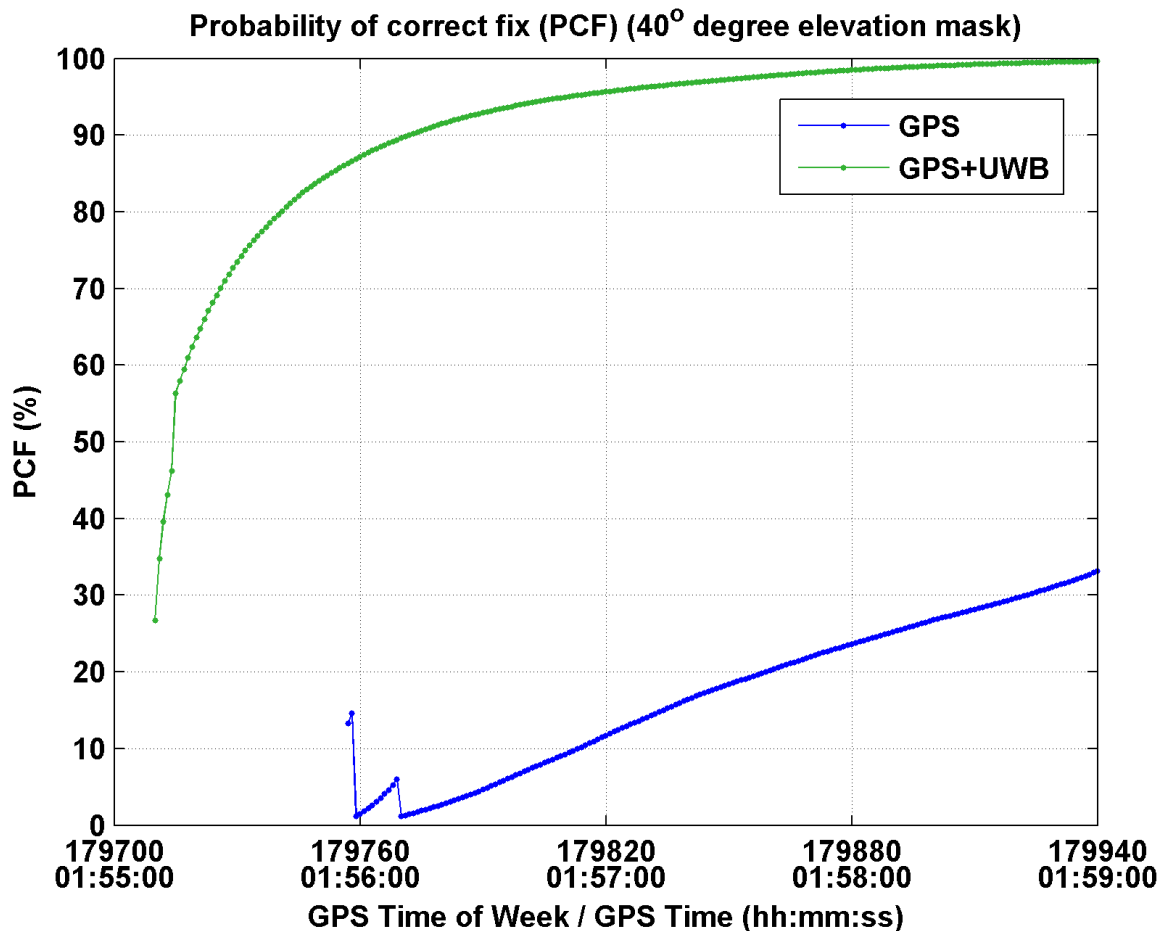


Figure 4.11: Static test: fixed solution probability of correct fix (40° mask)

Tables 4.1 and **4.2** provide a quantitative summary of the performance of the tightly-coupled GPS+UWB solution compared to the GPS-only solution for the case given the 40° elevation mask. The tables provide results for both the float solution and the epoch-by-epoch fixed solution. The GPS-only fixed solution does not provide any

improvement compared to the float solution because it fails to correctly determine the integer ambiguities. The GPS+UWB fixed solution statistics are computed after the solution has fixed correctly. In this case, the tightly coupled solution performs at the level normally expected of commercial RTK systems in open sky conditions.

Table 4.1: Comparison of Horizontal Errors for the Static Test (40° Elevation Mask)

	Float Solution GPS-Only (m)	Float Solution GPS+UWB (m)	Fixed Solution GPS-Only (m)	Fixed Solution GPS+UWB (m)
Max	10.744	0.053	11.819	0.044
Mean	0.830	0.022	0.793	0.011
1 σ	1.603	0.010	1.606	0.008
RMS	1.802	0.024	1.788	0.014

Table 4.2: Comparison of Vertical Errors for the Static Test (40° Elevation Mask)

	Float Solution GPS-Only (m)	Float Solution GPS+UWB (m)	Fixed Solution GPS-Only (m)	Fixed Solution GPS+UWB (m)
Max	0.778	2.353	0.637	0.072
Min	-21.905	0.020	-23.900	-0.073
Mean	-0.580	0.209	-0.686	-0.008
1 σ	3.657	0.186	3.531	0.024
RMS	3.695	0.279	3.590	0.025

4.2 Kinematic testing

The objective of kinematic testing is two-fold. Firstly, the ability to estimate UWB bias and scale factor states on-the-fly is assessed. It is expected that the error levels are sufficiently stable during a typical survey (while continuous power is maintained) to result in decimetre level range accuracy after error compensation. The high positioning accuracy of GPS RTK (e.g. 2 cm) under nominal conditions is used to facilitate the estimation of the UWB bias and scale factor states. Once these states are well estimated, the corrected UWB range measurements can enable and extend RTK accuracy into conditions that are hostile to GPS alone. Thus, the second objective of dynamic testing is to assess the performance of the combined system once the bias and scale factor states are well estimated.

Three MSS1 UWB reference stations, labeled 7, 8, and 9 in **Figure 4.12**, were set up, in a similar configuration as the static test, within 200 m of a GPS reference station located on the roof of the University of Calgary Engineering building. NovAtel OEM3 type GPS receivers were used for the reference station and the survey receiver.

In order to observe the UWB bias and scale factor states, a range of motion is required with good quality GPS conditions. Once these states are sufficiently estimated, a survey may proceed in degraded GPS signal conditions with the benefit of the corrected UWB measurements.

The test consists of a pre-survey initialization walk followed by walking a circular route on which there are three static test points which were pre-surveyed. This is illustrated in **Figures 4.13**. For the test system, an elevation mask of 40° is applied when entering the survey area.

To obtain a reference trajectory during the entire survey, GPS only results were ob-

tained for the entire test without the 40° elevation mask. Fixed ambiguity GPS-only RTK solutions were obtained using 7 satellites for the duration of the test. The reference test trajectory is shown in **Figure 4.13**.

- A range of motion is required with good RTK solution to observe the bias and scale factor states
- Initialization walk pre survey
7 satellites used ●●●●●●●
- RTK survey
3 satellites used ●●●●●●● (40° elevation mask)
- 3 UWB Ranges



Figure 4.12: The kinematic test

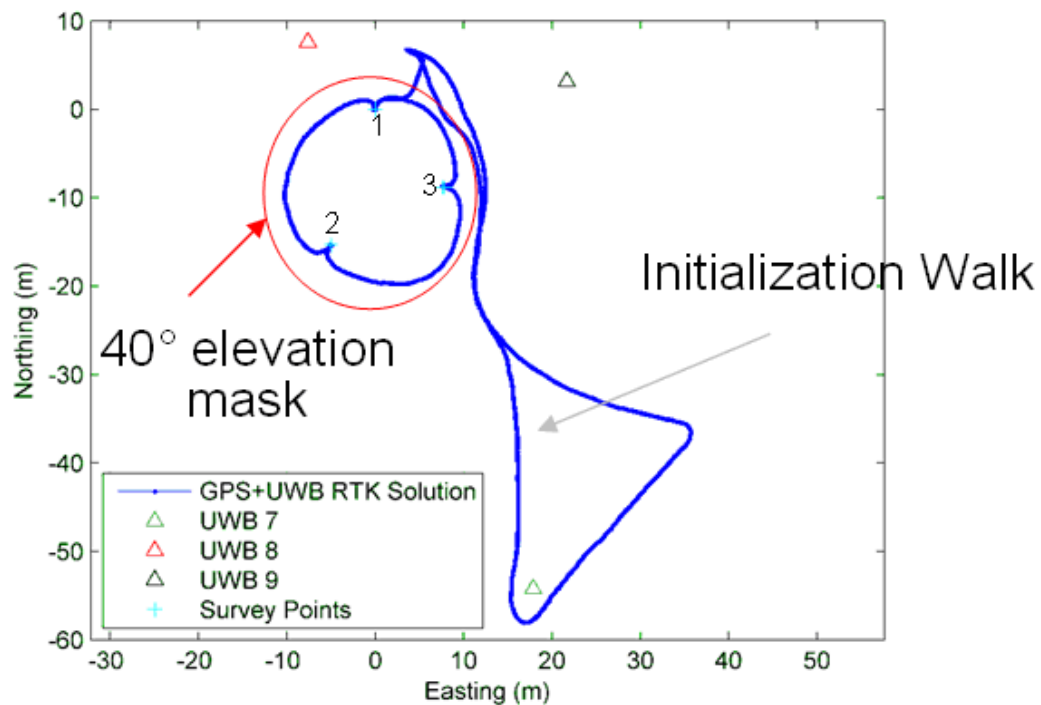


Figure 4.13: The kinematic test trajectory

4.2.1 Assessing UWB ranging

The ranges measured by the UWB pairs can be compared to the RTK solutions obtained using GPS only for the reference trajectory. This allows assessment of the actual range errors as the RTK derived ranges are accurate to a few centimetres. Bias and scale factor estimates are obtained using a best line fit of the UWB range errors versus the GPS RTK derived range. This is shown for all three ranging pairs in **Figure 4.14**. The figure shows the UWB range measurements and the RTK derived ranges for the entire test.

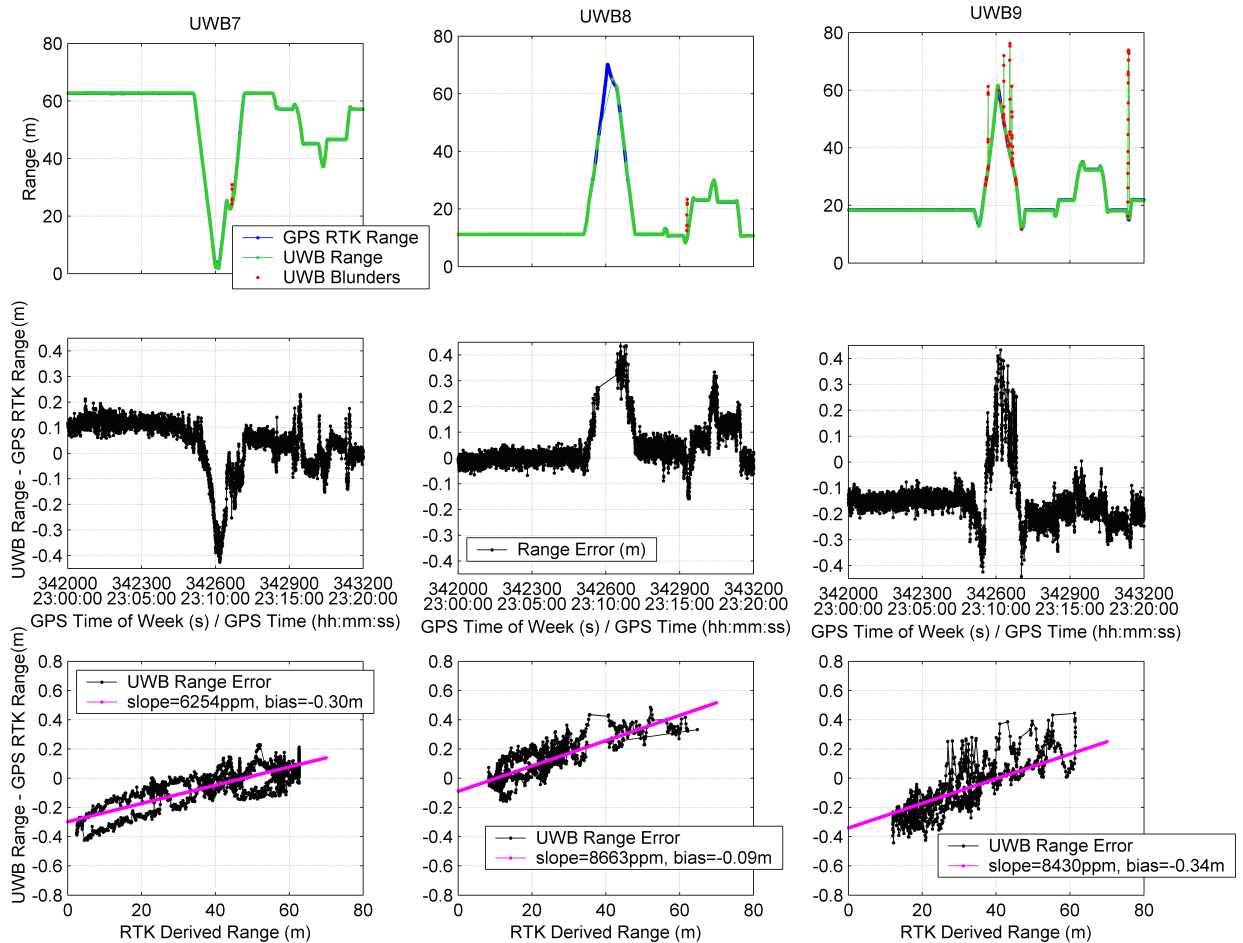


Figure 4.14: Kinematic test: UWB Ranging Errors. The top row of subplots show the raw measured UWB range and the reference GPS RTK derived range vs. time. At this scale, only data gaps and UWB range blunders are apparent. The difference between the UWB range and the GPS RTK derived range vs. time is shown in the second row of subplots. This is the UWB ranging error. The bottom row of subplots shows the UWB ranging error plotted as a function of the GPS RTK derived range. These plots show the error characteristics of the UWB measurements as a function of the best estimate of the true distance being measured. In each plot of the bottom row, a line fit of the data obtained by post-processing is shown. Of note: the bottom left subplot shows two distinct trend lines. It is possible that the turn-around-time bias changed during the test due to warming of the radios' oscillators.

Some interesting behaviour is observable in **Figure 4.14**. The UWB biases are not constant and change over time. For UWB7, the range measurements for the first static period (the first 8 minutes) are not consistent with the range measurements for the second static period (from approximately 23:12 to 23:14) despite occupying the same point. The apparent UWB bias changed by about 6 cm. The temperature during testing varied from -5°C to -10°C and the radios were turned on just as the test began. It is likely that the radios warmed up as the test proceeded and that the onboard oscillators exhibit frequency bias as a function of temperature. There are also clear multipath blunders especially for the range pair marked UWB9.

4.2.2 Tightly-coupled test results

Based on the results shown in the previous subsection, it should be possible to use the filter described in Chapter 3 to estimate the bias and scale factor errors in addition to the user position. In the following, results obtained using that filter are presented.

The number of double-difference ambiguities used in the GPS+UWB solution is shown in **Figure 4.15** along with the corresponding dilution of precision (DOP) values. The epoch when the 40° elevation mask is applied is clearly evident in the VDOP and PDOP plots. Note that the HDOP degrades only slightly because of good horizontal observability due to the UWB measurements. The GPS-only solution (with the elevation mask applied) lacks observability with only 3 satellites available and it cannot maintain fixed ambiguities. In the following analysis, the GPS+UWB solution is compared to the GPS-only RTK truth solution (obtained using a 13° elevation mask for the duration of the test). There are no GPS-only results with a 40° elevation mask angle because the solution is not usable due to the lack of observability.

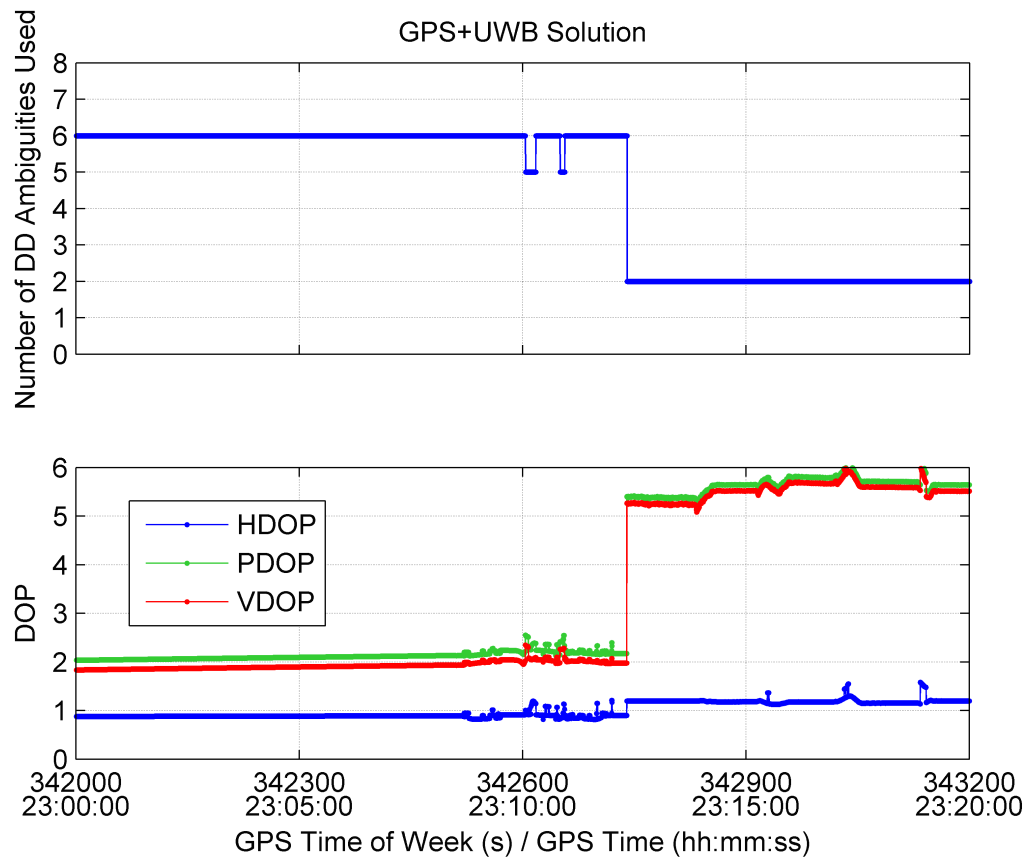


Figure 4.15: Kinematic test: GPS+UWB observations and DOP. The number of double difference ambiguities drops from 6 to 2 and there are large jumps in the DOP values when the 40° elevation mask is applied.

The GPS+UWB solution was able to maintain fixed ambiguity solutions for the duration of the test. The trajectory of the GPS+UWB solution closely matches that of the RTK truth solution. The differences in the computed positions are most apparent when examining the results for the static survey points. Both the GPS+UWB solution and the RTK truth solution are shown in **Figure 4.16** for these points. Statistics comparing the tightly-coupled GPS+UWB (40° elevation mask) solution to the GPS-Only (13° elevation mask) solution are provided in **Tables 4.3, 4.4, and 4.5**. The ability

to measure the static survey points corresponds reasonably well with the RTK truth solutions, especially considering the 40° elevation mask. The horizontal GPS+UWB solutions differ by less than 10 cm (maximum difference) from the GPS-Only (13° elevation mask) truth solution. The standard deviations of the solution differences are between 2 and 4 times larger for the GPS+UWB only case. This makes sense given the larger relative measurement variance of the UWB ranges compared to the GPS carrier phase measurements. In this test there are only 3 GPS satellites available and thus the UWB measurements have a strong influence on the position solution.

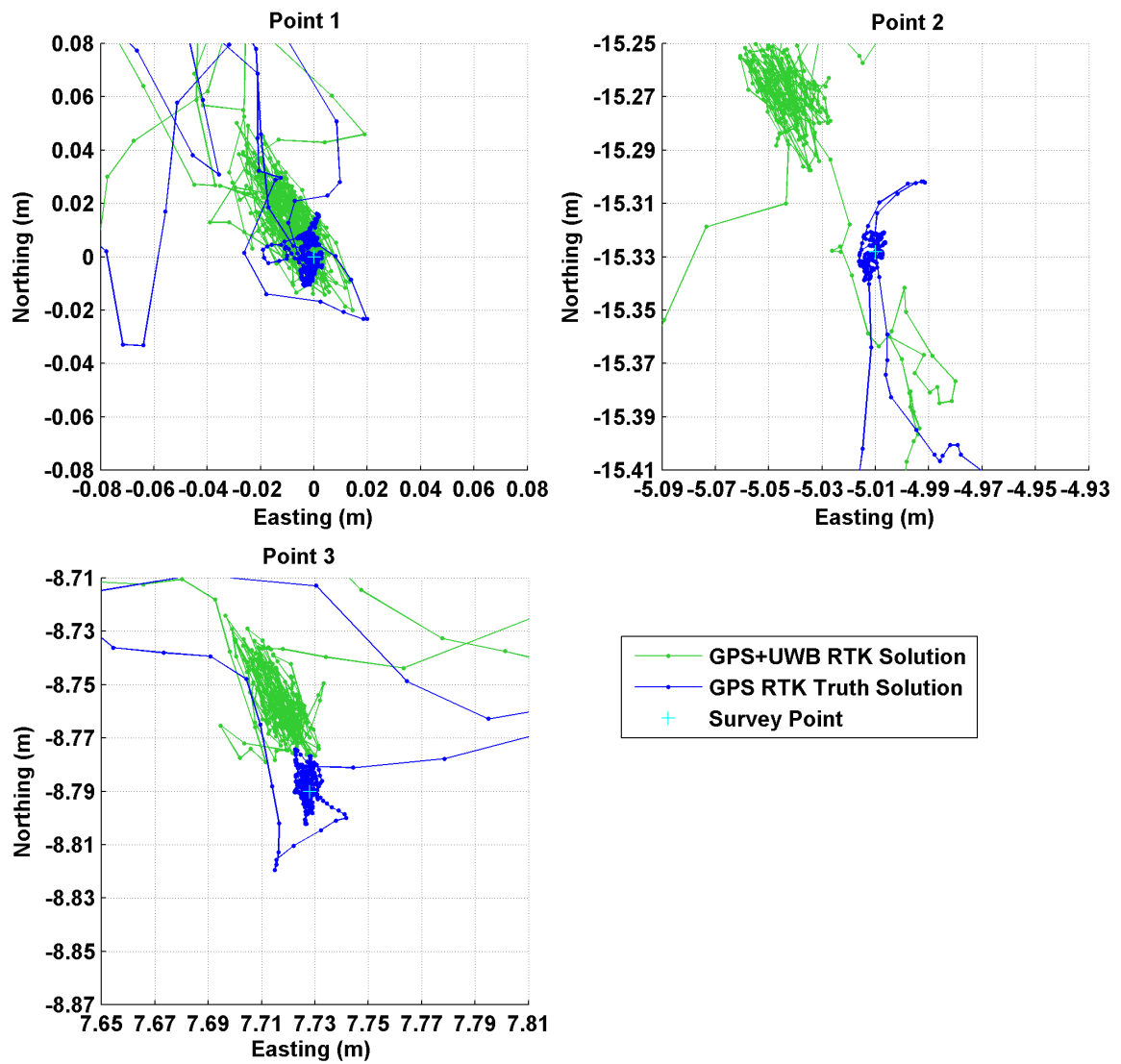


Figure 4.16: Kinematic test: survey points 1, 2, and 3 (GPS+UWB 40° elevation mask)

Table 4.3: Kinematic test: survey point 1 statistics (GPS+UWB 40° elevation mask vs. GPS-Only 13° elevation mask)

Point1	mean	min	max	σ	RMS	$\frac{\sigma}{\sigma_{\text{GPS-Only}}}$
GPS-Only East Error (cm)	0.0	-0.3	0.8	0.3	0.3	1.0
GPS-Only North Error (cm)	0.0	-0.3	0.5	0.2	0.2	1.0
GPS-Only Up Error (cm)	0.0	-0.6	0.9	0.4	0.4	1.0
GPS+UWB East Error (cm)	1.8	-2.8	5.0	1.2	2.1	3.8
GPS+UWB North Error (cm)	-0.9	-2.8	0.7	0.7	1.2	3.8
GPS+UWB Up Error (cm)	-2.6	-5.6	1.0	1.3	2.9	3.4

Table 4.4: Kinematic test: survey point 2 statistics (GPS+UWB 40° elevation mask vs. GPS-Only 13° elevation mask)

Point2	mean	min	max	σ	RMS	$\frac{\sigma}{\sigma_{\text{GPS-Only}}}$
GPS-Only East Error (cm)	0.0	-0.5	0.8	0.5	0.5	1.0
GPS-Only North Error (cm)	0.0	-0.5	0.5	0.3	0.3	1.0
GPS-Only Up Error (cm)	0.0	-0.7	0.3	0.3	0.3	1.0
GPS+UWB East Error (cm)	6.2	-5.2	9.3	1.1	6.3	2.6
GPS+UWB North Error (cm)	-3.3	-5.2	-1.9	0.7	3.4	2.2
GPS+UWB Up Error (cm)	-6.7	-9.9	-3.3	1.4	6.8	5.3

Table 4.5: Kinematic test: survey point 3 statistics (GPS+UWB 40° elevation mask vs. GPS-Only 13° elevation mask)

Point2	mean	min	max	σ	RMS	$\frac{\sigma}{\sigma_{\text{GPS-Only}}}$
GPS-Only East Error (cm)	0.0	-0.5	1.4	0.6	0.6	1.0
GPS-Only North Error (cm)	0.0	-0.5	0.6	0.2	0.2	1.0
GPS-Only Up Error (cm)	0.0	-0.9	1.4	0.6	0.6	1.0
GPS+UWB East Error (cm)	3.2	-3.1	6.6	1.1	3.4	2.9
GPS+UWB North Error (cm)	-1.1	-3.1	0.5	0.6	1.2	1.9
GPS+UWB Up Error (cm)	-2.7	-5.8	-0.6	1.2	2.9	1.9

The overall accuracy of the combined GPS+UWB solution is compared to the GPS only reference solution by comparing the 3D baseline obtained each epoch. The GPS+UWB system performs within 1 cm of the reference solution with the same GPS conditions (i.e. prior to the application of the 40° elevation mask) with the exception of a few error spikes due to the inclusion of some short delay UWB range blunders (all occurring close to 23:09:00). This is shown in **Figure 4.17**. When the GPS conditions are degraded using a 40° elevation mask and only 3 satellites are used, the performance of the system is typically better than 5 cm and better than 10 cm most of the time.

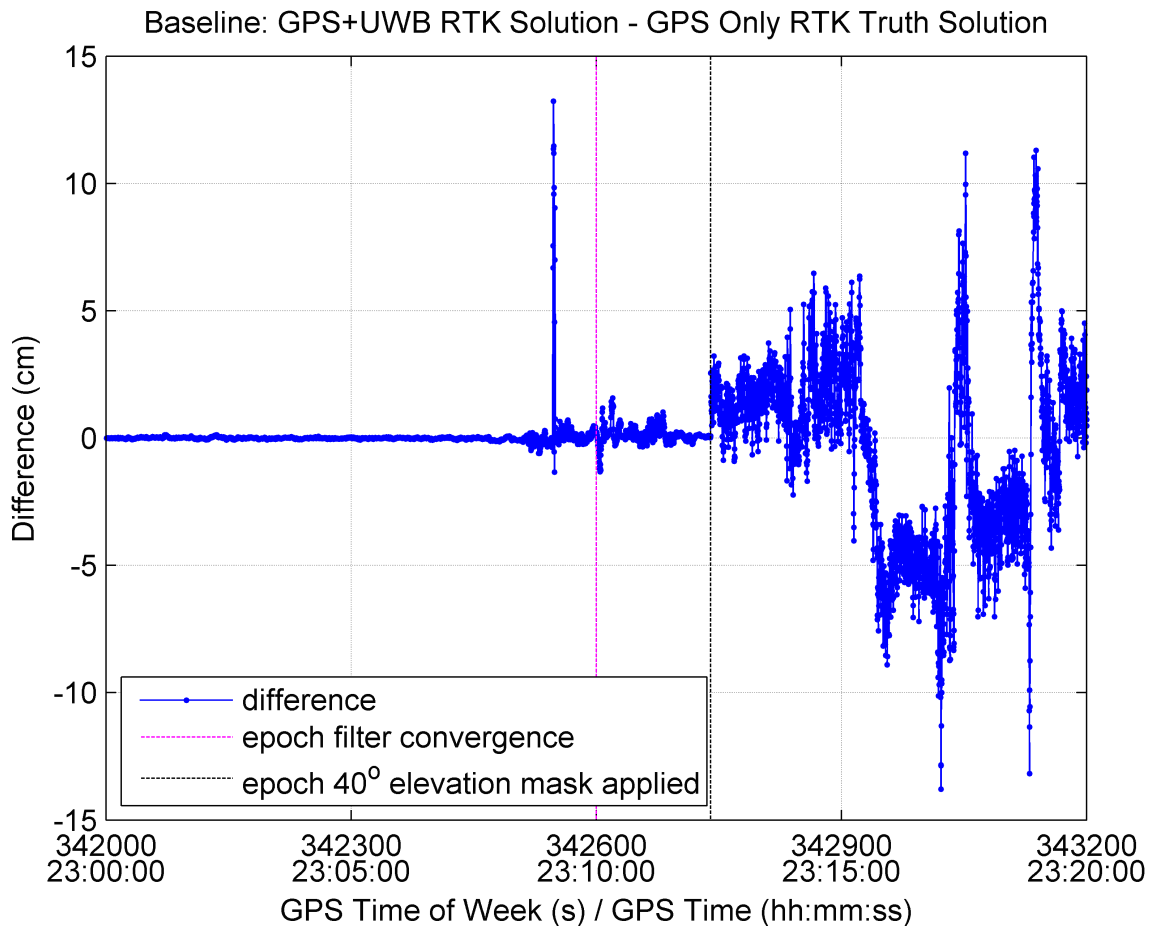


Figure 4.17: Kinematic test: baseline differences)

The filter estimated UWB bias values agree well with the post-processed line fit values. This is shown for UWB range pair UWB7 in **Figure 4.18**. Similar results were obtained for the other two range pairs, UWB8 and UWB9. It is clear from the bottom left subplot in **Figure 4.18** that the UWB bias requires the pre-survey initialization walk to estimate the UWB bias with sufficient estimated precision.

The estimate of the UWB scale factor value also agrees reasonably well with the post-processed line fit values. This is shown in **Figure 4.19**.

Analysis of the initial differences between the UWB bias and scale factor values and the values determined for the post-processed line fit shows that the bias and scale factor values cannot be observed distinctly prior to the initialization walk. The initial value of the scale factor is seeded based on a typical value from line of sight testing. This value differs from the post-processed line-fit by 1500 to 2000 ppm for UWB range pair 7. The difference is absorbed by the UWB bias estimate. The initial bias value is -0.13 m which corresponds to the 1500 to 2000 ppm difference at a distance of approximately 65 m. Hence, the bias and scale factor values cannot be observed distinctly without a range of motion to separate the states.

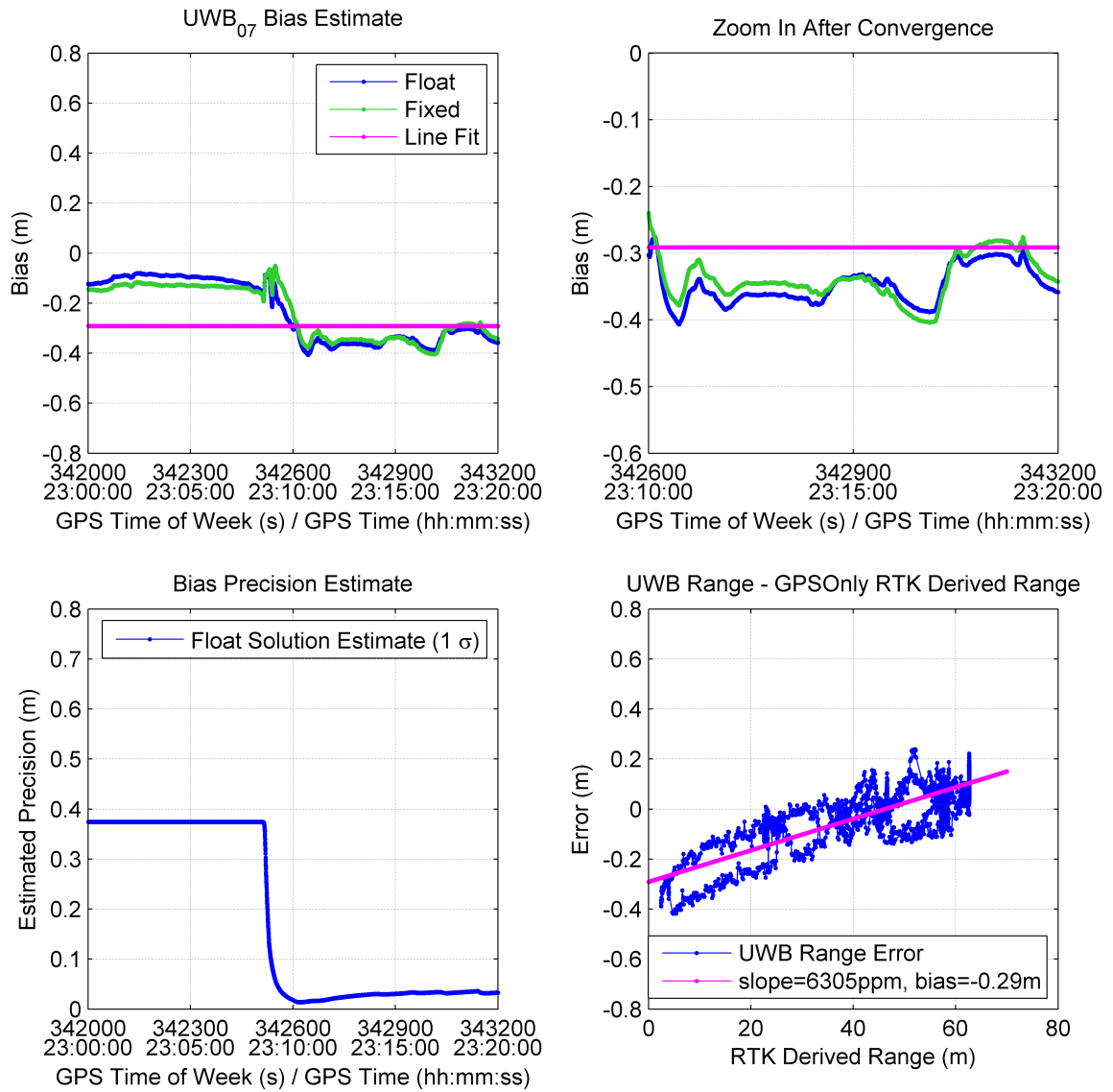


Figure 4.18: Kinematic test: UWB bias estimate. Convergence of the bias estimate only occurs after the user begins to move. The estimate of the bias converges after a sufficient range of motion is observed via the initialization walk.

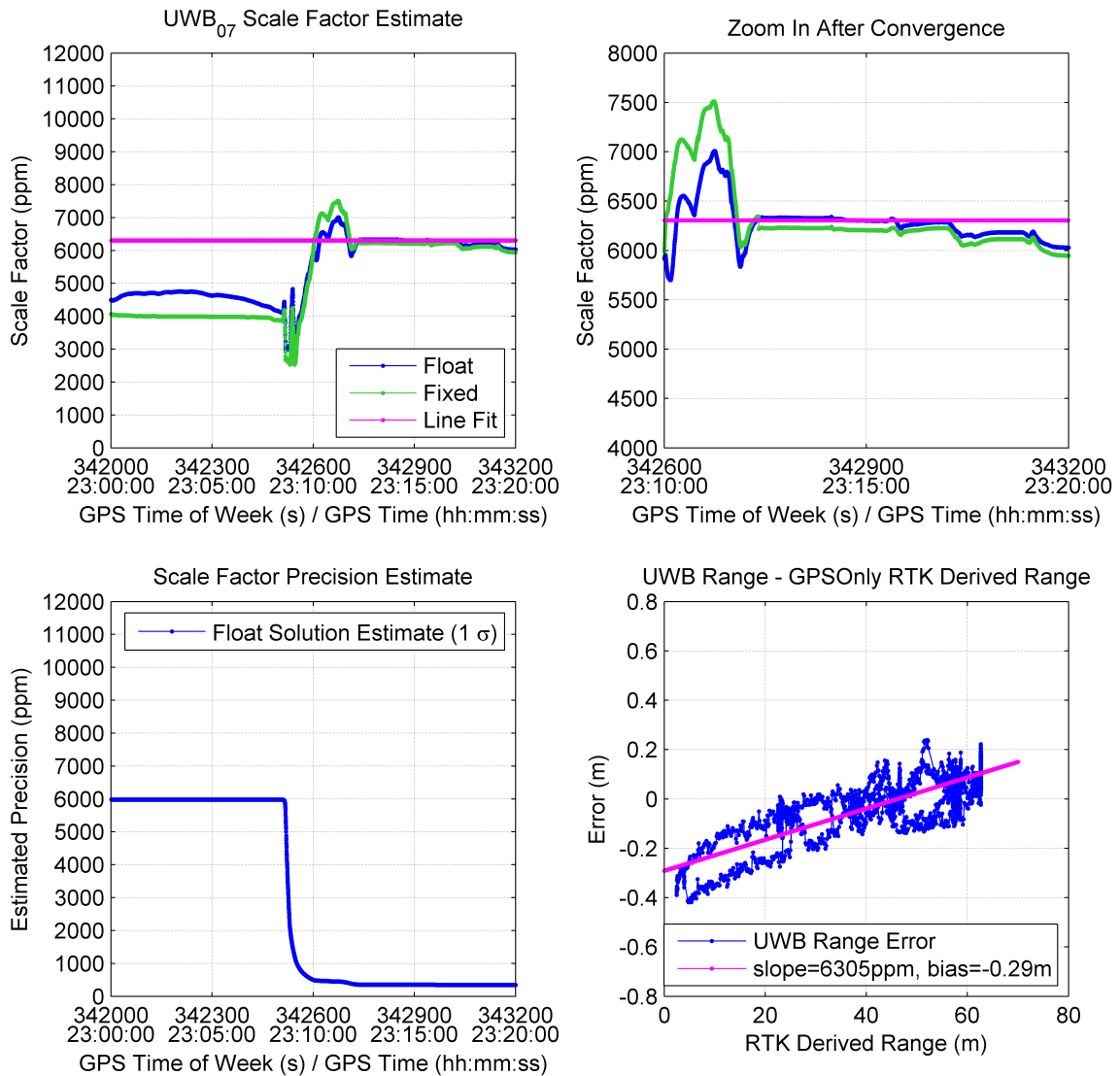


Figure 4.19: Kinematic test: UWB scale factor estimate. Convergence of the scale factor estimate only occurs after the user begins to move. The estimate of the scale factor converges after a sufficient range of motion is observed via the initialization walk.

Numerous UWB blunders were detected in testing as shown in **Figure 4.20**. For example, the UWB9 range pair exhibited multiple blunders with errors ranging from a few metres to tens of metres. The filter performed well in detecting most of these blun-

ders and excluding them from the filter. However, as shown in the baseline difference figure (**Figure 4.17**), a short delay multipath blunder went undetected and affected the solution accuracy.

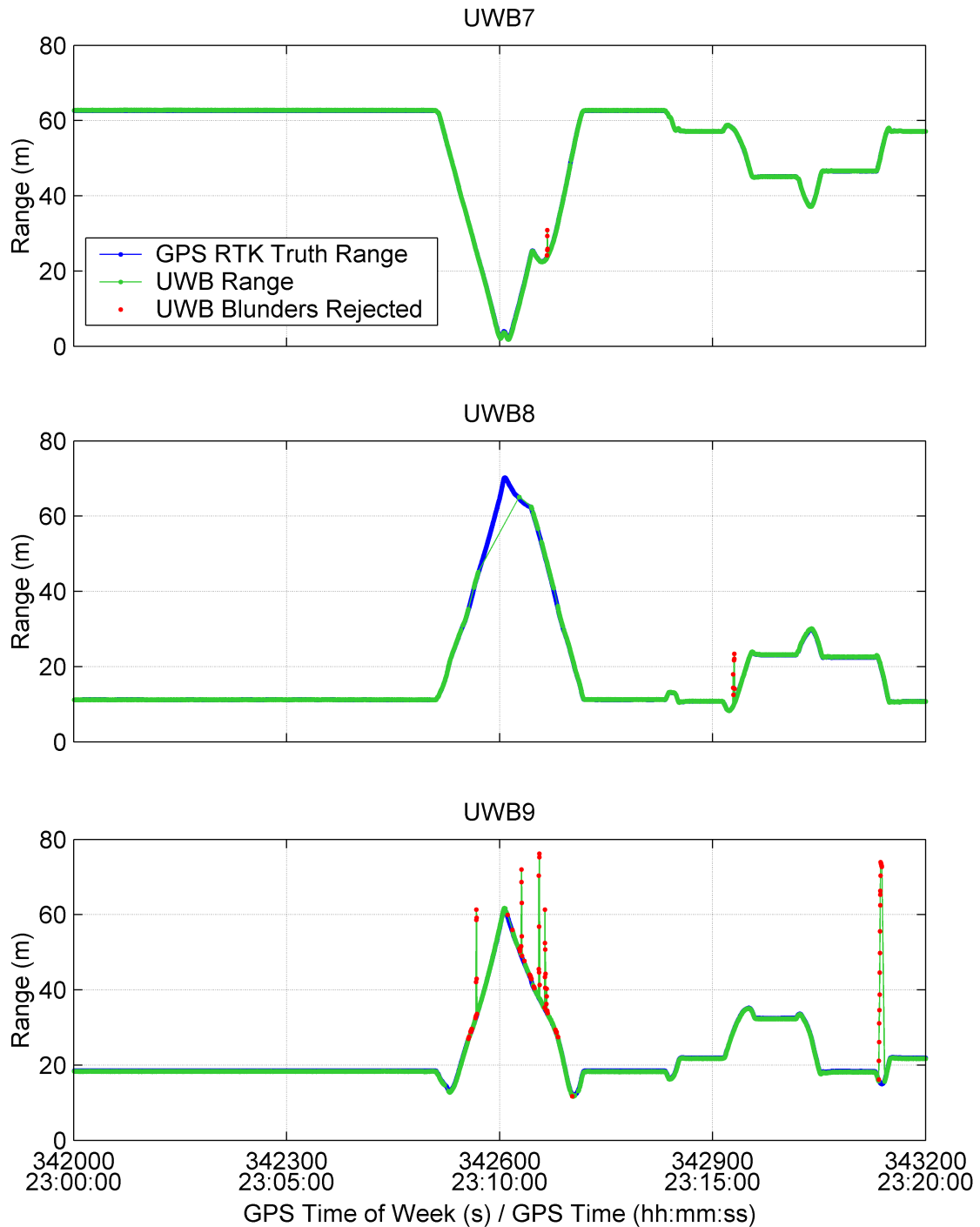


Figure 4.20: Kinematic test: UWB ranges and blunders. The subplots show the raw measured UWB range measurements (i.e. no corrections applied) and the reference GPS RTK derived range values. UWB range measurement blunders are clearly apparent in the plots. The blunders rejected by the filter are shown in red.

Comparing the raw range error with the range error corrected with the filter bias and scale factor values assesses the ability of the filter to 'correct' the UWB range measurements. This is shown in **Figure 4.21** and it is clear that the filter reduces the UWB measurement error but that there is room for improvement. Allowing the UWB transceivers warm-up time so that the temperature of their oscillators is stable should improve bias stability. The use of temperature controlled or ovenized oscillators would improve bias stability as well. The use a better pulse detection discriminator, such as the constant fraction discriminator ([Amann et al., 2001](#)), rather than the simple leading edge discriminator used by the UWB radios might decrease scale factor error and improve performance.

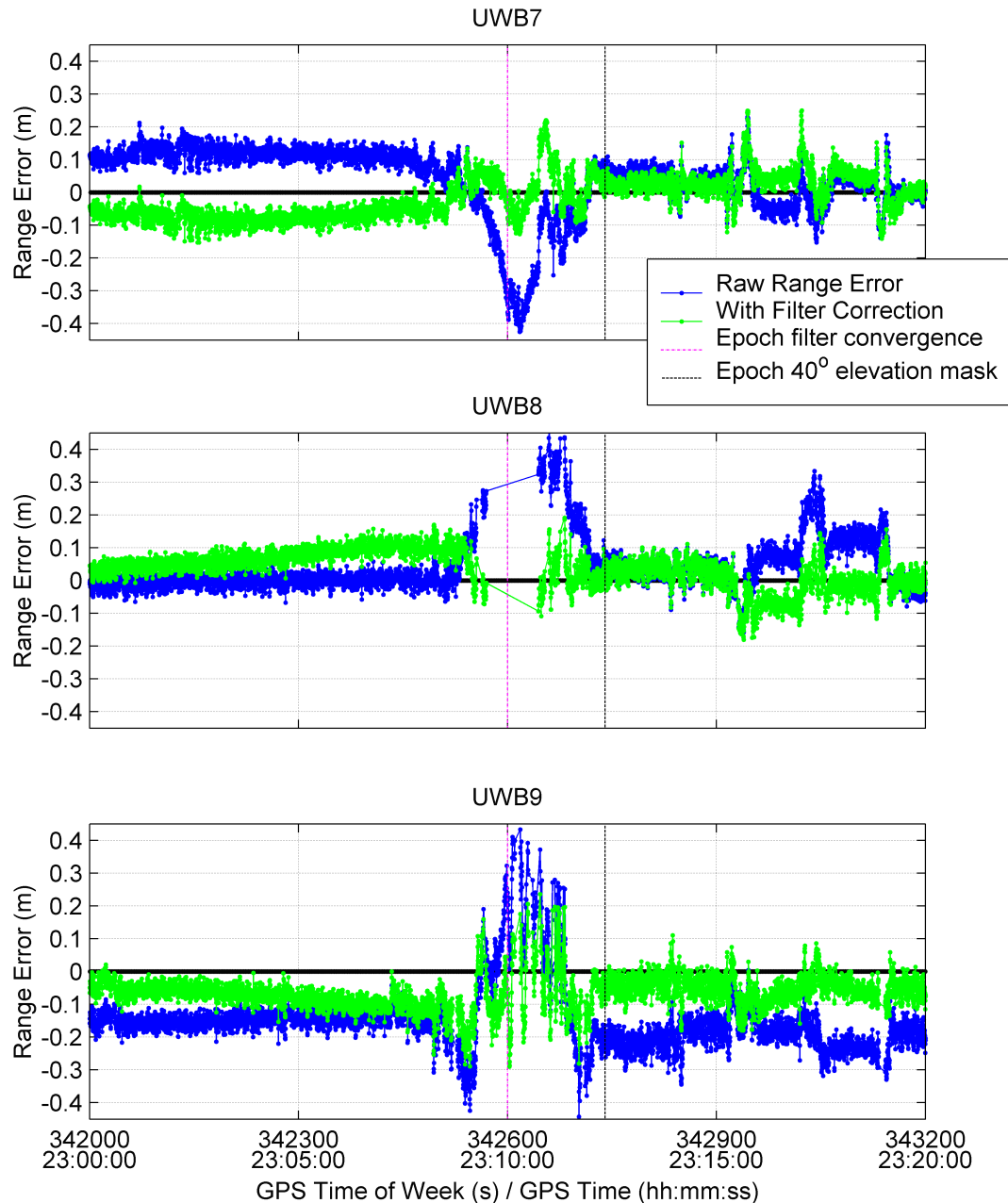


Figure 4.21: Kinematic test: Raw and corrected UWB range measurement errors. These subplots show the difference between the raw UWB range measurements and the reference GPS RTK derived ranges (i.e. UWB range error estimates). They also show the difference between the corrected UWB range measurements (using the estimated bias and scale factor estimates output by the filter for each epoch) and the reference GPS RTK derived ranges. The bias and scale factor corrections result in reduced UWB measurement error levels but systematic effects are not fully removed.

4.3 Summary

This work demonstrated tightly-coupled GPS and UWB using signal masking in post-processing. The degraded GPS environment was created artificially by simply excluding GPS satellites from the solution using an elevation mask. The next step is to test the method in a real-world environment. The next chapter assesses if the tightly-coupled approach of combining GPS and UWB measurements is feasible for RTK surveying in an urban canyon environment with realistic multipath and signal masking conditions.

Chapter 5

Results of testing in a difficult urban environment

This chapter presents results for the tightly-coupled filter in a difficult urban canyon environment. Bias and scale factor errors in the UWB measurements are estimated in-run and used with GPS pseudorange and phase measurements to survey several corner points of an eight story building. The tightly-coupled solution is compared to the GPS-only, UWB-only, and loosely-coupled solutions and UWB range errors are analyzed in detail for each of the static points surveyed. In the tests described in this chapter, both the MSSSI and TDC radios were used.

5.1 Description of the test

The test began with a static warm-up period in benign GPS signal conditions with 7 or more satellites available to allow the filter to converge and the integer GPS ambiguities to be resolved. A GPS base station was located less than 200 m away and 3 UWB reference radios were set up on precisely surveyed locations. NovAtel OEM3 GPS receivers were used.

A pre-survey initialization walk was performed with good GPS conditions to facilitate the estimation of UWB bias and scale factor states. The test system was then walked to four pre-surveyed test points located at the corners of a large glass and metal building (ICT building, 8 stories) on the University of Calgary campus and to one test point close to a large metal sign. The test was performed once for each set of UWB radios (TDC and MSSSI) resulting in two independent data sets. A photo of the test site is

shown in **Figure 5.1** and the trajectories for the tests are shown in **Figure 5.2**.

The UWB reference stations all have the same approximate height. Consequently, height observability must be obtained via GPS. Thus, for the UWB-only solution, a height constraint was employed for the duration of the test. For the GPS and GPS+UWB solutions, a height constraint was employed when fewer than 4 GPS satellites were available.

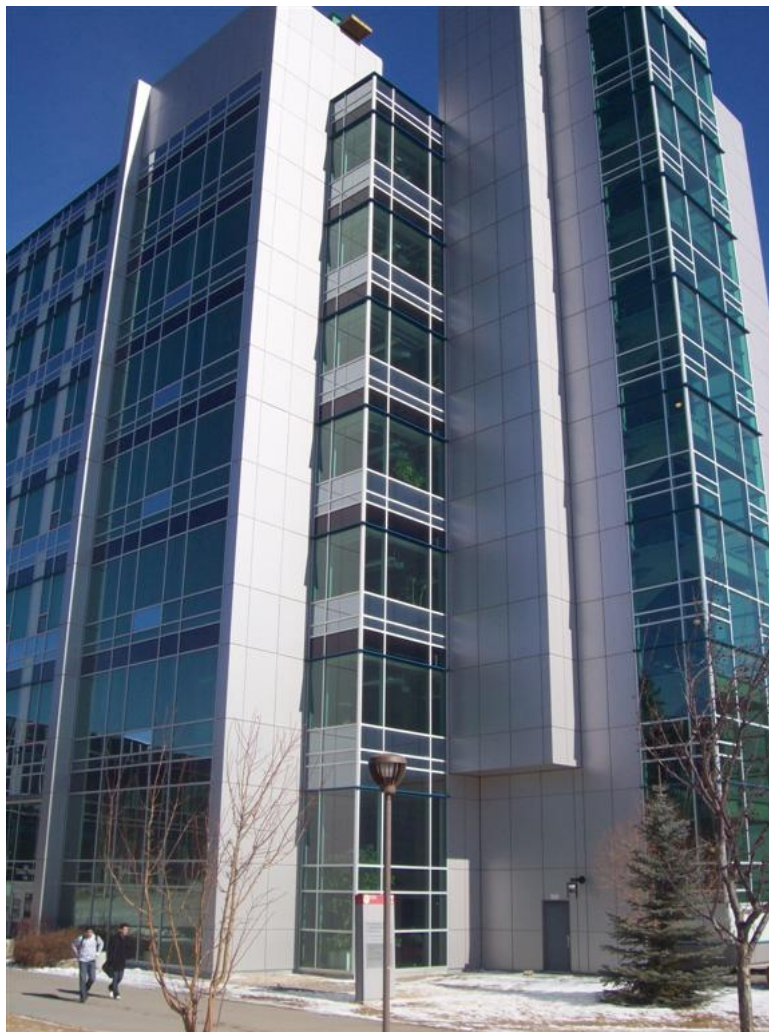


Figure 5.1: Photo of test area

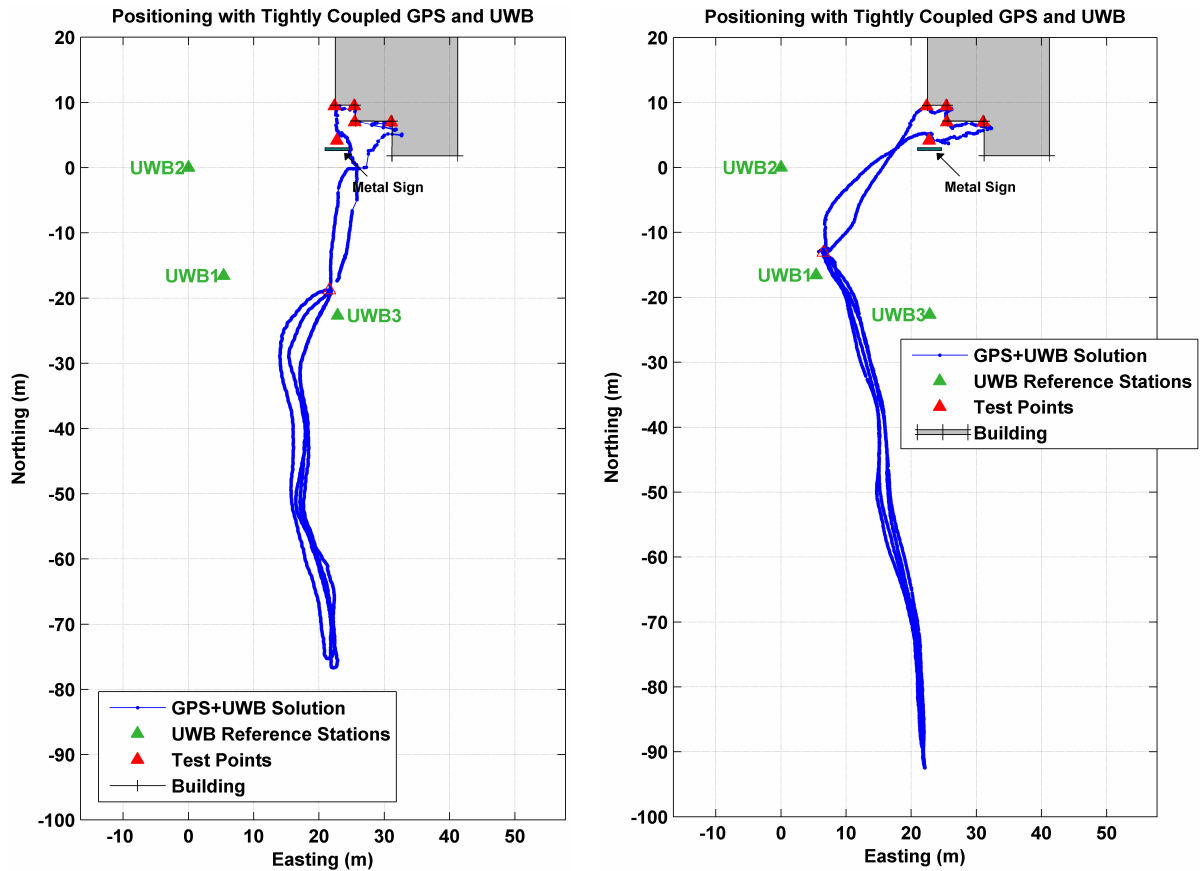


Figure 5.2: TDC test trajectory on left and MSSSI test trajectory on right

5.2 Results

Each test began with a pre-survey initialization walk away from obstructions and with excellent GPS and UWB availability. During both initialization walks, an UWB augmented fixed RTK solution was obtained. This allowed for estimation of the UWB error states similar to the results shown in the previous chapter. However, once the user approached the building, phase lock was generally lost and further fixed solutions could not be obtained. Additionally, significant multipath effects corrupted both the

GPS pseudorange and the UWB ranges. The position results, range errors and ability to detect and remove blunders for each filter and each test are discussed in the following.

5.2.1 Test results using the Time Domain Radios

For the test using the TDC radios, the GPS-only solution, the UWB-only solution, and the tightly-coupled GPS+UWB solution are shown in **Figures 5.3, 5.4 and 5.5** respectively. Periods of static data, as determined using the level sensor, are shown in green. The corresponding number of observations used in the solution is shown beside the plan view of the positioning results. A loosely-coupled solution obtained by combining the GPS-only solution and the UWB-only solution using weighted least-squares is shown in **Figure 5.6**.

The GPS-only solution suffers from signal masking close to the building corners such that the solution has only 2 satellites for points 1 and 2 and 1 satellite for point 3. The GPS-only solution thus relies on filter propagation of the position as it is not directly observable (3 unknowns, horizontal position, GPS receiver clock offset and only 1 or 2 observations in this case). The filter also has no ability to detect measurement errors as it cannot maintain an accurate solution and there is insufficient measurement redundancy for these points. Redundancy is defined on an epoch by epoch basis as the number of observations minus the number of unknowns.

The UWB-only solution estimates 3 of the 5 test points with sub-metre to one metre accuracy despite exhibiting periods in which measurement blunders cause the solution to jump considerably. It may appear that only 1 or 2 UWB ranges are used at the 5 Hz filter update rate. This is because the TDC radios do not make measurements simultaneously at the filter update rate. This does not mean that only one or two

stations are ranging. To show how many stations are ranging, the number of UWB observations used was resampled by accumulating separate ranging observations at 1 Hz. The UWB-only solution has sufficient observability but redundancy is only 1 at best (2 unknowns and up to 3 observations). This means the filter has limited ability to detect and remove UWB range outliers.

The tightly-coupled GPS+UWB solution exhibits few jumps in position and manages to maintain sub-metre level accuracy throughout the test. The loosely-coupled solution and the tightly-coupled solution perform better than either stand-alone solution as one expects; however, the loosely-coupled solution exhibits more jumps in position and poorer accuracy because it does not have the ability of the tightly-coupled solution to remove measurement outliers using innovation testing.

It is interesting and useful that the filter is able to continue to use the carrier phase measurements in the tightly-coupled solution compared to the GPS-only solution. The filter is able to maintain solution accuracy such that these measurements are not rejected by innovation testing.

The test with the TDC radios is pessimistic in the sense that there are very few GPS measurements and few UWB measurements each epoch. The GPS-only and UWB-only solutions have little if any ability to detect measurement blunders using innovation testing. The GPS-only and the UWB-only filter solutions cannot maintain the accuracy needed to identify blunders and there is insufficient measurement redundancy to detect the blunders in an epoch-by-epoch sense. The tightly-coupled solution achieves some redundancy as it is able to maintain three or more measurements (UWB ranges and GPS pseudorange) for most of the test. The filter uses a height constraint when an insufficient number of observations are available. This occurs for points 1, 2, 3, and part of point 4. In fact, there are generally five combined observations available and one or more GPS pseudorange or UWB range is rejected every epoch.

To better understand how the UWB measurements are used by both the UWB-only and the GPS+UWB solutions, the UWB range measurements obtained during the test are plotted in **Figure 5.7** and **Figure 5.8** for the UWB-only solution and the GPS+UWB solution respectively. The measurements flagged as outliers using innovation testing are shown in red. The true range which is known from the surveyed points is also plotted. There are subtle differences in the TDC ranges rejected between the UWB-only solution and the GPS+UWB solution. Upon close examination, there are a number of clear outliers that are used in the UWB-only solution but not in the combined solution. See the first part of the occupation of point 1 for range pair 1 as an example. The combined solution also rejects all the UWB measurements for point 5 and most of the UWB measurements afterward. The combined solution relies mostly on the GPS observations to navigate to point 5 and thereafter.

For range pair 2 at point 1, it is interesting that the TDC UWB ranges observed are consistently less than the true range. There are also a number of outliers that are less than the true range at other points. Multipath can only cause the measured range to be shorter than the line-of-sight signal if it is 180° out of phase with the line-of-sight signal and the range distortion is limited to less than half of the pulse width. For the TDC radios, the measured range can only be 3-5 cm shorter than the true range. The outliers observed are metre level. It may be that the radio is falsely detecting pulses emitted by the other ranging radios.

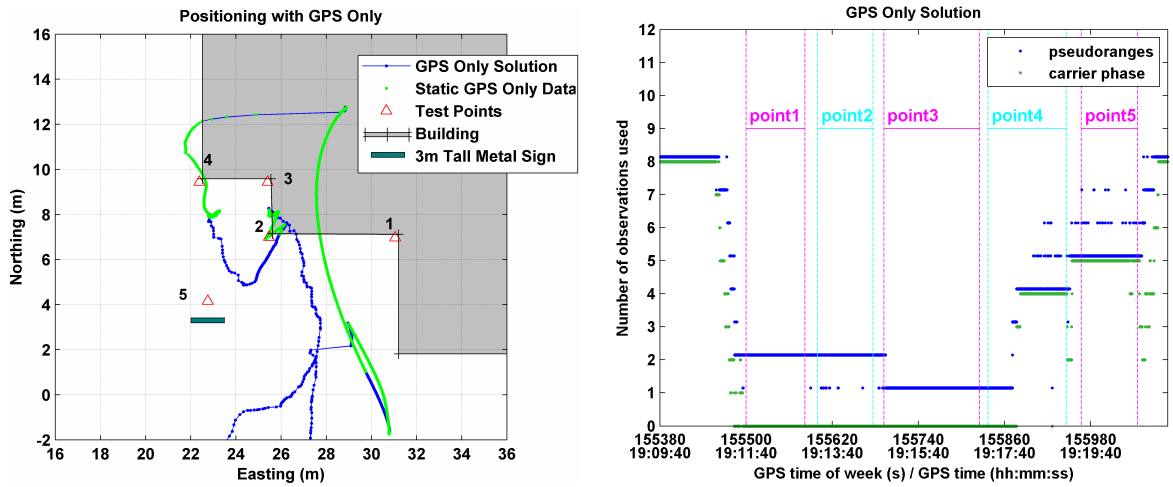


Figure 5.3: GPS-only results of test with TDC radios

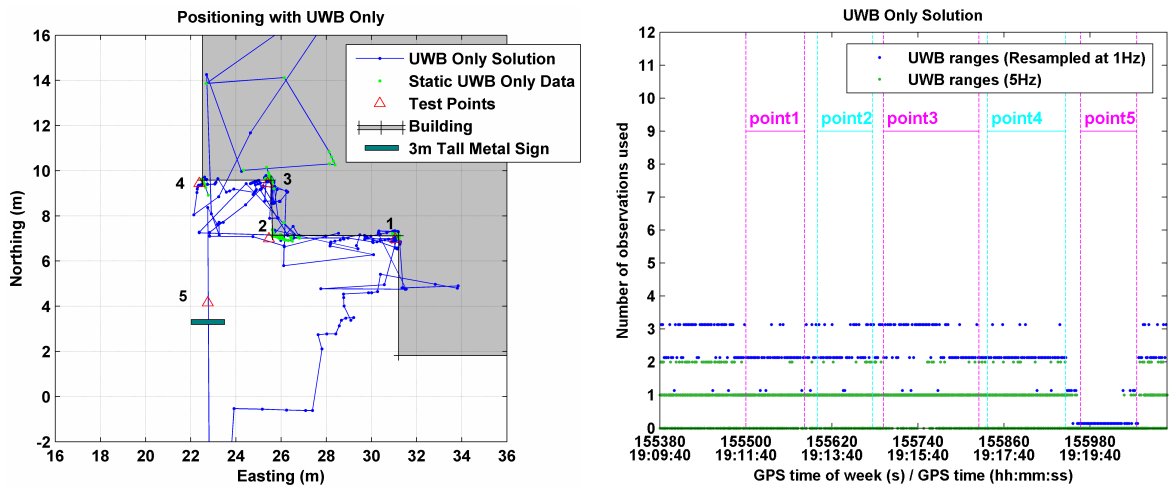


Figure 5.4: UWB-only results of test with TDC radios

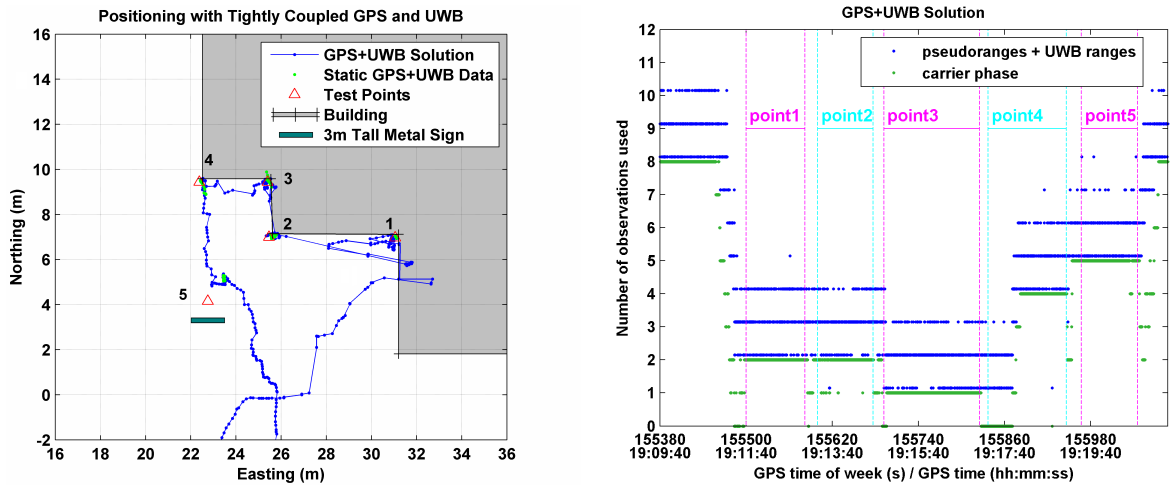


Figure 5.5: GPS+UWB results of test with TDC radios

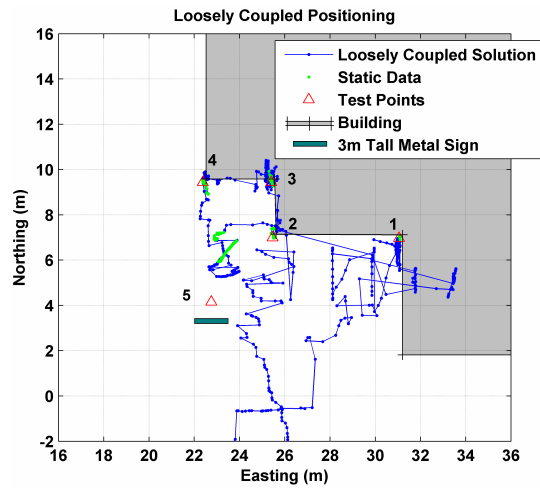


Figure 5.6: Loosely coupled solution using the TDC radios

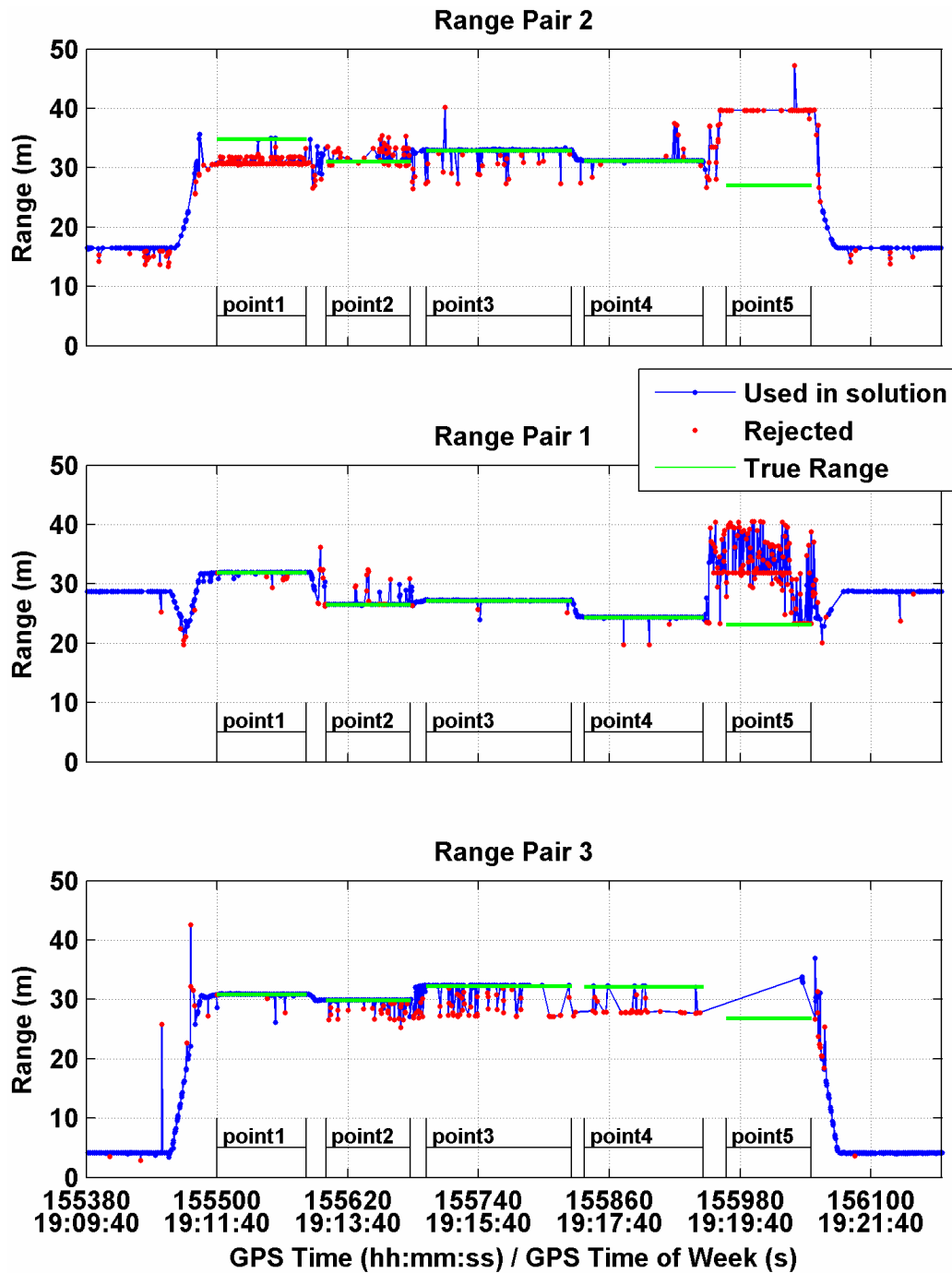


Figure 5.7: UWB ranges and rejected measurements for the TDC UW-B-Only solution

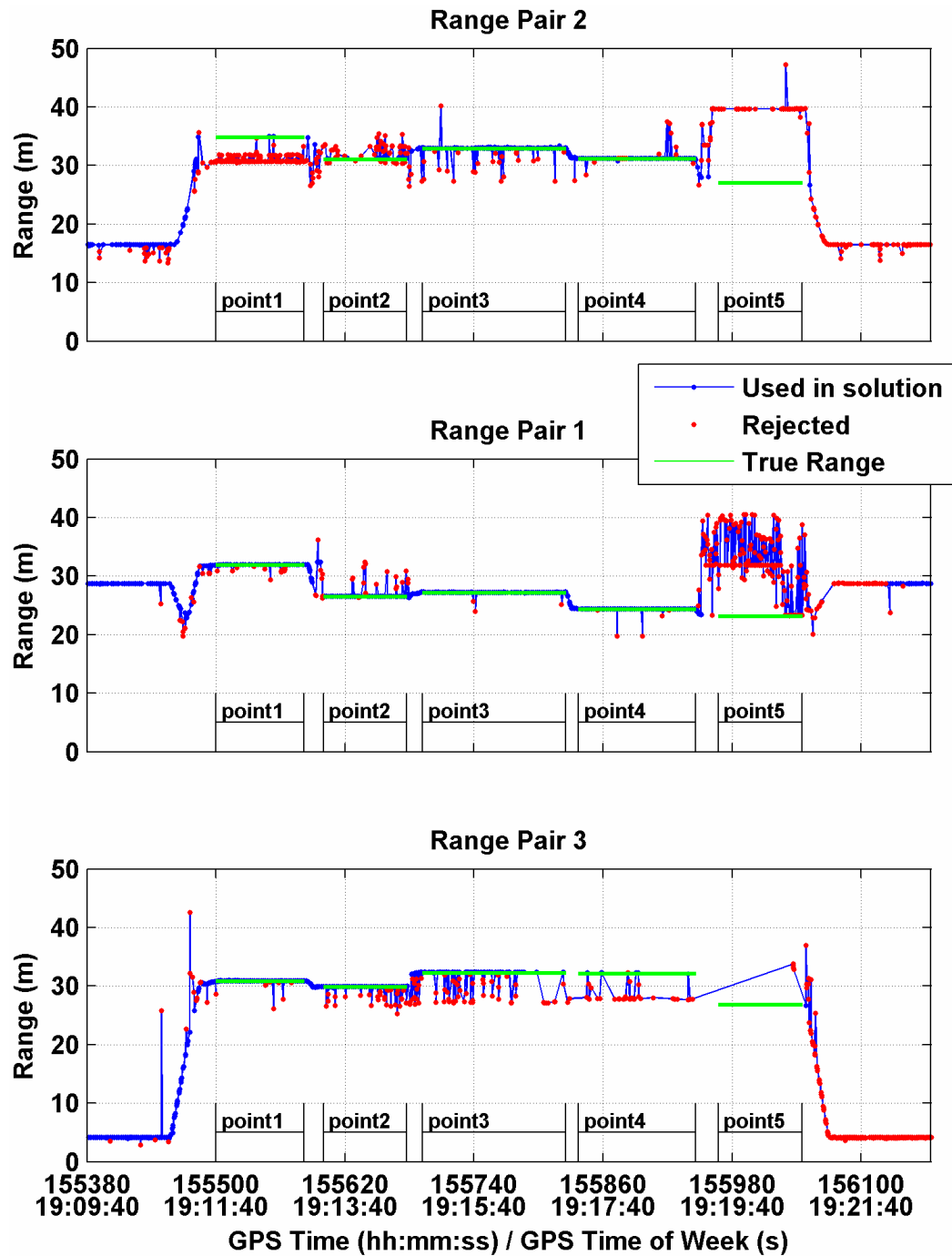


Figure 5.8: UWB ranges and rejected measurements for the TDC GPS+UWB solution

The UWB range errors for each range pair were calculated at all of the static points. Histograms of the raw UWB range errors, the range errors after applying the bias and scale factor corrections determined by the GPS+UWB solution, and the range errors without corrections used by the UWB-only solution are shown in **Figures 5.9, 5.10, and 5.11** for range pairs 1, 2, and 3 respectively. The portion of each bin for which the UWB ranges were rejected by the solution is indicated in red. If a bin is totally shown in red, all of the data in that bin was rejected by the filter.

It is difficult to observe any difference in the ability to detect and reject UWB range blunders based on the histogram for the GPS+UWB solution and the UWB-only solution. There are a few occurrences when good measurements are rejected by the tightly-coupled filter. The application of the bias and scale factor corrections results in a slightly more centralized distribution of the errors. This means the in-run estimation of the bias and scale factor errors is succeeding but may only be shifting the UWB range errors a small amount (e.g. 10 cm). A total of 56%, 83% and 85% of the range errors are contained within 0.5 m for range pairs 1, 2, and 3 respectively. A total of 84%, 85% and 99% of the range errors are contained within 1.0 m for range pairs 1, 2, and 3 respectively. This means that 15% of the UWB range measurements are outliers for range pairs 1 and 2. Again, it is also interesting that a large portion of the range errors are less than -1 m.

The distributions shown in **Figures 5.9, 5.10, and 5.11** represent the delay spread for the UWB channel for range pairs 1, 2, and 3 respectively. However, given that the width of the pulse used by the TDC radios is 0.23 ns (approximately 7 cm) it is not possible to observe a distribution comprised of the line-of-sight and short delay multipath when using 10 cm bins. The 10 cm bin size was selected to provide a common bin size for comparison with the MSSSI results (to follow). Following the next three figures, additional histograms with a finer bin size are discussed.

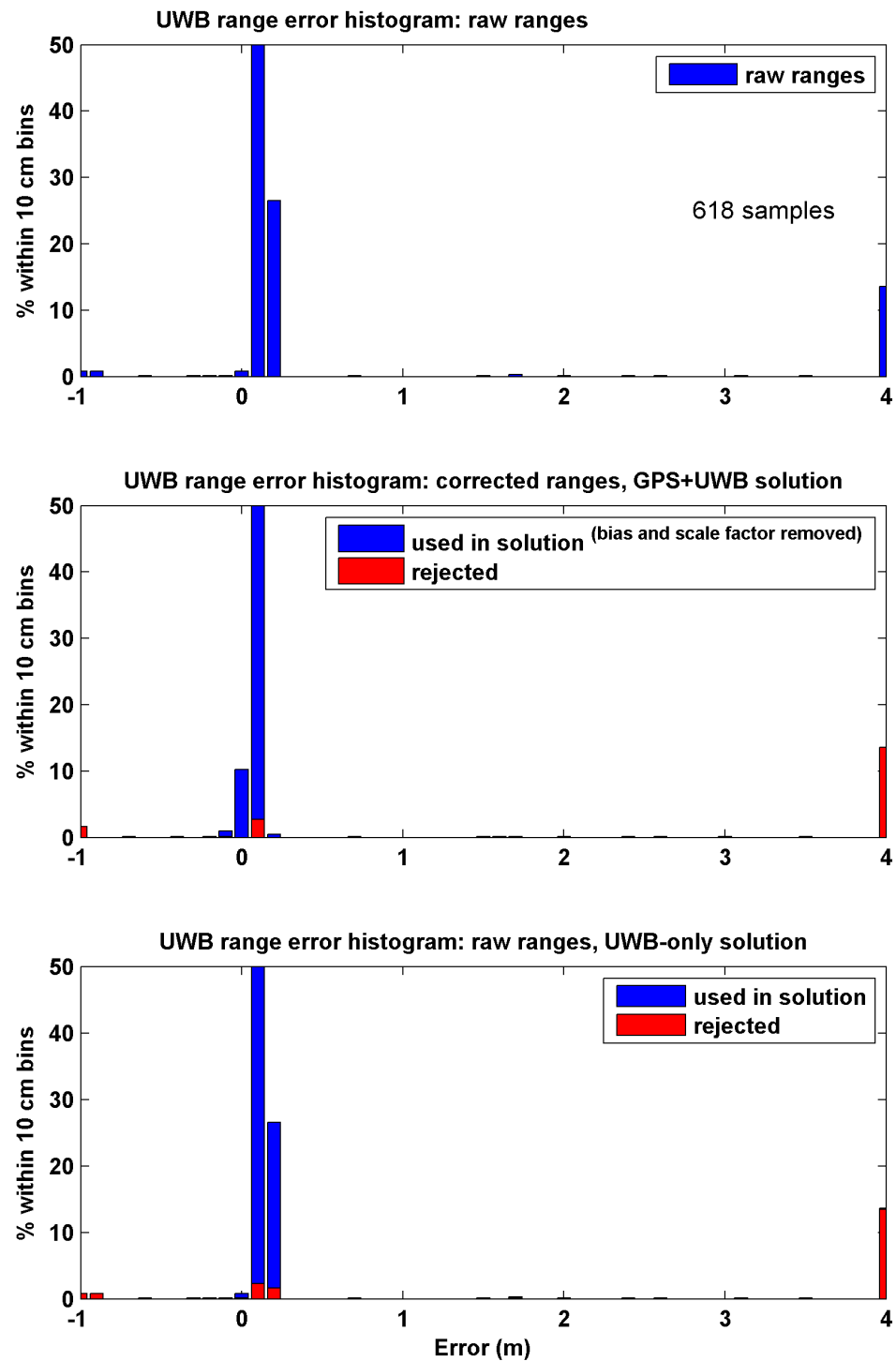


Figure 5.9: UWB range error histogram for range pair 1 (10 cm bin size)

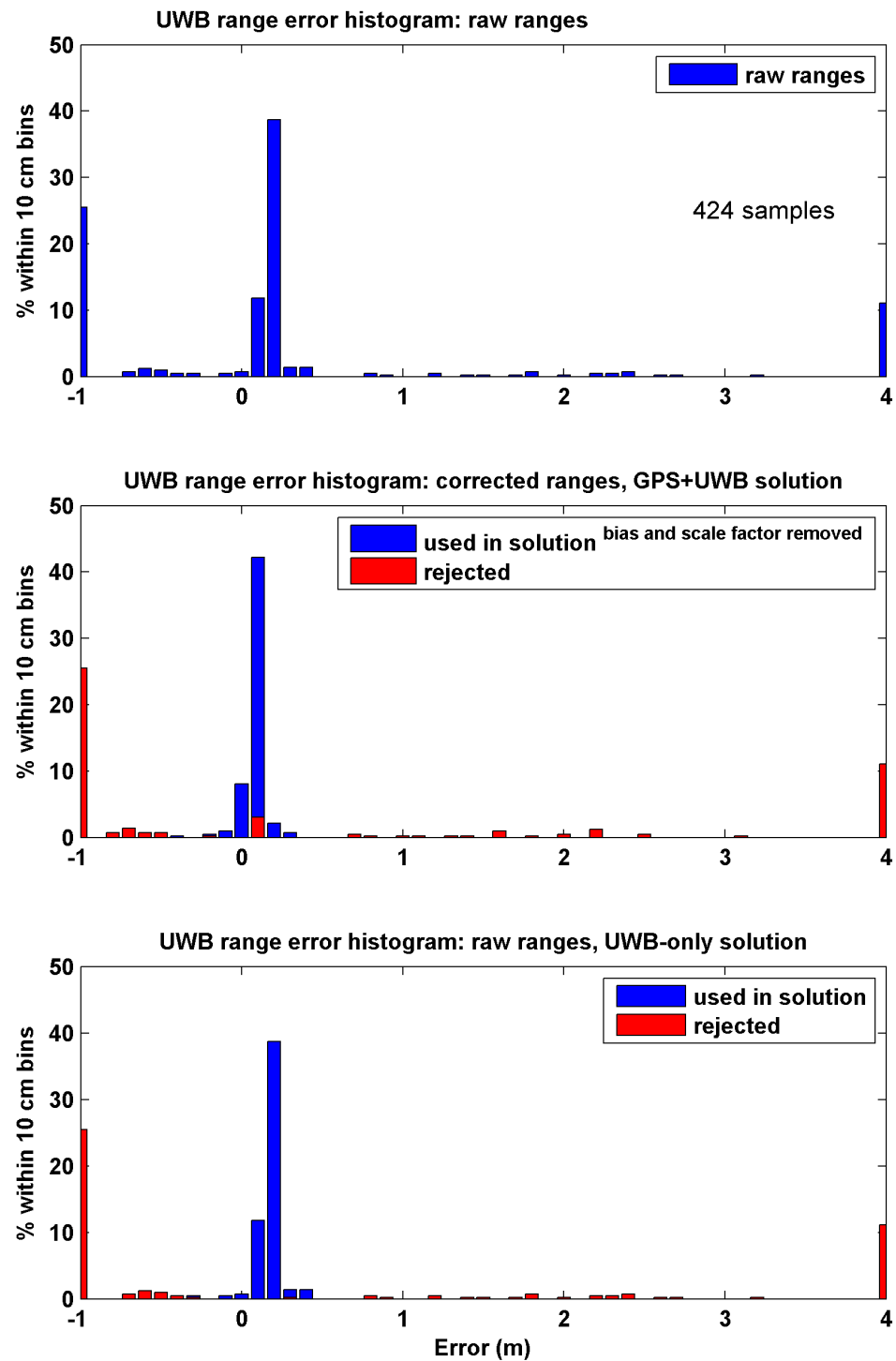


Figure 5.10: UWB range error histogram for range pair 2 (10 cm bin size)

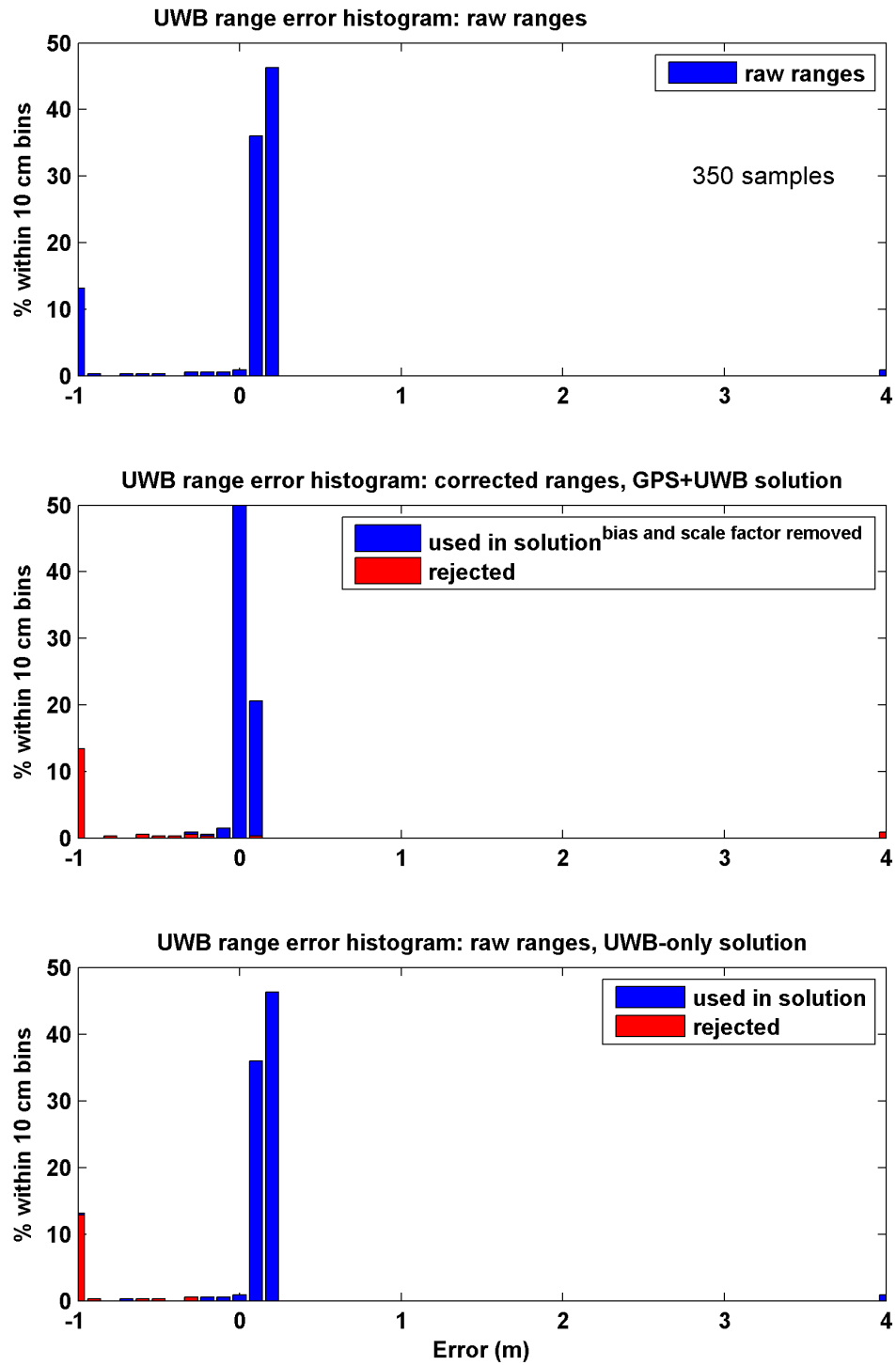


Figure 5.11: UWB range error histogram for range pair 3 (10 cm bin size)

The histograms were computed again for the TDC results using a 2 cm bin size and these are shown in **Figures 5.12, 5.13, and 5.14** for range pairs 1, 2, and 3 respectively. The impact of the bias and scale factor corrections is more apparent in these figures. Even with the corrections, the distributions for range pair 1 and 2 are biased by 5 to 8 cm. The bias and scale factor corrections improve the apparent UWB range errors but the extent of this is limited and this limits the accuracy attainable.

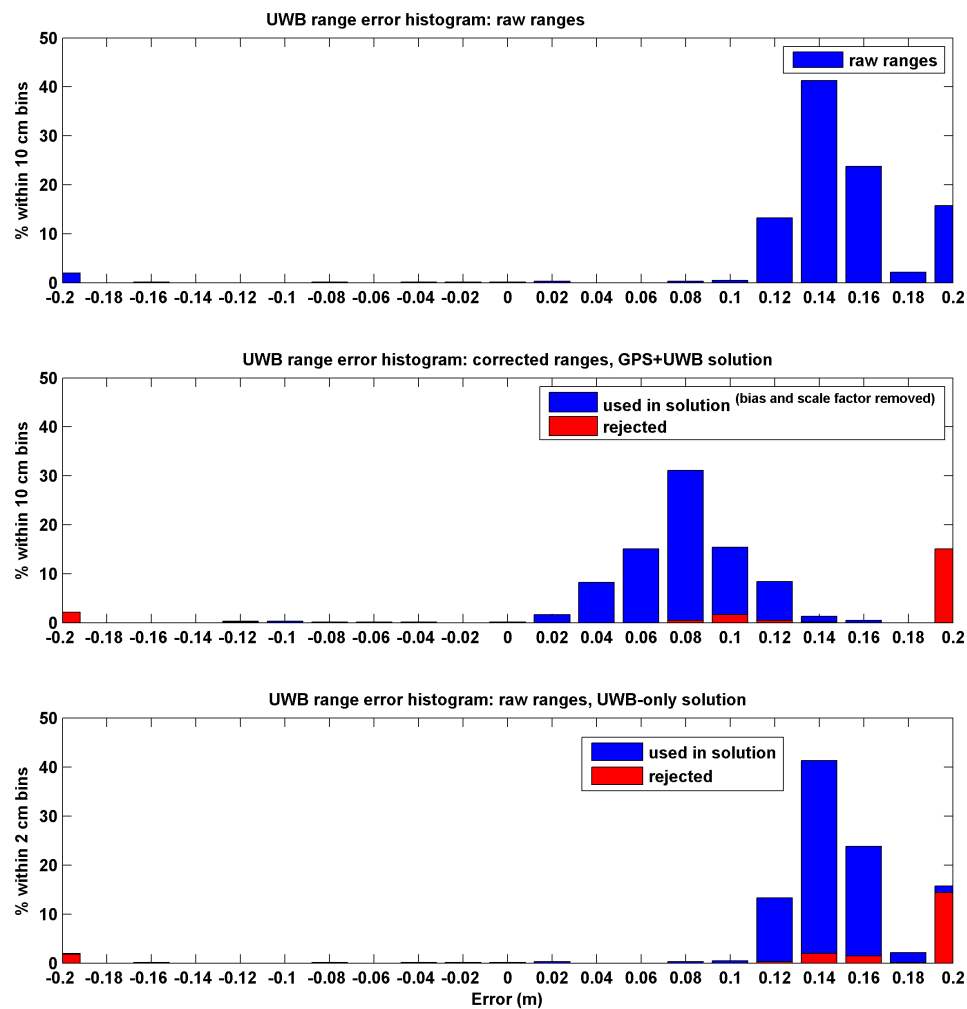


Figure 5.12: UWB range error histogram for range pair 1 (2 cm bin size)

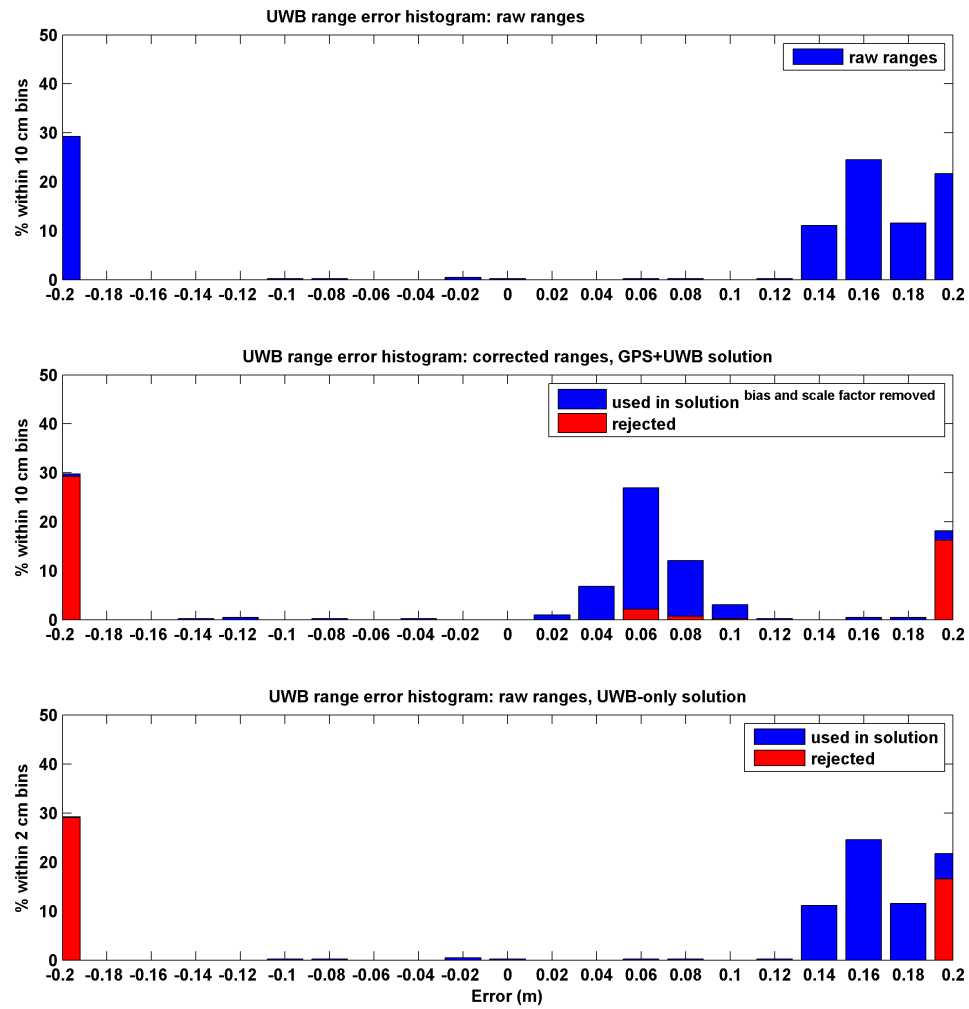


Figure 5.13: UWB range error histogram for range pair 2 (2 cm bin size)

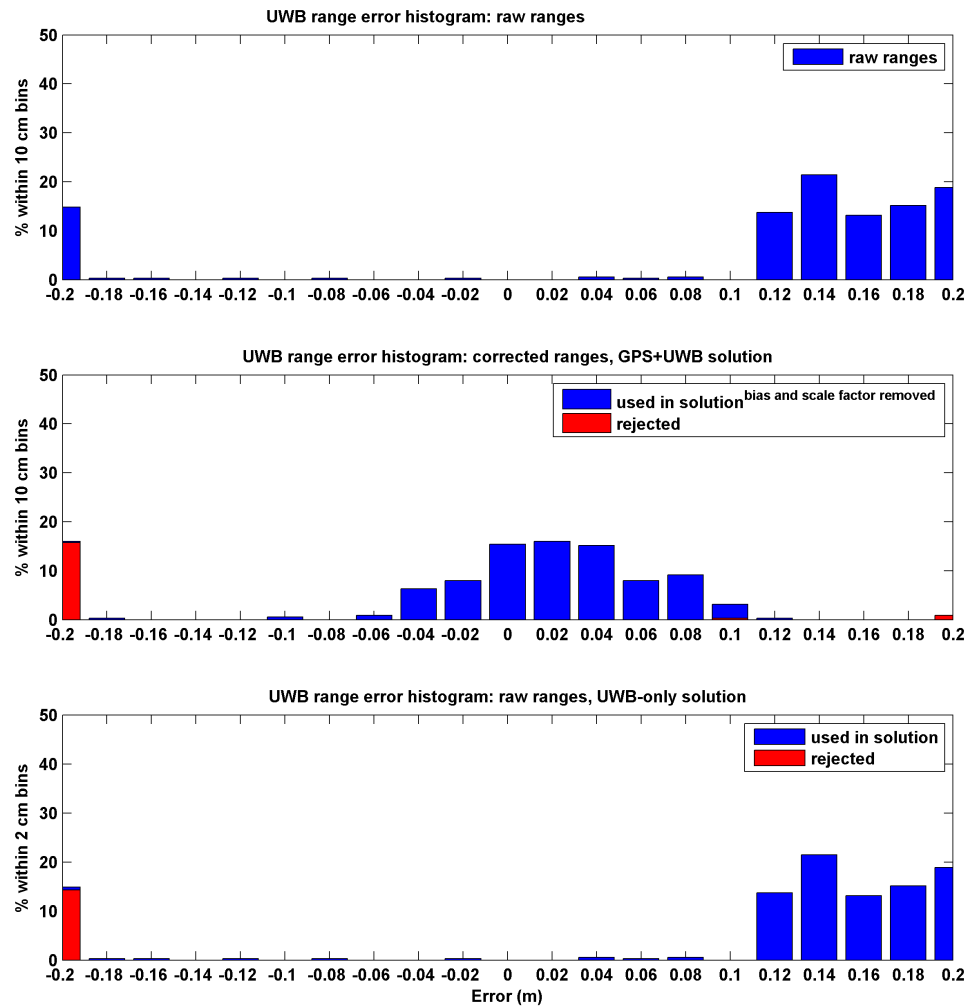


Figure 5.14: UWB range error histogram for range pair 3 (2 cm bin size)

5.2.2 Test results using the Multispectral Solutions Radios

The results using the MSSR radios for the GPS-only solution, the UWB-only solution, and the tightly-coupled GPS+UWB solution are shown in **Figures 5.15, 5.16, and 5.17**. The corresponding loosely-coupled solution is shown in **Figure 5.18**.

The GPS-only solution has 4 or more satellites for most of the test. This means the

filter is able to compute a solution at each epoch with some measurement redundancy. The filter is not able to maintain the integer carrier phase ambiguity estimates because of periodic loss of phase-lock for most of the satellite observations. This means the filter relies on the pseudorange measurements which are much more affected by multipath especially while close to strong specular reflection surfaces. Sub-metre accuracy cannot be achieved in this case. This is discussed further in the section concerning GPS measurement errors.

The UWB-only solution achieves sub-metre accuracy for 4 of the 5 test points. The inclusion of UWB range outliers clearly affects the solution for point 4 and for the solution obtained after moving away from the building from point 5. There are three UWB range measurements available for use at almost all epochs. The filter is often only using two of the three available as one is typically rejected by innovation testing.

The tightly-coupled GPS+UWB solution maintains sub-metre accuracy for all 5 test points. Redundancy is very good as there are often seven or more observations used in the filter. In fact, the solution is without a height constraint for most of the test and thus a 3D position solution is available. The measurement redundancy obtained using tight-coupling for estimation allows detection of UWB and GPS measurement blunders. Loose-coupling of the GPS-only and UWB-only solutions does not have this benefit and thus the tightly-coupled solution clearly outperforms the loosely-coupled solution as evident in the figures. The loosely-coupled solution does not perform as well as the UWB-only solution in this case.

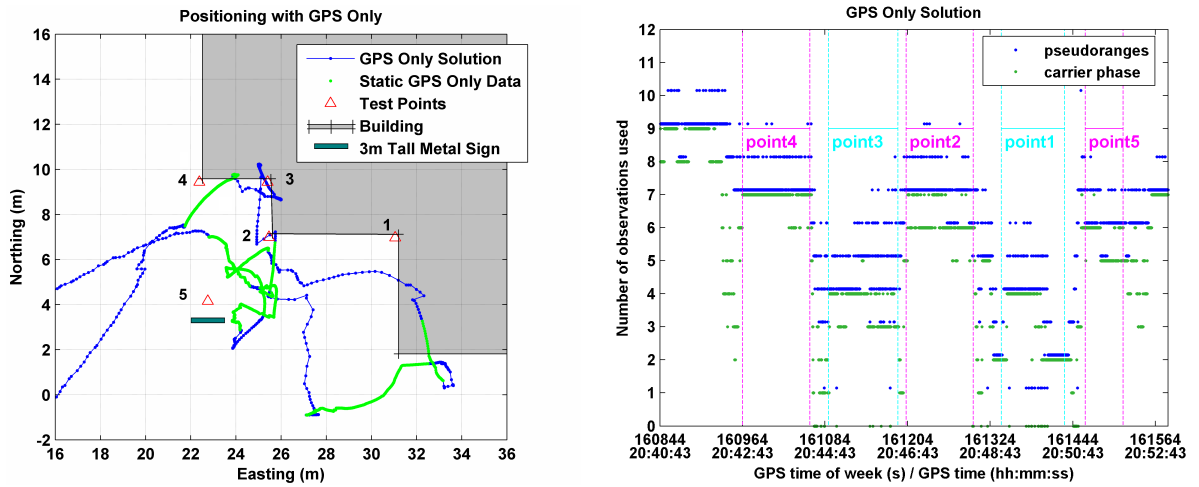


Figure 5.15: GPS-only results of test with MSSI radios

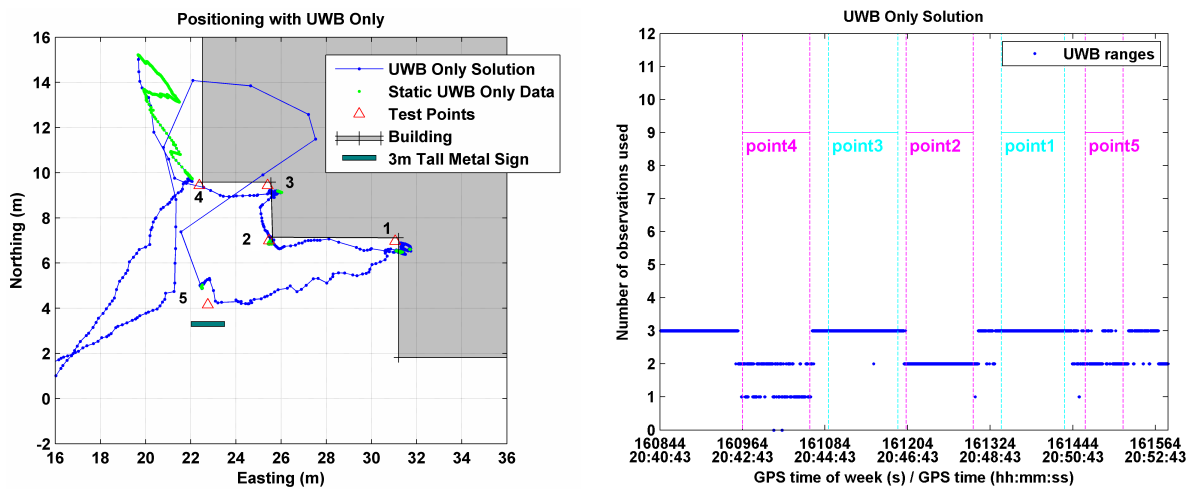


Figure 5.16: UWB-only results of test with MSSI radios

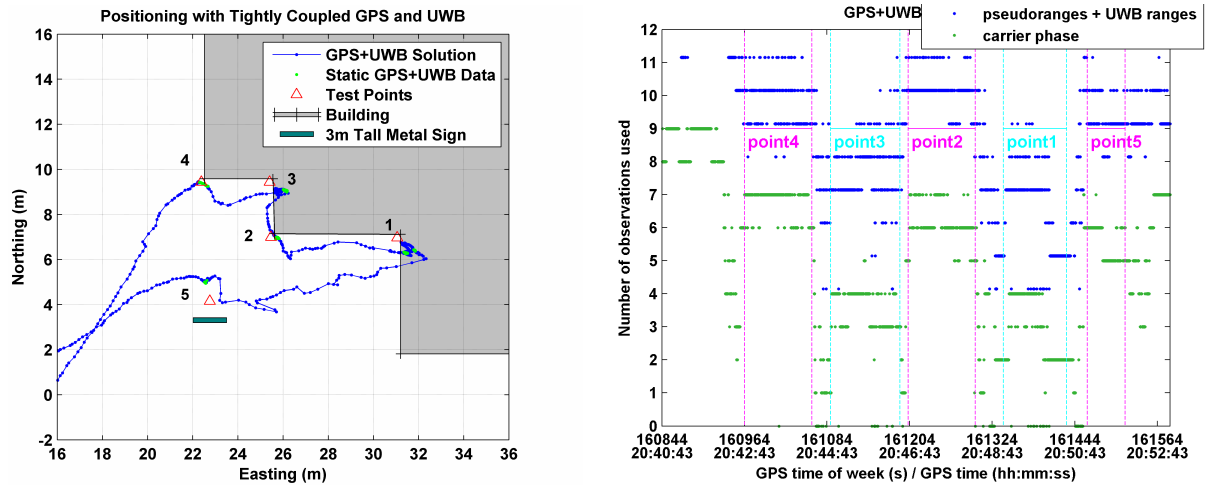


Figure 5.17: GPS+UWB results of test with MSSI radios

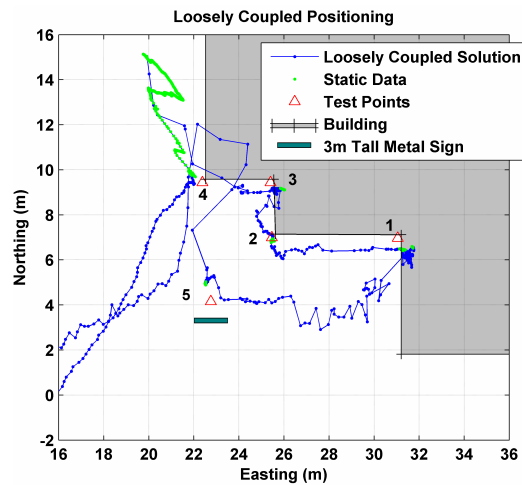


Figure 5.18: Loosely coupled solution using the MSSI radios

The MSSI UWB range measurements obtained during the test are plotted in **Figure 5.19** and **Figure 5.20** for the UWB-only and the GPS+UWB solutions respectively. The measurements flagged as outliers using innovation testing in the UWB-only and the GPS+UWB solutions are shown in red. The true range which is known from the

surveyed points is also plotted. There are obvious differences in the ranges rejected between the UWB-only solution and the GPS+UWB solution. For example, the UWB-only solution rejects range pair 2 for point 4 while using range pairs 1 and 3. This is a case of rejecting a good observation and including bad observations in the solution. Range pair 3 is exhibiting errors consistent with measuring reflected signals for points 4 and 5. The GPS+UWB solution performs very well by rejecting apparent measurement blunders. This is clear when the line-of-sight is obstructed (e.g. metal sign between user and south UWB reference station, for range pair 3 at points 4 and 5) and a significant number of non line-of-sight measurements are identified and rejected.

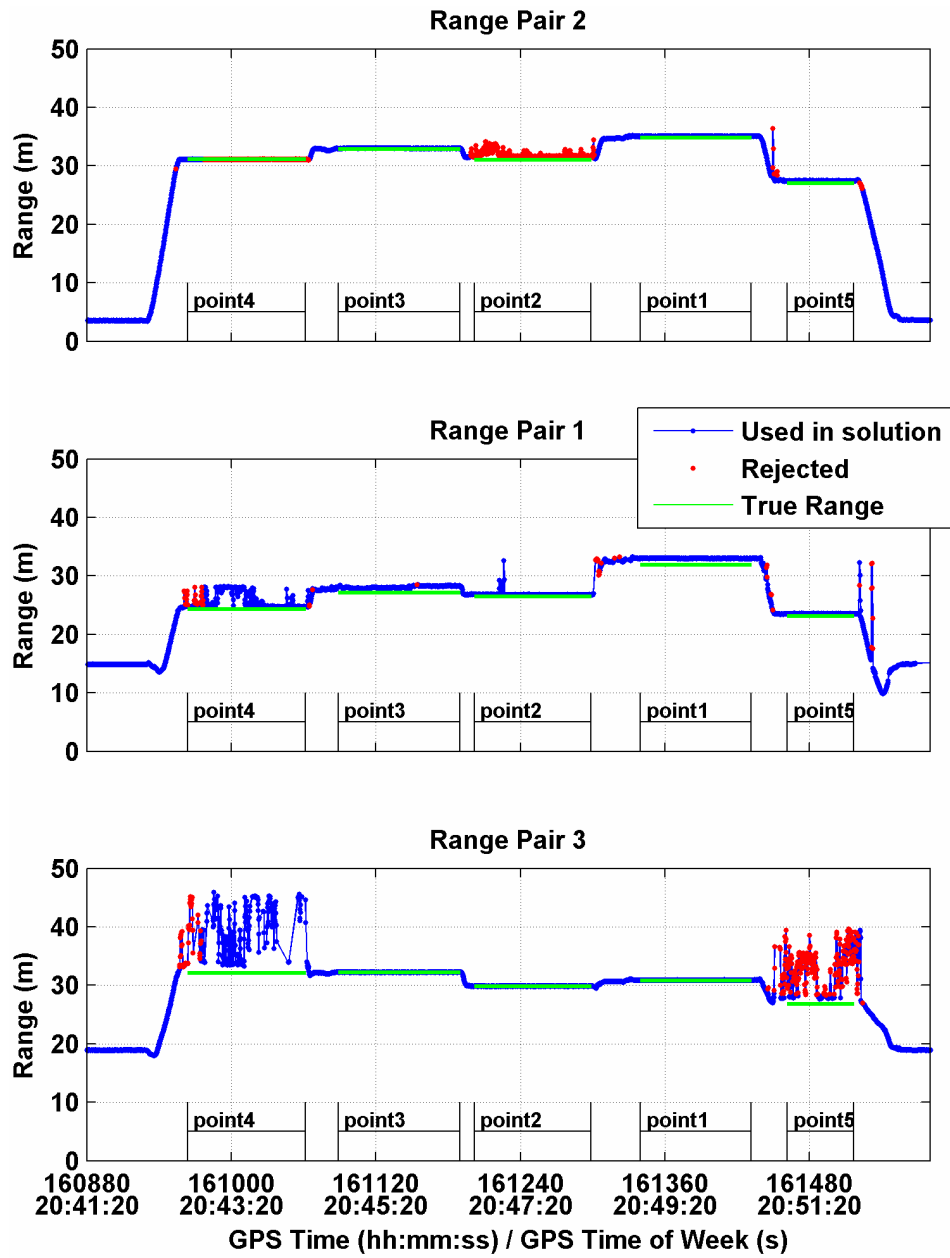


Figure 5.19: MSSSI UWB-Only solution UWB ranges and rejected measurements for the MSSSI UWB-Only solution

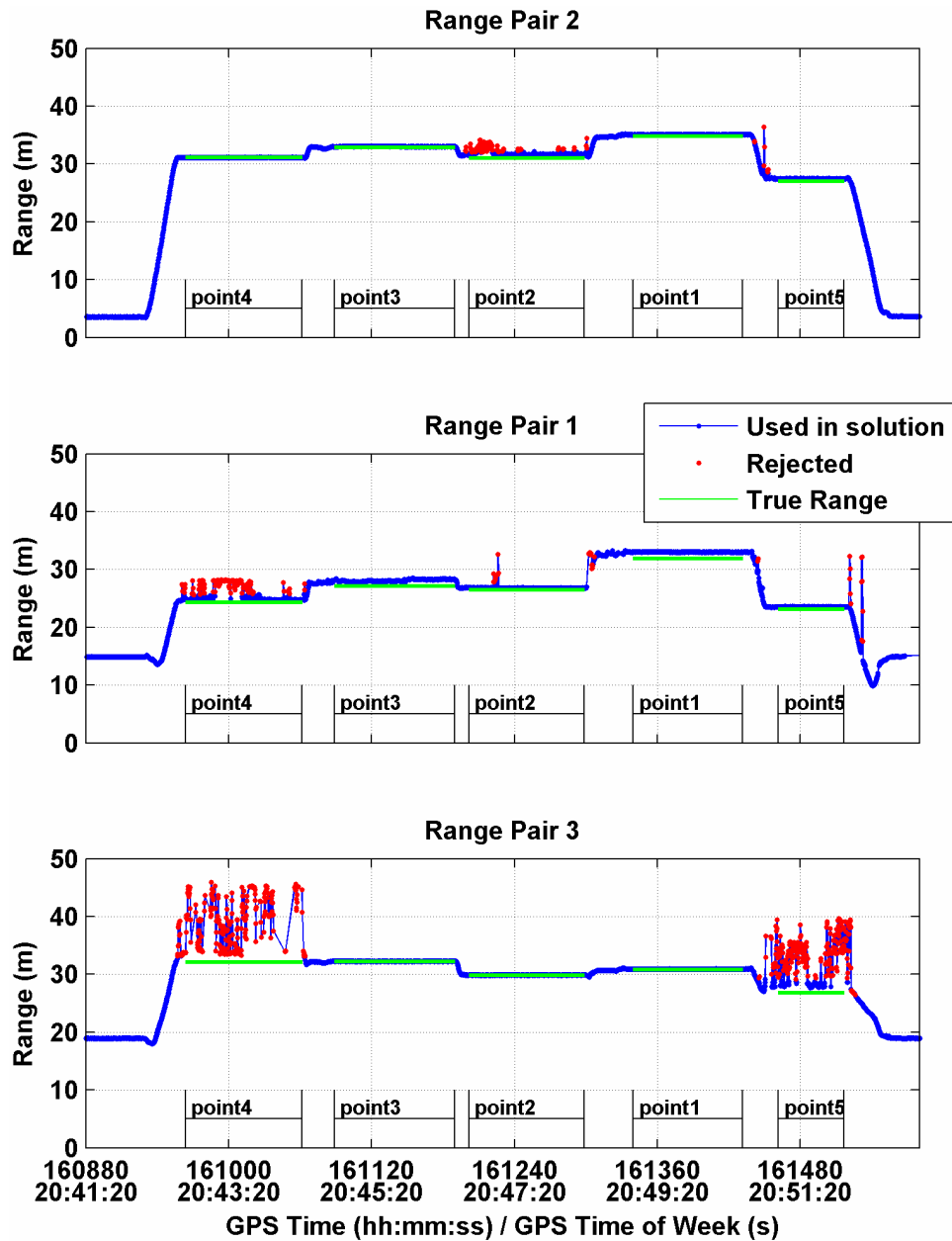


Figure 5.20: UWB ranges and rejected measurements for the MSS1 GPS+UWB solution

The UWB range errors for each range pair were calculated at all of the static points.

Histograms of the raw UWB range errors, the range errors after applying the bias and scale factor corrections determined by the GPS+UWB solution, and the range errors without corrections used by the UWB-only solution are shown in **Figures 5.21, 5.22, and 5.23** for range pairs 1, 2, and 3 respectively. The portion of each bin for which the UWB ranges were rejected by the solution is indicated in red. If a bin is totally shown in red, all of the data in that bin was rejected by the filter. It is difficult to see the rejected portions of the bins for range pair 1 for the UWB-only solution but there are small portions of the bins rejected in the bins that are more than the 1 m. The other figures provide clear indications of the portions of each bin that are rejected. The GPS+UWB solution performs well to detect and reject UWB range blunders. The UWB-only solution fails to reject gross blunders and often rejects good measurements.

The application of the bias and scale factor corrections results in a more centralized distribution of the errors. A total of 78% 44% and 74% of the range errors are contained within 0.5 m for range pairs 1, 2, and 3 respectively. A total of 95% 61% and 75% of the range errors are contained within 1.0 m for range pairs 1, 2, and 3 respectively. It can be concluded from this that a large portion of the UWB range measurements can be considered outliers.

The distributions of the UWB range errors for range pair 1 and range pair 2 are interesting. They are bimodal distributions (with an additional tail from outliers) that are likely comprised of line-of-sight measurements with short delay multipath interference (within half a pulse width, i.e. 1.5 ns or 45 cm) and some short delay reflection signals (i.e. no line-of-sight) that are not rejected by the filter.

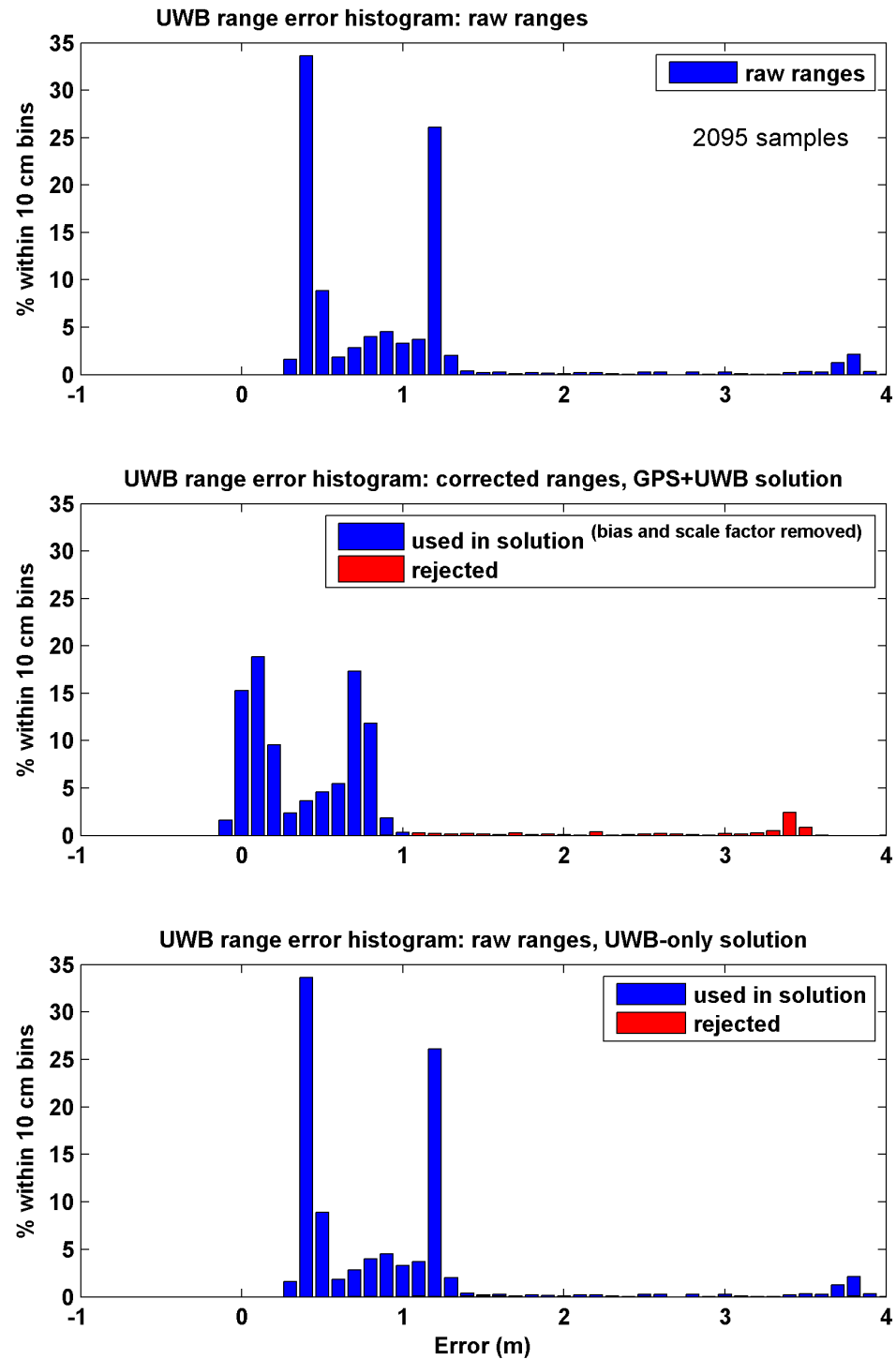


Figure 5.21: UWB range error histogram for range pair 1

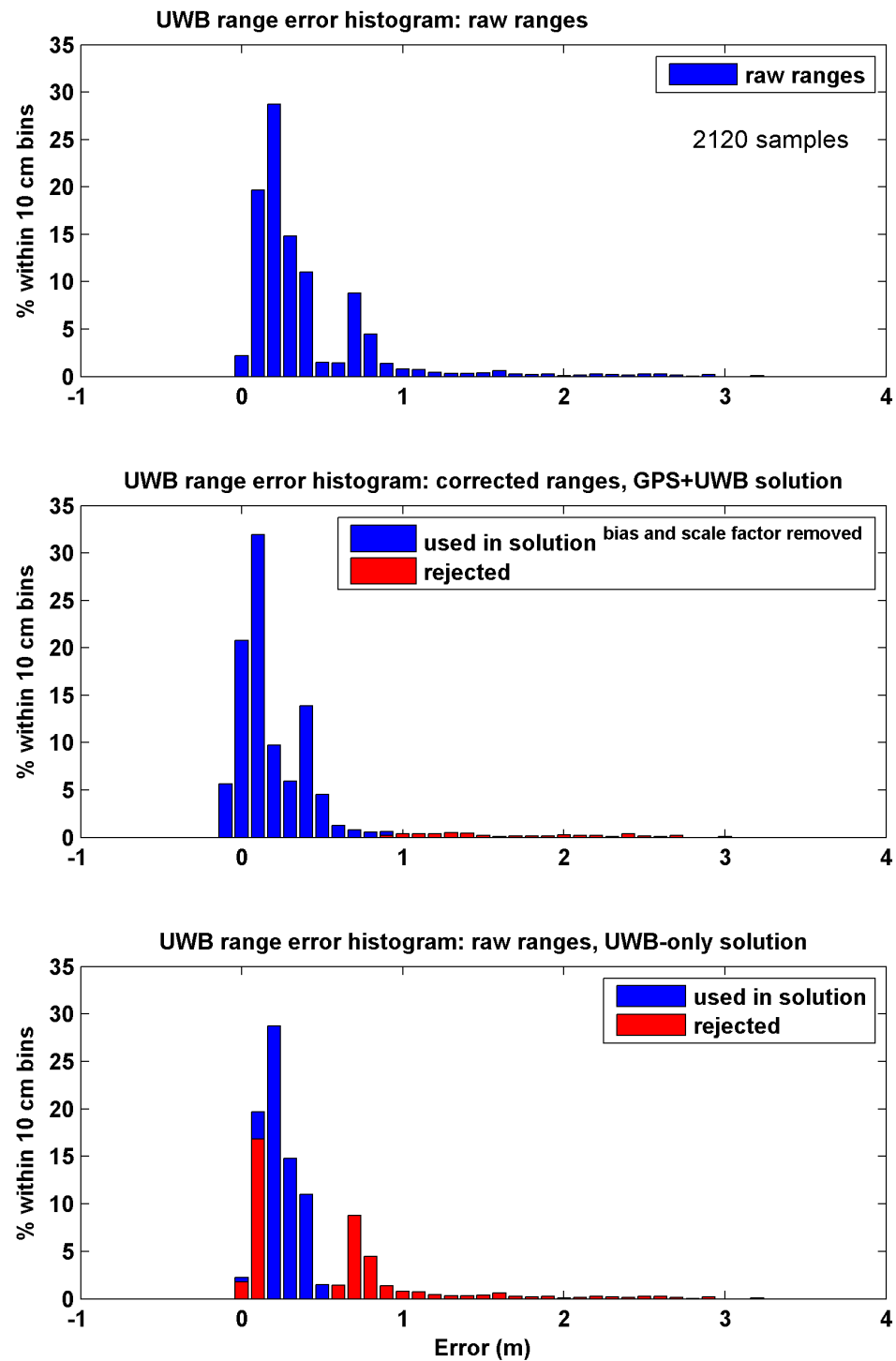


Figure 5.22: UWB range error histogram for range pair 2

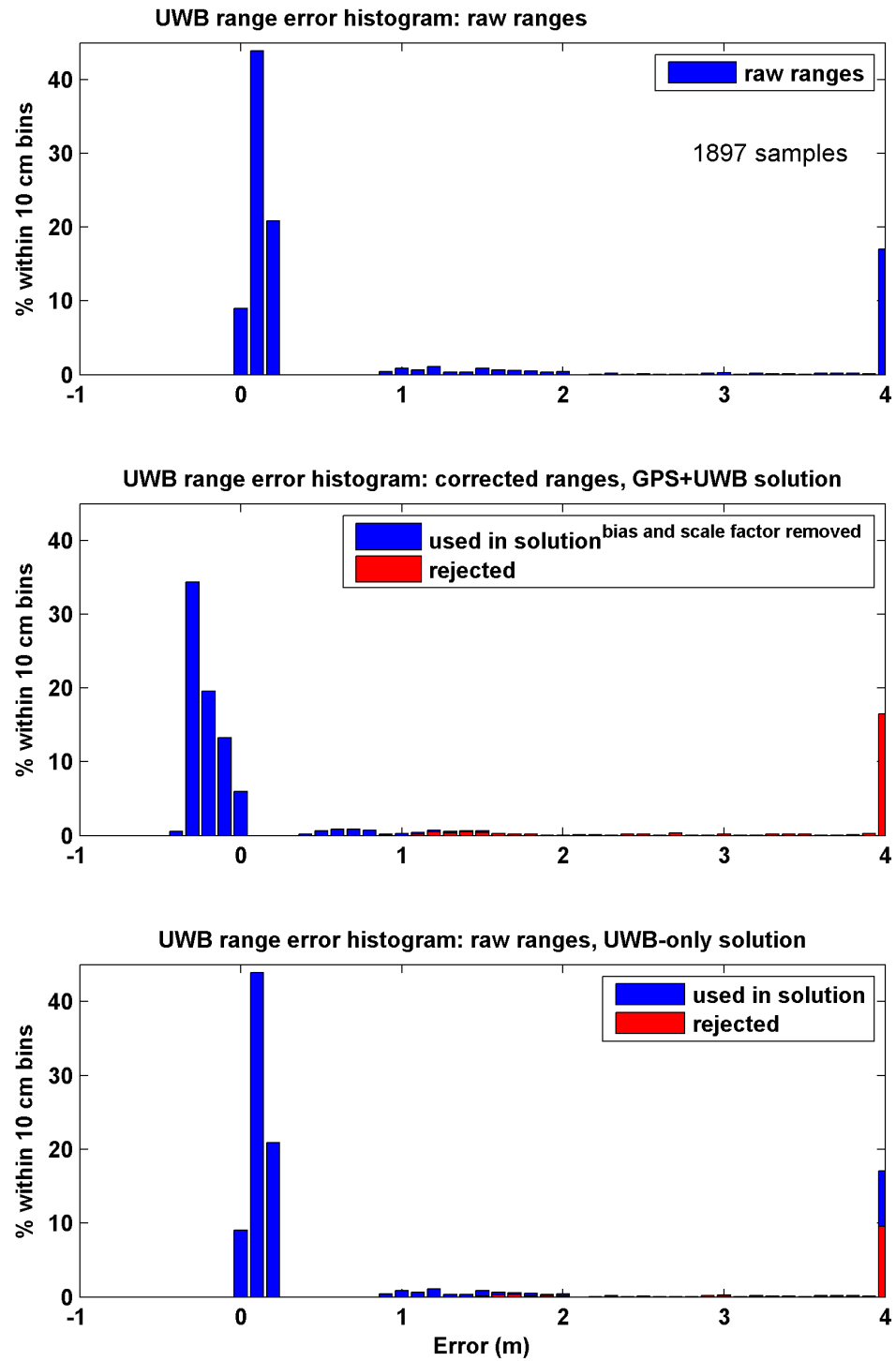


Figure 5.23: UWB range error histogram for range pair 3

5.2.3 GPS Pseudorange Errors

The urban canyon environment with large buildings having smooth glass and steel surfaces is problematic for GPS positioning in three ways. The first problem is a lack of satellite observations and restricted geometry due to signal masking. Hence there is need for augmentation with UWB ranges. The second problem is multipath induced tracking error which affects the pseudorange measurements. Lastly, situations arise in which buildings block the direct satellite signals while strong specular reflections due to others buildings are tracked. The attenuated direct signal may still reach the antenna but if the power of the reflected signal is greater, the receiver may track the echo-only (i.e. reflected) signal. This situation leads to large measurement errors greater than the maximum possible multipath error regardless of the type of correlator-based mitigation technique used by the receiver (MacGougan, 2008).

The effect of GPS multipath is evident in the observations by differencing the pseudorange and carrier phase observations (both in units of metres). This is conventionally called the code-minus-carrier metric. While the carrier phase of the signal is tracked without loss of phase lock, the difference between the carrier phase and pseudorange reflects the pseudorange measurement noise and multipath as well as a bias term which includes twice the ionospheric delay (a very low frequency term) and the carrier phase ambiguity. Given the pseudorange measurement model and carrier phase measurement model, the code-minus-carrier is found to be

$$\begin{aligned}
 P &= \rho + d\rho + c(dT - dt) + I + T + \varepsilon_P \\
 \Phi &= \rho + d\rho + c(dT - dt) - I + T + \varepsilon_\Phi + \lambda N \\
 P - \Phi &= 2I - \lambda N + \varepsilon_P - \varepsilon_\Phi \\
 \varepsilon_\Phi &\ll \varepsilon_P \\
 P - \Phi &\approx (2I - \lambda N) + \varepsilon_P
 \end{aligned} \tag{5.1}$$

where P is the pseudorange measurement (m), ρ is the geometric range, $d\rho$ is satellite

orbital error, dT is the receiver clock offset, dt is the satellite clock offset, I is the ionospheric delay, T is the tropospheric delay, ε_P is pseudorange noise and multipath, Φ is the carrier phase measurement (m), λN is the carrier phase ambiguity (m), and ε_Φ is carrier phase measurement noise.

The code-minus-carrier for PRN 22, which rises from an elevation angle of 29° to 38° during the MSSSI test, is shown in **Figure 5.24**. The azimuth of this satellite places it in the southwest corner of the sky and it is in a prime location for generating GPS multipath given the satellite and building geometry. The line-of-sight path from the satellite to the GPS antenna is not blocked and the building behind the GPS antenna acts as a specular reflector. There are clearly multipath effects characterized by oscillating pseudorange error as the multipath signal rotates in and out of phase with the line-of-sight signal. The GPS+UWB filter uses innovation testing to reject measurements and the rejected data is shown in red.

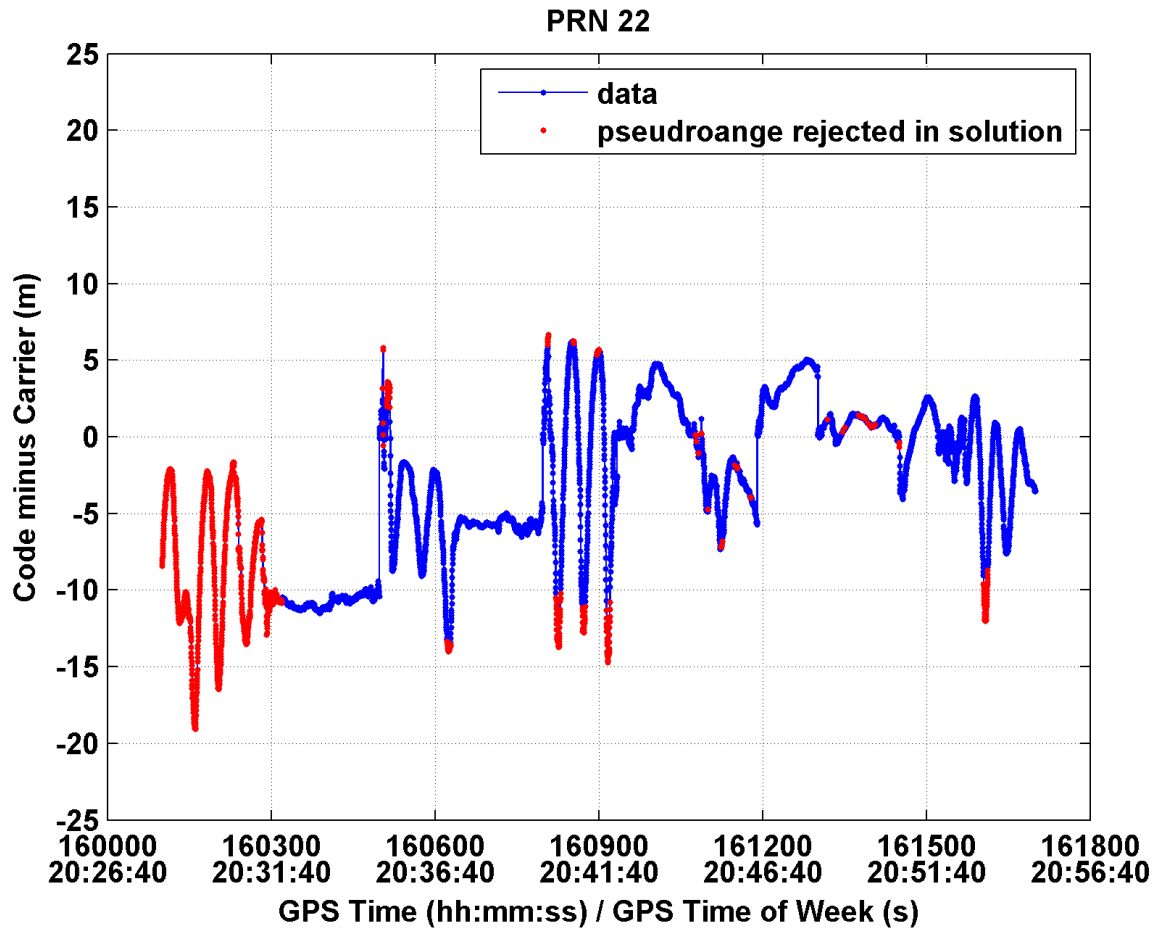


Figure 5.24: Code-minus-carrier for PRN 22

PRN16, which drops from an elevation angle of 19° to 12° during the MSSSI test, is partially masked by trees and a nearby building. The code-minus-carrier for PRN 16 is shown in **Figure 5.25**. There are large (10-15 m) multipath error oscillations and potentially echo-only signals tracked by the receiver. In the presence of such errors, innovation testing of the GPS observations is essential. This is especially important when the GPS carrier phase measurements are not usable and high accuracy is to be maintained.

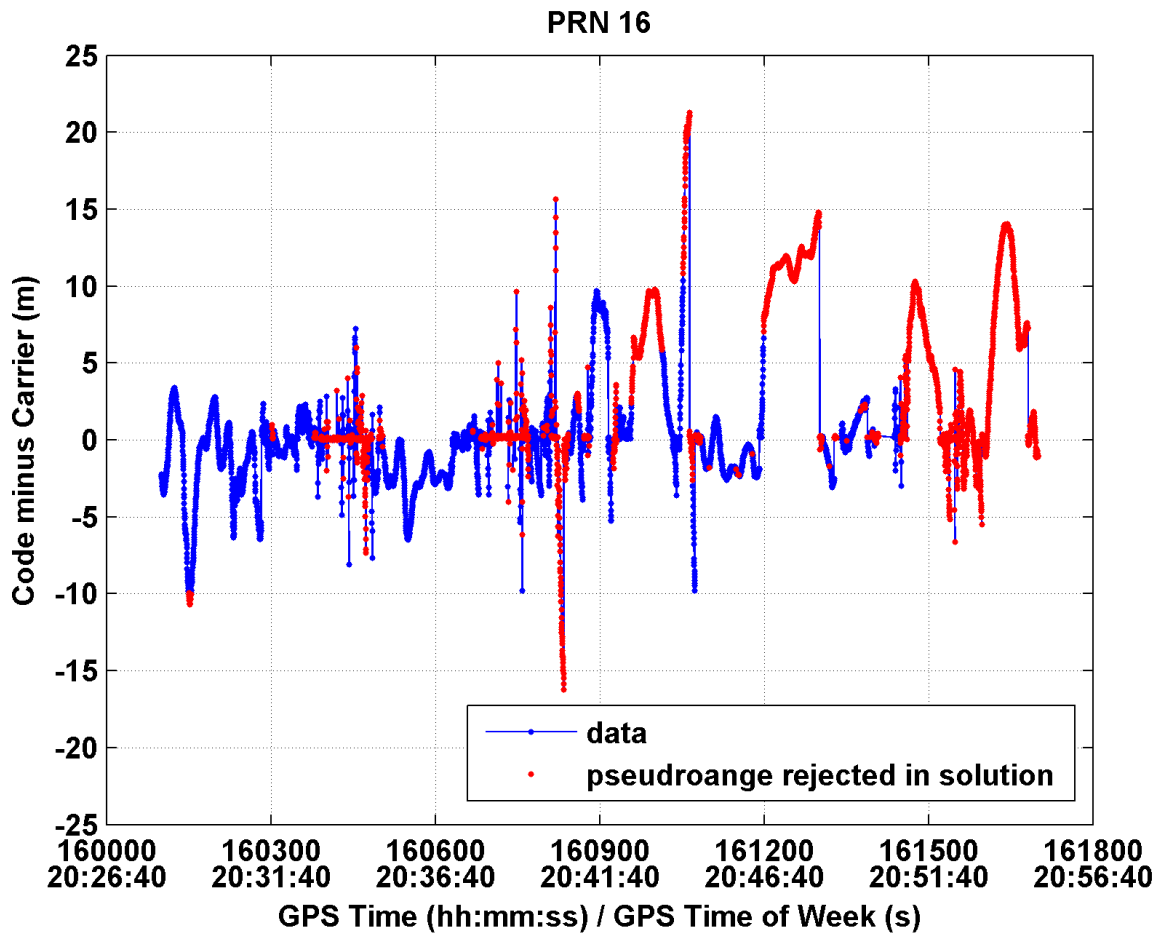


Figure 5.25: Code-minus-carrier for PRN 16

5.3 Summary

This chapter demonstrated tight-coupling of GPS and UWB using two types of UWB ranging technology in a difficult urban environment. The procedure used to perform the survey was time consuming and not optimal. This is not a problem for research applications but surveyors desire a tightly-coupled system that performs in real time without the need for extensive training. The next chapter discusses a novel method

to deploy the UWB equipment and perform a real-time survey using a tightly-coupled GPS+UWB system.

Chapter 6

System and method for tightly-coupled GPS+UWB surveying

GPS real-time-kinematic surveying is very useful for surveying companies because of the accuracy obtained using the technology without the need for highly skilled operators. The GPS+UWB integration described and tested in this thesis can be used to extend the accuracy achievable using RTK to new environments without dramatically increasing the level of skill required by the operators. A method of UWB reference receiver deployment and a procedure for performing tightly-coupled surveying using GPS and UWB is discussed in this chapter.

The combined apparatus for the UWB reference stations and the pole-mounted survey system was introduced in Chapter 3. The goal of the apparatus is to allow the UWB range measurements to translate to the phase center of the GPS antenna which is the position estimated in the tightly-coupled filter. The overall survey method involves three main tasks. The first task is the deployment of the UWB reference stations on either known points or at locations which can be surveyed using GPS and are in a good position to enable line-of-sight range measurements in the survey area. The second task is the initialization walk which is necessary to enable the estimation of UWB bias and scale factor states prior to the actual survey. The last task is the survey itself. It is possible to perform the entire procedure using a single GPS receiver (in addition to the GPS reference receiver for differential purposes).

6.1 UWB radio mounts

The UWB radio mounts are designed so that the phase center of the UWB antenna is aligned vertically above a threaded countersink (e.g. 5/8th inch) and below a threaded mounting bolt (e.g. 5/8th inch). This allows the mount to be placed on top of a standard surveying tribrach with a puck (with a threaded mounting bolt) or on a survey range pole and allows a GPS antenna to be placed above the UWB radio antenna. The mount used with the MSSSI UWB radio is shown in **Figure 6.1**.



Figure 6.1: MSSSI UWB radio mount

6.1.1 Tilt sensor

The use of a tilt sensor (also called an inclinometer) allows the lever arm between the GPS antenna and the UWB antenna to be monitored in real time. Electrolytic or accelerometer based tilt sensors can be used for this purpose. Given that 2° of tilt only corresponds to about 4 mm of ranging error for a 12 cm lever arm, this sensor need not be high accuracy (i.e. a 2° precision instrument is sufficient). The sensor can be mounted beside the UWB radio, on the range pole, or even on the GPS antenna.

6.2 Deployment of the UWB reference stations

The deployment of the UWB reference stations proceeds as follows. First and foremost, the deployment of the reference stations should proceed after identifying the area to be surveyed. It follows that the selection of the reference station locations depends on obtaining: the best line of sight UWB range measurements (i.e. minimal obstructions), and the best possible geometry for improving the solution (by trying to enclose a large volume with the UWB reference stations to obtain the best DOP).

Generally, the UWB reference stations are deployed at similar heights. This means that the UWB measurements do not contribute very much to the estimation of the height parameter (i.e. do not improve VDOP) but they do significantly improve HDOP. To obtain better VDOP and hence contribute more to the height solution, the UWB reference stations can be placed with significant height differences.

6.2.1 Deployment over known points

For UWB reference stations that are to be placed over previously surveyed coordinates, the UWB radio is set up (usually with a tripod and tribrach) using the UWB radio

mount and the height to the base of the threaded bolt on the top of the mount is recorded. The GPS antenna that will be used for the survey has a known phase center. The distance from the bottom of the threaded countersink of the antenna to this phase center is known. The virtual coordinates of the UWB reference station antenna are entered as the coordinates of the known point plus the height already recorded plus the GPS antenna phase center height. The UWB reference station antenna position is considered a virtual position because it pertains to a virtual point above the phase center of the actual UWB antenna. This concept is illustrated in **Figure 6.2**. An UWB range measurement between this reference station and another UWB radio mounted on an identical mount is equivalent to a range measurement between the virtual UWB antenna position and the phase center of the GPS antenna on the survey system (provided both the reference station and the survey system are aligned to the local gravity vector (i.e. plumb)).

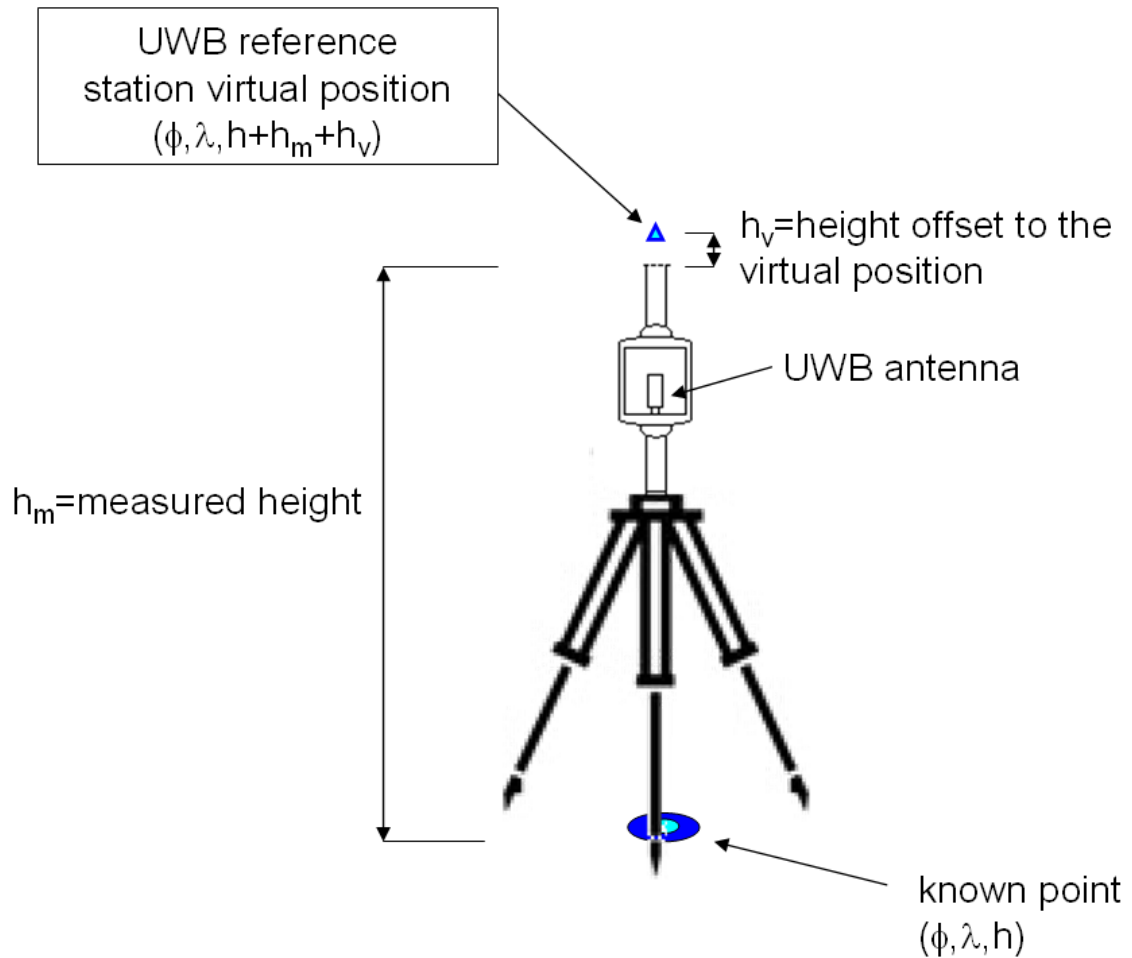


Figure 6.2: An UWB reference station over a known point

6.2.2 Deployment in the field using GPS

UWB reference stations can be deployed at unknown locations using a method that gains from other UWB reference stations that have already been deployed. This method only requires a single GPS survey antenna and receiver (in addition to the GPS system used to provide differential GPS corrections). Once suitable locations are selected, the UWB reference stations are set up (e.g. on tripods). The station with the best GPS

satellite visibility conditions is surveyed first. The GPS antenna is mounted over the first station's UWB antenna and an RTK position is determined. If UWB reference stations located on previously surveyed points are set up, the tightly-coupled RTK solution is used. The range measurement obtained from the UWB reference station to the reference station under survey is biased and in-run estimation of a bias and scale factor error model is not practical. A simple error model based on calibration testing of the radios could be applied but this is likely only a typical scale factor correction and the bias used in the model would be set to zero. Thus, the measurement is used by the estimation filter but with appropriate associated measurement variance. The solution still benefits from the tight coupling of the UWB and GPS measurements. The virtual position of the UWB reference station is then recorded as the position determined by the RTK system (tightly-coupled or simply GPS-only RTK for the first point). The estimated accuracy of the UWB reference station is also recorded. The GPS antenna and system are then moved and the antenna is mounted over the next UWB reference station with the second best GPS satellite visibility conditions. The UWB ranges between the first UWB reference station and perhaps some previously surveyed UWB reference stations are used with GPS measurements in a tightly coupled RTK solution to establish the virtual position and estimated accuracy of the second virtual UWB reference station. This concept is illustrated in **Figure 6.3**. Again, the UWB range measurements are biased but still used with appropriate measurement variance by the estimation filter. The virtual positions and estimated accuracies of the remaining UWB reference stations are determined using this method of moving the GPS antenna and utilizing UWB reference stations that are already set up.

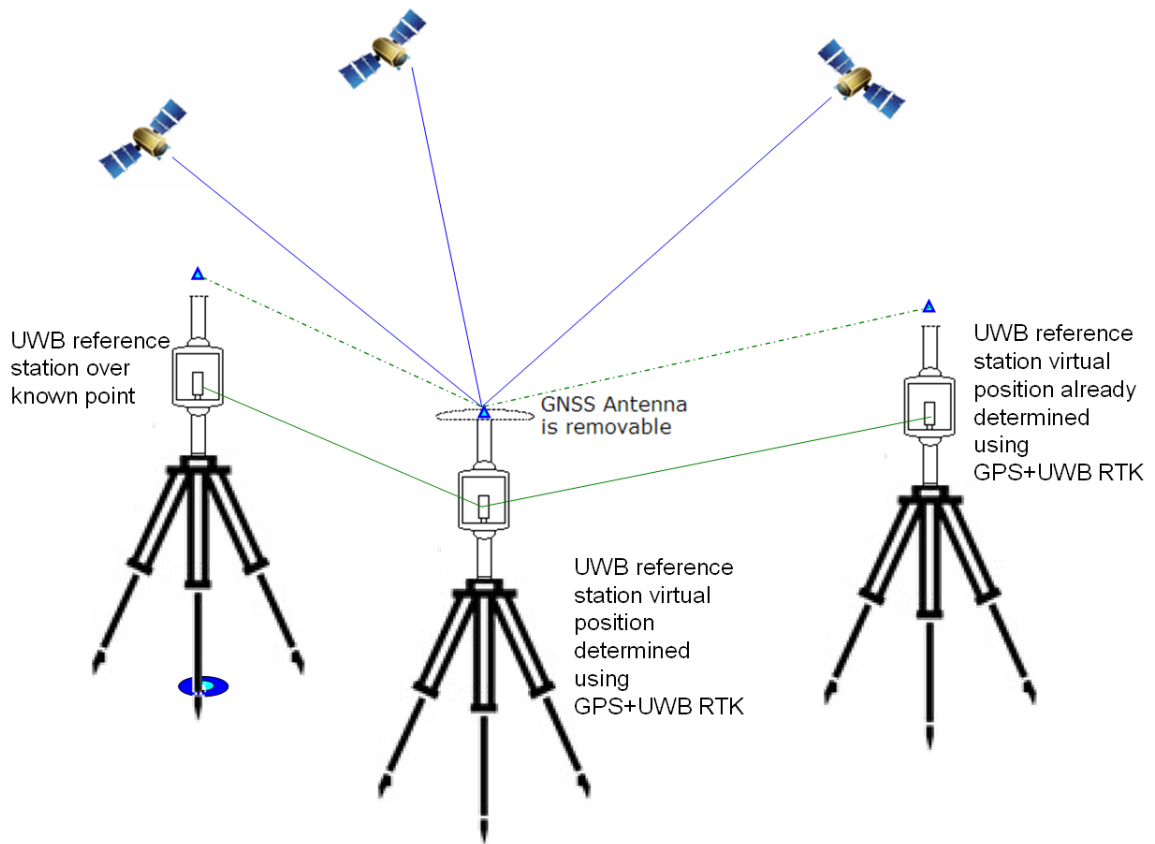


Figure 6.3: Surveying an UWB reference station over a new point

The virtual positions of the UWB reference stations and the associated measurement variance are recorded by the survey system during deployment. The estimated uncertainty in the UWB reference positions must be accounted for by additional UWB range measurement variance when the UWB range is used in the estimation filter. Some UWB ranges may be from accurate locations (i.e. within a centimetre) and some ranges may be from rough locations (i.e. metre level). Both types of observations will still benefit the tightly-coupled solution.

6.3 The initialization walk

Once the virtual antenna positions of all of the UWB reference stations are established, the GPS antenna is mounted on the survey system to be used in the survey area (e.g. a survey range pole). The combined apparatus is then taken for a walk while trying to keep the system as plumb as possible. The walk should occur in the best possible GPS satellite visibility conditions while maintaining line-of-sight to the UWB reference stations. This initialization walk allows the estimation of bias and scale factor states for each UWB range pair provided that a quality tightly-coupled RTK solution is computed.

6.4 The survey

Once the initialization walk is completed, the survey system is taken into the survey area. Points are occupied until the estimated accuracy of the solution is suitable. In other words, standard RTK surveying techniques are employed in the survey area.

6.5 Details

The bias and scale factor estimates are relatively stable during a survey. The bias states will change over time because they are a function of the oscillator stability of the UWB radios. These oscillators may exhibit frequency bias as a function temperature and thus a few minutes of initialization time prior to UWB radio use to let the internal temperature of the radio stabilize is a good idea. The scale factor state may change if the radio is powered off and on. This occurs for the MSSSI radios because they use a constant threshold fine timing discriminator. This threshold is set once based on

internal noise when the radio is turned on. Thus, cycling the unit's power will change the scale factor state. This is undesirable so the power on the UWB radios should be kept on during deployment, the initialization walk and during the survey.

6.6 Summary

The overall method is well summarized by the flowchart given in **Figure 6.4**. This survey method and claims are described the following patent application:

- K. O'Keefe, G.D. MacGougan, and D.S. Chiu (2008). System and methods for real time kinematic surveying using GNSS and ultra wideband ranging. United States provisional patent application. Filed in September 2008.

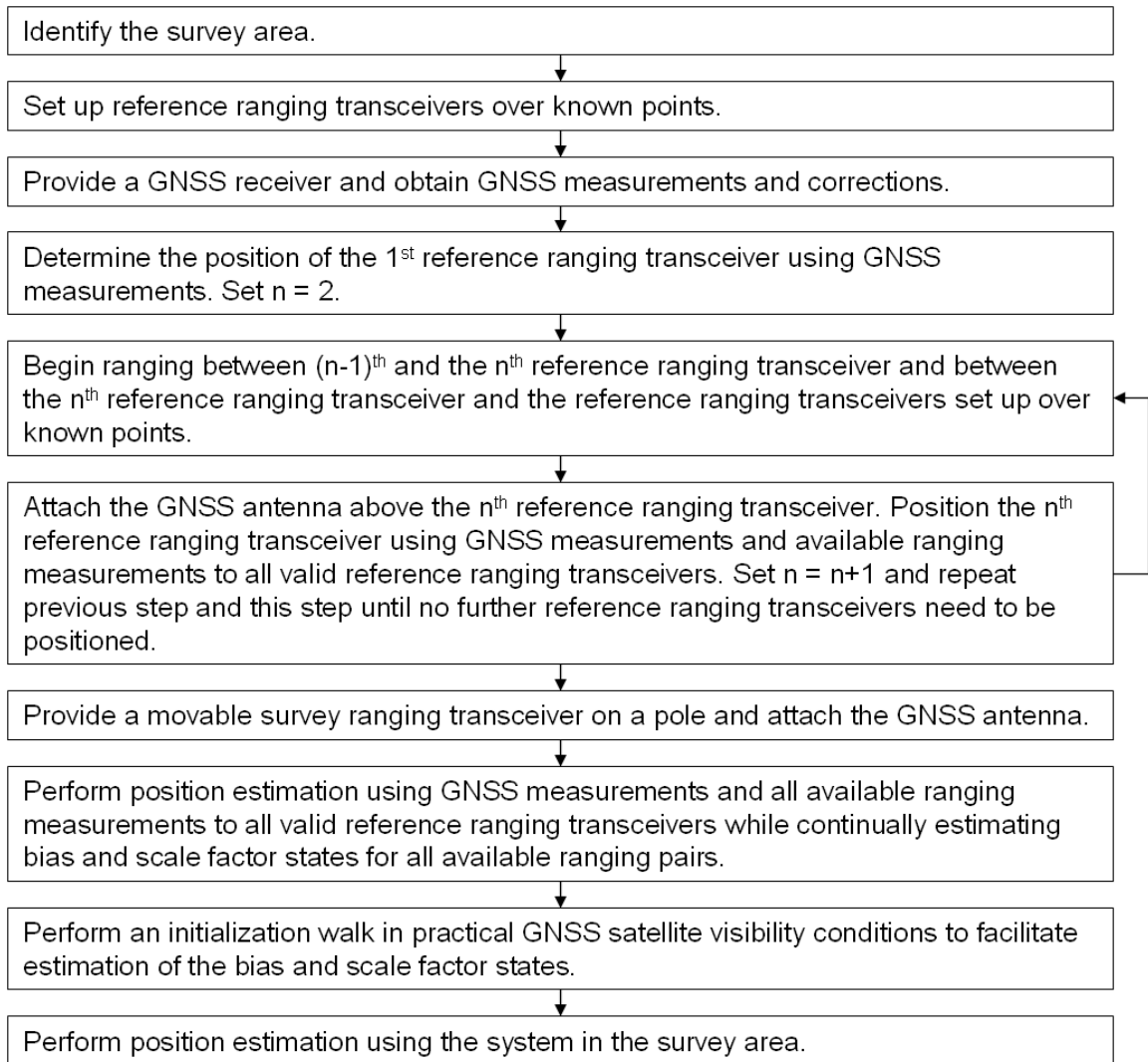


Figure 6.4: The GPS+UWB survey method

Chapter 7

Conclusions and future work

7.1 Summary

The recent decision by the FCC to allow unlicensed ultra-wideband transmissions offers promising potential for ranging applications. The Cramer-Rao lower bound analysis in Chapter 2 shows that UWB ranging has potential for sub-decimetre ranging precision. The two-way time-of-flight method is used by two types of UWB ranging radios evaluated in this research. This asynchronous ranging method produces direct ranging measurements without the need for complicated synchronization techniques and it is well suited for outdoor use (i.e. surveying) given the FCC restriction that outdoor UWB systems must not be set up using fixed infrastructure.

The two-way time-of-flight method induces a ranging bias error due to frequency bias in the oscillators used in the ranging radios during the fixed turn-around-time. In addition, the method used for pulse detection and fine-timing may induce a geometric walk error that is a function of the signal amplitude. This translates into a scale factor error as signal strength decreases with the distance measured.

Two types of UWB ranging radios, one from Multispectral Solutions Inc. (MSSI) and one from Time Domain Corp. (TDC) with bandwidths (10 dB) of 500 MHz and 3.2 GHz respectively, were evaluated in line-of-sight conditions. Both radios offer sub-metre ranging accuracy for range measurements up to 100 m without compensation for error effects. Line-of-sight testing showed that both types of radios exhibit ranging errors that fit a first order linear trend well. Thus, it is reasonable to model the ranging

errors with a bias term and scale factor term. The bias errors were observed to be less than 50 cm and 10 cm for the MSSSI and TDC radios respectively during testing. Scale factor errors are significant for both radio types. The TDC ranges exhibit scale factor errors of 2000 to 4000 ppm. The MSSSI ranges have scale factor errors ranging from 4000 to 13000 ppm based on the testing performed.

In theory, UWB is very resistant to multipath, provided the line-of-sight signal is detected. Testing was performed with signal blockage and strong specular reflection sources to evaluate the performance of the two ranging radio types in multipath conditions. In testing, the TDC radios likely measured strong reflection signals rather than the line-of-sight signal in the unobstructed cases and the radios failed to obtain measurements through a metal sign. The MSSSI radios exhibited line-of-sight measurements for the unobstructed case and errors characteristic of measuring strong reflected signals when the line-of-sight signal was blocked by a metal sign.

To facilitate tight-coupling of the GPS and UWB systems a co-axial mount was developed. The apparatus allows UWB measurements to translate to the phase center of the GPS antenna and it is the position of this phase center that is estimated by an estimation filter. The tight-coupling of the measurements from the two systems required the development of an estimation method and a method to deal with measurement blunders. A sequential discrete-time extended Kalman filter was selected for the tight-integration of GPS and UWB. Single-difference (between receiver) GPS measurements and UWB range measurements were used to update the filter. It included states for the position, a single-difference GPS receiver clock state, bias and scale factor states for each UWB range pair, and states for the single-difference GPS ambiguities. The filter used innovation testing to try to identify GPS and UWB measurement blunders before they could impact the solution. A single-difference float solution was employed rather than a double-difference float solution. The reasons and advantages for this

choice were discussed. The single-difference approach is computationally efficient and has advantages for detection of measurement blunders.

The results of static testing of the tightly-coupled system demonstrated that utilizing two-way time-of-flight UWB ranges with GPS RTK provides better accuracy, better ability to resolve integer ambiguities and enhanced fixed ambiguity solution availability compared to GPS alone in conditions with severe signal masking. In marginal GPS-only surveying conditions, with only 4 satellites present due to a 40° elevation mask, the GPS+UWB float solution performed more than an order of magnitude better than the GPS-only float solution in terms of both horizontal error and vertical error. For example, this was presented in **Table 4.1** with RMS float solution horizontal errors of 1.802 m and 0.024 m for the GPS-only and the GPS+UWB solutions respectively. The GPS+UWB solution was able to fix integer ambiguities correctly while the GPS-only solution could not. The GPS+UWB fixed solution RMS horizontal accuracy was 0.014 m while the GPS-only fixed solution performs no better than the GPS-only float solution.

To achieve RTK level positioning accuracy, it is important that UWB ranges are compensated for turn-around-time bias and for scale factor error. This work demonstrated that UWB errors can be successfully estimated in a real-time filter. In kinematic testing, when the GPS conditions were degraded using a 40° elevation mask and only 3 satellites were used, the accuracy of the system (3D baseline) was typically better than 5 cm and better than 10 cm most of the time compared to the GPS-only references solution. This is excellent performance compared to GPS-only which could not even provide a solution.

Initial testing demonstrated tightly-coupled GPS and UWB using signal masking in post-processing (albeit with a real-time approach). The degraded GPS environment was created artificially by simply excluding GPS satellites from the solution using an

elevation mask. The next step was to test the system in an environment with real signal masking and strong potential for multipath interference.

A difficult urban canyon environment with realistic multipath and signal masking conditions was selected for further testing. The tight-coupling of GPS and UWB ranging was evaluated by surveying 5 static points next to an eight story building. Sub-metre level position accuracy was maintained for all test points using tight-coupling in conditions where GPS-only, UWB-only, or loosely-coupled solutions are unavailable or unreliable. The loosely-coupled solution was shown to suffer from reliability problems due to the inclusion of measurement outliers in both the GPS and UWB solutions. The tightly-coupled solution was effective in detecting and removing measurement blunders in this case. The GPS-only solution and the UWB-only solution suffered from very poor redundancy and detecting and removing measurement outliers was problematic. The measurement redundancy obtained using tight-coupling for estimation allowed detection of UWB and GPS measurement blunders. Loose-coupling of the GPS-only and UWB-only solution did not have this benefit and thus the tightly-coupled solution clearly outperformed the loosely-coupled solution.

Surveyors using RTK expect horizontal positioning accuracy at the 1-3 cm level. Adding more UWB reference stations would help to improve the solution accuracy in the difficult urban canyon test with improved solution geometry and improved non-line-of-sight UWB measurement rejection. It is unfortunate that carrier phase lock could not be maintained in the difficult urban canyon test. Because of this, the phase measurements that were obtained did not contribute to the solution and a fixed solution could not be obtained. The fixed solution available away from the building was useful in improving the estimated UWB error states. This environment may have been too difficult to achieve RTK quality results but augmentation with UWB ranging technology clearly benefits the solution accuracy considerably.

7.2 Conclusions

The main conclusions resulting from this work are as follows:

- UWB range measurements have the potential to achieve 1 to 10 cm precision based on Cramer-Rao lower bound analysis.
- Current UWB range measurements obtained using two different UWB radio types that employ the two-way time-of-flight ranging method achieve 0.5 to 1 m accuracy without compensation for systematic errors.
- Line-of-sight UWB range measurement errors can be modeled reasonably well by a bias term and a scale factor term with residual systematic errors typically less than 10 cm RMS. The bias term is the turn-around-time bias associated with the two-way time-of-flight ranging method. The scale factor term arises because of systematic errors in fine-timing of UWB pulses.
- The bias and scale factor errors are stable during a typical survey period (e.g. 1 hour) while the units are powered continuously. However, they changed significantly each time the UWB radios were powered off and on. Thus, calibration was not optimal and real-time estimation of the parameters was needed. It is possible to estimate the bias and scale factor terms for each UWB range pair using an initialization walk prior to performing a GPS+UWB survey.
- UWB measurement blunders due to non-line-of-sight signal measurements are a concern.
- In marginal GPS conditions (i.e. 4 to 5 satellites available), RTK level (1-3 cm, 1σ horizontal) accuracy was maintained by the tightly-coupled GPS+UWB solution. In testing of this case, the GPS-only solution did not succeed in computing a correct fixed ambiguity solution and could only decimetre level accuracy.
- In non-functional GPS RTK conditions (i.e. less than 4 satellites and no GPS-only solution), 5-10 cm level accuracy was maintained using the tightly-coupled GPS+UWB solution in the case of signal masking using an artificial signal mask.
- In testing compared to GPS-only, UWB-only, and loosely-coupled solutions, the tightly-coupled GPS+UWB solution provided the best ability to detect and exclude measurement blunders and the best positioning accuracy.
- In testing in a severe urban canyon environment, the tightly-coupled GPS+UWB solution maintained sub-metre accuracy.

7.3 Future work

The method used to deploy the UWB reference stations and perform the survey has yet to be fully evaluated in a realistic challenging surveying environment (i.e. where some GPS carrier phase measurements can be maintained and used). This topic is the focus of further investigation during the summer of 2009.

The estimation method used in this research relied on only GPS L1 measurements and short baselines since this was sufficient to meet the objectives of this research. The use of GPS L2 measurements would improve the estimation performance for longer baselines and improve the time to fix ambiguities. The estimator should also make use of GLONASS and SBAS satellite observations to improve performance in poor GPS visibility environments.

The next research step, after improving the performance of the UWB radios and enabling more satellite observations in the tightly-coupled estimation method, is to assess the practical application of GPS+UWB for commercial RTK surveying. This requires test cases and working with appropriate industry groups.

7.4 Outlook

UWB ranging is receiving a lot of attention for indoor based positioning and navigation systems. It is limited in outdoor usage due to FCC restrictions to non-fixed infrastructure applications; however, with low cost, low complexity, and relatively easy deployment, UWB ranging can be used outdoors to augment GPS and GNSS for high precision surveying. The primary limitation of the technology is its operational range which for the UWB radios evaluated was limited to 200 m. With reduced pulse repetition frequencies, higher individual pulse energies, and time dithering of repeated pulses,

it is possible that the operational range of UWB technology can be increased to the kilometre level. The fact that non-FCC compliant equipment in [Fontana \(2002\)](#) has already been demonstrated 2 km level ranging suggests that the range can be extended. The question is how to do so with unlicensed UWB ranging technology.

UWB ranging radio technology is not yet specialized for high accuracy sub-metre applications. The use of better quality oscillators and better fine timing discriminators in the UWB radios would improve UWB range measurement accuracy by reducing bias and scale factor errors.

Tightly-coupled GPS+UWB for RTK surveying is a promising new technology that extends RTK surveying to new environments. In addition, in marginal GPS-only surveying environments, position accuracy and RTK solution availability are improved substantially. With improved performance and new potential application areas, it is hoped that this technology is commercialized in the near future.

Bibliography

- Amann, M., T. Bosch, R. Myllyla, and M. Rioux (2001). Laser ranging: a critical review of usual techniques for distance measurement. *Society of Photo-Optical Instrumentation Engineers*, 40(1), pages 10–19.
- Baarda, W. (1968). A Testing Procedure For Use In Geodetic Networks. Netherlands Geodetic Commission, Publication on Geodesy, New Series 2. No. 5, Delft, Netherlands.
- Barnes, J., C. Rizos, M. Kanli, and A. Pahwa (2006). A solution to tough GNSS land applications using terrestrial-based transceivers (LocataLites). In *Proceedings of the Institute of Navigation GNSS Conference*, pages 1487–1493. Fort Worth, TX.
- Barrett, T. (2001). History Of Ultra Wideband Communications And Radar, Part I. UWB Communications. *International Microwave Journal*, 44(1), pages 22–56.
- Barton, R. and D. Rao (2001). Performance Capabilities of Long-Range UWB-IR TDOA Localization Systems. *EURASIP Journal on Advances in Signal Processing*, Article ID 236791, 2008, page 17 pages.
- Bartone, C. and S. Kiran (2001). Flight Test Results of an Integrated Wideband Airport Pseudolite for the Local Area Augmentation System. *Navigation Journal of the Institute of Navigation*, 28(1), pages 35–48.
- Brodie, K. (2001). Improved chi-square fault detection for GPS navigation. In *Proceedings of the ION National Technical Meeting*, pages 438–446. Long Beach, CA.
- Brown, R. and P. Hwang (1997). *Introduction to Random Signals and Applied Kalman Filtering*, 3rd Edition. John Wiley and Sons.
- Bryson, A. E. and L. Henrikson (1968). Estimation Using Sampled Data Containing Sequentially Correlated Noise. *Journal of Spacecraft and Rockets*, 5(6), pages 662–665.
- Bryson, A. E. and D. Johansen (1965). Linear Filtering for Time-Varying Systems Using Measurements Containing Colored Noise. *IEEE Transactions on Automatic Control*, 10(1), pages 4–10.
- Cantor, S., A. Stern, and B. Levy (1999). Clock Technology. In *Proceedings of the Institute of Navigation ION Annual Meeting*, June 28-30, Cambridge, MA, pages 37–47.

- Cardinali, R., L. D. Nardis, M.-G. D. Benedetto, and P. Lombardo (2006). UWB Ranging Accuracy in High- and Low-Data-Rate Applications. *IEEE Transactions On Microwave Theory And Techniques*, 54(4), pages 1865–1875.
- Cardinali, R., L. D. Nardis, P. Lombardo, and M.-G. D. Benedetto (2005). Lower bounds for ranging accuracy with Multi Band FDM and Direct Sequence UWB signals. In *Proceedings of the IEEE International Conference on Ultra-Wideband*, pages 302–307.
- Chiu, D. (2008). Ultra Wideband Augmented GPS, December, 2008, UCGE Report No. 20277, Department of Geomatics Engineering, University of Calgary.
- Chung, W. and D. Ha (2003). An Accurate Ultra Wideband UWB Ranging For Precision Asset Location. In *Proceedings of the IEEE Conference on Ultra Wideband Systems and Technologies*, pages 389–393.
- Cobb, H. (1997). *GPS Pseudolites: Theory, Design, and Applications*. Phd, Stanford University.
- Counselman, C. and R. Abbot (1989). Method of resolving radio phase ambiguity in satellite orbit determination. *Journal of Geophysical Research*, 94(B6), page 70587064.
- Dai, L., J. Wang, C. Rizos, and S. Han (2002). Pseudo-Satellite Applications in Deformation Monitoring. *GPS Solutions*, 5(3), pages 80–87.
- Dardari, D., C. C. Chong, and M. Win (2006). Improved lower bounds on time-of-arrival estimation error in realistic UWB channels. In *Proceedings of the IEEE 2006 International Conference on Ultra-Wideband*, pages 531–537.
- DeJonge, P. and C. Tiberius (1996). Integer estimation with the LAMBDA method. In *Proceedings IAG Symposium No. 115*, pages 280–284. Springer Verlag.
- Denis, B., J. Keignart, and N. Daniele (2003). Impact of NLOS Propagation upon Ranging Precision in UWB Systems. In *Proceedings of the IEEE Conference on Ultra Wideband Systems and Technologies*, pages 379–383.
- DiBenedetto, M.-G., T. Kaiser, A. Molisch, I. Oppermann, C. Politano, and D. Porcino (2006). *UWB Communication Systems A Comprehensive Overview*. Hindawi Publishing Corp. ISBN 977-5945-10-0.
- ECMA-368 (2006). *High Rate Ultra Wideband PHY, 2nd Edition*. ECMA.

- Euler, H. and H. Landau (1996). Fast GPS Ambiguity Resolution On-the-fly for Real-time Applications. In Proceedings of 6th International Symposium on Satellite Positioning, pages 650–659. Columbus, Ohio.
- FCC (2002). Revision of Part 15 of the Commissions Rules Regarding Ultra-Wideband Transmission Systems. First Report and Order in ET Docket No. 98-153. Adopted February 14, 2002, released July 15, 2002.
- FCC (2005). Revision of Part 15 of the Commissions Rules Regarding Ultra-Wideband Transmission Systems. Second Report and Order and Second Memorandum Option and Order in ET Docket No. 98-153. Adopted December 15, 2004, released December 16, 2004.
- Fernandez-Madrigal, J., E. Cruz-Martin, J. Gonzalez, C. Galindo, and J. Blanco (2007). Application of UWB and GPS technologies for vehicle localization in combined indoor-outdoor environments. In Proceedings of the IEEE 9th International Symposium on Signal Processing and Its Applications, pages 1–4.
- Fontana, R. (1999). Ultra Wideband Receiver with High Speed Noise and Interference Tracking Threshold. US Patent US005901172, Assigned to Multispectral Solutions Inc. May 4, 1999.
- Fontana, R. (2000). Ultra Wideband Precision Geolocation System. US Patent US006054950, Assigned to Multispectral Solutions Inc. April 25, 2000.
- Fontana, R. (2002). Experimental Results from an Ultra Wideband Precision Geolocation System. In Proceedings of the Short Pulse Electromagnetics 5. Edited by P. D. Smith and S. R. Cloude, pages 215–223.
- Fontana, R., E. Richley, and J. Barney (2003). Commercialization of an ultra wideband precision asset location system. In Proceedings of the IEEE Conference on Ultra Wideband Systems and Technologies, pages 369–373.
- Galler, S., J. Schroeder, G. Rahmatollahi, K. Kyamakya, , and K. Jobmann (2006). Analysis and practical comparison of wireless LAN and ultra-wideband technologies for advanced localization. In Proceedings of the IEEE/ION position, location and navigation symposium, pages 198–203.
- Gelb, A. (1974). Applied Optimal Estimation. Analytical Sciences Corporation.
- Gezici, S., Z. Tian, G. Giannakis, H. Kobayashi, A. Molisch, H. Poor, and Z. Sahinoglu (2005). Localization via Ultra-Wideband Radios. IEEE Signal Processing Magazine.

- Gonzalez, J., J. Blanco, C. Galindo, A. O. de Galisteo, J. Fernandez-Madriral, F. Moreno, and J. Martinez (2007). Combination of UWB and GPS for indoor-outdoor vehicle localization. In Proceedings of the IEEE International Symposium on Intelligent Signal Processing, WISP, pages 1–6.
- Guvenc, I. and Z. Sahinoglu (2005). Threshold Selection for UWB TOA Estimation Based on Kurtosis Analysis. *IEEE Communications Letters*, 9(12), pages 1025–1027.
- Guvenc, I., Z. Sahinoglu, and P. Orlik (2006). TOA Estimation for IR-UWB Systems With Different Transceiver Types. *IEEE Transactions on Microwave Theory and Techniques*, 54(4), pages 1025–1027.
- IEEE802-15.4a (2007). Part 15.4: Wireless Medium Access Control and Physical Layer Specifications for Low-Rate Wireless Personal Area Networks. IEEE Standards.
- Kay, S. (1993). *Fundamentals of Statistical Signal Processing Estimation Theory*. Prentice-Hall Inc. ISBN 0-13-345711-7.
- Kelly, D., S. Reinhardt, R. Stanley, and M. Einhorn (2002). PulsON second generation timing chip: enabling UWB through precise timing. In Proceedings of the IEEE Conference on Ultra Wideband Systems and Technologies, pages 117–121.
- Kissick, W. (2001). (editor), *The Temporal and Spectral Characteristics of Ultrawideband Signals*. NTIA Report 01-383. January.
- Lanzisera, S., D. Lin, and K. Pister (2006). RF Time of Flight Ranging for Wireless Sensor Network Localization. In Proceedings of the Workshop on Intelligent Solutions in Embedded Systems. Vienna.
- Lathi, B. (1998). *Modern Digital and Analog Communication Systems 3rd Edition*. Oxford University Press. ISBN 0-19-511009-9.
- Lee, J.-Y. and R. A. Scholtz (2002). Ranging in a Dense Multipath Environment Using an UWB Radio Link. *IEEE Journal On Selected Areas In Communications*, 20(9).
- Leick, A. (2004). *GPS Satellite Surveying, 3rd Edition*. John Wiley And Sons Inc., Hoboken, New Jersey, USA.
- MacGougan, G. (2008). High sensitivity GPS performance analysis in degraded signal environments, UCGE Report No. 20176, Department of Geomatics Engineering.
- MacGougan, G., R. Klukas, and K. O’Keefe (2009). Cramer-Rao lower bound for UWB Ranging, optimistic factor of two discrepancies in the literature. *IEEE Microwave and Wireless Components Letters*, Submitted.

- McEwan, T. (1995). Phase coded, micro-power impulse radar motion sensor. US Patent US005519400. Filed June 6, 1995, Issue date May 21, 1996.
- Misra, P. and P. Enge (2004). *Global Positioning System Signals, Measurements, and Performance*. Ganga-Jamuna Press, Lincoln, Massachusetts, 01773.
- Moore, T., C. Hill, S. Ince, W. Ochieng, S. Feng, R. Ioannides, P. Cross, and L. Lau (2007). End-to-End Testing of an Integrated Centimetric Positioning Test-Bed. In *Proceedings of the Institute of Navigation ION GNSS*, pages 1128–1138. Forth Worth, TX.
- MSSI, M. S. S. I. (2007). *Multispectral Solutions Inc, Ranging Measuring Radio Data Sheet*.
- nzbuu (2009). Urban Canyon, <http://www.flickr.com/photos/nzbuu/3445439869/>, Creative Commons License.
- O’Keefe, K., M. Petovello, G. Lachapelle, and M. Cannon (2007). Assessing probability of correct ambiguity resolution in the presence of time-correlated errors. *Navigation*, 53(4), pages 269–282.
- Opshaug, G. and P. Enge (2001). GPS and UWB for indoor navigation. In *Proceedings of the Institute of Navigation GPS Conference*, page 7 pages. Salt Lake City, Utah.
- Opshaug, G. and P. Enge (2002). Integrated GPS and UWB navigation system: (motivates the necessity of non-interference). In *Proceedings of the IEEE Conference on Ultra Wideband Systems and Technologies*, pages 123–127. Long Beach, CA.
- OSD-DARPA (1990). *Assessment of Ultra-Wideband (UWB) Technology*. Ultra-Wideband Radar Review Panel, Report No. R-6280.
- Parikh, H. and W. R. Michalson (2008). Impulse Radio UWB or Multicarrier UWB for Non-GPS Based Indoor Precise Positioning Systems. *Navigation: Journal of the Institute of Navigation*, Spring, 55(1), pages 29–37.
- Petovello, M., M. Cannon, and G. Lachapelle (2003). Kalman filter reliability analysis using different update strategies. In *Proceedings of the CASI Annual General Meeting*, Montreal, QC.
- Petovello, M. G., K. O’Keefe, G. Lachapelle, and M. E. Cannon (2005). Quantifying Ambiguity Resolution Performance in the Presence of Time-Correlated Measurement Errors Using Geometric-Based Techniques. In *Proceedings of the Institute of Navigation Annual Meeting ION AM (27-29 June 2005, Cambridge, MA)*, pages 1073–1085.

- Petroff, A., R. Rienhardt, R. Stanley, and B. Beeler (2003). PulsON P200 UWB Radio: Simulation and Performance Results. In Proceedings of the IEEE Conference on Ultra Wideband Systems and Technologies, pages 344–348.
- Poor, H. (1988). An Introduction to Signal Detection and Estimation. Springer-Verlag, New York.
- Reed, J. (2005). An Introduction to Ultra Wideband Communication Systems. Prentice Hall, Upper Saddle River NJ.
- Richards, P. (1995). Constrained Kalman filtering using pseudo-measurements. IEE Colloquium on Algorithms for Target Tracking, pages 75–79.
- Ross, G. (1973). Transmission and reception system for generating and receiving base-band duration pulse signals without distortion for short base-band pulse communication system. U.S. Patent 3 728 632.
- Rüeger, J. (1990). Electronic Distance Measurement 3rd Edition. Springer-Verlag. ISBN 3-540-51523-2.
- Saberinia, E. and A. Tewfik (2008). Ranging in multiband ultrawideband communication systems. IEEE Transactions on Vehicular Technology, 57(4), pages 2523–2530.
- Sahinoglu, Z. and S. Gezici (2006). Ranging in the IEEE 802.15.4a Standard,. In Proceedings of the IEEE Annual Wireless and Microwave Technology Conference. Clearwater Beach, FL.
- Shen, Y. and G. Xu (2008). Simplified equivalent representation of GPS observation equations. GPS Solutions, 12(2), pages 99–108.
- Shimizu, Y. and Y. Sanada (2003). Accuracy of relative distance measurement with ultra wideband system. In Proceedings of the IEEE Conference Ultra Wideband Systems and Technologies, pages 374–378. Reston, VA.
- Stone, J. and J. D. Powell (1998). Precise positioning with GPS near obstructions by augmentation with pseudolites. In Proceedings of the IEEE Position Location and Navigation Symposium, pages 562–569.
- Sullivan, D., D. Allan, D. Howe, and F. L. Walls (1990). Characterization of clocks and oscillators, Technical Note 1337. National Institute of Standards and Technology.
- Tan, K. and C. Law (2007). GPS and UWB Integration for indoor positioning. In Proceedings of the IEEE 6th International Conference on Information, Communications and Signal Processing, pages 1–5. Singapore.

- Tanigawa, M., J. Hol, F. Dijkstra, H. Luinge, and P. Slycke (2008). Augmentation of low-cost GPS/MEMS INS with UWB positioning system for seamless indoor/outdoor positioning. In Proceedings of the Institute of Navigation ION GNSS, Sept 16-19, Savannah, GA, pages 1804–1811.
- TDC, T. D. C. (2008). Time Domain Corporation, P210 Starter Kit, Ranging Measuring Radio Data Sheet.
- Teunissen, P. (1989b). The mean and the variance matrix of the fixed GPS baseline. *Acta Geodaetica et Geophysica Hungarica*, 34(1-2).
- Teunissen, P. (1993). Least-squares estimation of the integer GPS ambiguities. IAG General Meeting, Invited Lecture, Section IV Theory and Methodology.
- Teunissen, P. (1998). Success probability of integer GPS ambiguity rounding and bootstrapping. *Journal of Geodesy*, 72, pages 606–612.
- Teunissen, P. and M. Salzmann (1989). A recursive slippage test for use in state-space filtering. *Manuscripta Geodaetica*, 14, pages 383–390.
- Teunissen, P. and S. Verhagen (2008). GNSS ambiguity resolution: when and how to fix or not to fix? In Proceedings of the International Association of Geodesy Symposia Vol 132, pages 143–148.
- Urkowitz, H. (1983). *Signal Theory and Random Processes*. Artech House, Norwell, MA.
- van Dierendonck, A. J., P. Fenton, and T. Ford (1992). Theory and Performance of Narrow Correlator Spacing in a GPS receiver. *NAVIGATION: Journal of The Institute of Navigation*, 39(3), pages 265–283.
- VanTrees, H. (1968). *Detection, Estimation, and Modulation Theory, Part I*. Wiley, New York.
- Verhagen, S. (2004). Integer ambiguity validation: an open problem. *GPS Solutions*, 8(1), pages 36–43.
- Wanniger, L. and S. Wallstab-Freitag (2007). Combined Processing of GPS, GLONASS, and SBAS Code Phase and Carrier Phase Measurements. In Proceedings of the Institute of Navigation ION GNSS, Sept 26-29, Fort Worth, TX, pages 866–875.
- Xu, H., L. Yang, and Y. Morton (2007). Positioning and navigation with ultra-wideband signals. In Proceedings of the Institute of Navigation ION GNSS, Sept 25-28, Fort Worth, TX, pages 1861–1866.

- Yang, L. and G. Giannakis (2004). Ultra-Wideband Communications An Idea Whose Time Has Come. *IEEE Signal Processing Magazine*.
- Yu, H. (2006). Long-Range High-Accuracy UWB Ranging for Precise Positioning. In *Proceedings of the Institute of Navigation GNSS Conference*, pages 83–94. Fort Worth, TX.
- Zimmerman, K., H. Cobb, F. Bauregger, S. Alban, P. Montgomery, and D. Lawrence (2005). A New GPS Augmentation Solution: Terralite XPS System for Mining Applications and Initial Experience. In *Proceedings of the Institute of Navigation GNSS Conference*, pages 2775–2788. Long Beach, CA.